IMMOBILIZATION OF METAL COMPLEXES (Pd, Mn) OVER MESOPOROUS MATERIALS: SYNTHESIS CHARACTERIZATION AND APPLICATION FOR OXIDATION, HYDROGENATION AND C-C COUPLING

A THESIS SUBMITTED TO THE

SAVITRIBAI PHULE PUNE UNIVERSITY FOR THE DEGREE OF

DOCTOR OF PHILOSOPHY

IN CHEMISTRY

BY

PRITI SHARMA

UNDER THE GUIDANCE OF

Dr. A. P. SINGH

CATALYSIS DIVISION

CSIR-NATIONAL CHEMICAL LABORATORY

PUNE 411008, INDIA

SEPTEMBER 2014

CERTIFICATE

Certified that the work incorporated in the thesis entitled: **"Immobilization of metal complexes (Pd, Mn) over mesoporous materials: Synthesis Characterization and application for oxidation, Hydrogenation and C-C coupling",** submitted by **Miss. Priti Sharma,** for the Degree of ***Doctor of Philosophy*****,** was carried out by the candidate under my supervision at Catalysis Division, CSIR-National Chemical Laboratory, Pune 411008, India. Material that has been obtained from other sources is duly acknowledged in the thesis.

Date: **Dr. Anand Pal Singh**

Place: **(Research Supervisor)**

DECLARATION BY THE CANDIDATE

I hereby declare that the thesis entitled **"Immobilization of metal complexes (Pd, Mn) over mesoporous materials: Synthesis Characterization and application for oxidation, Hydrogenation and C-C coupling"**, submitted for the Degree of ***Doctor of Philosophy*** to the Savitribai Phule Pune University, has been carried out by me during the period from August 2009 to till date at Catalysis Division, CSIR-National Chemical Laboratory, Pune 411008, India, under the supervision of Dr. A. P. Singh. The work is original and has not been submitted in part or full by me for any other degree or diploma to this or any other University.

Date: **Priti Sharma**

Place:

Dedicated

To my
Late Father

&

Almighty God

ACKNOWLEDGEMENTS

It gives me immense pleasure to express my deep sense of gratitude to my research guide Dr. A.P. Singh, who has helped me a lot to learn and think more about chemistry and for introducing me to the wonderful world of heterogeneous catalysis. I thank him for an excellent and inspiring guidance, constant encouragement, sincere advice and unstinted support during all the times of my Ph.D. work. His truly scientist intuition has made him as a constant oasis of ideas and passions in science, which exceptionally inspire and enrich my growth as a student, a researcher and a scientist want to be. My interactions with him have improved my quality of research life. I sincerely thank him for his splendid guidance, constant support and excellent work ethics that he bestowed on me. I learnt from him be it chemistry or patience or perseverance.

I would like to sincerely thank Dr. P. K. Tripathi for helping me in the last phase of my thesis by providing friendly discussions and suggestions and would also my earnest respect to all the senior scientists Dr. Ganesh Pande, Dr. C.V. Stynaryana, Dr. C. S. Gopinath, Dr. C. P. Vinod, Dr. Mrs. K. R. Kamble and Dr. P. N. Joshi, Dr. N. M. Gupta, Dr. Paresh Dhepe, Dr. T. Raja, Dr. SelvaRaj, Dr. Shubhangi for their valuable support during my course of study.

I wish to convey my sincere gratitude to Dr. Selvaraj, Dr. Nandhini Devi for low angle XRD, Dr. Shubhangi for FT-IR, all the NMR group members for solid and liquid state NMR analysis, Dr. N.E. Jacob and Mr. R.K. Jha for N_2-sorption analysis, Ms. V. Samuel for XRD, Dr. (Mrs.) S. S. Deshpande for UV-Vis, Dr. Patil of CMC and Dr. A. A. Bhalekhar, Mr. Gaikwad for SEM analysis, Micro analysis laboratory staffs for elemental analysis, divisional scientists and Dr. Kale from CMET. I would also like to thank Mr. Purushottaman, Mr. Madhu, Mr. Milind and all other scientific and nonscientific staff of the division for their valuable help and cooperation during my tenure as a research student.

I don't have words to express my feelings towards my friends and seniors Dr. Selvakumar, Mrs. Sheetal, Dr. Atul Kumar, Dr. Ramakanta Sahu, Dr. Ravinder Kumar, Dr. Asha, Dr. Dhermender Kumar, Dr. Anand Harbindu, Dr. Ankush, Dr. Sujeet, Dr. Rajender Salla, Dr. Priyanaka, Dr. Deepak, Dr. Guri Priya, Dr. Roshna without their invariable help and regular scientific discussions; it would have not been possible for me to submit this thesis.

With much appreciation, I would like to mention the crucial role of my lab mates and friends Anish, Shoy, Sanjay Negi, Monika, Jitesh. P. R, K. S. Sanjush, Shilpa Shanker, Rentona, Priyanka,

Aswath kumar, Anupam, Leena, Somya, Tanushree, Sager, Prsanjeet, Anup, Sandeep, Richa, Rajeesh, Jijil, Deepa, Sumona Ghosh, Hanmant Gurav, Nishita, Srikanth N. Dama, Richa, Santosh khokarale, Dr. Edwin, Lenin, Dr. Tussara, Dr. Mehjabeen Sheikh, Dr. Anuj Kumar Mourya, Dr. Bogesh, Dr. Trupti, Prakash Chandra, Swati, Ashok, Sunil Shekar, from catalysis division and Priyanaka Sharma, Ajeet Singh, Shrisht, Nevedita, Shashikant Shukla, Janki Ram, Govind, Krishanu, Arpan Manna, Priti Jain, Tanaya Bose, Alson Mart, Tamas Panda, Shubha Sahu other research scholars and my hostel friends Nalini, Praveen, Rubi Azghar, Manaswani, Priyanaka, Munmun, Manisha Kapoor from for such a friendly and cheerful working atmosphere, for their constant support, love and care throughout my stay in NCL.

I am forever indebted to my Father, Mother and sisters Poonam and Ritu for their love, understanding and encouragement throughout my life. Their blessings and encouragement have always made me to take proper decision in all difficult periods.

Finally, my thanks are due to Council of Scientific and Industrial Research, Government of India, for awarding the senior research fellowships and Dr. Sourav Pal, Director, Dr. B. D. Kulkarni, Deputy Director, Dr. P. A. Joy and all the Students Academic Committee (SAC) staffs, National Chemical Laboratory to carry out my research works, extending all infrastructural facilities and to submit this work in the form of a thesis for the award of Ph. D degree.

Priti Sharma

CONTENTS

DESCRIPTION

CHAPTER 1: INTRODUCTION AND LITERATURE SURVEY

CHAPTER 5: COVALENTLY ANCHORED 2, 4, 6-TRIALLYLOXY-1, 3, 5-TRIAZINE Pd(II) COMPLEX OVER MODIFIED SURFACE OF SBA-15

CHAPTER 6: SUMMARY AND CONCLUSIONS

PUBLICATIONS /SYMPOSIA /CONFERENCES/APPENDIX

LIST OF FIGURES

LIST OF TABLES

LIST OF SCHEMES

LIST OF ABBREVIATIONS

AAS	Atomic Absorption Spectroscopy
AES	Atomic Emission Spectroscopy
APTMS	3-Aminopropyltrimethoxy silane
ArMgBr	Phenyl magnesium bromide
AIBN	Azo-bisisobutyronitrile
Az-PTMS	3-azidopropyltrimethoxysilane
CP MAS	Cross Polarization Magic Angle Spinning
BET	Brunauer-Emmett-Teller
B-PMO	Benzene Periodic Mesoporous Organosilica
BJH	Barrett-Joyner-Halenda
BTEB	1,2-Bis (triethoxysilyl) benzene
BTSE	1,2-Bis(triethoxysilyl)ethane
BE	Binding Energy
CMC	Critical Micelle Concentration
CTABr	Cetyltrimethyl ammonium bromide
Cl-PTMS	3-Chloropropyl trimethoxysilane
CsF	Cesium Fluoride
DCM	Dichloromethane
DMG	Dimethylglyoxime
DIPEA	N,N-di-isopropylethylamine
DMSO	Dimethylsulfoxide

DMF	Dimethylformamide
Dp	Average Pore Diameter
EDTA	Ethylene diamine tetraacetic acid
SDPEN	(S,S)-DPEN or (S,S)-1,2-Diphenylethylenediamine
DNA	Deoxyribonucleic acid
DPEN	1,2-Diphenylethylenediamine
DTA	Differential Thermal Analysis
ee	Enantiomeric Excess
EN	Ethylenediamine
FSM	Folded Sheet Materials
FTIR	Fourier Transform Infrared
GC	Gas Chromatography
GCMS	Gas Chromatography – Mass Spectroscopy
GHSV	Gram Hourly Space Velocity
HMM	Hybrid Mesoporous Material
HMS	Hexagonal Mesoporous Silica
HRTEM	High Resolution Transmission Electron Microscopy
ICP-AES	Inductively Coupled Plasma – Atomic Emission Spectrometry
KCP	Kinetically Controlled Product
LCT	Liquid Crystal Template
MCM	Mobil's Crystalline Material
MLCT	Metal to Ligand Charge Transfer Transition
MPTS	3-Mercaptopropyl Trimethoxy Silane

NMR	Nuclear Magnetic Resonance
ODA	Octadecylamine
ODTA	Octadecyl Trimethyl Ammonium Bromide
PMO	Periodic Mesoporous Organosilica
SAED	Selected Area Electron Diffraction
SAMS	Self-Assembled Monolayers
SAMS	Self-Assembled Monolayers
SBA	Santa Barbara Amorphous
MCM	Mobil's Crystalline Material
SEM	Scanning Electron Microscopy
SLC	Silicatropic Liquid Crystals
TAT	2, 4, 6-triallyloxy-1, 3, 5-Triazine
TCP	Thermodynamically Controlled Product
TEOS	Tetraethyl Orthosilicate
TGA	Thermogravimetric Analysis
THF	Tetrahydrofuran
TON	Turnover Number
TPD	Temperature Programmed Desorption
TZ	4-(2-pyridyl)-1, 2, 3-Triazole Ligand
UOF MN	Unified Organically Functionalized Mesoporous Network
UV-Vis	Ultraviolet-Visible
XPS	X-Ray Photoelectron Spectroscopy
XRD	X-Ray Diffraction

XRF	X-Ray Fluorescence
Vp	Pore Volume

ABSTRACT

The surface modification of M41S type mesoporous materials by transition metal complexes or reactive organic functional groups allows the preparation of multifunctional heterogeneous catalysts with desired catalytic properties. Taking into account of environmental consideration the hetrogenization of organo-catalyst of transition metal complex over organic-inorganic hybrid mesoporous support such as PMO and SBA-15 are focused. The mesoporosity and very high surface area of the surface-functionalized mesoporous materials can also be exploited for the immobilization of different catalytically reactive species. The principal aim of this thesis is to investigate the approach of heterogenization of various transition metals complex over solid mesoporous supports (SBA-15) and organic-inorganic hybrid mesoporous materials (PMO) for oxidation, hydrogenation and C-C coupling reactions, under different reaction conditions.

Mesoporous silica materials represent a unique class of silica and organic-inorganic hybrid based materials *viz;* SBA-15 and PMO act as a support which have received much attention because of their uniform hexagonally ordered two dimensional mesoporous channels structure, high specific surface area, large pore volume, uniform pore size (between 2-50 nm), high hydrothermal stability and rich surface chemistry allowing ready diffusion of reactants to the active sites located in the nanopores. Their surface can be easily functionalized by organic molecules and these hybrid materials promise great opportunities for generation of new functional materials with improved and tailored properties. Immobilization of organo-catalysts on inorganic matrices has been a great area of research for academic and industrial points of view, as this method affords an ideal combination of the advantages of homogeneous catalysts and avoids their disadvantages related to handling and reusability of the catalyst. Homogeneous catalyst can be immobilized by different ways such as electrostatic interaction, covalent bonding and simply physical adsorption over support etc. Among the various types of immobilization covalent

interaction is superior, which involve direct bonding between organic moieties with heterogeneous support through linker group. The recent discovery of the Cu(I)-catalyzed 1, 3-dipolar cycloaddition of organic azides to alkynes has provided the most powerful "**click chemistry**" tool for conjugation between appropriately functionalized binding partners via an 1, 2, 3-triazole linkage. Additionally, the surface modification of the synthesized mesoporous materials were done by using various organic and organo silane groups, such as 3-aminopropyltrimethoxysilane (3-APTMS), 3-mercaptopropyltrimethoxysilane (3-MPTMS), 3-azidopropyltrimethooxysilan (3-Az-PTMS) (**click reaction**) for transition metal complexes anchoring by post synthetic route to develop new class of mesoporous catalysts. In-depth characterizations of all synthesized catalyst systems are highlighted to understand the mode of interaction of the active sites in transition metal complex with the mesoporous silicate network and to evaluate the structure-catalytic activity relations and stability of the mesoporous solids for oxidation, hydrogenation and C-C coupling reactions.

The present work is comprised of **six chapters**.

Chapter 1: **Introduction and Literature Survey**

This chapter gives an idea about current scenario in the field of mesoporous molecular sieve materials, precisely transition metal complex based mesoporous materials, more particularly Pd and Mn transition metal catalysed oxidation, hydrogenation and C-C coupling reactions. The different characteristic properties of these materials include shape selectivity, formation mechanisms etc., and further more literature survey over synthesis aspects, characterization techniques, and different catalytic applications has been discussed. The scopes and objectives of the present work were outlined at the end of this chapter.

Chapter 2: Mn(III) based Binaphthyl Schiff Base Complex Heterogenized over organo-modified SBA-15.

This chapter includes detailed synthesis and characterization of Chloro (S,S)(–)[N-3-tert-butyl-5-chloromethyl salicylidene]-N-[3,5-di tert-butyl salicylidene] 1,1-binaphthyl-2,2-diamine manganese(III) (homogeneous system) complex on modified SBA-15 by using 3-aminopropyl trimethyoxy silane (3-APTMS) as a reactive surface modifier to give supported catalyst. The surface properties of the functionalized catalyst were analyzed by a series of characterization techniques such as elemental analysis, XRD, N_2 sorption measurement isotherm, FT-IR, TGA-DTA, XPS, and solid state ^{13}C NMR. The XRD and N_2 sorption measurement, UV reflectance and CP MAS NMR spectroscopy (^{13}C and ^{29}Si) of the catalyst confirmed the structural integrity of the mesoporous hosts and the spectroscopic characterization technique proved the successful anchoring of the metal complex over the modified mesoporous support. The screening of the catalyst Mn(III)-L-SBA-15 and neat Mn(III)-L complexes was done in the oxidation reaction of thioanisole (methyl phenyl sulfide) by using TBHP as an oxidant. Mn(III)-L-SBA-15 catalyst shows higher activities and turnover number (TON) and exhibit enhanced enantiomeric excess comparable to homogeneous catalyst Mn(III)-L. Moreover bulkier alkene like 1,2-dihydronaphthalene was also efficiently epoxidized with the synthesized supported catalyst.

Chapter 3: Phosphine Free SBA-15-EDTA-Pd Highly Active Recyclable Catalyst for Heck, Suzuki and Sonogashira Reaction

This Includes phosphine obstructed highly efficient and reusable SBA-15-EDTA-Pd catalyst synthesis by anchoring Pd-EDTA complex over the surface of organo-functionalized SBA-15. The physiochemical properties of the organo-functionalized catalyst were analyzed by elemental analysis, ICP-OES, XRD, N_2 sorption measurement isotherm, TGA & DTA, solid state ^{13}C, ^{29}Si NMR spectra FT-IR, XPS DRS UV-Visible, SEM and TEM. XRD and N_2 sorption analyses of

synthesized catalyst confirm that ordered mesoporous channel structure was retained even after the multistep synthetic procedures. The (100), (110) and (200) reflections in SBA-15 provide good structural stability, existence of long range order and high pore wall thickness. The organic moieties anchored over the surface of SBA-15 and inside the pore wall were demonstrated by solid state ^{13}C NMR spectra and FT-IR spectroscopy. Further, solid state ^{29}Si NMR spectroscopy provides the information about degree of functionalization of surface silanol groups, of SBA-15 with organic moieties. The electronic environment and oxidation state of Pd metal in SBA-15-EDTA-Pd were monitored by XPS, DRS UV-visible techniques. Moreover, the morphologies and topographic information of synthesized catalyst were confirmed by SEM and TEM analysis. The synthesized catalyst SBA-15-EDTA-Pd was screened for the Heck, Suzuki and Sonogashira coupling reactions and show higher catalytic activity with higher TON (turn over number). The anchored solid catalyst can be recycled efficiently without major loss in reactivity.

Chapter 4: A Recyclable and Efficient Pd(II) 4-(2-Pyridyl)-1, 2, 3-Triazole Complex over the Solid Periodic Mesoporous Organosilica (PMO) Support by "Click Reactions"

An efficient highly reusable B-PMO-TZ-Pd(II) has been synthesized by anchoring 4-(2-pyridyl)-1, 2, 3-triazole ligand over the inner surface of organo-functionalized benzene containing periodic mesoporous organosilica (B-PMO) via "**Click reaction**" and subsequent complexation with $PdCl_2$. B-PMO materials with uniform hexagonal arrangement were prepared using C16 alkyl trimethyl ammonium bromide [CTAB] surfactant under basic conditions. The physiochemical properties of the functionalized catalyst were analyzed by elemental analysis, ICP-OES, XRD, N_2 sorption measurement isotherm, TGA & DTA, solid state ^{13}C, ^{29}Si NMR spectra FT-IR, XPS, DRS UV-Vis, SEM and TEM. The (100), (110) and (200) reflections in B-PMO provide good structural stability, existence of long range order and high pore wall thickness. TGA-DTA results reveal that thermal stability of synthesized catalyst

B-PMO-TZ-Pd(II) maintained at higher temperature. Furthermore, B-PMO-N_3 shows sharp absorbance at 2106 cm^{-1}; which is a characteristic stretching vibration of any organic azide (N_3). The absence of this peak at 2106 cm^{-1} in B-PMO-TZ-Pd(II) show that the azidopropyl group successfully incorporated to the 2-ethynylpyridine via **click reaction**. The electronic environment and oxidation state of Pd metal in B-PMO-TZ-Pd(II) were monitored by XPS, DRS UV-visible techniques. The synthesized catalyst was screened in the Stille and Kumada coupling reactions and show higher catalytic activities with high TONs. The anchored solid B-PMO-TZ-Pd(II) catalyst can be recycled efficiently and reused several time without major loss in reactivity.

Chapter 5: Covalently Anchored 2, 4, 6-Triallyloxy-1, 3, 5-Triazine Pd(II) Complex over Modified Surface of SBA-15

Highly efficient and reusable SBA-15-TAT-Pd(II) has been synthesized by anchoring 2, 4, 6-triallyloxy-1, 3, 5-triazine (TAT) complex over the surface of organo-functionalized SBA-15. The physiochemical properties of the organo-functionalized catalyst were analyzed by various characterizations. XRD and N_2 sorption analyses were done to find out textural properties of synthesized catalyst and confirm that ordered mesoporous channel structure was retained even after the multistep synthetic procedures. The organic moieties anchored over the surface of SBA-15 and inside the pore wall were demonstrated by solid state ^{13}C NMR spectra and FT-IR spectroscopy. The electronic environment and oxidation state of Pd metal in SBA-15-TAT-Pd(II) were monitored by XPS, DRS UV-visible techniques. The synthesized catalyst SBA-15-TAT-Pd(II) was screened for the hydrogenation reactions and show higher catalytic activity with high TON. The anchored solid catalyst can be recycled efficiently and reused several time (five times) without major loss in reactivity.

Chapter 6: Summary and Conclusions

This Chapter gives an overall summary of all the major conclusions of the present study with respect to the synthesis and characterization of immobilized catalysts and the successful attempt in using the catalytic properties of the catalyst for Oxidation, Hydrogenation and C-C coupling reactions.

CHAPTER-1

Introduction and

Literature Survey

1.1. GENERAL BACKGROUND

Jons Jakob Berzelius coined the term 'catalysis' (which means loosening down in Greek) in 1835 to refer certain chemicals that speed up reaction.[1] In general catalyst is defined as "*Substance that increases the rate of chemical attainment of chemical equilibrium without itself undergoing chemical change*". But, it follows from this definition that if the rate of forward reaction is speeded up in presence of particular catalyst, the reverse reaction will likewise be facilitated to the same degree. Catalyst generally react with one or more reactants to form a chemical intermediate that subsequently reacts to form the final reaction product while regenerating the catalyst. An acceleration of the rate of a process or reaction, brought about by a catalyst, usually present in small quantities and unaffected at the end of the reaction is called catalysis.

Catalysts can either be heterogeneous or homogeneous. Heterogeneous catalysts are present in different phases from the reactants (e.g. solid catalyst in liquid reaction mixture), whereas homogeneous catalysts are in the same phase (e.g. dissolved catalyst in liquid reaction mixture).[2] Heterogeneous catalysts provide surface on which the reactants (or substrates) temporarily become adsorbed. Bonds in the substrate become weakened sufficiently for new bonds to be created. The bonds between the products and the catalyst are weaker, so the products formation takes place. Active sites on the metal allow partial weak bonding to the reactant gases, which are adsorbed onto the metal surface. As a result, the bond within the molecule of a reactant is weakened and the reactant molecules are held in close proximity to each other.

Nevertheless, the efficiency of these processes can be improved even further through the employment of the corresponding heterogeneous catalysts that are derived from their homogeneous counterparts by immobilization, since the catalyst can be easily separated and recycled, and contamination with metal traces minimized.[3] The term heterogenization refers to a process, whereby a homogeneous transition metal complex (including free metal particles, biological molecules, organic species etc.) is either immobilized, or anchored, or incorporated or encapsulated in an inert organic (polymer) or inorganic support.

The organometallic complex can be immobilized on an organic or inorganic solid support through different anchored or immobilized methods. Amorphous oxides (in particular silica and, to a lesser extent, alumina),[4,5] zeolites,[6] pillared clays, LDHs[7] and clay minerals (in particular, smectite laminar minerals)[8] are most routinely used. A wide variety of organic supports, (principally insoluble polymers), take part in the common procedures for immobilizing ligands/catalysts. Although organic supports favour reaction rates that are higher than those of inorganic supports, the random distribution of the ligand units along the polymeric chain and swelling effects may be serious limitations. We have focused on the immobilization of catalysts on inorganic support (SBA-15) and periodic mesoporous organosilica (PMO) material, which are generally inert materials based on insoluble porous structures with a highly specific surface area.[9]

1.2. SYNTHESIS AND MECHANISM OF FORMATION OF MESOPOROUS MATERIAL

Porous materials have been extensively studied with regard to technical applications as catalysts and catalyst supports. According to the IUPAC definition, porous materials are divided into three classes depending on the pore size:

Type Pore Size	(Å)
Microporous	< 20
Mesoporous	20-500
Macroporous	> 500

The 'physical chemistry of organized matter' relies on the successful combination of sol-gel chemistry and self-assembly procedures, to uniquely control the texture of materials at the nanometer scale. The growth of soft chemistry derived inorganic or hybrid networks templated by organized surfactant assemblies (structure directing agents) allowed constructing a new kind of materials organized in the mesoscopic scale (2-50 nm): the best example is the ever growing family of meso-structured hybrids and derived mesoporous inorganic materials. Mesoporous silica (with regular

pore diameters between 20 and 500 Å) has recently been raised as novel class of materials in heterogeneous catalysis. Silica has no intrinsic catalytic property but it can be used as support and therefore functionalized either by framework substitution or by post-synthesis surface modification. Mesoporous molecular sieves have attracted considerable attention in recent years since the discovery of the M41S family of mesoporous materials by researchers of the Mobile Oil Corporation. The materials are synthesized by using a silica source and an organic structure-directing agent e.g., cationic surfactants containing long alkyl chain quaternary ammonium compounds containing 10-20 carbons, often followed by then addition of co-surfactants. Originally, this family has been classified into three subgroups: a hexagonal (MCM-41, Mobile Composition of Matter: 2D hexagonal); a cubic (MCM-48), and a lamellar phases (MCM-50). More recently, the so-called SBA-15 (University of California at Santa Barbara; 2D-hexagonal) materials have been prepared by using neutral triblock co-polymers (Pluronic triblock polymer, poly (ethylene oxide)-poly (propylene oxide)-poly (ethylene oxide); $[EO_nPO_mEO_n]$.

1.2.1. Liquid Crystal Templating (LCT) Mechanism

The researchers of Mobil Corporation proposed a *"liquid crystal templating (LCT) mechanism*" to explain the formation of M41S type mesoporous materials.[10] The mesostructure formation depends on the hydrocarbon chain length of the surfactant tail group[11], the effect of variation of the surfactant concentration and the additional organic swelling agents. The lowest concentration at which the surfactant molecules aggregate to form spherical isotropic micelles is called critical micelle concentration (CMC1). Further increase in the surfactant concentration initiates aggregation of spherical into cylindrical or rod-like micelles (CMC2). There are three main liquid crystalline phases with hexagonal, cubic and lamellar structures (**Scheme 1.1**). The hexagonal phase is the result of hexagonal packing of cylindrical micelles, the lamellar phase corresponds to the formation of surfactant bilayers and the cubic phase may be regarded as a bicontinous structure. The Mobil researchers proposed two synthesis mechanisms[10a,b]. In first route, the $C_nH_{2n+1}(CH_3)_3N^+$ surfactant species organize into lyotropic liquid crystal phase, which can serve as template for

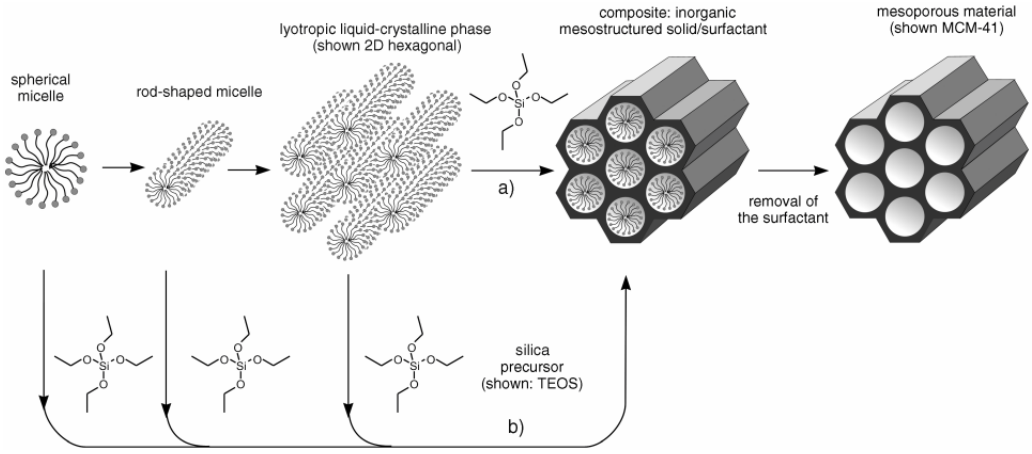

Scheme 1.1 Formation of mesoporous materials by structure directing agents.

the formation of hexagonal MCM-41 structure.

First the surfactant micelles aggregate into a hexagonal array of rods, followed by interaction of silicate or aluminate anions present in the reaction mixture with the surfactant cationic head groups. Thereafter condensation of the silicate species occurs, leading to the formation of an inorganic polymeric species. After combusting off the surfactant template by calcination, hexagonally arranged inorganic hollow cylinders are produced. However, the drawback of this synthesis pathway was pointed out by *Cheng et. al*,[12] according to whom the hexagonal liquid-crystal phase does not form below 40 % of surfactant concentration. It is known that MCM-41 may be formed at low surfactant concentrations (1 wt. %) with respect to water content, and in situ ^{15}N NMR spectra indicated that the hexagonal liquid crystalline phase was not present anytime during formation of MCM-41.

In the second route[10a,11], the hexagonal ordering is initiated by the presence of silicate species in the reaction mixture. *Chen et.al* explained that randomly distributed surfactant micelles with rod-like morphology form initially, and their interaction with silicate oligomers generate randomly oriented surfactant micelles surrounded by two or three silica monolayers[13] **(Scheme 1.2)**. The presence of rod-like micelles in solution was supported by isotropic in situ ^{14}N NMR.[14] Further condensation between silicate species on adjacent rods occurs on heating, initiating long-range hexagonal ordering.

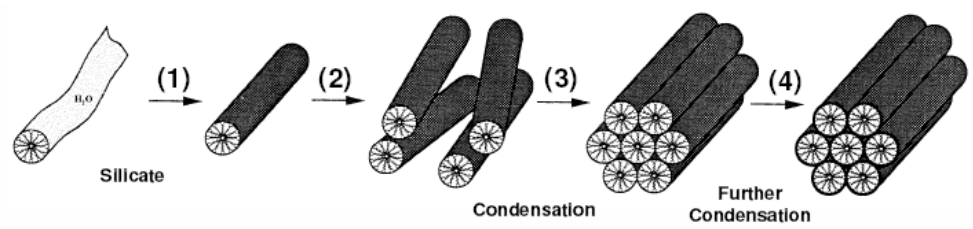

Scheme 1.2. Silicate rod assembly proposed for the formation of MCM-41; (1) and (2) random ordering of rod-like micelles and interaction with silicate species, (3) spontaneous packing of the rods, and (4) remaining condensation of silicate species on further heating.

1.2.2. Charge Density Matching

The "charge density matching" model proposed by Stucky *et al.* suggested that condensation occurs between initially formed silicate species by the electrostatic interaction between the anionic silicates and the cationic surfactant head groups. This eventually reduces the charge density and therefore, curvature was introduced into the layers to maintain the charge density balance with the surfactant head groups, which

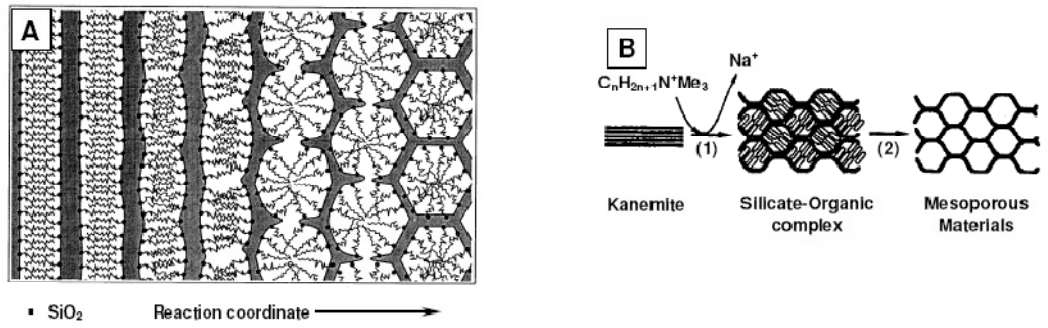

Scheme 1.3. Transformation of surfactant-silicate systems from lamellar to hexagonal mesophases; (A) hexagonal mesophase obtained by charge density matching, and (B) folding of kanemite silicate sheets around intercalated surfactant molecules. (Ref. 15, 16)

leads to transformation of the lamellar mesostructure into the hexagonal one **(Scheme 1.3)**. Although this silica-initiated synthesis mechanism has been widely accepted, the

presence of an intermediate lamellar species has been disputed.

1.2.3. Folded Sheet Mechanism

The "folded-sheet mechanism" postulated by *Inagaki et al.*[16] indicated the presence of intercalated silicate phases in the synthesis medium of the reaction products. The flexible silicate layers of kanemite fold around the surfactant cations, and cross-linking of the interlayer occurs by condensation of silanol groups on adjacent silicate sheets. On increase of pH, the amount of occluded $C_nH_{2n+1}(CH_3)_3N^+$ cations in kanemite increases resulting in expansion of the kanemite interlayers to form another class of regular hexagonal structure called FSM 16.

1.2.4. Silicatropic Liquid Crystals

Firouzi et al. have developed a model based on cooperative organization of inorganic and organic molecular species into 3D structured arrays.[17] According to this model, the physicochemical properties of a particular system were not determined by the organic arrays having long-range pre-organized order, but by the dynamic interplay among ion-pair inorganic and organic species, so that different phases can readily be obtained through small variation of controllable synthesis parameters. The exchange of silicate anions with the surfactant halide counter ions formed the 'silicatropic liquid crystal' (SLC) phase, which exhibited very similar behaviour to that of typical lyotropic systems and finally condensed irreversibly in to MCM-41.

1.2.5. Generalized Liquid Crystal Templating Mechanism

1.2.5.1. Ionic Route (Electrostatic Interaction)

Huo et al.[18] proposed a generalized mechanism for the formation of mesostructures, which was based on specific types of electrostatic interaction between an inorganic precursor (I) and a surfactant head group (S). In this concept, four different approaches were proposed to synthesize transition metal oxide mesostructures. The first route involves the charge density matching between surfactant cations and inorganic anions (will be referred to as S^+I^- hereafter). The second route deals with the charge-reversed situation, *i.e.*, anionic surfactant and

cationic inorganic species (S^-I^+). Both the third and fourth routes are counter ion mediated pathways. The third one demonstrates the assembly of cationic species *via* halide ions ($S^-X^+I^-$), while the fourth one depicts the assembly of anionic species *via* alkali metal ions ($S^+X^-I^+$) **(Scheme 1.4)**. These synthesis strategies are acceptable for

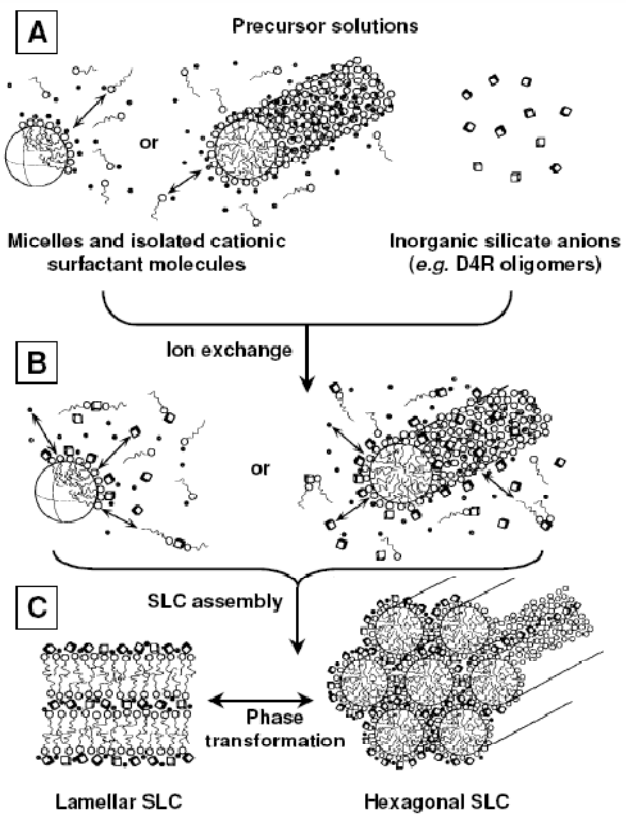

Scheme 1.4. Cooperative organization for the formation of silicatropic liquid crystal phase/silicate-surfactant mesophases; (A) organic and inorganic precursor solutions, (B) preliminary interaction of the two precursor solutions after mixing and (C) multidentate interaction of the oligomeric silicate units with the surfactant molecules.

the formation of a wide variety of lamellar, hexagonal or cubic mesophases. However, a general problem negotiated very often is the poor stability of the inorganic framework, which frequently collapses after removal of the surfactant.

1.2.5.2. Neutral Templating Route (Hydrogen Bonding Interaction)

Tanev and Pinnavaia proposed another route to synthesize hexagonal mesoporous silicas (HMS) having thicker pore walls, high thermal stability and smaller crystallite size but, having higher amounts of inter particle mesoporosity and lower degree of long-range ordering of pores than MCM-41 materials.[19] This route is essentially based on hydrogen bonding between neutral primary amines (S^0) and neutral inorganic precursors (I^0), wherein hydrolysis of tetraethyl orthosilicate (TEOS) in an aqueous solution of dodecylamine yields neutral inorganic precursor. Using the same approach, porous lamellar silicas with vesicular particle morphology have been synthesized with the aid of double headed alkylamines linked by a hydrophobic alkyl chain (α, β-dialkylamine).

1.2.5.3. Ligand-Assisted Templating Route (Covalent Interaction)

Antonelli and Ying have proposed a ligand-assisted templating mechanism for the synthesis of hexagonally packed mesoporous metal oxide completely stable to surfactant removal.[20] In a typical synthesis, the surfactant was dissolved in the metal alkoxide precursor before addition of water to allow nitrogen-metal covalent bond formation between the surfactant head group and the metal alkoxide precursor. The existence of this covalent interaction was confirmed by ^{15}N NMR spectroscopic studies. In this approach, the structure of the mesophases could be controlled by adjustment of the metal/surfactant ratio, which led to a new class of mesoporous transition metal oxides analogous to M41S family.

1.3. BLOCK COPOLYMERS AS TEMPLATES

Since the pioneering work of the Mobil scientists, a permanent effort is made to develop meso-textured inorganic or hybrid phases, which are potential candidates for a variety of applications, in the fields of catalysis, optics, photonics, sensors, separation, drug delivery, sorption, acoustic and electrical insulation. In the case of mesoporous oxides, the templating relies on supramolecular arrays: micellar systems formed by surfactants or block copolymers (BC) are indeed interesting as supra molecular templates because they are capable to impart larger pores and thicker walls,

apart from being industrially available, hazard-free and easy to remove from the mineral framework (by thermal treatment or solvent extraction). The initial works related to meso structured oxides described the use of ionic surfactants such as the cationic alkyltrimethylammonium(CTAB, n=8-18), anionic alkylsulfonates ($C_nSO_3^{2-}$, n = 12-18) or alkyl phosphates as supramolecular templates. These syntheses were performed in extreme (acid or alkaline) pH conditions, yielding materials with controlled pore size (15-100 Å). However, two main limitations exist:

1. Typical wall thickness of 8-13 Å, which is a serious limitation regarding stability for catalysis;
2. Limited pore size offered by molecular surfactants.

The only way to go beyond 50 Å pore size consisted in employing swelling agents (such as trimethylbenzene), involving complicated synthesis, and irreproducibility (linked to emulsion formation or phase separation). Thus, more versatile supra-molecular templates were needed. Amphiphilic BC belongs to an important family of surfactants, widely used in detergency, emulsifying, coating, thickening, etc. The self-assembly characteristics of these BC permit to control the superstructure, to vary the typical length scales and to add specific functions. Indeed, the properties of BC can be continuously tuned by adjusting solvent composition; molecular weight or polymer architecture. Pinnavaia and co-workers were the first to bring the idea of using nonionic surfactants (alkyl amines (C_nNH_2), oligomeric alkyl poly (ethyleneoxide) ($C_n(PEO)_mOH$), or $(PEO)_m(PPO)_n(PEO)_m$, EO = $-CH_2-CH_2O-$, and PO = $-CH(CH_3)CH_2O-$ as progen species, in neutral media. Some advantages of using neutral non-ionic surfactants over the ionic ones were immediately noticed: (a) larger inorganic wall thickness (15-40 Å), enhancing the hydrothermal stability of the mesoporous oxides; (b) easier pore diameter tuning, by varying both the type and the concentration of the surfactant, (c) easier solvent removal, by solvent extraction; H bonding (instead of electrostatic) interactions between the template and the inorganic framework should be easier to dissociate. The first mesoporous materials issued MSU-X from the so-called neutral route (S^oI^o) presented low-order wormlike structures. In 1998, the use of neutral surfactant has been extended to ordered meso-

structured silicas by *Stucky et.al*. The hexagonal SBA-15 silicas are prepared in acidic condition, TEOS being introduced as silica source and a triblock co-polymer [polyethyleneoxide-polypropyleneoxide-polyethyleneoxide (EO_n-PO_m-EO_n) possessing two medium length EO_n hydrophilic blocks surrounding a long and less hydrophilic PO_m block] as surfactant. At low concentration in water, these copolymers from cylindrical aggregates, with the dehydrated PO_m blocks in their cores, surrounded by a corona formed by the hydrated EO_n blocks. At the low pH used for synthesis (<2), the EO groups are protonated. Their interaction with positively charged silicate oligomers are mediated by Cl^- anions and the weak $S^+Cl^-I^+$ (S = surfactant; I = inorganic) interactions, is therefore an easy way to induce an increase in the wall thickness of mesoporous silicas and to stabilize them.

1.4. SURFACE MODIFICATION OF MESOPOROUS MATERIALS

The application of pure mesoporous silicates or alumina-silicates as catalysts is rather limited because of the limitations in the nature of their active sites, leading to limited scope of the reactions they could accomplish. To utilize these mesoporous materials for several specific applications including catalysis and also sorption, ion exchange, sensing *etc*., the introduction of reactive organic functional groups by modifying the inner surfaces of these materials, to form inorganic-organic hybrid materials, is essential.[21] The inorganic components of these inorganic-organic hybrid materials can provide mechanical, thermal or structural stability, while the organic components can introduce flexibility into the framework and can more readily be modified for specific applications.[22] The presence of large amount of silanol groups in the surfaces of M41S materials could be exploited for anchoring of desired organic functional groups by condensation with necessary alkoxysilane precursors.[23] These parent organic functional groups, with or without further modification; can facilitate anchoring of different types of catalytically reactive metal particles or organometallic complexes inside the mesoporous network.[24] Different methods for organic modification of mesoporous surfaces will be briefly highlighted in this section.

1.4.1. Grafting Methods

Grafting refers to post synthesis modification of the inner surface of mesoporous silica, where the organic functional groups are introduced as the terminal groups of an organic monolayer.[25] The large concentration of surface silanol [(-SiO)$_3$Si-OH] groups present in mesoporous silica can be utilized as convenient moieties for anchoring of organic functional groups.[26] The surface modification with organic functional groups is generally carried out by silylation, as depicted in Scheme

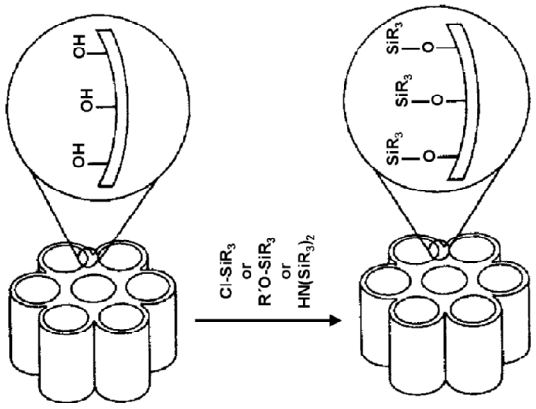

Scheme 1.5. Functionalization of inner walls of mesoporous silicates by grafting (Ref. 21).

1.5. The surfactant molecules from the mesopores are usually removed either by calcination or by extraction with appropriate solvents. At typical calcinations temperatures (~500 °C) several surface silanol groups are lost after condensation of unreacted silanol groups. However, it is necessary to maintain a large concentration of surface silanol groups after calcination, if a high coverage of organic functional groups on the surfaces is desired. This can be achieved by treatment of calcined mesoporous silica with boiling water[27] or steam[28], or by acid hydrolysis.[29] Solvent-extraction processes reduce the possibility of loss of surface silanol groups, although thermal treatments after extraction can increase the surface reactivity towards silylation.

1.4.1.1. Grafting with Passive Surface Groups

Organic functional groups with lower reactivity such as alkyl or phenyl groups could be grafted to alter the accessible pore volume of mesoporous silica, thereby enhancing the hydrophobicity of the surface and protecting towards hydrolysis. The pore diameters of ordered mesoporous materials could be adjusted by varying the alkyl chain length of the silylating agent or the quantity of the silylating agent.[30] The most commonly used surface modifying agents containing lower reactive functional groups are trimethylchlorosilane (Me_3SiCl)[31], and hexamethyldisilaxane [$(Me_3Si)_2NH$].[32]

1.4.1.2. Grafting with Reactive Surface Groups

Grafting of the mesopore surfaces with reactive functional groups like olefin, cyanide, thiol, amine, halide, epoxide *etc*. permits further functionalization of the surface. Further functionalization includes hydroboration[33] and bromination[34] of olefins (vinyl groups), hydrolysis of cyanides to carboxylic acids[35], oxidation of thiols to sulfonic acids[36] alkylation and nucleophilic substitution of amines[37] and nucleophilic substitution of halides.[38] After the desired modification of the reactive functional groups, a rational design for anchoring of catalytically active transition metal complexes onto mesoporous network could be made.[39]

1.4.1.3. Site-Selective Grafting

For grafting of organic functional groups, the external surfaces of the mesoporous materials are kinetically more accessible than the internal surface and are functionalized predominantly.[40] To minimize the grafting on the external surface, it is necessary to passivate the silanol groups on the external surface before functionalizing those on the internal surface. Shephard et al. have carried out the passivation of external surface with dichlorodiphenylsilane (Ph_2SiCl_2) first, and functionalization of internal surface with 3-aminopropyltrimethoxysilane [$(MeO)_3Si(CH_2)_3NH_2$] thereafter.[41] The existence of the amine functional groups almost entirely on the internal surface was confirmed by high resolution transmission electron microscopy (HRTEM). In a different approach, grafting of the external

surface by Me_3SiCl was carried out on the as-prepared mesoporous material without the surfactant being removed from the mesopores.[42] Grafting occurred mainly on the external surface due to steric constraint of the surfactant. After solvent extraction of the surfactant the internal surface was functionalized with the desired organic group. An alternate pathway by *Antochshuk and Jaroniec* describes simultaneous grafting of Me_3SiCl and extraction of surfactant template, by refluxing as-synthesized MCM-41 material with neat Me_3SiCl.[43] Since the calcination step is not required in these two processes, larger numbers of surface silanol groups are likely to be present inside the mesopores.

1.4.2. Co-condensation Reactions

In the grafting methods, incorporation of organic groups is done by attachment of the organosiloxane precursor with surface Si atoms through Si-O-Si-C covalent bond formation. Then Si-O can be cleaved at some reaction conditions as experienced by *Price et al.*[25] Therefore, in some cases it would be desirable to have, direct formation of a C-Si (surface) covalent bond. Thus, the "one-pot" co-condensation method, where condensation occurs between a tetra alkoxysilane and one or more trialkoxy organosilanes through sol-gel chemistry, seems to have distinct advantages over the grafting methods (**Scheme 1.6**).[44]

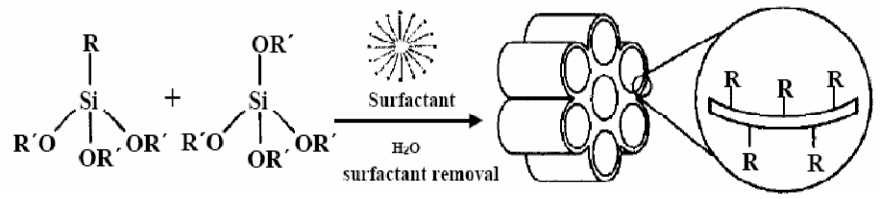

Scheme 1.6. Synthesis of organo-functionalized mesoporous silicates by co-condensation (ref. 22).

Several research groups have employed this method to prepare inorganic–organic hybrid mesoporous materials under a wide range of synthesis conditions.[45]

1.5. CLICK CHEMISTRY

In 2001 *Sharpless* and co-workers coined the prototypical concept of click chemistry.[46] Click chemistry enables a modular approach to generate novel products by utilizing a collection of reliable chemical reactions.[46] Those reactions thus give products stereo-selectively in high yields, produce inoffensive by-products, are insensitive to oxygen and water, utilize readily available starting materials and have a thermodynamic driving force of atleast 20 kcal mol^{-1}. *Sharpless* and co-workers classified following reactions under click chemistry category: 1) cycloaddition reactions of unsaturated species, such as 1, 3-dipolar cycloaddition reactions, and hetero Diels -Alder reactions; 2) nucleophilic substitution chemistry, particularly ring-opening reactions of strained heterocyclic systems such as epoxides, aziridines, aziridinium ions, and episulfonium ions; 3) carbonyl chemistry of the "non-aldol" type; such as formation of ureas, thioureas, aromatic heterocycles, oxime ethers, hydrazones, and amides and 5) additions to carbon-carbon multiple bonds, especially oxidative reactions such as epoxidation, dihydroxylation, aziridination, and sulfenyl halide addition, but also Michael additions of Nu-H reactants.[46] Recently, addition of thiols to alkenes (also called as thiol-ene coupling, TEC) has also been classified as click chemistry reaction.[47] Of all the click reaction reported so far, the most widely studied and used is *Huisgen* [3 + 2] cycloaddition between a terminal alkyne and an azide to yield substituted 1,2,3-triazoles.[48] This reaction has been termed the "cream of the crop" of "**click reactions**"[46] and has found application in various fields of research as diverse as organic synthesis, polymer and material science, drug discovery, medicinal chemistry, bioconjugation, dendrimers, molecular biology, and biotechnology **(Scheme 1.7)**.[49] The great success of this reaction as a ligation tool relies on the efficiency and selectivity (regio- and chemo-), the ready occurrence of the process under aerobic conditions, and compatibility with a broad repertoire of functional groups. The formation of a robust linker such as the 1,4- disubstituted 1,2,3-triazole ring which displays biological and pharmacological activities[49a] of its own, is an added advantage of the synthetic utility of the CuAAC reaction in the discovery of novel covalent immobilization.

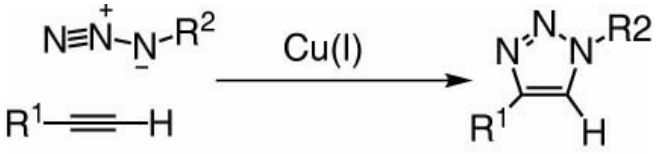

Scheme 1.7. CuAAC reaction between an alkyl azide and alkyne.

Although many methods have been developed for the heterogenization of homogeneous catalysts[50], they mainly use inorganic materials, dendrimers[51] and organic polymers as supports.[52] Further, it has been well accepted that covalent immobilization of metal complexes to the solid support offers high catalytic efficiency and better recycling without having the inherent problems of leaching of complex/ligand during the reaction. The area of organic chemistry that has gained precedence in recent years is the "**click**" reaction chemistry.[47] This broad area of organic synthesis incorporates any reaction that has high atom efficiency, low by-product levels, and high yields. The ultimate "**click**" reaction is defined by a complete conversion of all starting materials, no side-product formation, and relatively mild reaction conditions. The most widely used reaction under the "**click**" heading is the copper- (I)-catalyzed *Huisgens* 1, 3-dipolar cycloaddition reaction between an alkyne and an azide, yielding a single isomer of a 1, 2, 3-triazole, the 1, 4-isomer.[53] Recent work has shown the application of "click" chemistry for the tethering of molecules to both organic and inorganic polymeric supports.[54,55] In recent years, azide-alkyne [3+2] cycloaddition "**click reaction**" owing to its simplicity in use, mild reaction conditions and high conversion has proven to be one of the most powerful tools for the covalent attachment between appropriately functionalized molecules or their ligation to solid supports *via* a 1, 2, 3-triazole linkage.

Furthermore, the copper catalysed "**click reaction**" demonstrate high regioselectivity to give the 1, 4-linked triazoles in excellent yields. Even though substituted 1, 2, 3-triazoles should be good candidates for acting as ligands in coordination chemistry, their use as ligands has been much less explored in comparison to their 1, 2, 4-counterparts. There have been some recent reports on the use of such ligands as "analogues of terpyridine and bipyridine".[56] Copper complexes

have been reported with potentially tetradentate 1, 2, 3-triazole ligands where the question of the mechanism of the click reaction was also addressed.[57] Triazole ligands have been known for a long time, and their coordination has been investigated with a variety of transition metals.[58] These highlighted advantages have considerably renewed the interest in 1, 2, 3-triazolyl derivatives. Little use has been made in inorganic chemistry, however, although the di-substituted 1, 2, 3-triazole ligands formed in this "**click reaction**" can also coordinate transition metals. The click method provides an extremely convenient route for the synthesis of (2-pyridyl)-substituted 1, 2, 3-triazoles which could potentially be used as "2, 2-bipyridine analogues".[59] In comparison to 2, 2-bipyridine it is relatively easy to vary the steric and electronic properties of such triazole ligands.

1.6. PERIODIC MESOPOROUS ORGANOSILICAS (PMO): ORGANIC-INORGANIC HYBRIDS WITH ORGANIC MOIETY IN THE FRAMEWORK

The diverse applications of periodic mesoporous silica and organic-inorganic hybrid mesoporous materials have stimulated the search for materials with new structures and framework compositions. The combination of organic and inorganic fragments inside the structure of porous materials that are self-assembled into architectures with dimensions spanning multiple length scales can give rise to new materials preserving the unique characteristic of both organic and inorganic materials.[60] Thus an alternative strategy in the synthesis of organic-inorganic hybrid mesoporous materials is to replace one or more of the siloxane links with organic groups.[61] Since the organic groups integrated inside the channel walls is the carrier of the desired property, it finds interesting to tailor the properties of these materials by the replacement of the bridging oxygen group by bridging organic groups in the wall channels. The organic component is capable of modifying the properties of bulk material and using these approach new materials with interesting morphologies can be developed according to the nature of the organic groups in the silicate network.[62]

Inagaki et al. have first reported the synthesis of "periodic mesoporous organosilica" (PMO) with organic functional groups uniformly incorporated in the mesoporous walls, using 1, 2-bis(triethoxysilyl)ethane as the framework precursor

and octadecyl trimethylammonium chloride[61a] as the surfactant. *Asefa et al*. and *Melde et al.* have also described the co-condensation of either 1, 2-bis(triethoxysilyl)ethane or 1,2- bis(triethoxysilyl) ethylene with silica precursors to synthesize hexagonal hybrid framework materials, under basic reaction conditions.[61b,c] *Melde et al.* designated their materials as 'unified organically functionalized mesoporous networks' (UOFMN), having worm-like channel systems and lacking long-range ordering. Thus the co-condensation of silsesquioxane precursors of the type, $(R'O)_3Si$-R-$Si(OR')_3$, where R = $-(CH_2)_x-$, $-C_6H_4-$, -CH=CH-, etc, and their self assembly over an organized surfactant species can create organic-inorganic hybrid materials having long-range ordering and organic moiety as component of the solid network **(Scheme 1.8)**.[63] These materials are unique compared to the first generation periodic mesoporous silica materials (PMS), since unlike MCM-41, the bridging organics inside the channel wall of periodic mesoporous organosilicas offer a diversity of function and potential uses. Moreover, organic groups like ethylene, phenyl and biphenyl in the framework exhibits crystalline wall channels and thus the discovery of periodic mesoporous organosilicas is considered as a major breakthrough in the field

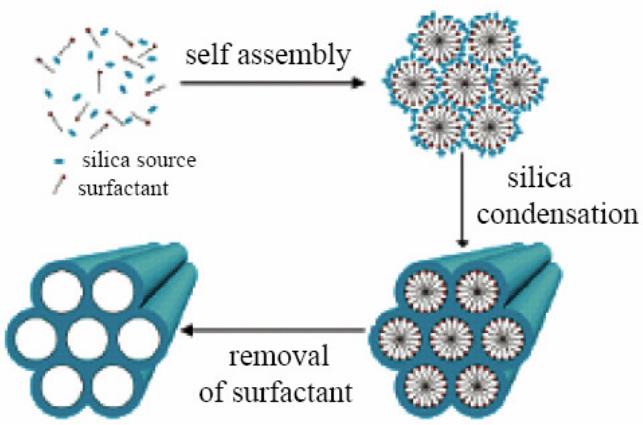

Scheme 1.8. Synthesis of organic-inorganic hybrid mesoporous materials having organic groups in the frame wall positions. Silica source: Bridged Silsesquioxanes, $(R'O)_3Si$-R-$Si(OR')_3$, where R = $-(CH_2)x-$, $-C_6H_4-$, -CH=CH-.

of materials science.[64] The crystal-like ordering of the wall structures is thought to form through self-organization of the precursor molecules as a result of hydrophobic hydrophilic interaction of hydrolyzed $(OH)_3Si\text{-}R\text{-}Si(OH)_3$ species or π-π interactions of aromatic groups. Now, a wide range of synthetic routes to mesoporous organosilicas with different mesophases and morphologies has been reported including the use of cationic, neutral and non-ionic surfactants and surfactant mixtures under basic, acidic and neutral conditions.[65]

Compared to the conventional organic-functionalized heterogeneous mesoporous materials, where the organic groups are '*dangling'* inside the pores of the hybrid mesoporous materials, the periodic mesoporous organosilica materials exhibit quite different pore wall structure and surface properties.[66] Although the conventional grafting of organic functional groups on the inorganic framework offers the advantage of introducing catalysis and adsorption properties, the inactivation of catalytic sites on the inorganic framework through coverage with organic groups as well as the accompanied decrease in porosity of the material highlights the relevance of PMO materials. Other important advantages of the PMO materials than the conventional organic-inorganic hybrid mesoporous materials are due to: (i) organic moieties in PMO are homogeneously dispersed inside the wall channels with a maximum loading of 100 %, which are not achievable with the organic pendant groups grafted, (ii) bridging organics inside the channel walls do not block the pores, (iii) the soft organic groups integrated within the channel walls impart interesting physical and mechanical properties of the host and (iv) the organic groups integrated inside the channel walls can be varied to produce a wide range of materials with potentially interesting characteristics.[67]

The union of the two main branches of chemistry *viz.,* the inorganic chemistry and organic chemistry there by allows the preparation of a myriad of new nano-composites in which the organic groups can be integrated into an inorganic material. The organosilane compound with two or more alkoxy groups can make stable framework because the alkoxy groups at the both sides of the silsesquioxane precursor will condense to form a three dimensional stable network containing organic groups in the framework with a better periodic arrangement under surfactant templating

conditions. These are the first type of mesoporous materials whose framework has a completely uniform distribution of organic groups integrated within the inorganic framework at the molecular level and having a periodic pore arrangement. Further,

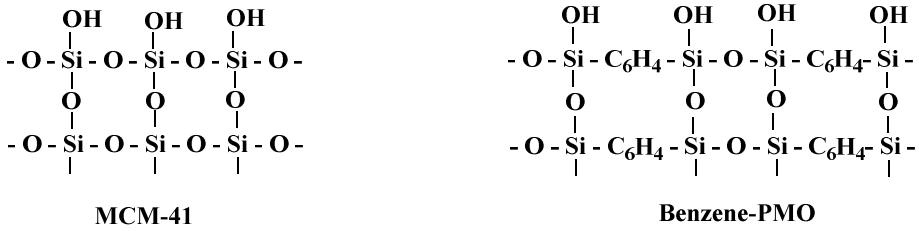

Scheme 1.9. Composition and surface characteristics of: (A) periodic mesoporous silica (PMS) and (B) organosilica (PMO) material having benzene bridges.

this is the first type of mesoporous materials having only T type [$Si(OH)R(OSi)_2$] silicons, without any Q type [$Si(OSi)_n(OH)_{4-n}$, n = 2-4] silicon species. However, similar to M41S materials, the hybrid mesoporous materials also posses residual silanol sites, as T^2 type silicon species.[68] The peak intensity ratio of the T^2/T^3 signals of the PMO is almost similar to the Q^3/Q^4 sites, which indicates that the hybrid materials posses similar silanol density as of M41S materials. Further adsorption isotherm of water vapour showed that the hybrid materials has more hydrophobic surface than siliceous MCM-41, which suggests that the organic fragments are exposed on the surface and thereby increase the surface hydrophobicity (**Scheme 1.9**).[69] Thus it is ideal to mention that this new approach extends the realm of mesoporous materials to ***'chemistry of the channel walls'*** rather than limiting it to the ***'chemistry of the void space'.***[70]

1.7. MESOPOROUS SILICA AS SUPPORT OR HOST FOR THE HETEROGENIZATION OF HOMOGENEOUS CATALYSTS

Materials with well-defined pores belong to the most interesting class of compounds, because they can be converted into organic-inorganic hybrid

nanocomposites by various surface modifications. The microporous and organized mesoporous materials obtained after the hydrothermal synthesis are in fact a nonporous organic-inorganic hybrid since the organic structure director (template or surfactant) is usually trapped in the cavities of the solid. Hence, to obtain completely porous solid and to introduce reactive organic functional groups inside the channels of ordered materials, it is necessary to remove the entrapped organic species from the as-made samples. The commonly employed method for the removal of surfactant consist of calcining the materials, in a flow of air, typically >400 ^{o}C. However, the high-cost template reactant is destroyed and such treatments further cause damage to the porous materials, since during calcination high local temperature and water formation may occur, and therefore extra framework sites may be formed.[71] An alternative method involves the removal of the template by mild treatments such as liquid extraction using acidic solutions, alcohols or a mixture of both.[72] This method is especially effective for mesoporous materials where the framework-surfactant interactions are weak (electrostatic, vander-Waals or hydrogen bonding interactions) and because of the larger pore sizes. An added advantage of this method is that under acidic extraction conditions, exchange of sodium ions for protons is also achieved simultaneously with the removal of surfactants. Moreover, the mild routes for the removal of templates help in the reuse of the organic templates for a subsequent synthesis with similar textual properties.[73] The materials obtained after the removal of surfactant groups contains ordered pore channels with abundant silanol sites. These mesoporous hosts can be utilized for the synthesis of organic-inorganic hybrid mesoporous materials having reactive functional groups and have stimulated fundamental research interests in the inclusion of metals and metal complexes inside the mesoporous channels.[74,75]

During the last few years, organic-inorganic hybrid mesoporous materials constitutes an emerging area in the field of materials science and had shown its impact in a wide range of heterogeneous catalysis reactions.[76] However, the main problem encountered in heterogenized catalysts is that the bonds between metal and ligand are often broken and reformed during catalytic reactions, leading to leaching of the metal from the catalyst in the product, thus decreasing the reaction rate and activity.[77] Hence

the nature of interaction between the homogenous catalysts and the support surface decides the overall stability and reusability of the heterogenized catalysts and in general, if the anchoring is covalent, it can be robust enough to withstand the harsh conditions of the catalytic reactions. The most common immobilization techniques used for this purpose include grafting or tethering, physical entrapment, ship-in-a-bottle synthesis and supported liquid phase catalysis.[78] Earlier, the supports used to tether the homogeneous catalyst are the organic polymers, which are soluble in the reaction media. The advantage of this support is that the active sites are distributed throughout the reaction solution and hence the catalyst architecture is similar to that of the homogeneous catalyst that it is trying to mimic.[79] Insoluble supports are preferable than the homogeneous supports because of several reasons *i.e*., they are readily recovered, they have potential applications in flow process and they do not need extra solvents for precipitation. Insoluble organic polymers are effective supports, but the polymer had to be carefully chosen and tuned so as to avoid swelling and to ensure that the homogeneous complex catalyst is tightly bound with the support not merely occluded inside. In contrast to the insoluble organic polymers, inorganic silica materials like amorphous silica gels or mesoporous silicas did not swell or dissolve in organic solvents. However, because of the lack of ordered pore channels, amorphous silica gels are unable to provide the size/shape specificity properties.

Hence the immobilization of various homogeneous metal catalysts over solid organic-inorganic hybrid mesoporous supports as a mean of 'heterogenization' has particular significance. Heterogenization of useful homogenous catalysts or active centers will improve the overall efficiency of the catalytic process due to: (i) it is easier to separate the catalyst from the liquid by simple filtration, where the homogenous catalysts often leads to complicated and laborious extraction or distillation requirements, (ii) often the catalysts can be regenerated and recycled, (iii) confinement of the catalyst in the mesopores provides a means of introducing the size/shape selectivity and thus a greater specificity to a desired reaction. Moreover, if the functional groups or the catalytic active site was attached firmly to the solid support, the leaching problem greatly reduced.

1.8. PHYSICOCHEMICAL CHARACTERIZATION

Understanding the structural and electronic properties of the catalyst by spectroscopic techniques is one of the major goals in catalysis research. In catalytic research, a number of techniques will be used to characterize a sample and a summation of all characterization techniques will reveal the active sites in a catalyst and these in turn will helps in the design of a new catalyst or to improve the catalytic performances. The commonly used characterization techniques, their principles, advantages and limitations are briefly described in this section.

1.8.1. X-Ray Diffraction (XRD)

XRD has been applied as the most important tool to determine the structure of the materials characterized by long-range ordering, to identify bulk phases, to monitor the kinetics of bulk transformations and to estimate particle sizes.[80,81] The XRD method involves the interaction between the incident monochromatized X-rays (like *Cu Kα or MoKα* source) with the atoms of a periodic lattice. X-rays scattered by atoms in an ordered lattice interfere constructively in directions given by Bragg's law*:* $n\lambda = 2d \sin\theta$, where, λ is the wavelength of the X-rays, d is the distance between two lattice planes, θ is the angle between the incoming X-rays and the normal to the reflecting lattice plane and n is an integer known as the order of reflection.[82] Bragg peaks are measured by observing the intensity of the scattered radiation as a function of scattering angle 2θ. The angles of maximum intensity enable one to calculate the spacing between the lattice planes and allow phase identifications while the width of diffraction peaks carries information on the dimensions of the reflecting planes. The width of the diffraction lines can be further used to estimate the crystal size by the Debye-Scherrer formula: $Dhkl = k\lambda/\beta\cos\theta$, where *Dhkl*, λ, β and θ are the volume averaged particle diameter, X-ray wavelength, full width at half maximum (FWHM) and diffraction angle, respectively, and *k* is a constant, often taken as 1.[82]

Isomorphous substitution of heteroatoms in the framework of molecular sieves can be calculated from the changes in the unit cell parameters and unit cell volume. Unit cell parameter (a_o) of a hexagonal lattice can be calculated from, $a_o = 2d_{100}/\sqrt{3}$ and a cubic lattice can be determined by the following equation: $a_o = d_{211}\sqrt{6}$. The unit

cell dimension determined by XRD is also used to calculate the frame wall thickness (FWT) of the channels of the mesoporous materials. A major limitation of XRD is that this technique requires samples, which possess sufficient long-range order. Amorphous phases and small particles give either broad or weak diffraction lines or no diffraction at all, which makes them virtually invisible for XRD.

1.8.2. Adsorption Isotherm and BET Method

1.8.2.1. Brunauer-Emmett-Teller (BET).

Despite of some theoretical limitations, the Brunauer-Emmett-Teller (BET) method continues to be the most widely used method for the evaluation of surface area, pore volumes and pore size distributions of porous solids from N_2 physisorption isotherm data. The BET equation can be represented as follows,

$$\frac{p}{v(p_0 - p)} = \frac{1}{v_m c} + \frac{c-1}{v_m c}\frac{p}{p_0}$$

where v = volume of N_2 adsorbed by the sample under pressure p, p_0 = saturated vapor pressure at the same temperature, v_m = volume of N_2 adsorbed when the surface is covered with a uni-molecular layer, and c = constant for a given adsorbate.[83] The equation suggests that the plot of $p/v(p_0–p)$ versus p/p_0 should be linear, and from the intercept $1/V_mC$ and slope $C–1/V_mC$ the values of v_m and C can be determined as follows: $v_m = (\text{slope} + \text{intercept})^{-1}$.

$$S = \frac{N_0 v_m A}{22414m}$$

Thus the specific surface area (S) of a sample can be determined as follows, where N_0 = Avogadro number, m = amount of solid adsorbent, A = cross-section of the gas molecules (16.2 $Å^2$ for N_2), and S is expressed in $cm^2\ g^{-1}$ unit.

Several computational procedures are available for the derivation of pore size distribution of mesoporous samples from physio-sorption isotherms. Most popular

among them is the *Barrett-Joyner-Halenda (BJH) model*, which is based on speculative emptying of the pores by a stepwise reduction of p/p_0, and allowance being made for the contraction of the multilayer in those pores already emptied by the condensate.[84] The mesopores size distribution is usually expressed as a plot of $\Delta Vp/\Delta rp$ versus rp, where Vp = mesopore volume, and rp = pore radius. It is assumed that the mesopores volume is completely filled at high p/p_0. N_2 adsorption-desorption was conducted by NOVA 1200 (Quantachrome) at –196 °C. For this particular measurement, before analysis the samples were oven-dried at 100 °C and evacuated at 180 °C for 3 h under vacuum and then the adsorption-desorption was conducted by passing nitrogen into the sample, which was kept under liquid nitrogen.

1.8.2.2. The t- and β Plots

The *t*-plot analysis, a plot of the amount adsorbed versus the thickness of the adsorbed gas on the walls of the pores, is mostly applied to differentiate between the adsorption mechanisms in micropores, mesopores and macropores. Lippens and de Boer showed that if the multimolecular layer of adsorbed nitrogen could be formed freely on the surface, the statistical thickness, t (in nm) of the adsorbed layer could be calculated according to the equation.

$$t = 0.3538(V_a/V_m) = f_1(p/p_0)$$

If the adsorption data are presented in the form of a *t*-plot, two linear regions are obtained. The first linear region represents both micropore filling and surface coverage of larger pores. The second linear region gives the layer-by layer adsorption taking place in meso and macropores but not in micropores. The y-axis intercept multiplied by the ratio of the gas and liquid densities of the adsorbate (0.00156 for nitrogen) will provide the micropore volume in cc per gram of the solid. The slope of the second linear region gives the surface area provided by pores with radii larger than 10 Å, *i.e.,* the mesopore area. The first linear region extrapolates to the origin and the slope of this line gives the value of the total surface area of the material provided by all pores. Usually this number agrees with the BET surface area within 10-15 %.

Micropore volume can also be observed from the β plot also where Three different regions can be seen on these plots: (i) a linear region due to multilayer adsorption in mesopores; (ii) a steep region due to capillary condensation within these mesopores; and (iii) a last linear region due to multilayer formation onto the external surface of

$$\beta - \left[\ln(0.4) / \ln(p/p_0) \right]^{1/2.7}$$

the grains. Micropore and mesopore volumes can be obtained by the intercept between the adsorbed amount (y-axis) and the linear segments (i) and (iii). These two extrapolations give V_{micro} and (V_{micro} + V_{meso}) respectively. The β plots of SBA-15 yield non-zero V_{micro} values, thus indicating the presence of micropores.

1.8.2.3. Pore Volume and Pore Size Distribution

The total pore volume is derived from the amount of vapour adsorbed at relative pressure close to unity assuming that all the pores are filled with condensed absorptive in normal liquid state. Pore size distribution is the distribution of pore volume with respect to pore size. The computation of pore size distribution involves a number of assumptions (pore shape, mechanism of pore filling, validity of Kelvin equation etc). It is generally accepted that desorption isotherm is more appropriate than adsorption isotherm for evaluating the pore size distribution of the adsorbent. The mesopore size calculations are made assuming cylindrical pore geometry using Kelvin equation in the form:

$$r_k = \frac{-2\gamma V_m}{RT \ln(p/p_0)}$$

Where γ= surface tension of nitrogen at its boiling point, V_m = Molar volume of liquid nitrogen, R= gas constant, T= boiling point of liquid nitrogen, p/p_0 = relative pressure of nitrogen, r_k = the Kelvin radius of the pore. If the radius of cylindrical pore is r_p and correction is made for the thickness of a layer already adsorbed on the pore walls, i.e.

the multilayer thickness, t, then,

$$r_p = r_k + t$$

Several computational procedures are available for the derivation of pore size distribution of mesoporous samples from physiosorption isotherms. Among the classical macroscopic theories, most popular is the Barrett-Joyner-Halenda (BJH) model, which is based on speculative emptying of the pores by a stepwise reduction of p/p_0, and allowance being made for the contraction of the multilayer in those parts already emptied by the condensate.[84b] The mesopore size is usually expressed as a plot of $\Delta vp/\Delta rp$ versus rp, where vp = mesopore volume, and rp = pore radius. It is assumed that the mesopore volume is completely filled at high p/p_0. But classical macroscopic, theories like DR, BJH, HK etc. do not give a realistic description of the filling of micropores and even narrow mesopores. This leads to an underestimation of pore sizes. Microscopic theories like Non Local Density Functional Theory (NLDFT)[85] consider the sorption and phase behaviour of fluids in narrow pores on a molecular level. The NLDFT correctly describes the local fluid structure near curved solid walls; adsorption isotherms in the model pores are determined based on the intermolecular potentials of the fluid-fluid and solid-fluid interactions. The relation between isotherms determined by these microscopic approaches and experimental isotherm of a porous solid can be interpreted in terms of a Generalized Adsorption Isotherm (GAI) equation. The pore size distribution is then derived by solving the GAI equation numerically via a fast non-negative least square algorithm.

1.8.3. Chemical Composition by CHN-S Analysis

Analysis of the organic content, carbon Nitrogen and sulphur present in the catalysts was estimated using a *Carlo-Erba CHN analyzer* (EA1108 Elemental Analyzer).

1.8.4. Fourier Transforms Infrared Spectroscopy

Fourier transforms infrared (FT-IR) spectroscopy deals with the vibration of chemical bonds in a molecule at various frequencies depending on the elements and types of bonds. After absorbing the electromagnetic radiation the frequency of vibration of a bond increases leading to transition between ground state and several excited states. The energy corresponding to these transitions corresponds to the infrared region (4000–400 cm^{-1}) of the electromagnetic spectrum. The term Fourier transform (FT) refers to a recent development in the manner in which the data are collected and converted from an interference pattern to an infrared absorption spectrum that is like a molecular "fingerprint".[86] In case of SBA-15, stretching vibrations observed in the range of 3600–3400 cm^{-1} region are attributed to the hydrogen-bonded silanol groups and the band observed near 797 cm^{-1} and 1076 cm^{-1} are due to the symmetric and asymmetric vibrations of the Si–O–Si group, respectively. In this study, all the synthesized catalysts FT-IR spectra were obtained in a range of 400 to 4000 cm^{-1} on a Shimadzu FTIR 8201PC using a Diffuse Reflectance scanning disc technique.

1.8.5. Cross-Polarization Magic Angle Spinning NMR Spectroscopy

Nuclear magnetic resonance (NMR) spectroscopy is one of the most powerful tools to investigate structure and dynamics of a molecular system in liquid phase. Atomic nuclei consisting of odd number of protons and/or neutrons possessing a nuclear spin $I \neq 0$ and consequently a magnetic moment $\mu = \gamma hI$ (γ = gyromagnetic ratio), when placed in a magnetic field of strength B_0, Zeeman interaction results in quantized orientations of the nuclear magnetic moments. The nucleus can adopt $2I+1$ Eigen states with energies $E(m) = -m\gamma hB_0$, where m = (I, I–1,…., –I). Transitions between neighbouring energy states ($\Delta m = \pm 1$) can be induced by electromagnetic radiation (energy $E = h\nu$) of frequency

$$\nu_0 = \gamma B_0/2\pi.$$

The chemical shift interaction arises from secondary local magnetic fields induced by the interaction of the electrons surrounding the nucleus. The induced local field opposes B_0 and hence shields the nucleus under observation. The shielding is spatially anisotropic due to the non-spherical electron distribution around the nucleus.[87] With the advent of sophisticated solid-state NMR techniques, it has become possible to obtain NMR spectra of solids with spectral resolution comparable to that of liquids.[88] Modern high-resolution solid-state NMR spectroscopy allows to elucidate the chemical and structural environment of several atoms (*e.g.* ^{13}C, ^{27}Al, ^{29}Si, ^{31}P, ^{51}V *etc*.) in a solid matrix like that of porous materials.[89] The most popular technique to get high-resolution NMR spectra with narrow line width is the magic angle spinning (MAS), where the solid sample is fast rotated about an axis inclined at a "magic" angle $\theta = 54°44'$ to the direction of B_0.[90]

Cross-polarization (CP) technique does not affect the line width of the spectra, but is applied to improve the sensitivity, i.e., the signal to noise ratio (SNR) of the spectra of nuclei with low natural abundance (e.g. ^{13}C, ^{29}Si, ^{31}P etc.), and to monitor the spatial proximity of nuclei.[91] CP involves indirect excitation of the less abundant nucleus through magnetization transfer from an abundant spin system (*e.g.* ^{1}H). Bruker DRX–500 and DSX–300 NMR spectrometers were used. The resonance frequencies of ^{29}Si and ^{13}C were 59.6 and 75.5 MHz, respectively. The chemical shifts were determined using tetraethyl orthosilicate (δ = 82.4 ppm from TMS) and adamantine (δ = 28.7 ppm from TMS) as the reference compounds for ^{29}Si and ^{13}C, respectively.

1.8.6. UV-Visible Spectroscopy

UV-Vis spectroscopy deals with the study of electronic transitions between orbital or bands of atoms, ions or molecules in gaseous, liquid and solid state. In the case of transition metal ions or atoms, any change in their coordination sphere may affect their optical properties and therefore can be characterized by UV-Vis.[92] For solid substances like transition metal containing mesoporous materials, diffuse reflectance UV-Vis spectroscopy (DRUV-Vis) is applied to determine the ligand field symmetry and oxidation state of the metal inside the solid matrices. Thus DRUV-Vis

is a sensitive probe to examine the type of the sites, framework or extra-framework in which that metal ion or cluster exist.[93] For a vast period of time metallic nano-particles have fascinated researchers due to their colourful colloidal solutions.[94]

Mie explained the origin of this colour theoretically by solving Maxwell's equation for the absorption and scattering of electromagnetic radiation by small metallic particles.[95] This absorption of electromagnetic radiation by metallic nanoparticles originates from the coherent oscillation of the valence band electrons induced by an interaction with the electromagnetic field. These resonances are known as surface plasmons, which occur only in the case of nanoparticles and not in the case of bulk metallic particles.[96] Hence, DRUV-Vis can be utilized to study the unique optical properties of the hybrid mesoporous materials containing occluded metallic nanoparticles, exploiting the size and shape dependent surface Plasmon resonance.[97]

1.8.7. X-Ray Photoelectron Spectroscopy

XPS is based on the photoelectric effect. Routinely used X-ray sources are MgKα ($h\nu$ = 1253.6 eV) and AlKα ($h\nu$ = 1486.3 eV). In XPS one measures the intensity of photoelectrons N(E) as a function of their kinetic energy E_k. Because a set of binding energies is characteristic for an element, XPS can be used to analyze the composition of samples. Binding energies are not only element specific but contain chemical information as well; the energy levels of core electrons depend on the chemical state of the atom. Photoelectron peaks are labeled according to the quantum numbers of the level from which the electron originates. An electron coming from an orbital with main quantum number n, orbital quantum number l (0, 1, 2, 3,.. indicated as s, p, d, f,..) and spin quantum number s(+1/2 or –1/2) is indicated as nl_{l+s}. Almost all photoelectrons used in the laboratory XPS have kinetic energy in the range of 0.2 to 1.5 keV, and probe the outer layer of the catalyst.

X-ray photoelectron spectra (XPS) were obtained using a VG Microtech Multilab-ESCA-3000 spectrometer equipped with a twin anode of Al and Mg. All the measurements are made on as received powder samples using *Mg Kα* X-ray at room temperature. Base pressure in the analysis chamber was 4×10^{-10} Torr. Multichannel detection system with nine channels is employed to collect the data. The overall

energy resolution of the instrument is better than 0.7 eV, determined from the full width at half maximum of 4f 7/2 core level of gold surface. The errors in all BE (binding energy) values were within ±0.1 eV.

1.8.8. Atomic Absorption and Emission Spectrometry

The principle of atomic absorption is based on energy absorbed during transitions between electronic energy levels of an atom. When some sort of energy is provided to an atom in ground state by a source such as a flame (temperature ranging from 2100–2800 °C), outer-shell electrons are promoted to a higher energy excited state. The radiation absorbed as a result of this transition between electronic levels can be used for quantitative analysis of metals and metalloids present in solid matrices, which have to be dissolved by appropriate solvents before analysis. The basis of quantitative analysis depends on measurement of radiation intensity and the assumption that radiation absorbed is proportional to atomic concentration.[98] Analogy of relative intensity values for reference standards is used to determine elemental concentrations. Atomic emission spectrometry (AES) is similar to atomic absorption spectrometry (AAS). In both the cases the sample must be atomized in order to obtain usable absorption spectra. However, in contrast to AAS, in AES the sample is heated at a very high temperature (8000–10000 °C), where the atoms in the sample are excited to higher energy levels. When the excited atoms are relaxed and fall back to the ground energy level, radiations are emitted. Measurement of the intensities of the emission forms the basis of quantitative determination.[99] Here, all the synthesized catalysts were studied by Varian Spectra AA220.

1.8.9. Scanning Electron Microscopy

Scanning electron microscopy (SEM) is an important tool for morphological characterization of mesoporous molecular sieve materials. A scanning electron microscope can generate an electron beam scanning back and forth over a solid sample. The interaction between the beam and the sample produces different types of signals providing detailed information about the surface structure and morphology of the sample. When an electron from the beam encounters a nucleus in the sample, the

resultant coulombic attraction leads to a deflection in the electron's path, known as Rutherford elastic scattering. A fraction of these electrons will be completely backscattered, reemerging from the incident surface of the sample. Since the scattering angle depends on the atomic number of the nucleus, the primary electrons arriving at a given detector position can be used to produce images containing topological and compositional information.[100]

The high-energy incident electrons can also interact with the loosely bound conduction band electrons in the sample. However, the amount of energy given to these secondary electrons as a result of the interactions is small, and so they have a very limited range in the sample. Hence, only those secondary electrons that are produced within a very short distance from the surface are able to escape from the sample. As a result, high resolution topographical images can be obtained in this detection mode.[101] Here, all the synthesized catalysts were studied by JEOL-JSM-5200 scanning microscopy.

1.8.10. Transmission Electron Microscopy

Transmission electron microscopy (TEM) is typically used for high resolution imaging of thin films of a solid sample for micro-structural and compositional analysis. The technique involves: (i) irradiation of a very thin sample by a high-energy electron beam, which is diffracted by the lattices of a crystalline or semi crystalline material and propagated along different directions, (ii) imaging and angular distribution analysis of the forward-scattered electrons (unlike SEM where backscattered electrons are detected), and (iii) energy analysis of the emitted X-rays.[102] The topographic information obtained by TEM in the vicinity of atomic resolution can be utilized for structural characterization and identification of various phases of mesoporous materials, *viz.*, hexagonal, cubic or lamellar.[103] TEM also provides real space image on the atomic distribution in the bulk and surface of a nanocrystal. A JEOL JEM-1200EX instrument with 120 kV of acceleration voltage was used to probe the materials.

1.8.11. Thermal Analyses

The thermo analytical techniques, *viz*., thermo gravimetric analysis (TGA) and differential thermal analysis (DTA) have been widely used to establish the thermal stability of ordered mesoporous silica. Both TGA and DTA provide important information about the following: (i) temperature programmed desorption (TPD) and removal of physisorbed water below 150 °C, (ii) oxidative decomposition of the occluded organic materials, accompanied by one or several exotherms within 150 °C and 600 °C, and (iii) dehydroxylation occurring from condensation of adjacent silanol groups to form siloxane bonds at or above 600 °C.[104] Further, DTA can also detect any phase transitions if occur. Thermal analysis of all the samples were carried out by Mettler Toledo 851^{e} using an alumina pan under a nitrogen (80 ml/min) atmosphere from ambient to 1000 °C with the increasing rate of 20 K/min.

1.9. ANALYSIS OF PRODUCTS

1.9.1. Gas Chromatography

Gas chromatography-specifically gas-liquid chromatography involves a sample being vaporized and injected onto the head of the chromatographic column. The sample is transported through the column by the flow of inert, gaseous mobile phase. The column itself contains a liquid stationary phase which is adsorbed onto the surface of an inert solid. The carrier gas must be chemically inert. Commonly used gases are Nitrogen, Helium, Argon and Carbon-dioxide. For optimum column efficiency, the sample should not be too large and should be introduced onto the column as a plug of vapor. Micro syringe is used to inject sample through a rubber septum into a flash vaporizer port at the head of the column. Two types of column are present Packed and Capillary columns. For precise work, column temperature must be controlled within tenths of a degree. Many detectors are used in Gas chromatography. Different detectors give different selectivity. Flame ionization detector (FID), Thermal conductivity detector, Electron Capture detector, Flame photometric detector, Photo ionization detector, Nitrogen-Phosphorous detector, Hall electrolytic conductivity. Flame ionization detector is a useful general detector for the analysis of organic compounds, has high sensitivity, large linear response range, low noise,

Robust, easy to use but destroys the sample.

1.9.2. Gas Chromatography/Mass Spectrometry (GC/MS)

GC/MS is a GC detector that is very expensive but very powerful version of the mass spectrometer. When coupled to a GC the detection system itself is often referred to as the mass selective detector or more simply the mass detector. This powerful analytical technique belongs to the class of hyphenated analytical instrumentation (since each part had a different beginning and can exist independently) and is called gas chromatography/mass spectrometry (GC/MS). The power of this technique lies in the production of mass spectra from each of the analytes detected instead of merely an electronic signal that varies with the amount of analyte. These data can be used to determine the identity as well as the quantity of unknown chromatographic components with an assuredness simple unavailable by other techniques. Major components of the GC/MS. Ionization source, Mass separator- (1) Quadrapole and (2) Ion trap, Ion detector.

1.9.3. Liquid State NMR

NMR (Nuclear Magnetic Resonance) spectra arise from the spinning of nucleus. It is widely used as one of the instrumental techniques available for structure analysis. Modern NMR spectroscopy is frequently divided into several categories;

- High resolution mode on homogenous solutions.
- High power mode on highly relaxing nuclei which exhibit very broad lines, or polymers etc.
- The study of solids using eg Magic angle spinning techniques.
- NMR 3D imaging to resolutions of ~ 1 mm.

The types of information accessible via high resolution NMR include;

- Functional group analysis (chemical shifts)
- Bonding connectivity and orientation (J coupling),
- Through space connectivity (Over Hauser effect)

- Molecular Conformations, DNA, peptide and enzyme sequence and structure.
- Chemical dynamics (Line shapes, relaxation phenomena).

The number of peaks in the low-resolution spectrum depends on the number of different environments that the hydrogen atoms have in the molecule. There are four aspects of an NMR spectrum that will allow us to determine the identity of the molecule.

- The number of NMR signals
- The position of each signal relative to a reference signal
- The relative area under each signal

1.10 CATALYTIC APPLICATIONS AND PROSPECTS

In recent years, environmental and economic considerations have raised strong interest to redesign commercially important process so that the use of harmful substances and the generation of toxic wastes can be avoided.

Through the development of hybrid organic-inorganic mesoporous solids, much progress has been made in the last few years towards the applications of mesoporous solids in various areas of heterogeneous catalysis. The concept of '*heterogenization'* of homogenous catalysts over organic-inorganic hybrid mesoporous materials possessing reactive functional sites provides the prospective for extending the benefits of heterogeneous catalysis to homogeneous systems. These benefits include easier separation of catalyst and reaction products leading to shorter work up times, improved process efficiency and better reuse of the supported catalysts. However, the prime requirement of the heterogenization approach is to maintain the stability of the heterogenized complex, such that it does not decompose or leach out from the solid support to the liquid phase during the course of reaction, and at the same time, it retains high activity and selectivity. Reactions that have been studied in this thesis using functionalized mesoporous solids include oxidations, hydrogenation and C-C coupling catalytic reactions that produce fine chemicals are discussed.

In this section, the catalytic applications and prospects of organo-modified mesoporous materials for various oxidation[105], hydrogenation[106] and C-C coupling[107] reactions are briefly reviewed.

1.10.1. Oxidation Reaction

The discovery of efficient method for catalytic epoxidation is an important goal in synthetic chemistry as there is a growing interest in using epoxides as a building block in organic synthesis. The first examples of liquid phase catalytic oxygen transfer dates back to 1936. The so-called Milas reagents were formed by reaction of transition metal oxides with a solution of H_2O_2 in tert-butanol resulting in soluble inorganic peracids.[108] These catalysts were used for the vicinal dihydroxylation of olefins but with certain metal oxides like MoO_3 or WO_3, selective epoxidation was observed. From these basics, a great deal of effort has been put into the development of transition metal based catalysts, as homogeneous and heterogeneous, for various selective oxidation reactions.[109]

In a catalytic epoxidation and oxidation reaction a wide variety of organic molecules, organic peroxides as well as hydrogen peroxide were used as single oxygen donors. Even though, organic peroxides are more active oxidants than hydrogen peroxide, they are more expensive and the active oxygen content is rather low. Moreover, usage of organic peroxides generates stoichiometric amount of corresponding alcohols, which in most cases complicates the separation process. Hence the preferred oxidant in most of the oxidation or epoxidation process is hydrogen peroxide, with respect to the active oxygen content (47 %) and the nature of byproduct formed *viz.,* water.[110] Immobilization of transition-metal complexes on solid supports can provide catalysts which are easier to handle and which may possibly exhibit improved selectivity and activities because of the support environment. Mn(III) Schiff-base complexes have become highly valuable catalysts in homogeneous alkene epoxidation reactions using readily available oxygen donors such as, H_2O_2 or TBHP. Over the past few decades researchers has focused on the development of a variety of homogeneous catalysts. The design and synthesis of ligands that, upon coordination with metal ion can induce high stereoselectivity for organic transformations and constitute an important issue in modern coordination chemistry.[111]

1.10.2. Hydrogenation Reaction

Liquid-phase hydrogenation of olefins using heterogeneous catalysts is an industrially relevant process. Along with olefin, hydrogenation of nitro compounds to amines has become one of the most important chemical reactions because organic amines are essential materials for the production of agrochemicals, dyes, pharmaceuticals, polymers and rubbers.[112] For more than 100 years chemists have used heterogeneous catalysts based on noble metals on various supports. Homogeneous hydrogenation catalysis was developed in the 1960's and is reviewed frequently.[113] It is well known that Pd-catalyzed reactions are of significant importance in modern chemical transformations. There is a growing demand for organo-metallic reagents that exhibit favorable chemo selectivity and stereo selectivity in hydrogenation reactions. Generally reaction proceeds using N-ligand based palladium catalysts. However, most of these ligands are expensive, which significantly limited to their industrial applications.[114] These new ligands are not easily available and contain tedious and expensive synthesis processes and hardly stable in catalytic systems. Therefore simple and easily accessible stable catalyst is desired for heterogeneous reactions.

1.10.3. C-C Coupling Reaction

Cross coupling reactions are one of broadest area for the synthesis of symmetrical and unsymmetrical binary compounds, which are the key components of the several natural products as well as in the field of engineering materials, such as conducting polymers, molecular wires and liquid crystals.[115] Palladium complexes with or without phosphine ligands can catalyze the C-C coupling reactions. The phosphine-assisted approach is the classical and well-established methods,[116] which gives excellent results in a majority of cases; whereas phosphine ligands are expensive, toxic, and unrecoverable and also a major drawback of the phosphine ligands in a catalytic reaction is the oxidation of phosphine to a phosphine oxide as well as cleavage of the P-C bond, causing degradation of the catalytic cycle. In large-scale industrial applications, the phosphines might be a more serious economical burden than even palladium itself, which can be recovered at any stage of production

or from wastes. Therefore, the development of phosphine-free catalysts for C-C bond-forming reactions would be an important topic of interest of the current industrial research.[117]

1.10.3.1. Heck C-C Coupling Reaction

Palladium catalyzed Mizoroki-Heck reaction of olefin and aryl halide is one of the most fundamental reactions for carbon-carbon bond formation in organic synthesis. Several reports have been published on Heck reaction for the synthesis of symmetrical and unsymmetrical binary compounds, which are the key components of the several natural products.[118] Among the basic types of palladium catalyzed transformation the C-C coupling reactions related chemistry occupied a special place in organic synthesis.

1.10.3.2. Suzuki C-C Coupling Reaction

Among the basic types of palladium catalyzed transformations, Suzuki reaction related chemistry occupied a special place.[119] The Suzuki cross-coupling reaction of organo-boron reagents with organic halides represents one of the most versatile and straightforward methods for carbon-carbon bond formation. The reaction is largely unaffected by water, tolerating a large range of functionality and yielding non-toxic by-products.

1.10.3.3. Sonogashira Coupling Reaction

The original Sonogashira reaction often required highly dry organic solvent, inert atmosphere, highly strong base, prolonged reaction time and phosphine containing catalyst. Generally a copper co-catalyst is needed in Sonogashira coupling reaction. However, the addition of copper, although beneficial in terms of increasing the reactivity of the system, added some shortcomings. The principal being the necessity of avoiding the presence of oxygen in order to block the undesirable formation of alkyne homocoupling through a copper mediated Hay/glasier reaction. The copper-acetylides formed in-situ could undergo oxidative dimerization to give diaryldiacetylenes when they are exposed to air or an oxidant (a reaction known as the

Glaser coupling). These by-products are generally difficult to separate from the desired products. Furthermore, the copper acetylide is a potential explosive reagent. To address such a problem, a solution was to eliminate the copper in the so-called ‘‘copper-free’’ Sonogashira reaction.[120] Furthermore, Sonogashira coupling of phenyl acetylenes and aryl halides is one example of palladium catalyzed reaction that allows connecting a C≡C triple bond substituent in an aromatic ring.

1.10.3.4. Stille Coupling Reaction

Palladium catalyzed cross-coupling reactions of aryl halides or halide equivalents with various nucleophiles have been shown to be highly effective and practical methods for the formation of C-C bonds. These coupling reactions make use of a variety of trans metalating agents such as organoboron, organomagnesium, organosilicon, organostannane and organozinc reagents.[121] Stille reaction involves coupling of an organotin compound with a sp^2-hybridized organic halide catalyzed by palladium. Stille reaction popularity is usually attributed to the stability in air and functional group tolerance of stannanes, as well as their chemo selectivity and broad scope in terms of reaction. This transformation has become a useful synthetic tool for carbon-carbon bond formation and can also be extended to numerous organic electrophiles.[122]

1.10.3.5. Kumada-Corriu-Tamao Coupling Reaction

In the class of C-C coupling reactions the organo magnesium compounds are generally more readily available than any alternative organometallic nucleophile. The improvement of the functional group tolerance of the Kumada-Corriu-Tamao coupling has become a very important and practical impact on the current scenario of metal-catalyzed C-C coupling reactions in organic synthesis.[123]

1.11. SCOPE AND OBJECTIVES OF THE THESIS

The principal aim of this thesis is to investigate the approach of heterogenization of various transition metals complex over solid mesoporous supports and organic-inorganic hybrid mesoporous materials for oxidation, hydrogenation and C-C coupling reactions, under different reaction conditions. During the last few years, the catalytic transformations of bulky molecules over various organo-modified supported metal complex mesoporous materials constitute an interesting research area in the field of fine chemical synthesis. Hence, the immobilization of different metal complex over the pore channels of different mesoporous materials had been systematically studied, characterized and also used as catalysts in various industrially relevant organic transformations. By keeping the above objectives in mind, the following specific work was selected for the present thesis:

The specific problems chosen are:

- Heterogenization method of the salen binaphthyl Schiff base ligand over organo-modified SBA-15. Determination of extent of the increased stability of the synthesized catalyst with regard to the homogeneous catalyst in the epoxidation and sulfoxidation reactions.
- Synthesis of Pd-EDTA complex and its immobilization over aminofunctionalized ($-NH_2$) organomodified SBA-15 phases, reaction condition optimization and their catalytic properties in Heck, Suzuki and Sonogashira coupling reactions as heterogeneous catalyst.
- Synthesis of periodic mesoporous organosilicas (PMO) having organic moieties like benzene ($-C_6H_4-$) in the frame wall positions.
- Attempt to graft Pd metal complexes of 4-(2-pyridyl)-1, 2, 3 triazole, a version of "**click reaction**" product ligand, and its derivatives into B-PMO phases and their catalytic properties in Stille C-C coupling reaction.
- Heterogenization of 2, 4, 6-triallyloxy-1, 3, 5-triazine (TAT) Pd(II) complex over organic group modified SBA-15 support, and to measure the catalytic properties in hydrogenation reaction.
- To characterize the synthesized catalysts by various characterization

techniques. The textural characteristics of these new heterogenized catalyst will be determined by FT-IR, ^{1}H, ^{13}C, ^{29}Si, MAS NMR spectroscopy, high resolution transmission electron spectroscopy (HRTEM), diffuse reflectance UV-Vis spectroscopy, X-ray diffraction (XRD), scanning electron microscopy (SEM), nitrogen adsorption analysis to determine surface area, pore size and typical N_2 adsorption and desorption isotherm. Another objective is to compare the reactivity obtained over heterogenized complexes with the corresponding homogeneous analogues.

- To study the regenerability of all the catalytic systems.

1.12. ORGANIZATION OF THE THESIS

The present thesis is divided into six chapters; **Chapter 1** gives an idea about current scenario in the field of mesoporous molecular sieve materials, precisely transition metal complex based mesoporous materials, more particularly Pd and Mn transition metal catalysed oxidation, hydrogenation and the C-C coupling reactions. The different characteristic properties of these materials including shape selectivity, formation mechanisms etc., and further more literature survey related to synthesis aspects, characterization techniques, and different catalytic applications has been discussed. The scopes and objectives of the present work were outlined at the end of this chapter.

Chapter 2: This chapter includes detailed synthesis and characterization of Chloro (S,S)(−)[N-3-tert-butyl-5-chloromethyl salicylidene]-N-[3,5-di tert-butyl salicylidene] 1,1-binapthyl-2,2-diamine manganese(III) (homogeneous system) complex on modified SBA-15 by using 3-aminopropyltrimethoxy silane as a reactive surface modifier to give supported catalyst. The surface properties of the functionalized catalyst were analyzed by a series of characterization techniques, which confirmed the structural integrity of the mesoporous hosts and the spectroscopic characterization technique proved the successful anchoring of the metal complex over the modified mesoporous support. The screening of the catalyst Mn(III)-L-SBA-15 and the neat Mn(III)-L complexes were done in the oxidation reaction of thioanisole (methyl

phenyl sulfide) by using TBHP as an oxidant. Mn(III)-L-SBA-15 catalyst shows comparable activities and turnover number (TON) and exhibit improved enantiomeric excess compared to homogeneous catalyst Mn(III)-L.

Chapter 3: Phosphine obstructed highly efficient and reusable SBA-15-EDTA-Pd(II) has been synthesized by anchoring Pd-EDTA complex over the surface of organo-functionalized SBA-15. The physiochemical properties of the organo-functionalized catalyst were analyzed by various characterization techniques. The synthesized catalyst SBA-15-EDTA-Pd(II) was screened for the Suzuki and Sonogashira coupling reactions show higher catalytic activity with high TON (turn over number). The anchored solid catalyst can be recycled efficiently and reused several times (five times) without major loss in reactivity.

Chapter 4: An efficient and highly reusable B-PMO-TZ-Pd(II) has been synthesized by anchoring 4-(2-pyridyl)- 4-(2-pyridyl)-1, 2, 3-triazole ligand over the inner surface of organo-functionalized benzene containing periodic mesoporous organosilica (B-PMO) via "**Click reaction**" and subsequent complexation with $PdCl_2$. B-PMO materials with uniform hexagonal arrangement were prepared using C16 alkyl trimethyl ammonium bromide [CTAB] surfactant under basic conditions. The synthesized catalyst was screened in the Stille and Kumada coupling reactions and show higher catalytic activities with high TONs. The anchored solid B-PMO-TZ-Pd(II) catalyst can be recycled efficiently and reused several times.

Chapter 5: This chapter consist of details of highly efficient and reusable SBA-15-TAT-Pd(II) synthesis by anchoring 2, 4, 6-triallyloxy-1, 3, 5-triazine (TAT) complex over the surface of organo-functionalized SBA-15. The synthesized catalyst SBA-15-TAT-Pd(II) was screened for hydrogenation reactions and show higher catalytic activity with high TON. The anchored solid catalyst can be recycled efficiently and reused without major loss in reactivity.

Chapter 6: This chapter gives an overall summary of all the major conclusions of the present study with respect to the synthesis and characterization of immobilized catalysts and the successful attempt in using the catalytic properties of the catalyst for oxidation, hydrogenation and C-C coupling reactions.

1.13. REFERENCES

[1] J. J. Berzelius, P. A. Reseanteckningar, Norstedt, Soner, *Stockholm*, **1903**.

[2] W. A. Herrmann, B. Cornils, *Angew. Chem. Intl. Ed.* **1997**, 36, 1048.

[3] Manassen*, J. in Catalysis, Progress in Research, Eds.: F. Basolo, Jr. Burwell, E. R, Plenum Press: New York,* **1973**, 177.

[4] T. Wasaki, Y. Aoiuma, *J. Am. Chem. Soc.***1999**, 121, 4793.

[5] C. J. Brinker, G. W. Scherer, *In Sol-gel Science, the Physics and Chemistry of Sol-gel Processing; Academic Press* **1999.**

[6] a) J. M. Thomas, S. Ramdas, G. R. Millward, J. Klinowsky, M. Audier, J. Conzalex Calbet, C. A. Fyfe, *J. Solid. State Chem.***1982,** 45, 368.; b) A. Corma, *Chem. Rev.* **1997,** 97, 2373.; c) S. Scurrell, *In La Chimica e l'industria* **1979,** 69, 219.; d) M. Berry, R. K. Champaneria, J. A. S. Howell, *J. Mol. Catal.* **1986,** 37, 243.; e) M. E. Davis, J. Schnitzer, J. A. Rosin, *J. Mol. Catal.* **1987,** 39, 243.; f) J. M. Fraile, J. I. García, J. A. Mayoral, *Chem. Commun.* **1996,** 1319.; g) A. Guerte, M. Iglesias, F. Sánchez, *J. Organomet. Chem.* **1999,** 58, 186.

[7] F. Cavani, F. Trifiro, A. Vaccari, *Catal. Today.* **1991,** 11, 173.

[8] a) Y. Yermakow, I. Yu, B. N. Kuznetsow, V. A. Zakharow, *In Studies in surface science and catalysis; Elveir scientific publishing company: Amsterdam* **1981**, 8.; b) T. J. Pinnavaia, *Science* **1983,** 220, 365; c) J. M. Andersen, *Platinium Metals Rev.* **1997,** 41, 132.; d) P. Gamez, B.Donjic, F. Fache, M. J. Lemaire, *J. Chem. Soc., Chem. Commun*. **1994**, 1417.

[9] D. Zhao, J. Feng, Q. Huo, N. Melosh, G. H. Fredrickson, B. F. Chmelka, G. D. Stucky, *Science,* **1998**, 279, 548.

[10] a) C. T. Kresge, M. E. Leonowicz, W. J. Roth, J. C. Vartuli, J. S. Beck, *Nature,* **1992**, 359, 710.; b) J. S. Beck, J. C. Vartuli, W. J. Roth, M. E.

Leonowicz, C. T. Kresge, K. D.Schmitt, C. T. W. Chu, D. H. Olson, E. W. Sheppard, S. B. Mc Cullen, J. B. Higgins, J. L. Schlenker, *J. Am. Chem. Soc.* **1992**, 114, 10834.

[11] J. S. Beck, J. C. Vartuli, G. J. Kennedy, C. T. Kresge, W. J. Roth, S. E. Schramm, *Chem. Mater.* **1994**, 6, 1816.

[12] a) A. Monnier, F. Schuth, Q. Huo, D. Kumar, D. I. Margolese, R. S. Maxwell, G. D. Stucky, M. Krishnamurthy, P. Petroff, A. Firouzi, M. Janicke, B. F. Chmelka, *Science.* **1993**, 261, 1299.; b) G. D. Stucky, A. Monnier, F. Schuth, Q. Huo, D. I. Margolese, D. Kumar, M. Krishnamurthy, P. Petroff, A. Firouzi, M. Janicke, B. F. Chmelka, *Mol. Cryst. Liq. Cryst.* **1994**, 240, 187.

[13] C. Y. Chen, S. L. Burkett, H. X. Li, M. E. Davis*, Micro. Mater.* **1993,** 2, 27.

[14] S. Inagaki, Y. Fukushima, K. Kuroda, *J. Chem. Soc., Chem. Commun.* **1993**, 680.

[15] a) A. Monnier, F. Schuth, Q. Huo, D. Kumar, D. I. Margolese, R. S. Maxwell, G. D. Stucky, M. Krishnamurthy, P. Petroff, A. Firouzi, M. Janicke, B. F. Chmelka, Science. **1993,** 261, 1299.; b) G. D. Stucky, A. Monnier, F. Schuth, Q. Huo, D. I. Margolese, D. Kumar, M. Krishnamurthy, P. Petroff, A. Firouzi, M. Janicke, B. F. Chmelka, *Mol. Cryst. Liq. Cryst.* **1994**, 240, 187.

[16] S. Inagaki, Y. Fukushima, K. Kuroda, *J. Chem. Soc., Chem. Commun.* **1993**, 680.

[17] a) A. Firouzi, D. Kumar, L. M. Bull, T. Besier, P. Sieger, Q. Huo, S. A. Walker, J. A. Zasadzinski, C. Glinka, J. Nicol, D. I. Margolese, G. D. Stucky, B. F. Chmelka, *Science* **1995,** 267, 1138.; b) A. Firouzi, F. Atef, A. G. Oertli, G. D. Stucky, B. F. Chmelka, *J. Am. Chem. Soc.* **1997,** 119, 3596.

[18] a) Q. Huo, D. I. Margolese, U. Ciesla, P. Feng, P. Sieger, R. Leon, P. Petroff, F. Schuth, G. D. Stucky, *Nature* **1994,** 368, 317.; b) Q. Huo, D. I. Margolese, U. Ciesla, D. G. Demuth, P. Feng, T. E. Gier, P. Sieger, A. Firouzi, B. F. Chmelka, F. Schuth, G. D. Stucky, *Chem. Mater.* **1994,** 6,

1176.

[19] a) P. T. Tanev, T. J. Pinnavaia, *Chem. Mater.* **1996,** 8, 2068.; b) P. T. Tanev, T. J. Pinnavaia, *Science* **1996,** 271, 1267.; c) P. T. Tanev, T. J. Pinnavaia, *Science* **1995**, 267, 865.

[20] D. M. Antonelli, J. Y. Ying, *Angew. Chem. Int. Ed.* **1996,** 35, 426.

[21] A. Stein, B. J. Melde, R. C. Schroden, *Adv. Mater.* **2000,** 12, 1403.

[22] A. P. Wight, M.E. Davis, *Chem. Rev.* **2002,** 102, 3589.

[23] X. Feng, G. E. Fryxell, L.-Q. Wang, A. Y. Kim, J. Liu, K. M. Kemner, *Science*. **1997**, 276, 923.

[24] D. E. De Vos, M. Dams, B. F. Sels, P. A. Jacobs, *Chem. Rev.* **2002,** 102, 3615.

[25] P. M.Price, J. H. Clarck, D.J. Macquarrie, *J. Chem. Soc., Dalton Trans.* **2000,** 101.

[26] K. Moller, T. Bein, *Stud. Surf. Sci. Catal.* **1998,** 117, 53.

[27] J. Liu, X. Feng, G. E. Fryxell, L.-Q. Wang, A. Y. Kim, M. Gong, *Adv. Mater.* **1998,** 10, 161.

[28] K. K. Unger, *Porous Silica–Its Properties and Use as Support in Column Liquid Chromatography, Vol. 16, Elsevier, Amsterdam,* **1979.**

[29] L. Mercier, T. J. Pinnavaia, *Environ. Sci. Tech.* **1998,** 32, 2749.

[30] T. Kimura, S. Saeki, Y. Sugahara, K. Kuroda, *Langmuir*. **1999,** 15, 2794.

[31] J. S. Beck, D. C. Calabro, S. B. McCullen, B. P. Pelrine, K. D. Schmitt, J. C. Vartuli, *Method for* Functionalizing Synthetic Mesoporous Crystalline Material, Mobil Oil Corporation, USA, 1992.

[32] R. Anwander, I. Nagl, M. Widenmeyer, G. Engelhardt, O. Groeger, C. Palm, T. Roser, *J. Phys. Chem. B*, **2000,** 104, 3532.

[33] M. H. Lim, C. F. Blanford, A. Stein, *J. Am. Chem. Soc.* **1997,** 119, 4090.

[34] R. Anwander, I. Nagl, M. Widenmeyer, G. Engelhardt, O. Groeger, C. Palm, T. Roser, *J. Phys. Chem. B*. **2000,** 104, 3532.

[35] M. H. Lim, C. F. Blanford, A. Stein, *Chem. Mater.* **1998,** 10, 467.

[36] a) W. M. van Rhijn, D. E. De Vos, B. F. Sels, W. D. Bosaert, P. A. Jacobs, *Chem. Commun.***1998**, 317.; b) D. Margolese, J. A. Melero, S.C.

Christiansen, B. F. Chmelka, G.D. Stucky, *Chem. Mater.* **2000**, 12, 2448.

[37] J. H. Clark, D. J. Macquarrie, *Chem. Commun.***1998,** 853.

[38] D. Brunel, *Micropor. Mesopor. Mater.***1999,** 27, 329.

[39] P. Sutra, D. Brunel, *Chem. Commun.***1996**, 2485.

[40] M. H. Lim, A. Stein, *Chem. Mater.* **1999,** 11, 3285.

[41] D. S. Shephard, W. Zhou, T. Maschmeyer, J. M. Matters, C. L. Roper, S. Parsons, B. F. G. Johnson, M. J. Duer, *Angew. Chem. Int. Ed.* **1998,** 37, 2719.

[42] F. D. Juan, E. R. Hitzky, *Adv. Mater.* **2000,** 12, 430.

[43] V. Antochshuk, M. Jaroniec, *Chem. Commun.* **1999,** 2373.

[44] C. Sanchez, F. Ribot, *New. J. Chem.* **1994,** 18, 1007.

[45] a) S. L. Burkett, S. D. Sims, S. Mann, *Chem. Commun.* **1996,** 1367.; b) S. D. Sims, S. L. Burkett, S. Mann, *Mater. Res. Soc. Symp. Proc.* 8, **1996**.; c) D. J. Macquarrie, *Chem. Commun.* **1996,** 1961.; d) Q. Huo, D. I. Margolese, G. D. Stucky, *Chem. Mater.* **1996,** 8, 1147.

[46] H. C. Kolb, M. G. Finn, K. B. Sharpless, *Angew. Chem. Int. Ed.* **2001,** 40, 2004.

[47] a) A. Dondoni, *Angew. Chem. Int. Ed.*, **2008,** 47, 8995.; b) L. M. Campos, I. Meinel, R. G. Guino, M. Schierhorn, N. Gupta, G. D. Stucky, C. J. Hawker, *Adv. Mater.*, **2008,** 20, 3728.

[48] R. Huisgen, *Proc. Chem. Soc.***1961**, 357.

[49] a) H. C. Kolb, K. B. Sharpless, *Drug Discovery Today*. **2003,** 8, 1128.; b) J. E. Moses, A. D. Moorhouse, *Chem. Soc. Rev.*, **2007,** 36, 1249.; c) Y. L. Angell and K. Burgess, *Chem. Soc. Rev*., **2007**, 36, 1674.; d) S. Dedola, S. A. Nepogodiev, R. A. Field, *Org. Biomol. Chem.* **2007**, 5, 1006.

[50] a) C. E. Song, S. Lee, *Chem. Rev.* **2002,** 102, 3495.; b) J. M. Notestein, A. Katz, *Chem. Eur. J.* **2006,** 12, 3954.; c) A. Corma, H. Garcia, *Adv. Synth. Catal.* **2006,** 348, 191.

[51] a) R. van de Coevering, R. J. M. Klein. Gebbink, Van. Koten, G. Prog. *Polym. Sci.* **2005,** 30, 474.; b) A. Berger, R. J. M. Klein Gebbink, G. van Koten, *Top. Organomet. Chem.* **2006,** 20 *Dendrimer Catalysis*, 1. (i) R.

Andres, E. De Jesus, J. C. Flores, *New J. Chem.* **2007,** 31, 1161.; c) S. H. Hwang, C. D. Shreiner, C. N. Moorefield, G. R. Newkome, *New J. Chem.* **2007,** 31, 1192.

[52] a) S. J. Shuttleworth, S. M. Allin, R. D. Wilson, D. Nasturica, *Synthesis.* **2000,** 8, 1035.; b) B. Clapham, T. S. Reger, K. D. Janda, *Tetrahedron.* **2001,** 57, 4637.; c) T. J. Dickerson, N. N. Reed, K. D. Janda, *Chem. Rev.* **2002,** 102, 3325.; d) S. Kobayashi, R. Akiyama, *Chem. Commun*. **2003,** 449.; e) P. Mastrorilli, C. F. Nobile, *Coord. Chem. Rev.* **2004,** 248, 377.

[53] H. C. Kolb, M. G. Finn, K. B. Sharpless, *Angew. Chem., Int. Ed.* **2001,** 40, 2004.

[54] a) N. D. Gallant, K. A. Lavery, E. J. Amis, M. L. Becker, *Adv. Mater.* **2007,** 19, 965. (b) H. Nandivada, H. Y. Chen, L. Bondarenko, Lahann, *J. Angew. Chem. Int. Ed.* **2006,** 45, 3360. c) C. Gauchet, G. R. Labadie, C. D. Poulter, *J. Am. Chem. Soc.* **2006,** 128, 9274.

[55] A. Gissibl, C. Padie, M. Hager, F. Jaroschik, R. Rasappan, Cuevas. E. Yanez, C. O. Turrin, A. M. Caminade, J. P. Majoral, Reiser, *O. Org. Lett*. **2007,** 9, 2895.

[56] a) Y. Li, J. C. Huffman, A. H. Flood, *Chem. Commun.*, **2007,** 2692.; b) B. Schulze, C. Friebe, M. D. Hager, A. Winter, R. Hoogenboom, H. Gorls, U. S. Schubert, *Dalton Trans.* **2009,** 787.; c) B. Happ, C. Friebe, A. Winter, M. D. Hager, R. Hoogenboom, U. S. Schubert, *Chem. Asian J.*, **2009,** 4, 154.; d) J. T. Fletcher, B. J. Bumgarner, N. D. Engels, D. A. Skoglund, *Organometallics*, **2008,** 27, 5430.

[57] P. S. Donnelly, S. D. Zanatta, S. C. Zammit, J. M. White, S. J. Williams, *Chem. Commun.*, **2008**, 2459.

[58] a) M. Barz, E. Herdtweck, W. R. Thiel, *Angew. Chem., Int. Ed.* **1998,** 37, 2262.; b) PtII complexes: S. Komeda, M. Lutz, A. L. Spek, Y. Yamanaka, T. Sato, M. Chikuma, J. Reedjik, *J. Am. Chem. Soc.* **2002,** 124, 4738.; c) CuI complexes: T. R. Chan, R. Hilgraf, K. B. Sharpless, V. V. Fokin, *Org. Lett.* **2004**, *6*, 2853.

[59] J. T. Fletcher, B. J. Bumgarner, N. D. Engels, D. A. Skoglund,

Organometallics, **2008**, 27, 5430.

[60] a) D. A. Loy, K. J. Shea, *Chem. Rev*. **1995**, 95, 1431.; b) K. J. Shea, D. A. Loy, O. Webster, *J. Am. Chem. Soc*. **1992,** 114, 6700.; c) D. A. Loy, G. M. Jamison, B. M. Baugher, S. A. Myers, R. A. Assink, K. J. Shea, *Chem. Mater*. **1996,** 8, 656.

[61] a) S. Inagaki, S. Guan, Y. Fukusima, T. Ohsuma, O. Terasaki, *J. Am. Chem. Soc*. **1999,** 121, 9611.; b) T. Asefa, M. J. Mac. Lachlan, N. Coombs, G. A. Ozin, *Nature.* **1999,** 402, 867.; c) B. J. Melde, B. T. Holland, C. F. Blanford, A. Stein, *Chem. Mater*. **1999,** 11, 3302.

[62] a) B. Hatton, K. Landskron, W. Whitnall, D. Perovic, G. A. Ozin, *Acc. Chem. Res*. **2005,** 38, 305.; b) S. Guan, S. Inagaki, T. Ohsuna, O. Terasaki, *J. Am. Chem. Soc*. **2000,** 122, 5660.; c) M. P. Kapoor, S. Inagaki, *Chem. Mater*. **2002,** 14, 3509.; d) A. Sayari, S. Hamoudi, Y. Yang, I. L. Moudrakovski, J. R. Ripmeester, *Chem. Mater*. **2000,** 12, 3857.; e) C. H. Lee, S. S. Park, S. J. Choe, D. H. Park, *Microporous Mesoporous Mater*. **2001,** 46, 257.

[63] a) B. Hatton, K. Landskron, W. Whitnall, D. Perovic, G. A. Ozin, *Acc. Chem.Res*. **2005,** 38, 305.; b) S. Guan, S. Inagaki, T. Ohsuna, O. Terasaki, *J. Am. Chem. Soc*. **2000,** 122, 5660.; c) M. P. Kapoor, S. Inagaki, *Chem. Mater*. **2002,** 14, 3509.; d) A. Sayari, S. Hamoudi, Y. Yang, I. L. Moudrakovski, J. R. Ripmeester, *Chem. Mater*. **2000,** 12, 3857.; e) C. H. Lee, S. S. Park, S. J. Choe, D. H. Park, *Microporous Mesoporous Mater*. **2001,** 46, 257.

[64] a) S. Hamoudi, S. Kaliaguine, *Chem. Commun*. **2002,** 2118.; b) Y. Lu, H. Fan, N. Doke, D. A. Loy, R. A. Assink, D. A. La Van, C. J. Brinker, *J. Am. Chem. Soc*. **2000,** 122, 5258.; c) J. R. Matos, M. Kruk, L. P. Mercuri, M. Jaroneic, T. Asefa, N. Coombs, G. A. Ozin, T. Kamiyama, O. Terasaki, *Chem. Mater*. **2002,** 14, 1903.

[65] a) S. Inagaki, S. Guan, T. Ohsuna, O. Terasaki, *Nature.* **2002,** 416, 304.; b) M. P. Kapoor, Q. Yang, S. Inagaki, *Chem. Mater.* **2004**, 16, 1209.; c) W. Wang, S. Xie, W. Zhou, A. Sayari, *Chem. Mater.* **2003**, 15, 4886.; d) M. P.

Kapoor, Q. Yang, S. Inagaki, *J. Am. Chem. Soc*. **2002**, 124, 15176.; e) K. Okamoto, Y. Goto, S. Inagaki, *J. Mater. Chem*. **2005**, 15, 4136.

[66] a) C. Y. Ishii, T. Asefa, N. Coombs, M. J. Mac Lachlan, G. A. Ozin, *Chem. Commun*. **1999**, 2539.; b) K. Nakajima, D. Lu, J. N. Kondo, I. Tomita, S. Inagaki, M. Hara, S. Hayashi, K. Domen, *Chem. Lett*. **2003,** 32, 950.

[67] M. J. M. Lachlan, T. Asefa, G. A. Ozin, *Chem. Eur. J*. **2000,** *6*, 2507.

[68] S. Inagaki, S. Guan, F. Fukushima, T. Ohsuna, O. Terasaki, *Stud. Surf. Sci. Catal*. **2000**, 129, 155.

[69] a) M. P. Kapoor, A. K. Sinha, S. Seelan, S. Inagaki, S. Tsubota, H. Yoshida, M. Haruta, *Chem. Commun*. **2002,** 2902.; b) E. B. Cho, K. W. Kwon, K. Char, *Chem. Mater*. **2001**, 13, 3837.

[70] T. Asefa, M. J. Mac Lachlan, H. Grondey, N. Coombs, G. A. Ozin, *Angew. Chem. Int. Ed*. **2000,** *39*, 1808.

[71] J. Patarin, *Angew. Chem. Int. Ed.* **2004,** *43*, 1.

[72] a) S. Hitz, R. Prins, *J. Catal*. **1997**, 168, 194.; b) P. T. Tanev, T. J. Pinnavaia, *Chem. Mater*. **1996**, 8, 2068.

[73] H. Lee, S. I. Zones, M. E. Davis, *Nature.* **2003,** 425, 385.

[74] a) N. Husing, *Angew. Chem. Int. Ed*. **2004,** 43, 3216.; b) C. H. Lee, T. S. Lin, C. Y. Mou, *J. Phys. Chem. B.* **2003,** 107, 2543.; c) C. D. Nunes, M. Pillinger, A. A. Valente. J. Rocha, A. D. Lopes, I. S. Goncalves, *Eur. J. Inorg. Chem*. **2003**, 3870.; d) L. L. Welbes, A. S. Borovik, *Acc. Chem. Res*. **2005**, 38, 765.

[75] a) A. Taguchi, F. Schuth, *Microporous Mesoporous Mater*. **2004,** 77, 1.; b) C. T. Fischel, R. J. Davis, J. M. Garcer, *J. Catal*. **1996,** 163, 141.; c) R. Ryoo, C. H. Ko, J. M. Kim, R. Howe, *Catal. Lett*. **1996,** 37, 29.

[76] a) J. Jamis, J. R. Anderson, R. S. Dickson, E. M. Campi, W. R. Jackson, *J. Organomet. Chem.* **2001,** 627, 37.; b) K. Mukhopadhyay, B. R. Sarkar, R. V. Chaudhari, *J. Am. Chem. Soc*. **2002**, 124, 9692.; c) C. Baleizao, B. Gigante, M. J. Sabatier, H. Garcia, A. Corma, *Appl. Catal. A. Gen*. **2002,** 288, 279.; d) S. Xiang, Y. Zhang, Q. Xin, C. Li, *Angew. Chem. Int. Ed*. **2002,** 41, 821.; e) A. Poppl, P. Baglioni, L. Kevan, *J. Phys. Chem.* **1995,**

99, 14156.; f) W. Bohlmann, K. Schandert, A. Poppl, H. C. Semmelhack, *Zeolites.* **1997,** 19, 297.

[77] D. J. Cole Hamilton, *Science.* **2003**, 299, 1702.

[78] a) W. F. Maier, J. A. Marten, S. Klein, J. Heilmann, R. Parton, K. Vercruysse, P. A. Jacobs, *Angew. Chem. Int. Ed.* **1996,** 35, 180.; b) N. A. Herron, *Inorg. Chem.* **1986**, 25, 4714.

[79] C. A. M. Namara, M. J. Dixon, M. Bradley, *Chem. Rev*. **2002,** 102, 3275.

[80] J. W. Niemantsverdriet, *Spectroscopic Methods in Heterogeneous Catalysis*, VCH, Weinheim, **1993**.

[81] a) S. Biz, M. Occelli, *Catal. Rev-Sci. Eng*. **1998,** 40, 329.; b) G. Bergeret in: *Handbook of Heterogeneous Catalysis*, Vol. 2, Eds, G. Ertl, H. Knozinger, J. Weitkamp, Wiley-VCH, Weinheim, **1997,** pp. 464.

[82] W. H. Bragg, W. L. Bragg, *The Crystalline State*, Vol. 1, McMillan, New York, **1949.**

[83] S. Brunauer, P. H. Emmett, E. Teller, *J. Am. Chem. Soc.* **1938**, *60,* 309.

[84] a) C. Y. Chen, H. X. Li, M. E. Davis, *Microporous Mater.***1993**, *2,* 17.; b) E. P. Barrett, L. G. Joyner, P. P. Halenda, *J. Am. Chem. Soc.* **1951**, *73*, 373.

[85] a) R. Evans, U. M. B. Marconi, P. Tarzona, *J. Chem. Soc., Faraday Trans. II* **1986**, *82*, 1763.; b) P. I. Ravikovitch, G. L. Haller, A. V. Neimark, *Adv. Colloid Interfac.* **1998**, *203,* 76.

[86] C. C. Freyhardt, M. Tsapatsis, R. F. Lobo, K. J. Balkus, M. E. Davis, *Nature.***1996**, *381*, 295.

[87] M. Mehring, *High Resolution NMR Spectroscopy in Solids*, Springer-Verlag, Berlin, **1976.**

[88] G. Engelhardt, D. Michel, *High-Resolution Solid-State NMR of Silicates and Zeolites*, John Wiley and Sons Ltd., Chichester, **1987**.

[89] G. Engelhardt, in: *Handbook of Heterogeneous Catalysis*, *Vol. 2*, Eds: G. Ertl, H. Knozinger, J. Weitkamp, Wiley-VCH, Weinheim, **1997**, *P. 525.*

[90] J. W. Robinson, *Atomic Absorption Spectroscopy*, Marcel Dekker, New York, **1975.**

[91] J. W. Robinson, *Atomic Absorption Spectroscopy*, Marcel Dekker, New

York, **1975**.

[92] C. K. Jorgensen, *Absorption Spectra and Chemical Bonding in Complexes, Pergamon, New York,* **1962**.

[93] G. Kortum, *Reflectance Spectroscopy, Springer, Berlin,* **1969**.

[94] M. Faraday, *Philos. Trans.* **1857**, 147, 145.

[95] G. Mie, Ann. Physik **1908**, 25, 377.

[96] G. C. Papavassiliou, Prog. *Solid State Chem.* **1980**, 12, 185.

[97] a) S. Link, M. A. El-Sayed, *J. Phys. Chem. B.* **1999**, 103, 4212.; b) C. Burda, T. Green, C. Landes, S. Link, R. Little, J. Petroski, M. A. El-Sayed, in: *Characterization of Nanophase Materials, Ed:* Z. L. Wang, Wiley-VCH, Weinheim, **2000**, Chapter 7, pp. 197.

[98] G. L. Moore, *Introduction to Inductively Coupled Plasma Atomic Emission Spectrometry*, Elsevier, Amsterdam, **1988.**

[99] G. Lawes, *Scanning Electron Microscopy, X-Ray Microanalysis*, John Wiley and Sons Ltd., Chichester, **1987**.

[100] D. E. Newbury, D. C. Joy, P. Echlin, C. E. Fiori, J. I. Goldstein, *Advanced Scanning Electron Microscopy and X-Ray Microanalysis*, Plenum Press, New York, **1986**.

[101] J. R. Fryer, *Chemical Applications of Transmission Electron Microscopy*, Academic Press, San Diego, **1979**.

[102] V. Alfredsson, M. Keung, A. Monnier, G. D. Stucky, K. K. Unger, F. Schuth, *J. Chem. Soc., Chem. Commun.***1994,** 921.

[103] Z. L. Wang, in: *Characterization of Nanophase Materials*, Ed: Z. L. Wang, Wiley-VCH, Weinheim, **2000,** Chapter 3, P. 37.

[104] M. Chamumi, D. Brunel, F. Fajula, P. Geneste, P. Moreau, J. Solof, *Zeolites*. **1994,** 14, 283.

[105] M. Dusi, T. Mallat, A. Baiker, *Catal. Rev. Sci. Eng.* **2000**, 42, 213.

[106] a) O. Schmidt, *Chemical Reviews*. **1933**, 12, 363.; b) R. A. W. Johnstone, A. H. Wilby, I. D. Entwistle, *Chem. Rev.* **1985**, 85, 129.; c) C. M. Crudden, D. Allen, M. D. Mikoluk, J. Sun, *Chem. Comm.* **2001**, 1154.

[107] a) C. M. Crawforth, I. J. S. Fairlamb, A. R. Kapdi, J. L. Serrano, R. J. K. Taylor G. Sanchez, *Adv. Synth. Catal.* **2006,** 348, 405.; b) M. Lamblin, L. N. Hardy, J. C. Hierso, E. Fouquet, F. X. Felpin, *Adv. Synth. Catal.* **2010**, 352, 33.; c) X. F. Wu, H. Neumann, M. Beller, *Chem. Commun*. **2011,** 47, 7959.

[108] a) N. A. Milas, S. Sussman, *J. Am. Chem. Soc*. **1936**, *58*, 1302.; b) N. A. Milas, S. Sussman, *J. Am. Chem. Soc*. **1937**, *59*, 2345.; c) N. A. Milas, *J. Am. Chem. Soc.***1937**, *59*, 2342.

[109] K. A. Jorgensen, *Chem. Rev*. **1989**, *89*, 431.

[110] M. L. W. Vorstenbosch, Ph. D *Thesis, Schuit Institute of Catalysis, Eindhoven University of Technology, The Netherlands,* **2002**.

[111] K. C. Gupta, A. K.Sutar, *Coor. Chem. Rev.* **2008,** 252, 1420.

[112] a) B. Chen, U. Dingerdissen, J. G. E. Krauter, H. G. J. Lansink Rotgerink, K. M¨obus, D. J. Ostgard, P. Panster, T. H. Riermeier, S. Seebald, T. Tacke H. Trauthwein, *Appl. Catal: A*, **2005**, 280, 17.; b) K. Nomura, *J. Mol. Catal. A: Chem.*, **1998**, 130, 1.

[113] a) H. U. Blaser, C. Malan, B. Pugin, F. Spindler, H. Steiner, M. Studer, *Adv. Synth. Catal.* **2003,** 345, 103.; b) R. M. Magdalene, E. G. Leelamani, N. M. N. Gowda, *J. Mol. Catal. A: Chem.* **2004,** 223, 17.

[114] a) D. H. Lee, J. Y. Jung, M. J. Jin. *Chem. Commun.* **2010,** 46, 9046.; b) J. Yang, L. Wang. *Dalton Trans.* **2012,** 41, 12031.; c) I. Blaszczyk, A. M. Trzeciak. *Tetrahedron.* 2010, 66, 9502.

[115] a) I. P. Beletskaya, V. Andrei, Cheprakov, *Chem. Rev*. **2000,** 100, 3009; b) V. Polshettiwar, A. Molnar, *Tetrahedron.* **2007**, 63, 6949.; c) S. P. Stanforth, *Tetrahedron.* **1998**, 54, 263.

[116] a) C. Amatore, A. Jutand, M. Amine, M. Barki, *Organometallics* **1992,** 11, 3009.; b) H. A. Dieck, R. F. Heck, *J. Org. Chem* **1975,** 40, 1083.; c) C. A. Fleckenstein, H. Plenio, *Chem. Soc. Rev*. **2010** 39, 694.

[117] A. Zapf, M. Beller, *Top. Catal* **2002,** 19, 101.; b) L.X. Yin, J. Liebscher, *Chem. Rev.* **2007,** 107, 133.

[118] a) M. Lamblin, L. N. Hardy, J. C Hierso, E. Fouquet, F. X. Felpinb, *Adv. Synth. Catal.* **352**, 2010, 33.; b) T. N. Glasnov, S. Findenig, C. O. Kappe. *Chem. Eur. J.*, **1001**, 2009, 15.; c) E. Chorell, P. Das, F. Almqvist, *J. Org. Chem.* **72,** 2007, 4917.

[119] a) C. M. Crawforth, I. J. S. Fairlamb, A. R. Kapdi, J. L. Serrano, R. J. K. Taylor, G. Sanchez, *Adv. Synth. Catal.* **2006,** 348, 405.; b) M. Lamblin, L. N. Hardy, J. C. Hierso, E. Fouquet, F. X. Felpin, *Adv. Synth. Catal.* **2010**, 352, 33.; c) X. F. Wu, H. Neumann, M. Beller, *Chem. Comm*. **2011,** 47, 7959.

[120] a) T. Ljungdahl, T. Bennur, A. Dallas, H. Emtenas, J. Mårtensson. *Organometallics*. **2008,** 27, 2490.; b) T. Ljungdahl, K. Pettersson, B. Albinsson, J. Mårtensson, *J. Org. Chem.* **2006,** 71, 1677.

[121] a) N. S. Miyaura, *A. Chem. Rev*. **1995,** 95, 2457.; b) K. Tamao, K. Sumitani, M. Kumada, *J. Am. Chem. Soc*. **1972,** 94, 4374.; c) T. Hiyama, *J. Organomet. Chem.* **2002**, 653, 58.; c) J. K. Stille, *Angew. Chem, Int. Ed.* **1986,** 25, 508.; d) E. Negishi, *Acc. Chem. Res*. **1982,** 15, 340.

[122] a) G. Lu, C. Caib, B. H. Lipshutz, *Green Chem.* **2013,** 15, 105.; b) C. Chiappe, G. Imperato, E. Napolitanob, D. Pieraccini, *Green Chem*. **2004**, 6, 33.

[123] a) C. A. Hillier, A. G. Grasa. S. M. Viciu, H. M. Lee, Y. Chuluo, A. C. Nolan. J. O*rgano. Chem.* **2002,** 653, 69.; b) P. Knochel, A. Krasovskiy, I. Sapountzis, *Handbook of Functionalized Organometallics, Vol. 1 (Ed.: P. Knochel), Wiley-VCH, Weinheim.* **2005**, 109.

CHAPTER-2

Mn(III) Based Binaphthyl Schiff Base Complex Heterogenized over Organo-modified SBA-15

2.1. INTRODUCTION

The discovery of efficient method for catalytic epoxidation is an important goal in synthetic chemistry as there is a growing interest in using epoxide as a building block in organic synthesis. Mn(III) schiff-base complexes have become highly valuable catalysts in homogeneous alkene epoxidation reactions using readily available oxygen donors such as, H_2O_2 or TBHP.[1,2] On the other hand, immobilization of transition-metal complexes on solid supports can provide catalysts which are easier to handle and which may possibly exhibit improved selectivity and activities because of the support environment.[3-10] Over the past few decades, researchers has focused on the development of a variety of homogeneous catalysts that deliver high levels of activities and enantio or diastereoselectivities.[11] The design and synthesis of chiral ligands that, upon coordination with metal ion can induce high stereoselectivity for organic transformations constitute an important issue in modern coordination chemistry.[12] In this context, a lot of attention has been directed to C_2-symmetric binaphthyl ligands such as BINAP and binaphthol and chiral Schiff-base ligands.[13] Recently, there has been increasing interest in utilizing a 'hybridized' form of binaphthyl ligands and salens, *i.e.* binaphthyl Schiff base ligand.

Since the synthesis of ordered mesoporous materials in 1992 sparked worldwide interest in the field of heterogeneous catalysis and separation science, SBA-15 has became the most popular member of the group possessed extremely high surface areas, easily accessible, uniform pore sizes and stability.[14] SBA-15 porous structures possess with unusually large inter lattice 'd' spacing of 74.5–320 Å between the (100) planes, pore sizes from 46–300 Å, pore volume fractions up to 0.85, and silica wall thicknesses of 31–64 Å.[15] To extent the applicability of SBA-15 materials, it is necessary to modify the surface by organic functional groups for anchoring metals and metal complexes.[16] Grafting of functional organosilanes by using surface hydroxyl groups as anchor points has been widely used. Furthermore the leaching of active site can also be avoided as the organic moieties are covalently attached to the inorganic support. Along with these affordable reasons the deciding factor for solid support ends over the SBA-15.

Herein, this chapter we described the covalent bonding of the chloro (S, S)(–

)[N-3-tert-butyl-5-chloromethyl salicylidene]-N′-[3′,5′-di tert-butyl salicylidene] 1,1′-binaphthyl-2,2′-diamine manganese (III) (homogeneous system) complex on modified SBA-15 by using 3-aminopropyl trimethoxy silane as a reactive surface modifier to give supported catalyst and their catalytic properties in sulfide oxidation by TBHP. The immediate goal of our study was to evaluate the heterogenization method of the salen binaphthyl Schiff base ligand over SBA-15 and to determine the extent of the increased stability of the catalyst with regard to the homogeneous catalyst as well as their recycling properties.

2.2. EXPERIMENTAL

2.2.1. Materials

Tetraethylorthosilicate (TEOS), Pluronic 123 (P_{123}, Average Mol. Wt = 5800), 3-tert-butyl-2-hydroxy benzaldehyde, 3-aminopropyl trimethoxy silane (3-APTMS), dimethoxydimethylsilane ($(MeO)_2Me_2Si$), (S)-(–)-1, 1′-Binaphthyl-2, 2′-diamine 1, 2-dihydronaphthalene, thioanisole (methyl phenyl sulfide) were purchased from Aldrich. Glacial acetic acid, paraformaldehyde, HCl (36.5 %) was purchased from Thomas Baker (India). 5-Chloromethyl-3-tertbutyl-2-hydroxy benzaldehyde was synthesized according to literature procedure with slight modification. The dry reagent grade solvents were obtained from Merck (India) and dried before use according to standard methods.

2.2.2. Synthesis Procedure of Catalyst

2.2.2.1. Synthesis of parent and organo-functionalized SBA-15

The synthesis of mesoporous SBA-15 was carried out hydrothermally under the autogeneous pressure in an autoclave. The polymer surfactant P_{123} was used as a template and hydrochloric acid served as a mineralizer. The gel composition was as follows;

0.043 TEOS: 4.4 g P_{123} Mavg= 5800 = [EO_{20} - PO_{70} - EO_{20}]: 8.33 H_2O : 0.24 HCl.

4.4 g of tri block co-polymer dispersed in 30 g of distilled water was stirred for 1.5 h. To the resultant solution, 120 g of 2 M HCl was added under stirring and the stirring

was continued for 2 h. Finally, 9 g of TEOS was added drop wise and the mixture was maintained at 40 ºC for 24 h with continuous stirring. The mass was submitted to a hydrothermal treatment (100 ºC, 48 h) under static condition. The precipitate was filtered, washed with distilled water, dried in an oven (90 ºC, 12 h) and then calcined in air (500 ºC, 6 h) to remove the template.

Surface modification of SBA-15 was achieved by a post synthesis grafting method [Scheme 2.1(D)]. One gram of SBA-15 was suspended in a 100 ml of dry toluene and refluxed with 2.5 mmol of 3-aminopropyltrimethoxysilane (3-APTMS) for 8 h under N_2 atmosphere. The material was filtered after cooling to ambient temperature, washed with dry toluene and dichloromethane, respectively. Soxhlet extraction was carried out for 24 h in dichloromethane (DCM) to remove the occluded organosilane. The sample was dried in vacuum for 10 h. The obtained material is designated as NH_2-SBA-15. The free –OH groups present in NH_2-SBA-15 were protected by adding 1.5 mmol of dimethoxydimethylsilane [$(MeO)_2Me_2Si$] to a stirred suspension of 1 g of NH_2-SBA-15 in dry toluene (50 mL), followed by stirring of 12 h at reflux temperature under inert atmosphere. The obtained material was filtered, washed, with toluene and further soxhlet extracted with DCM for 24 h. The obtained material was named as –OH protected NH_2-SBA-15 as per scheme [Scheme 2.1(E)].

2.2.2.2. Synthesis of 5-chloromethyl-3-tert-butyl-2-hydroxybenzaldehyde

3-tert-butyl-2-hydroxy benzaldehyde 2 g (0.01 mol) and para-formaldehyde 10.09 g (2.97 mol) was stirred in a round bottom flask and the resulting emulsion was refluxed for 48 h with 25 ml con. HCl. The reaction mixture was extracted with DCM.[17,18] The organic phase was washed with saturated aqueous sodium bicarbonate followed by brine solution and dried over Na_2SO_4. Resultant residue was further concentrated in vacuum to give 5-chloromethyl-3-tert-butyl-2-hydroxybenzaldehyde as the viscous oil [Scheme 2.1(A)]. (93 % yield, 1.86 g, 8.21 mmol). ^{13}C NMR 300 MHz, $CDCl_3$, δ (ppm) - 29.12 (s, 3C); 34.98 (s, 1C); 45.92 (s, 1C); 120.32 (s, 1C); 128.26 (s, 1C); 131.76 (s, 1C); 134.54 (s, 1C); 139.16 (s, 1C); 161.28 (s, 1C); 196.74 (s, 1C). ^{1}H NMR (200 MHz, $CDCl_3$, δ (ppm) - 1.43 (m, 9H); 4.5 (s, 2H); 5.34 (s, 1H); 7.45 (s, 1H); 7.52 (s, 1H); 9.88 (s, 1H); 11.86 (s, 1H).

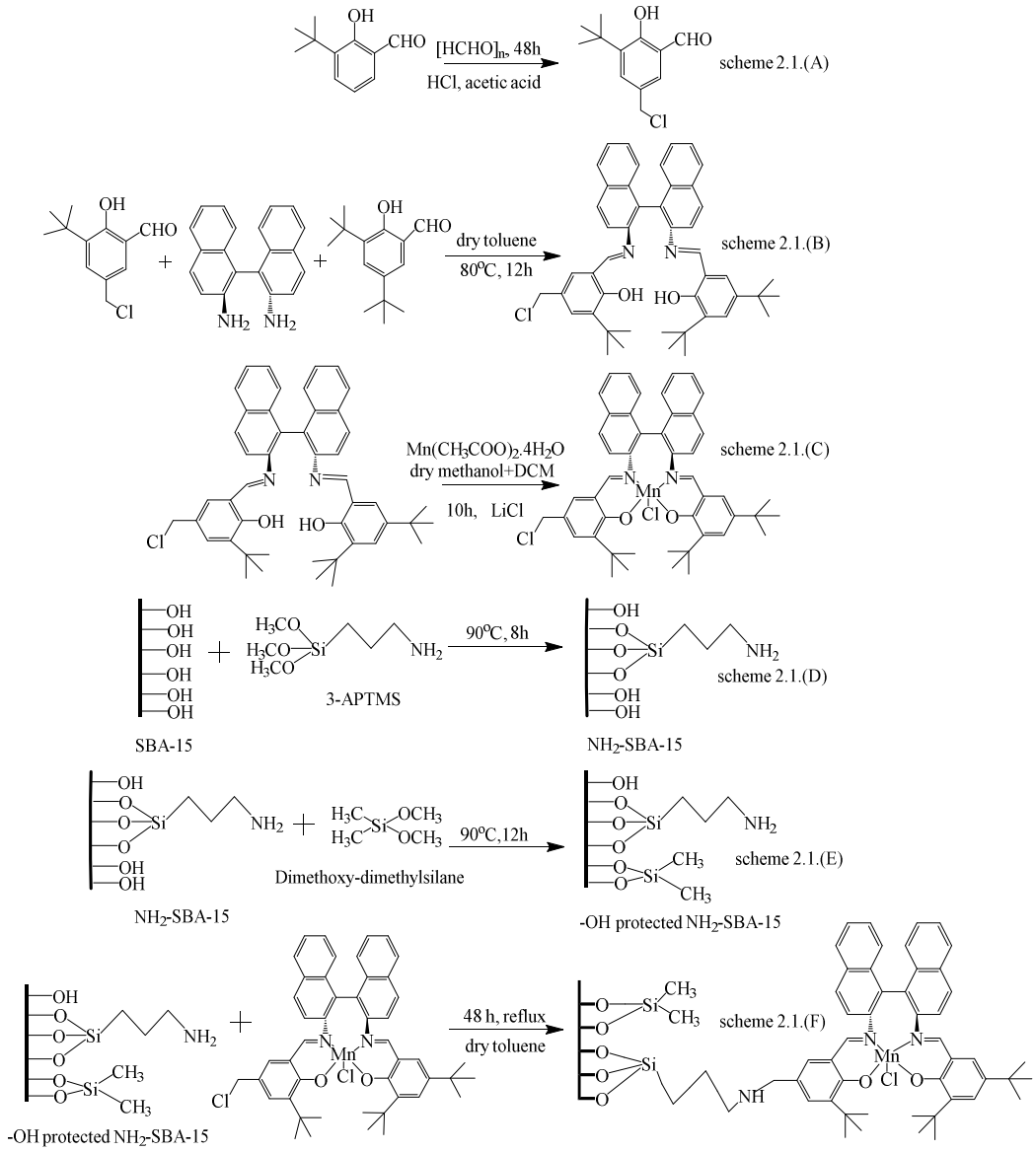

Scheme 2.1. Functionalization of SBA-15 and heterogenization of ligand, 2.1.(A) Chloromethylation of 3-tert-butyl-2-hydroxybenzaldehyde, 2.1.(B) Schiff Base ligand synthesis, 2.1.(C) Metalation of salen schiff base, 2.1.(D) Surface Modification of SBA-15, 2.1.(E) Capping of SBA-15, 2.1.(F) Heterogenization of salen metal complex.

2.2.2.3. [L] Synthesis of chloro (S,S)(–)[N-3-tert-butyl-5-chloromethyl salicylidene]-N'-[3',5'-di tert-butyl salicylidene] 1,1'- binaphthyl-2,2'-diamine manganese(III)

To a stirred solution of S-(–)-1,1-binaphthyl -2,2-diamine (0.704 mmol, 200 mg) in 30 ml, 5-chloromethyl-3-tertbutyl-2-hydroxybenzaldehyde (1.05 mmol, 238.68 mg) and 3,5 di-tert-butyl-2-hydroxybenzaldehyde (0.35 mmol, 82.41 mg) were added with powder molecular sieves (200 mg) and excess amount of magnesium sulphate [50-70 mmol]. The resulting suspension was refluxed for 24 h and the solvent was evaporated in vacuum [Scheme 2.1(B)].[19,20] The crude mixture was dissolved in dry dichloromethane (DCM). Magnesium sulphate was removed by filtration and the pure deep orange ligand was obtained by evaporation to dryness. Deep orange colored crystals (75 % yield, 0.53 mmol, and 0.75 g) were obtained. On complexation with $(MnCH_3COO).4H_2O$ and its aerial oxidation in the presence of LiCl, this gives the complex Mn(III)-L [Scheme 2.1(C)]. ^{1}H NMR (200 MHz, $CDCl_3$), δ (ppm) - 1.22 (s, 18H); 2.1 (s, 9H); 4.32 (s, 2H); 6.9-7.3 (m, 14H); 7.5 (d, 2H); 8.65 (s, 2H); 11.55 (s, 2H). IR (KBr) cm^{-1}: 3420, 3050, 3000, 2956, 2909, 2863, 1650, 1629, 1501, 1430, 1388, 1335, 1276, 1209, 1155, 1032, 967, 927, 867, 806, 774, 744, 693.

2.2.2.4. Grafting of chloro (S,S)(–)[N-3-tert-butyl-5-chloromethyl salicylidene]-N'-[3',5'-di-tert-butyl salicylidene] 1,1'- binaphthyl-2,2'-diamine manganese(III) inside the –OH protected NH_2-SBA-15

The surface modified SBA-15 (2 g) was added to a solution of the unsymmetrical Schiff base (0.79 mmol, 560.8 mg) in dry toluene (25 ml) and the resulting suspension was refluxed for 48 h under inert atmosphere. The supported catalyst was filtered, washed thoroughly with dry toluene and diethyl ether and extracted repeatedly on a soxhlet extractor until the washing become colourless. The final material is designated as Mn(III)-L-SBA-15 [Scheme 2.1(F)].

2.2.3. INSTRUMENTS FOR CHARACTERIZATION

Powder X-ray diffractograms (XRD) of the materials were recorded using a PAN analytical X'pert Pro dual goniometer diffractometer. A proportional counter detector was used for low angle experiments. The radiation used was Cu Kα (1.5418

Å) with a Ni filter and the data collection was carried out using a flat holder in Bragg-Brentano geometry (0.5–5 °; 0.2 °min^{-1}). N_2 adsorption–desorption isotherms, pore size distributions as well as the textural properties of the hybrid materials were determined by using a Micromeritics ASAP 2020 instrument and Autosorb 1C Quantachrome USA. The program consisting of both an adsorption and desorption branch and typically ran at –196 °C after samples were degassed at 250 °C for 2 h. Specific surface areas were calculated via the BET model at relative pressures of P/Po = 0.06–0.3. A JEOL JEM-3010 and Tecnai (Model F30) both operating at 300 KV were used for HRTEM samples observation. Samples were crushed and dispersed in isopropenol with low power sonication before putting a drop over carbon coated Cu grid for observation. Chemical analysis was carried out in a Lab Tam 8440 Plasma lab sequential mode ICP–OES Spectrometer and a Spectro Arcos ICP–OES instrument. Standard solution was used for calibration purpose. The scanning electron micrographs of the samples were obtained in dual beam scanning electron microscope (FEI company, model Quanta 200 3D) operating at 30 kV. The samples were loaded on stubs and sputtered with thin gold film to prevent surface charging and also to protect from thermal damage due to electron beam.

^{1}H NMR spectra were recorded on Bruker AC–200 instruments using deuteriated solvent. Chemical shifts are reported in ppm. Liquid ^{13}C NMR spectra were recorded on Bruker AC–200 instruments operating at 50 MHz. ^{13}C NMR chemical shifts are reported in ppm relative to the central line of $CDCl_3$ (d 77.0). Solid-state ^{13}C CP MAS NMR and ^{29}Si MAS NMR spectra were recorded on a Bruker MSL 300 NMR spectrometer with a resonance frequency of 75.5 MHz and 59.6 MHz for ^{13}C and ^{29}Si, respectively, and the chemical shifts were referenced to glycine and TMS respectively. Infrared spectra were recorded using a Perkin Elmer, Spectrum one FTIR spectrophotometer. The liquid samples or dilute solution of the solid samples in THF were spread over KBr plates and their spectra were recorded. IR spectra were recorded in the range of 4000–400 cm^{-1}. Optical rotations were measured on a JASCO P–1030 Polarimeter. Thermal analyses (TGA–DTA) of the samples were conducted using a Pyris Diamond TGA analyzer with a heating rate of 10 ºC min^{-1} under air atmosphere.

2.3. Results and Discussions

2.3.1. Powder X-ray Diffraction (XRD)

The uniqueness of mesoporous structure, phase purity, degree of orderedness and unit cell parameters of all the siliceous and surface modified mesoporous materials were determined by powder X-ray diffraction (XRD). XRD pattern of the (a) calcined SBA-15, (b) as-synthesized SBA-15, (C) –OH protected NH_2-SBA-15 and (d) heterogenized salen Mn(III)-L-SBA-15 complex is visualized in Figure 2.1. The typical hexagonal phase of the SBA-15 [main (100), (200), and (210)] reflections

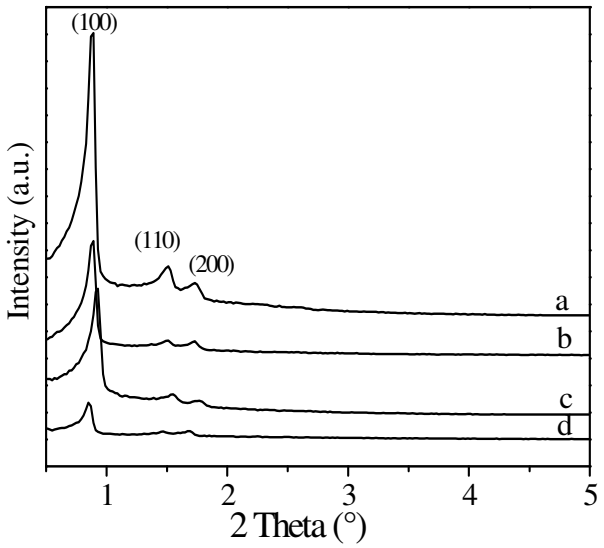

Figure 2.1. XRD pattern of (a) calcined SBA-15, (b) as-synthesized SBA-15, (C) -OH protected NH_2-SBA-15 and (d) Mn(III)-L-SBA-15.

are clearly visible in calcined SBA-15.[21] In all the samples, (110) reflection is more intense than the (200) reflection. As evident from the Figure 2.1. the XRD patterns of the samples synthesized after treatment with 3-APTMS and $(MeO)_2SiMe_2$ are almost similar to the parent SBA-15 sample with small decrease in overall intensity to the (100), (110) and (200) reflections. From the XRD pattern it is clear that after anchoring of the chiral complex Chloro (S,S)(–)[N-3-tert-butyl-5-chloromethyl salicylidene]-N′-[3′,5′-di-tert-butyl salicylidene] 1,1′-binaphthyl-2,2′-diamine manganese(III) an inconsequential decrease in peak intensities to the (100), (110) and

(200) reflections were observed without changing the peak positions.[22] This perseverance of peak positions indicates that, even the presence of a large amount of organic moieties by the partial filling of inside of the mesopores is less detrimental to the quality of the SBA-15 material. The persistence of the (100), (110) and (200) reflections not only proved the structural stability and existence of long range ordering to the mesophase but also the survival of undisturbed pore wall thickness even after a number of treatments with organic molecules in solvents under radical conditions. All the observations clearly show that the ordered mesoporosity and structural stability of the samples have retained after incorporation of organometallic complex.

2.3.2. FT-IR Spectra

The presence of isolated surface silanols, hydrogen bonded hydroxyl groups, anchored complex and amorphous structures of the wall are evidenced from the IR spectrum of the calcined SBA-15 and its modified samples. The FTIR spectra of the parent host material (a) SBA-15, (b) –OH protected NH_2-SBA-15, (c) immobilized Mn(III)-L-SBA-15 complex and (d) neat Mn(III)-L complex is shown in Figure 2.2. The ν –OH stretching vibrations observed in the 3600–3400 cm^{-1} region are attributed to the hydrogen-bonded silanol groups and the sharp band at 3740 cm^{-1} corresponds to the isolated surface silanol groups. Stretching vibrations of geminal silanols are also observed in the same region of isolated silanols; hence distinguishing these in the IR spectral patterns is very difficult.[23-26] In the present analysis, after 3-APTMS functionalization, complete disappearance of the isolated peak at 3740 cm^{-1} or a sharp decrease in its intensity with a peak shift to lower value is seen, demonstrating the role of surface silanols in modifications. Moreover, it is also observed that the intensity of the hydrogen-bonded silanol groups in the 3600–3400 cm^{-1} decreases after 3-APTMS and later on dimethoxydimethylsilane functionalization. Generally, the free and geminal silanol sites are the active silanol sites participating in the condensation reactions with the silylating agents, whereas the hydrogen bonded silanol groups do not actively participate due to the efficient hydrophilic networks

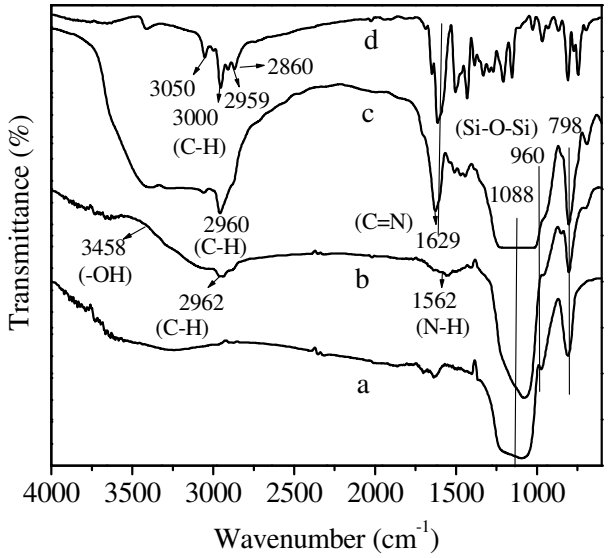

Figure 2.2. FT-IR spectrum of (a) calcined SBA-15, (b) -OH protected NH_2-SBA-15, (c) Mn(III)-L-SBA-15 and (d) neat Mn(III)-L complex.

formed among them. However, the present results imply that the hydrogen bonded silanol groups are also vulnerable in the reaction with aminopropyl groups. Anchoring of 3-APTMS groups and capping by dimethoxydimethylsilane in the pore channels of mesoporous materials is identified by the ethylene stretching bands in the 2950–2850 cm^{-1} regions from IR experiment.[27-29] The band at 1088 cm^{-1} is assigned to the asymmetric ν_{as} (Si–O–Si) vibrations and the band at 798 cm^{-1} is assigned to symmetric vibrations of (Si–O) SBA-15, while the band at 960 cm^{-1} is attributed to *v* (Si–OH) vibrations. Symmetric and asymmetric mode of (Si–O–Si) is clearly visible with the same intensity in all samples [figure 2.2. (a), (b) and (c)]. Absorption band at 960 cm^{-1} in the case of (b), (c), and (d) are assigned to (Si–O) mode of the Si–OH group.

After Mn(III)-L complex immobilization, the band due to N–H vibration gets disappeared with the formation of new band at 1629 cm^{-1}, which is characteristic stretching vibration of C=N band.[30,31] Specially these two results clearly indicate the anchoring of neat Mn(III)-L complex over the amino group of modified SBA-15 surface as shown in Scheme 2.1. In neat Mn(III)-L complex IR spectrum from *v* 1450–1600 cm^{-1} and *v* at 3000 to 3050 cm^{-1} correspond to C–C stretching and C–H

stretching vibrations, respectively indicating to the aromatic region of binaphthyldiamine as well as salicyaldehyde unit of chiral Schiff base.[32] Thus, all the results indicate chiral salen Mn(III)-L complex was incorporated to the modified wall of SBA-15 successfully.

2.3.3. Thermal Analyses

The thermal stability of synthesized catalysts was studied by thermo gravimetric analysis in air atmosphere from ambient temperature to 1000 °C with a temperature ramp of 10 °C min^{-1}. As evident from Figure 2.3A, The TGA curve of as-synthesized SBA-15 [Figure 2.3.A(a)] shows weight loss in one step only and DTA curve of (Figure 2.3.B) as-synthesized SBA-15 shows one exothermic peak in the same region of temperature 170–220 °C which is attributed to the removal of surfactant (triblock–copolymer) from the as-synthesized SBA-15. Whereas, in the case of calcined SBA-15 Figure 2.3.B.(b), sharp peak in the range of 170–220 °C is not visible in DTA pattern; which clearly supports complete removal of surfactant from the SBA-15 channels.[33] TGA results shows that only 7 % weight loss is observed in calcined SBA-15 whereas in case of as-synthesized SBA-15, 43.16 % weight loss was observed. All data are evidently supporting the fully removal of organic surfactant from as-synthesized SBA-15.[34,35] In –OH protected NH_2-SBA-15 sample TGA result Figure 2.3.A(c) showing three step of weight loss. In the first step, weight loss between 70 and 150 °C corresponds to the loss of loosely bounded water, adsorbed moisture. In the second step weight loss was observed in the region of 250–350 °C. TGA analysis and a sharp visible exothermic peak in DTA analysis in the same temperature region (250-350 °C) is attributed to the decomposition of 3-APTMS (amino functionalized). Third weight loss step visible in TGA analysis, in the region of 380–450 °C corresponds to removal of dimethoxydimethylsilane [$(MeO)_2SiMe_2$] which is evidently supported by DTA analysis showing one strong exothermic peak in the sample temperature range. TGA result of –OH protected NH_2-SBA-15 quantitatively shows ~21.27 % weight loss, which is greater than calcined SBA-15; strongly supports the successful anchoring of 3-APTMS and [$(MeO)_2SiMe_2$] group over SBA-15.

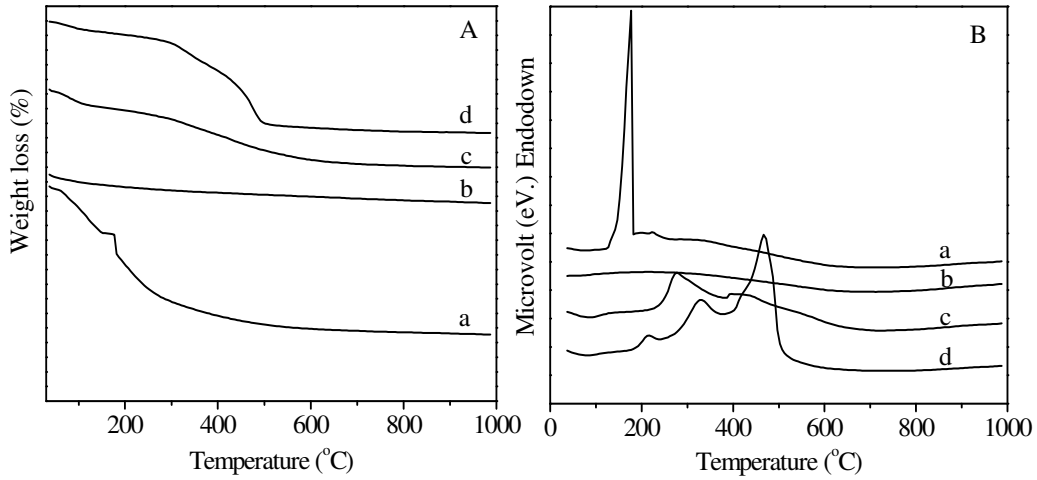

Figure 2.3. TGA (A) and DTA (B) pattern of (a) as-synthesized SBA-15, (b) calcined SBA-15, (c) –OH protected NH_2-SBA-15 and (d) Mn(III)-L-SBA-15.

In the case of heterogenized metal complex [Mn(III)-L-SBA-15] one extra peak was observed along with two peaks shown in capped amino functioned SBA-15, in the region of 400–510 °C assigned to salen [Mn(III)-L] complex. Note that decomposition of Mn(III)-L complex occurred at elevated temperature revealing the high thermal stability of complex. Direct comparison of weight loss between heterogenized complex Mn(III)-L-SBA-15 (35.62 % weight loss), and capped amino functionalized SBA-15 (21.24 % weight loss) shows 14.3 % loading of chiral salen complex over SBA-15. All these results show that the Mn(III)-L-SBA-15 is formed and principally located, inside the SBA-15 pore channels.

2.3.4. Electron Microscopy

TEM micrograph of the SBA-15 revealed the hexagonally arranged pore structure when viewed along the pore direction, along with parallel lattice fringes on a side view analysis. The shown TEM images confirm the SBA-15 having 2D p6 mm hexagonal structure (Figure 2.4.).[14,15] The ordered mesoporous structure of the support was unaffected by anchoring of Mn(III)-L salen complex. SEM micrograph revealed that SBA-15 sample consist of small agglomerate whose morphology does

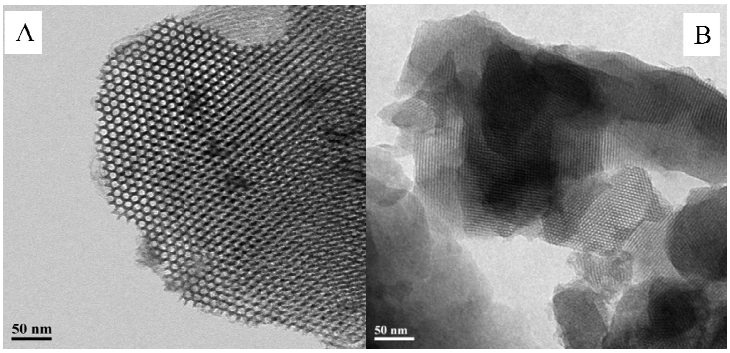

Figure 2.4. TEM images of (A) calcined SBA-15 and (B) Mn(III)-L-SBA-15.

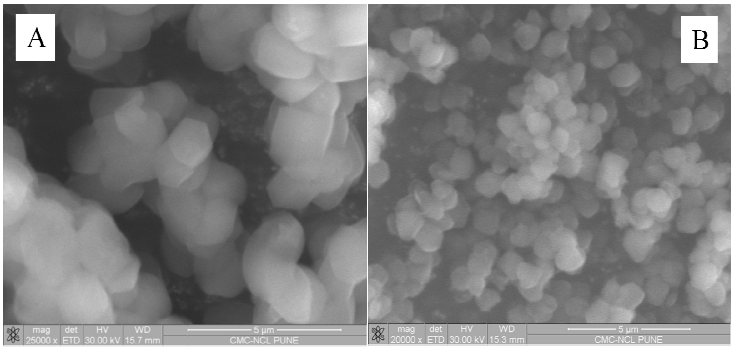

Figure 2.5. SEM images of (A) calcined SBA-15 and (B) Mn(III)-L-SBA-15.

not change in the supported catalyst Mn(III)-L-SBA-15. Calcined SBA-15 shows the hexagonal structure with uniform in particle size (Figure 2.5). The uniformity of the particle size gets reduced after the grafting of various organic moieties on the inner pore wall of the SBA-15, indicating that the various treatments can affect the morphology of the SBA-15.

2.3.5. ^{13}C CP MAS NMR Study

In the solid state ^{13}C CP MAS NMR spectra of NH_2-SBA-15, –OH protected NH_2-SBA-15 and Mn(III)-L-SBA-15 the peak observed at 8.6 ppm can be accounted for carbon atom bonded to the silicon. The signal at 21 ppm corresponding to methylene carbon (C_2) and signal at 42.7 ppm can be attributed to the carbon atom attached to NH_2 group (Figure 2.6.1.). After –OH group of NH_2-SBA-15 protection

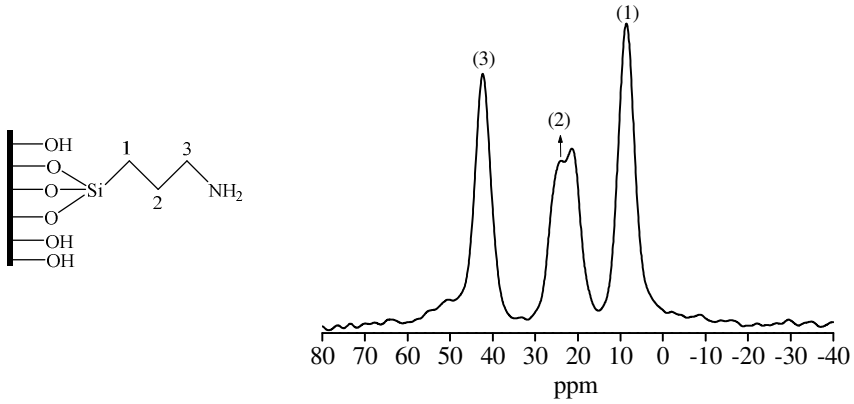

Figure 2.6.1. Solid-state ^{13}C MAS NMR spectrum NH_2-SBA-15.

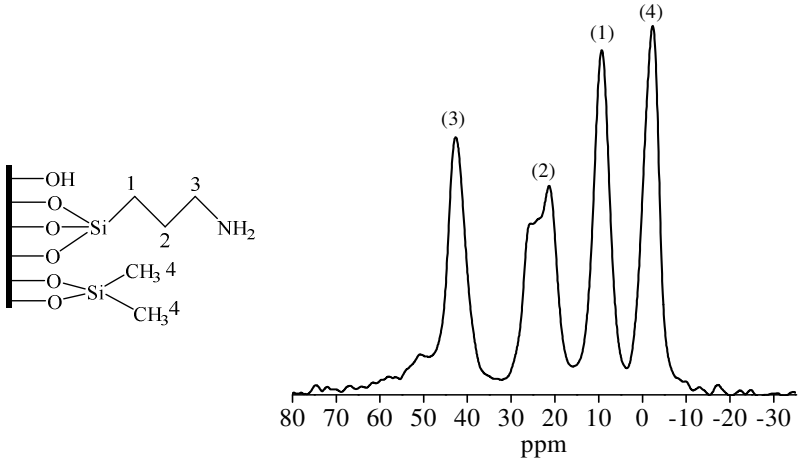

Figure 2.6.2. Solid-state ^{13}C MAS NMR spectrum –OH protected NH_2-SBA-15.

by dimethoxydimethylsilane, along with all three peak of NH_2-SBA-15, one extra peak is clearly visible at 2.2 ppm corresponds to methyl group from the capping agent, dimethoxydimethylsilane (Figure 2.6.2.). No peaks was observed for the methoxy group which confirms that all the methoxy groups were hydrolysed and attached over the support and confirm the successful anchoring of 3-APTMS. Grafting of binaphthyl salen ligand is confirmed by the presence of new resonance in the ^{13}C CP/MAS NMR spectrum of Mn(III)-L-SBA-15. First in the 112–170 ppm region, distinct peaks are observed corresponds to aromatic region of binaphthyl group and salicyaldimine groups.

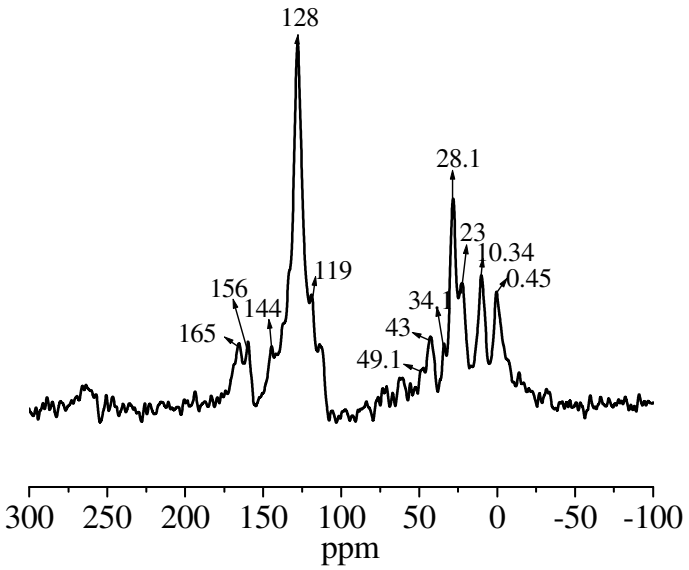

Figure 2.6.3. Solid-state ^{13}C MAS NMR spectrum of Mn(III)-L-SBA-15.

Moreover in the region of 0–50 ppm, additional two resonance peaks at 28.1 and 34.1 ppm were observed after anchoring of metal complex (Figure 2.6.3.), which attributed to the methyl carbon of t-butyl and t-butyl carbon of (salicyaldimine groups), respectively. Whereas one shoulder peak at 49.1 ppm correspond to carbon, which is directly attached to linker group of NH_2. All the observed data clearly demonstrating the successful anchoring of salen binaphthyl Schiff base complex to modified solid surface of SBA-15.

2.3.6. ^{29}Si CP MAS NMR Study

^{29}Si MAS NMR of surfactant-extracted, mesoporous organofunctionized SBA-15 exhibit peaks at –112, –102, –67 and –60 ppm which are usually assigned to Q^4 [$Si(OSi)_4$, siloxane], Q^3 [$Si(OH)(OSi)_3$, single silanol], T^3 [$SiR(OSi)_3$] and T^2 [$Si(OH)R(OSi)_2$] sites, respectively (Figure 2.7.).The unmodified SBA-15 sample shows a broad resonance peaks from –93.89 to –102.91 ppm, indicative for a range of Si–O–Si bonds and it is noteworthy that the sample contains large amounts of Q^4 sites showing a high framework cross-linking. Compared with calcined SBA-15, amine-functionalized SBA-15 show decrease in Q^2 and Q^3 site with a corresponding increase

in the percentage of Q^4 sites, demonstrating that the silylating agents effectively consume the geminal as well as the free silanol sites.[36-37] In general, Q^3 sites are considered to be rich with isolated Si–OH groups, which may be free or hydrogen-bonded, whereas Q^2 sites have the geminal silanol sites. A decrease in Q^3 values after silylation over all of the support materials shows that these silanol groups are highly accessible to the silylating agents.

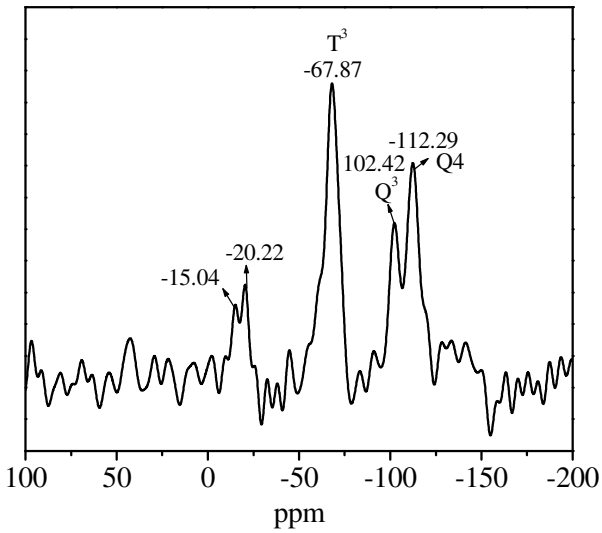

Figure 2.7. Solid-state ^{29}Si MAS NMR spectrum of Mn(III)-L-SBA-15.

The 3-APTMS functionalized SBA-15 shows additional peaks at –68.48 ppm. and at –60.87 ppm which are assigned to T^3 [$SiR(OSi)_3$] and T^2 [$Si(OH)R(OSi)_2$] sites, respectively (Figure 2.7.). The decreased T^2/T^3 ratio in NH_2-SBA-15 shows that more silanes are linked to each other than in the pore channels of NH_2-SBA-15. After protection of –OH group in NH_2-SBA-15 by dimethoxydimethylsilane, it is clearly visible that T^2 site [$Si(OH)R(OSi)_2$] disappeared along with the appearance of new peak of dimethoxydimethylsilane at –22.36 ppm. With this two significant changes evidently proved the free silanol group of NH_2-SBA-15, the T^2 site [$Si(OH)R(OSi)_2$] get blocked by the condensation with methoxy group of dimethoxydimethylsilane (capping agent). Whereas after anchoring with Mn(III)-L complex one significant

difference was observed in the peak of dimethoxydimethyl silane at –22.36 ppm which splits into two peak may be due to the methyl groups which are attached to Si (capping agent dimethoxydimethylsilane) experience the different electronic environment around it. All these Si NMR results supporting the successful formation of SBA-15 and its modification along with anchoring of Mn(III) salen complex.

2.3.7. X-ray Photoelectron Spectra (XPS)

X-ray photoelectron spectroscopy (XPS) is the powerful tool to investigate the electronic properties of the species formed on the surface, such as the electronic environment, e.g. oxidation state and or /multiplicity influences the binding energy of the core electron of the metal. Both of the Mn(III)-L-SBA-15 and homogeneous catal-

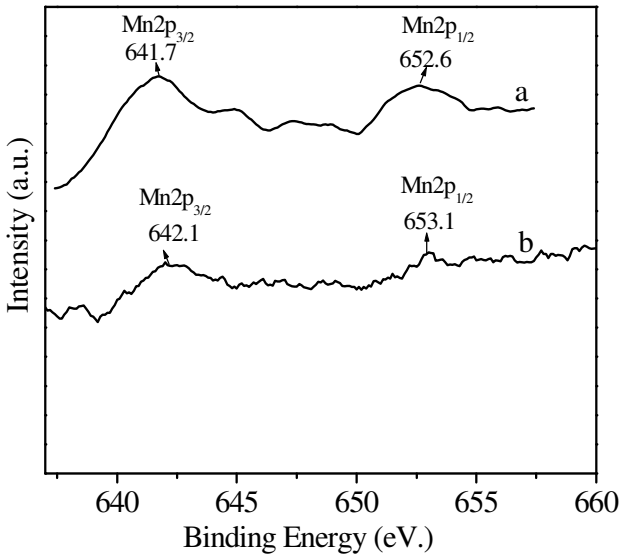

Figure 2.8. XPS spectra of (a) $Mn2p_{3/2}$ Mn(III) and (b) $Mn2p_{1/2}$ Mn(III) binding energy.

-ysts were characterized by XPS analysis. The accuracy of the measured binding energy (BE) was ±0.3 eV. The spectrum was given in Figure 2.8. In heterogeneous catalyst Mn(III)-L-SBA-15, XPS spectra showing two clear band at 641.7 eV and at 652.6 eV, which corresponds to Mn(III)$2p_{3/2}$ and Mn(III)$2p_{1/2}$ binding energy of the Mn metal respectively; whereas in homogeneous neat catalyst [Mn(III)-L], XPS

spectra showing two resolved peaks at 642 eV. and 653.1 eV.[38] This indicates the oxidation state of Mn ion is +3 in both of the catalysts (Figure 2.8.). The binding energies of Mn(III)$2p_{3/2}$ in the homogeneous Mn(III)-L catalyst and the anchored catalyst, Mn(III)-L-SBA-15 are 642.0 and 641 eV., respectively (Figure 2.8.). The difference in the binding energy between them is the result of the anchored ligand strongly coordinating with Mn^{3+} compared to the Mn(III)-L. The strong coordination ability can increase the electron density around the Mn ion, which decreases the binding energy of the ion. In the N 1s region of homogeneous Mn(III)-L as well as heterogeneous catalyst Mn(III)-L-SBA-15, there is only one broad band observed at BE = 399.3 eV, typical of sp^2 C=N bond and assigned to the nitrogen of the C=C aromatic ring.[39,40]

2.3.8. UV-Vis Spectra

The UV-Vis spectra of neat chiral salen Mn(III)-L complex and heterogenized chiral salen Mn(III)-L-SBA-15 complex are shown in Figure 2.9. Typically, Mn(III) salen complexes show charge transfer transition of salen ligand at ~ 335 nm, ligand to metal (LMCT) charge transfer transition at ~ 430 nm and d-d transition at ~500 nm.[41]

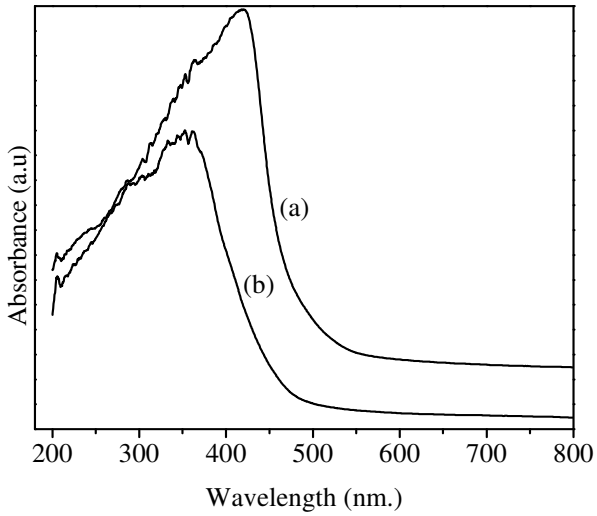

Figure 2.9. UV–vis spectra (a) neat Mn(III)-L complex, (b) heterogeneous Mn(III)-L-SBA-15 catalyst.

However, in the present study, all the three absorption bands of Mn(III)-L are overlapped and show a broad electronic transition from 300–530 nm region. Similar absorption bands were also noticed for the heterogenized chiral complex [Mn(III)-L-SBA-15]. reported by *J. Hu et al.,* [42] . Pure siliceous mesoporous materials (MCM-41 and SBA-15) usually show absorption in the UV region at ~220 nm. The blue shift absorption between 200 to 470 nm in the case of Mn(III)-L-SBA-15 compared to neat Mn(III)-L complex clearly shows the strong coordination of neat chiral metal complex over amino functionalized SBA-15. This result is supported by the XPS binding energy shift due to the complexation of metal with ligand.

2.3.9. Nitrogen Sorption Studies

The nitrogen adsorption–desorption results of calcined SBA-15 and Mn(III)-L-SBA-15 samples and their corresponding pore size distribution curves are plotted in Figure 2.10. N_2 adsorption-desorption isotherms of both the samples show Type IV isotherms, According to IUPAC classification, type IV isotherms relate to capillary condensation steps, characteristic of the mesoporous materials (20–500 Å), with completely reversible nature, uniformly sized mesopores.[15] The surface area, average pore diameter and the pore volume observed for the calcined SBA-15 and Mn(III)-L-SBA-15 samples are summarized in Table 2.1. It is well known that the introduction of homogenous catalysts or metals on porous supports shows a decrease in its specific surface area and pore volume. The support, mesoporous calcined SBA-15 shows a high surface area of 665 m^2/g and pore volume of 2.1 cm^3/g (Figure 2.10.). After metal complex functionalization, the surface area gets reduced to 232 m^2/g and pore volume reduced to 0.437 cm^3/g for Mn(III)-L-SBA-15 samples (Table 2.1.). Thus, the decrease in total mesoporous pore volume (20.55 %) and surface area (34.88 %) after metal immobilization is indicative of the grafting of metal complex inside the channels of mesoporous calcined SBA-15 (Table 2.1.). It is clear from Table 1 that even though silylation procedures changed the textural properties of the mesoporous material, the decrease is more prominent after complex immobilization and due to the presence of bulkier organic moieties inside the pore channel of the support. In detail,

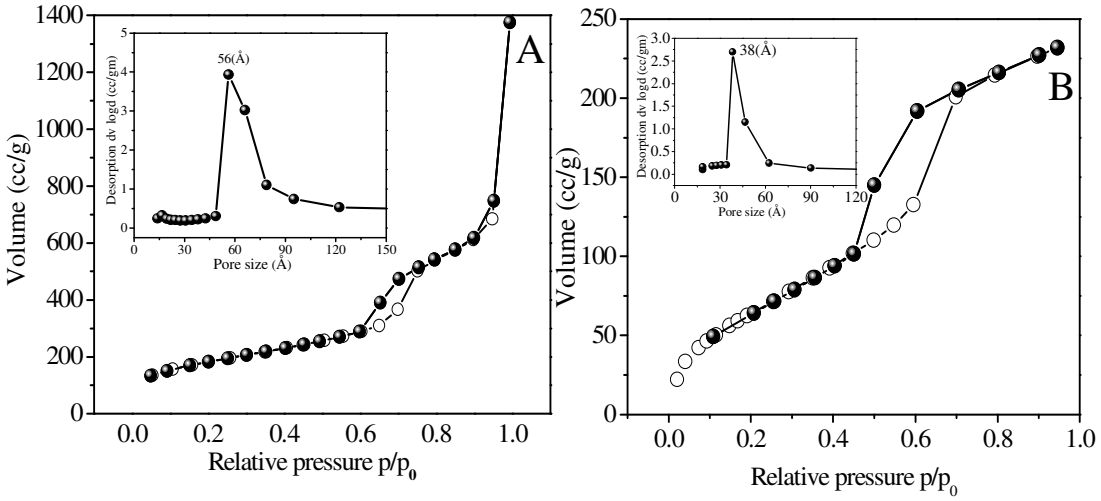

Figure 2.10.(A) Nitrogen adsorption–desorption isotherm and pore size distribution of (inset) calcined SBA-15, **Figure 2.10.(B)** Nitrogen adsorption-desorption isotherm and (BJH) pore size distribution (inset) of Mn(III)-L-SBA-15.

Table 2.1.

Textural properties of mesoporous calcined SBA-15 and Mn(III)-L-SBA-15.

Sample	BET surface area (m^2/g)	Pore diameter (Å)	Pore volume (cm^3/g)
Calcined SBA-15	665	56	0.4397
Mn(III)-L-SBA-15	232	31	0.3043

the mesoporous SBA-15 support shows an inflection in the *P*/*P*o ~0.6 range, while after complex immobilization, the *P*/*P*o value changed to a lower value of ~0.5, indicative of some sort of structural damage to the material after modifications and are consistent with the XRD results. Moreover, the BJH pore size distribution analysis shows that the material posses uniformly sized mesopores centered at ca. 56 Å for SBA-15 support and centered at 31 Å for the metal complex functionalized samples.

2.3.10. Catalytic Activity

2.3.10.1. Catalytic Oxidation of Sulfide

Oxidation reaction was carried out in 10 ml flask equipped with magnetic stirrer. The flask was charged with 3 mL of solution or suspension of the catalyst [15 mg Mn(III)-L complex (neat homogeneous complex) or 50 mg Mn(III)-L-SBA-15 (heterogeneous catalyst)] in dichloromethane (DCM). After stirring for 15 minutes, methyl phenyl sulfide (2 mmol) along with oxidant 3 mmol (TBHP or H_2O_2) were added with continuous stirring. Chemical yield and enantiomeric excess (ee) were measured by GC/MS and polerimeter.

The synthesized and characterized materials neat Mn(III)-L complex and Mn(III)-L-SBA-15 were applied for the liquid phase sulfoxidation of methyl phenyl sulfide with TBHP as an oxidant at room temperature (25 °C). To determine the performance of the synthesized catalysts, catalytic properties were compared from the conversion profiles of the three different systems; over Neat Mn(III)-L complex, Mn(III)-L-SBA-15 and the blank reaction (without any catalyst). The immobilized Mn(III)-L-SBA-15 shows enhanced catalytic activity with 94 % conversion of thioanisole along with 95 % selectivity towards sulfoxide (main product) in 5 h (Table 2.2.). The immobilized metal complex followed the different reaction pathway, which lead to neat selective oxygen transfers reaction. In terms of time period, the reaction time increases from 1 h for homogeneous metal complex to 5 h for heterogenized complex. This strongly suggests that the reaction took place in the pores where the presence of oxidant and substrate are regulated by the pore size. Also the heterogeneous catalyst (Mn(III)-L-SBA-15 complex) enhances enantioselectivity (ee) (2 %) whereas only 0.5–1 % enatioselectivty was obtained in the case of homogeneous catalyst (Neat Mn(III)-L complex). To explain the poor enantioselectivty[12] of thioanisole sulfoxidation reaction products, the obtained results agrees with the previous data of the binaphthyl based salen type complexes. According to "*Katia bernardo, Simon Leppard et al"*. The unexpected poor enantioselectivity of the binaphthyl based manganese complex as oxidation catalysts is due to its steric hindrance near the reactive site of metal which is not favourable for accessing the TBHP and H_2O_2 oxidizing agents.[43,44] One more possible explanation

for the poor catalytic activity in terms of enantioselectivity is that, in spite of chiral manganese environment, the highly distorted geometry of the salen binaphthyl

Table 2.2.

Oxidation of thioanisole by supported Mn(III)-L-SBA-15 and Neat Mn(III)-L catalysts.

S. No.	Catalyst	Time (h)	Conversion (%)	Selectivity to sulfoxide (%)	TON[d]
1.	No catalyst	12	20	55	-
2.	Neat Mn(III)-L complex	1	93	61	132.8
3.	Mn(III)-L-SBA-15	5	94	95	152.3
4.	Mn(III)-L-SBA-15[a]	5	70	77	113.4
5.	Mn(III)-L-SBA-15[b]	5	40	82	64.0
6.	Mn(III)-L-SBA-15[c]	2	95	63	153.9

Reaction condition: catalyst amount =50 mg (heterogeneous catalyst), 15 mg (homogeneous catalyst); thioanisole = 2 mmol; TBHP = 2.5 mmol; DCM = 2 ml; reaction temperature = 25 °C (room temperature).
[a] with anhydrous TBHP.
[b] with H_2O_2 oxidant.
[c] At 35 °C temperature.
[d] Turn over number is calculated by the expression moles of substrate converted per mole of metal.

ligands, more compatible with tetrahedral rather than octahedral or square-pyramidal coordination. Further in order to evaluate the importance of oxidant we had probed the catalytic activity with different oxidant such as TBHP (70 %), anhydrous TBHP and H_2O_2 for sulfoxidation reaction by using Mn(III)-L-SBA-15 as a catalyst (Table 2.2.). In the case of H_2O_2 as an oxidant sulfoxidation of thioanisole gives only 40 % conversion which is not appreciable results. Although H_2O_2 is an environmentally benign oxidant, the activation energy required for thioanisole oxidation is high. Whereas TBHP enhances the catalytic activity to many folds (94 %) in sulfoxidation reaction (table 2.2.). In the case of anhydrous TBHP, thioanisole oxidation product

observed was 70 % in the same time period (5 h) but not remarkable changes were observed towards selectivity of sulfoxide (Table 2.2.). The sulfoxidation of thioanisole reaction is remarkably influenced by reaction temperature as examined at different temperature 25 °C and 35 °C (Table 2.2.). At higher temperature thioanisole conversion was enhanced at the cost of decreased selectivity towards sulfoxide (63 %). In the series of catalytic activity, epoxidation of 1,2 dihydronaphthalene (1 mmol) was also performed over neat Mn(III)-L complex (15 mg) and Mn(III)-L-SBA-15 (50 mg) for 30 h at 40 °C in dichloromethane (2 mL) using TBHP (3.5 g) as an oxidant and pyridine-N-oxide (123 mg) as an axial oxidant. The conversion of 1, 2 dihydronaphthalene was found to be 60 %. Selectivity towards 1, 2-dihydronaphthalene epoxide and TON over Mn(III)-L-SBA-15 were found to be 83 % and 48.62 %, respectively. In the absence of the catalyst, no epoxide of 1, 2-dihydronaphthalene was detected. In terms of enatioselectivity (ee), immobilized Mn(III)-L-SBA-15 complex catalyzed reaction gave 5 % (ee), where as Mn(III)-L gave 3 % (ee). The lower reaction rates obtained with the Mn(III)-L-SBA-15 catalysts compared to homogeneous counterpart could have been anticipated in the view of the restrictions imposed on the diffusion substrate and products through the micropores of the solid.

2.3.11. Recycling Studies

In order to verify whether the observed catalytic activity arises due to heterogeneous catalysis; the Mn(III)-L-SBA-15 was recovered from the methyl phenyl sulfide reaction mixture after completion of the sulfoxidation reaction by simple centrifugation. The recovered catalyst was washed thoroughly with dichloromethane and dried in vacuum for 6 h before reuse. The stability of metal complex Mn(III)-L-SBA-15 was tested two times (fresh + one cycle) in the sulfoxidation reaction. The conversion of thioanisole decreased from 90 % to 71 % from fresh first cycle. The difference in the conversion (~20 %) between fresh and 1st recycle may be due to the leaching of some of the chiral metal complex in oxidizing condition, Further, recyclability test was done up to 4th cycle and result shows almost similar conversion and selectivity from 2nd to 4th cycles (~71 % conversion at the end

of 4th cycle). The observed reactivity data supporting the heterogeneity of the synthesized catalyst Mn(III)-L-SBA-15. The ICP analysis of the filtrate after the catalytic reaction shows the loss of Mn element from the heterogeneous catalyst Mn(III)-L-SBA-15 is less than 2 % compared with the total amount of the Mn(III)-L complex grafted over the modified surface of the SBA-15.

2.4. REFERENCES

[1] M. Dusi, T. Mallat, A. Baiker, *Catal. Rev. Sci. Eng.* **2000**, 42, 213.

[2] I. W. C. E. Arends, R. A. Sheldon, *Appl. Catal. A.* **2001**, 212, 175.

[3] a) T. Katsuki, *J. Mol. Catal. A: Chem.* **1996**, 113, 87; b) T. Katsuki, *Coord. Chem. Rev.* 1995 **140,** 189.

[4] L. Canali, D.C. Sherrington, *Chem. Soc. Rev.* **1999,** 28, 85.

[5] N. E. Leadbeater, M. Marco*, Chem. Rev.* **2002,** 102, 3217.

[6] Q. H. Fan, Y. M. Li, A. S. C. Chan, *Chem. Rev.* **2002,** 102, 3385.

[7] C. Bianchini, P. Barbaro, *Top. Catal.* **2002,** 19, 17.

[8] E. Song, S. G. Lee, *Chem. Rev.* **2002,** 102, 3495.

[9] P. M. Morn, G. Hutchings, *J. Chem. Soc. Rev.* **2004,** 33, 108.

[10] C. Li, *Catal. Rev. Sci. Eng.* **2004,** 46, 419.

[11] A. R. Silva, C. Freire, B. D. Castro, *New. J. Chem.* **2004,** 28, 253.

[12] K. C. Gupta, A. Kumar Sutar, *Coord. Chem. Rev.* **2008,** 252, 1420.

[13] C. M. Che, J. S. Huang, *Coord. Chem. Rev.* **2003,** 242, 97.

[14] J. Y. Ying, C. P. Mehnert, M. S. Wong, *Angew. Chem. Int. Ed.* **1999,** 38, 56.

[15] D. Zhao, J. Feng, Q. Huo, N. Melosh, G. H. Fredrickson, B. F. Chmelka, G. D. Stucky, *Science. VOL.* **1998,** 279, 548.

[16] R. I. Kureshy, A. H. Khan, K. Pathak, V. Jasra, *Tetra. Asymm.* **2005**, 16, 3562.

[17] M. F. Pini, A. D. Petri, P. Salvadori, *Tetra Asymm.* **1996,** 7, 2293.

[18] L. Canali, E. Cowan, H. Deleuze, C. L. Gibson, D. C. Sherrington, *J. Chem. Soc. Perkin Trans.* **2000,** 1, 2055.

[19] C. Baleizão, B. Gigante, M. J. Sabater, H. Garcia, A. Cormab, *App. Catal. A. Gen.* **2002,** 228, 279.

[20] K. Bernardo, S. Leppard, A. Robert, G. Commenges, F. Dahan, B. Meunier,

Inorg Chem. **1996,** 35, 387.

[21] C. Yu, B. Tian, J. Fan, G. D. Stucky, D. Zhao, *J. Am. Chem. Soc.* **2002,** 124, 4556.

[22] G. J. de, A. A. Soler-Illia, C. Sanchez, B. Lebeau, J. Patarin, *Chem. Rev.* **2002**, 102, 4093.

[23] M.D. Alba, Z. Luan, J. Klinowski, *J. Phys. Chem.* **1996,** 100, 2178.

[24] T. Ishikawa, M. Matsuda, A. Yasukawa, K. Kandori, S. Inagaki, T. Fukushima, S. Kondo*, J. Chem. Soc. Faraday Trans:* **1996,** 92, 1985.

[25] Jentys, N.H. Pham, H. Vinek, *J. Chem. Soc. Faraday Trans:* **1996,** 92 3287.

[26] T.W. Dijkstra, R. Duchateau, R.A. van Santen, A. Meetsma, G.P.A. Yap, *J. Am. Chem. Soc:* **2002,** 124, 9856.

[27] X. Wang, Y. H. Tseng, J. C. C. Chan, S. Cheng, *J. Catal.* **2005**, 266.

[28] A. B. Bourlinos, T. Karakoatas, D. Petridis, J. *Phys. Chem. B.* **2003,** 107, 920.

[29] H. Yoshitake, T. Yokoi, T. Tatsumi, *Chem. Mater.* **2002,** 14, 4603.

[30] P. Karandikar, M. Agashe, K. Vijaymohanam, A. J. Chandwadkar, *Appl. Catal. A Gen.* **2004,** 257, 133.

[31] X. G. Zhou, X. Q. Yu, J. S. Huang, S. G. Li, L. S. Li, C. M. Che, *Chem. Comm.***1999,** 1789.

[32] K. Yu, Z. Gu, R. Ji, L. L. Lou, F. Ding, C. Zhang, S. Liu, *J. of Cat.* **2007,** 252, 312.

[33] M. Chidambaram, A. P. Singh, *App. Cat. A: Gen.* **2006,** 310, 79.

[34] S. Shylesh, A. P. Singh, *J. Catal.* **2004,** 228, 333.

[35] S. C. Laha, P. Mukherjee, S. R. Sainkar, R. Kumar, *J. Catal.* **2002,** 207, 213.

[36] A. Rosa Silva, C. Freire, B. de Castro, *New. J. Chem.* **2004,** 28, 253.

[37] H. Yoshitake, T. Yokoi, T. Tatsumi, *Chem. Mater.* **2002,** 14, 4603.

[38] G. Zampieri, M. Abbate, F. Prado, A. Caneiro, *Solid State Comm.* **2002,** 123, 81.

[39] C. Li, C. B. Cao, H. S. Zhu, *Mater. Lett.* **2004,** 58, 1903.

[40] I. K. Biernacka, *J. of Mol. Catal. A: Chem.* **2007,** 278, 82.

[41] J. Hu, Kexin Li, W. Li, F. Ma, Y. Guo, *App. Catal. A: Gen*. **2009,** 364, 211.

[42] I. Domínguez, V. Fornés, M. J. Sabater, *J. of Catal*. **2004**, 228, 92.

[43] K. Bernardo, S. Leppard, A. Robert, G. Commenges, F. Dahan, B. Meunier, *Inorg. Chem.* **1996**, 35, 387.

[44] C. W. Ho, W. C. Cheng, M. C. Cheng, S. M. K. Cheng, *J. Chem. Soc. Dalton Trans.***1996**, 405.

CHAPTER-3

Phosphine Free SBA-15-EDTA-Pd Highly Active Recyclable Catalyst for Heck, Suzuki and Sonogashira Reactions

3.1. INTRODUCTION

There are several homogenous metal complexes widely used for organic transformation; however, separation and recycling of the homogeneous catalysts rather expensive and impart difficulties. Heterogenization of such homogenous catalysts on solid supports can mitigate these problems. Furthermore, heterogeneous catalysts have clear advantages over their homogeneous counterparts, which can be easily separated from the reaction medium. "Heterogeneous catalytic system includes polymer/dendrimer supported palladium catalysts, palladium on carbon, palladium supported metal oxides, clays and molecular sieves.[1]" Since the synthesis of ordered mesoporous materials in 1992 sparked worldwide interest in the field of heterogeneous catalysis and separation science; SBA-15 has become the most popular member of the group, which possessed extremely high surface areas, easily accessible uniform pore sizes and stability.[2]

To extent the applicability of SBA-15 materials, it is necessary to modify the surface by organic functional groups for anchoring metals and metal complexes. Grafting of functional organosilanes by using surface hydroxyl groups as anchor points has been widely used. Furthermore, the leaching of the active site can also be avoided as the organic moieties are covalently attached to the inorganic support.

Palladium complexes with or without phosphine ligands can catalyze the C-C coupling reactions. The phosphine-assisted approach is the classical and well-established methods,[3] which gives excellent results in a majority of cases; whereas phosphine ligands are expensive, toxic, and unrecoverable and also a major drawback of the phosphine ligands in a catalytic reaction is the oxidation of phosphine to a phosphine oxide as well as cleavage of the P–C bond, causing degradation of the catalytic cycle. In large scale industrial applications, the phosphines might be a more serious economical burden than even palladium itself, which can be recovered at any stage of production or from wastes. Therefore, the development of phosphine free catalysts for C-C bond-forming

reactions would be an important topic of interest of the current industrial research.[4]

The accurate selection of the ligands for the complex synthesis is the key factor for the synthesis of the complex. Recently a number of nitrogen base compounds in phosphine free condition were commonly used as a ligand such as C based heterocyclic carbenes, C-N based 2-aryl-2-oxazolines, aryl (hetroaryl) oximes, arylimines, N, N-based diazobutadienes, DMG and salen complexes.[5] However, these ligands are not easily available and contain tedious and expensive synthesis processes and hardly stable in catalytic systems. Therefore, simple easily accessible stable catalyst is desired for the high temperature reactions.

Cross coupling reactions are one of the broadest area for the synthesis of symmetrical and unsymmetrical binary compounds, which are the key components of the several natural products as well as in the field of engineering materials, such as conducting polymers, molecular wires and liquid crystals.[6] Among the basic types of palladium catalyzed transformations, Suzuki, Sonogashira and Heck reactions related chemistry occupied a special place.[7] The Suzuki cross-coupling reaction of organo-boron reagents with organic halides represents one of the most versatile and straightforward methods for carbon-carbon bond formation. The reaction is largely unaffected by water, tolerating a large range of functionality and yielding non-toxic by-products. Furthermore, Sonogashira coupling of phenyl acetylenes and aryl halides is one example of palladium catalyzed reaction that allows connecting a C≡C triple bond substituent in an aromatic ring. Palladium catalyzed Mizoroki-Heck reaction of olefin and aryl halide is one of the most fundamental reactions for carbon-carbon bond formation in organic synthesis. Several reports have been published on the Heck reaction for the synthesis of symmetrical and unsymmetrical binary compounds; which are the key components of the several natural products as well as in the field of engineering materials, such as conducting polymers, molecular wires and liquid crystals.[8]

In 2005, *Korolev et. al.* described the synthesis of $PdCl_2$–EDTA complex as a homogeneous catalyst for the Suzuki–Miyaura reactions in water.[9] However, this catalytic system was not stable enough to store for longer time period and unfortunately, no catalyst recovery was possible. In this context, we decided to immobilize the Pd-complex over the surface of organo-functionalized SBA-15 in order to recycle the catalyst. Herein, we report grafting of Pd-EDTA complex, and its derivatives into SBA-15 phases and their catalytic properties in Heck, Suzuki and Sonogashira coupling reactions as heterogeneous catalyst. The immediate goals of our study were (i) to evaluate the heterogenization method of the Pd-ethylenediaminetetraacetic acid complex over organo-modified mesoporous SBA-15 support, (ii) to measure the catalytic properties in Heck, Suzuki and Sonogashaira C-C coupling reaction (iii) to optimize the reaction parameter such as temperature, solvent and base in the both coupling reaction, (iv) to determine the extent of stability of the catalysts as well as their recycling properties.

3.2. EXPERIMENTAL

3.2.1. Synthesis Procedure of Catalyst

SBA-15 was synthesized according to the reported procedure using tri-block P_{123} as a template under acidic conditions.[9] Pluronic 123 (2 g) was dissolved in a solution of HCl (60 mL of 2.0 M) and H_2O (60 mL). The solution was stirred at 38 ºC for 1 h. After that time, tetraethylorthosilicate (TEOS) was added, and the resultant solution was left stirring at 38 ºC for further 4 h and then aged at 100 ºC for 24 h. Surface modification of SBA-15 was achieved by a post synthesis grafting method [scheme 3.1(A)]. One gram of SBA-15 was suspended in a 100 ml of dry toluene and refluxed with 2.5 mmol of 3-aminopropyltrimethoxysilane (3-APTMS) for 8 h under N_2 atmosphere. The material was filtered after cooling to ambient temperature, washed with dry toluene and dichloromethane. Soxhlet extraction was carried out for 24 h in dichloromethane (DCM) to remove occluded organosilane. The sample was dried in vacuum for 10 h. The obtained material is designated as NH_2-SBA-15.

The free –OH groups present in NH_2-SBA-15 were protected [scheme 3.1(B)] by adding 1.5 mmol of dimethoxydimethylsilane [$(MeO)_2Me_2Si$] to a stirred suspension of 1 g of NH_2-SBA-15 in dry toluene (50 mL), followed by stirring for 12 h at reflux temperature under inert atmosphere.[9] The obtained material was filtered, washed with toluene and soxhlet extracted with DCM for 24 h and named as –OH protected NH_2-SBA-15.

3.2.2. SBA-15-Pd-EDTA Synthesis

$PdCl_2$ (0.5 mmol) in 5 ml distilled water was treated with 0.186 g (0.5 mmol) of EDTA and 1 mmol of sodium carbonate (Na_2CO_3) and stirred to give yellow red solution. To the resultant solution the calculated amount (1.0 g) of organo-modified SBA-15 was added along with the slow addition of 25 ml of Millipore water.[9] The final mixture was stirred at 75 °C for 24 h and washed with distilled water and soxhlet extracted to remove the unanchored materials from the SBA-15 surface [scheme. 3.1(D)]. The resultant material is named as SBA-15-EDTA-Pd(11). Similarly, 7 and 15 wt. % of Pd loading were also synthesized by using corresponding amount of modified SBA-15 and $PdCl_2$ and obtained materials were designated as SBA-15-EDTA-Pd(7) and SBA-15-EDTA-Pd(15), respectively.

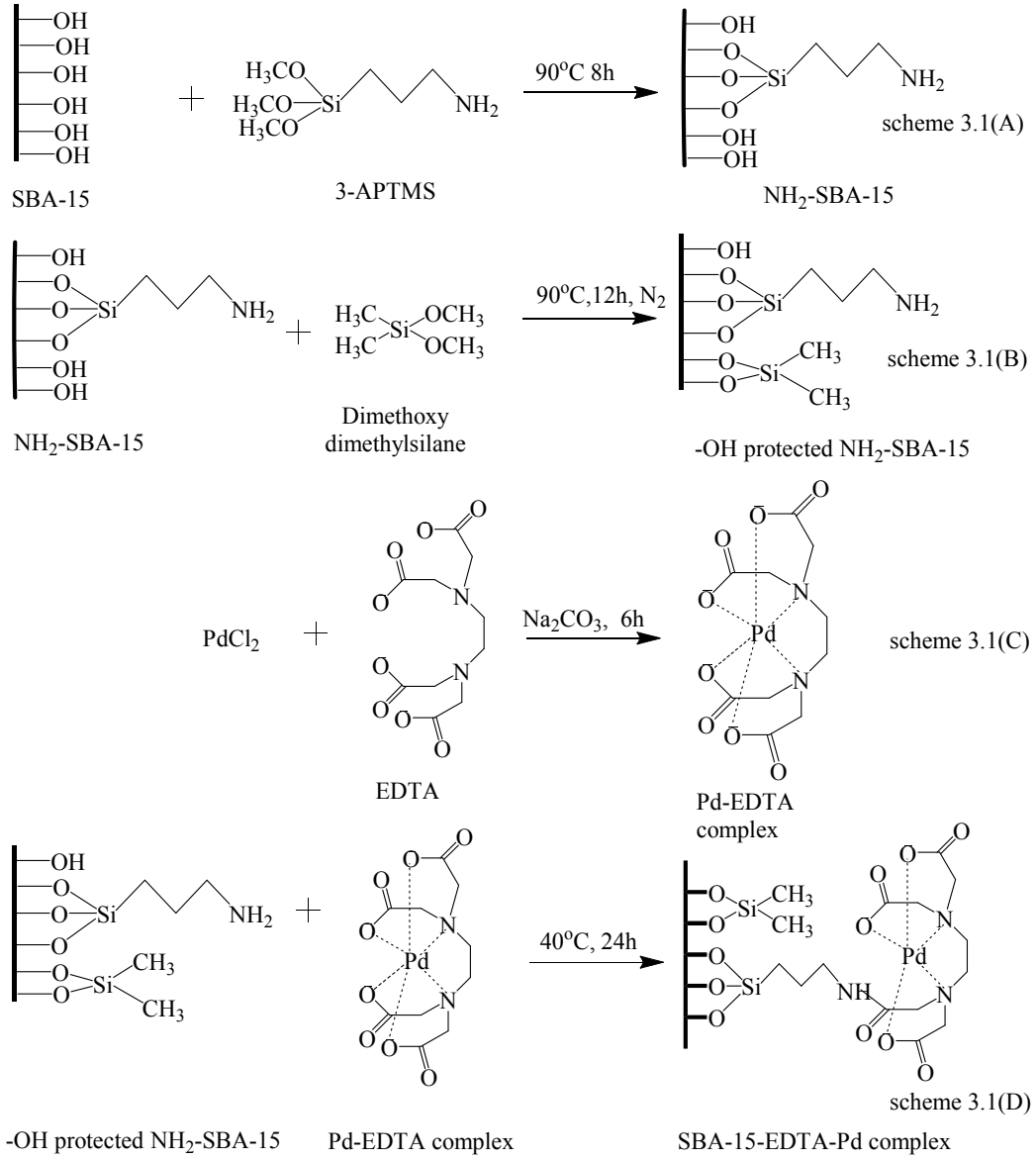

Scheme 3.1. Schematic diagram of SBA-15 Functionalization and heterogenization of Pd-EDTA-SBA-15. 3.1(A) Amino ($-NH_2$) functionalization, 3.1(B) Capping of SBA-15, 3.1(C) Pd-EDTA complex Formation, 3.1(D) anchoring of Pd-EDTA complex over modified surface of SBA-15.

3.2.2. Instruments for Characterization

Powder X-ray diffractograms (XRD) of the materials were recorded using a PAN analytical X'pert Pro dual goniometer diffractometer. The radiation used was Cu Kα (1.5418 Å) with a Ni filter and the data collection was carried out using a flat holder in Bragg-Brentano geometry (0.5 to 5 °; 0.2 °/min).

N_2 adsorption–desorption isotherms, pore size distributions as well as the textural properties of the hybrid materials were determined by using a Micromeritics ASAP 2020 instrument and Autosorb 1C Quantachrome USA. Pore size distribution curves were obtained via the NLDFT model assuming cylindrical pore geometry and the micropore volume calculated via t-plot analyses as a function of relative pressure using the Broekhoff de Boer model for thickness curve measured between 3.5–5.0 Å.

A JEOL JEM-3010 and Tecnai (Model F30) both operating at 300 KV were used for HRTEM samples observation. Chemical analysis was carried out in a Lab Tam 8440 Plasma lab sequential mode ICP–OES Spectrometer and a Spectro Arcos ICP–OES instrument. The scanning electron micrographs of the samples were obtained in dual beam scanning electron microscope (FEI company, model Quanta 200 3D) operating at 30 kV. The samples were loaded on stubs and sputtered with thin gold film to prevent surface charging and also to protect from thermal damage due to electron beam.

^{1}H NMR spectra were recorded on Bruker AC–200 instruments using deuteriated solvent. Chemical shifts are reported in ppm. Liquid ^{13}C NMR spectra were recorded on Bruker AC–200 instruments operating at 50 MHz. ^{13}C NMR chemical shifts are reported in ppm relative to the central line of $CDCl_3$ (d 77.0). Solid-state ^{13}C CP MAS NMR and ^{29}Si MAS NMR spectra were recorded on a Bruker MSL 300 NMR spectrometer with a resonance frequency of 75.5 MHz and 59.6 MHz for ^{13}C and ^{29}Si, and the chemical shifts were referenced to glycine and TMS respectively. Infrared spectra were recorded using a Perkin Elmer, Spectrum one FTIR spectrophotometer. The liquid samples or dilute solution of the solid samples in THF were spread over KBr

plates, and their spectra were recorded. Thermal analysis (TG–DTA) of the samples was conducted using a Pyris Diamond TGA analyzer with a heating rate of 10 ºC min^{-1} under air atmosphere.

3.3. CHARACTERIZATION

3.3.1. Powder X-Ray Diffraction

XRD pattern of (a) calcined SBA-15, (b) -OH protected NH_2-SBA-15 and (c) Pd-EDTA-SBA-15(11) complexes are visualized in Figure 3.1(A) and (a) SBA-15-EDTA-Pd(7), (b) SBA-15-EDTA-Pd(11), (c) SBA-15-EDTA-Pd(15) in Figure 3.1(B). The typical hexagonal phase of the SBA-15 [main (100), (200), and (210)] reflections are clearly visible in calcined SBA-15. In all the samples, (110) reflection is more intense than the (200) reflection.

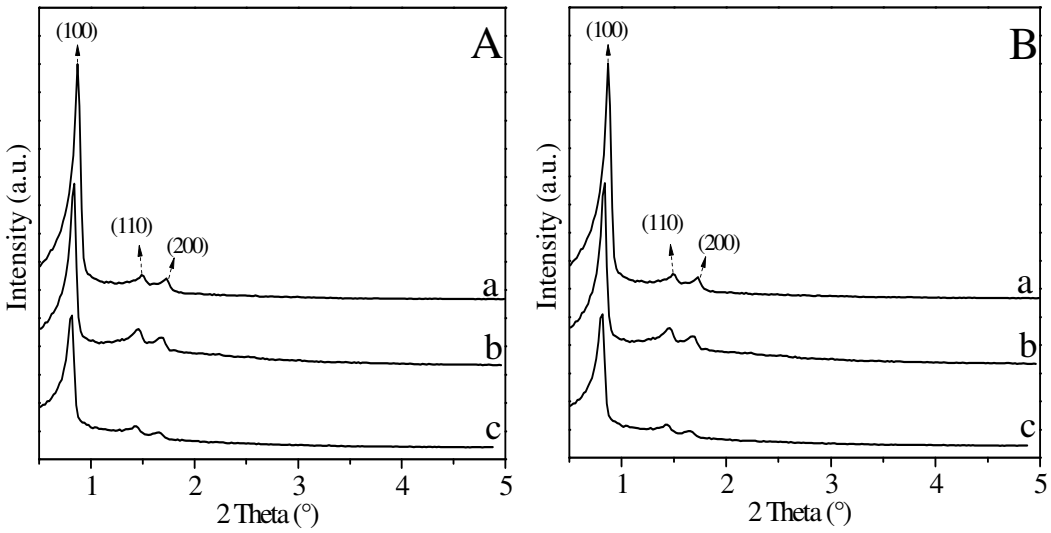

Figure 3.1. (A) XRD pattern of (a) calcined SBA-15 (b) -OH protected -NH_2-SBA-15 (c) SBA-15-EDTA-Pd(11). **Figure 3.1.** (B) XRD pattern of (a) SBA-15-EDTA-Pd(7), (b) SBA-15-EDTA-Pd(11), (c) SBA-15-EDTA-Pd(15).

As evident from the figure 3.1(A) the XRD patterns of the samples synthesized after treatment with 3-APTMS and [$(MeO)_2SiMe_2$] are almost

similar to the parent SBA-15 sample with small decrease in overall intensity to the (100), (110) and (200) reflections. From the XRD pattern it is clear that after anchoring of Pd-EDTA complexes with different weight % ratio (7 %, 11 %, 15 %) an inconsequential decrease in peak intensities to the (100), (110) and (200) reflections were observed without changing the peak positions (Figure 3.1.A). This perseverance of peak positions indicates that, even the presence of a large amount of Pd-EDTA complex moieties by partial filling the inside of the mesopores is less detrimental to the quality of the SBA-15 material.[10] The persistence of the (100), (110) and (200) reflections (Figure 3.1 A, B) not only proved the structural stability and existence of long range ordering of mesophase but also the survival of undisturbed pore wall thickness even after a number of treatments with organic molecules in solvents.

3.3.2. Nitrogen Adsorption Desorption Isotherm

The nitrogen adsorption-desorption results of calcined SBA-15 and SBA-15-EDTA-Pd(7), SBA-15-EDTA-Pd(11), SBA-15-EDTA-Pd(15) samples and their corresponding pore size distribution curves are plotted in Figure 3.2(A, B), respectively. The observed surface area, average pore diameter, pore volume and wall thickness for calcined SBA-15 and SBA-15-EDTA-Pd(7), (11) and (15) derivatives samples are summarized in the Table 3.1. All samples show type IV N_2 adsorption desorption isotherms, according to the IUPAC classification, indicating the uniformity of the mesopores. Due to the capillary condensation of N_2 within the uniformly sized mesopores the capillary condensation step where observed at P/Po = 0.3–0.4. The total surface area, average pore diameter and pore volume observed for calcined SBA-15, SBA-15-EDTA-Pd(7), SBA-15-EDTA-Pd(11) and SBA-15-EDTA-Pd(15) were found to be 739 m^2g^{-1}, 65 Å, 1.173 cm^3g^{-1}, 665 cm^3g^{-1}, 64.3 Å, 0.439 cm^3g^{-1}, 363 m^2g^{-1}, 56 Å, 0.478 cm^3g^{-1} and 187 m^2g^{-1}, 48.5 Å, 0.36 cm^3g^{-1}, respectively. The decrease in total mesoporous surface area (10 %, 50 %, 74 %), pore diameter (2 %, 13 %, 26 %) and pore volume (62 %, 59 %, 69 %) after

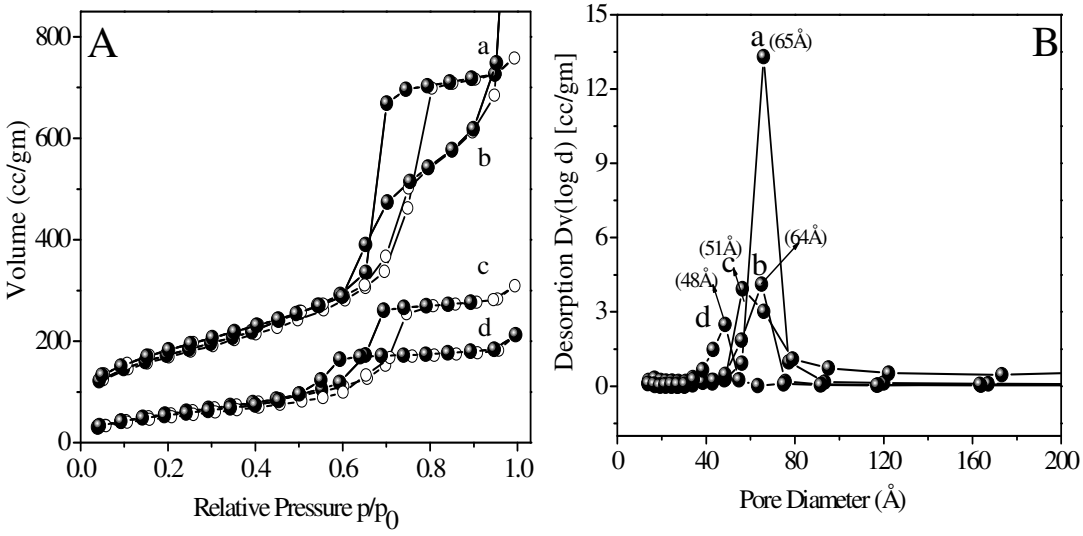

Figure 3.2. (A) Nitrogen adsorption-desorption isotherm of (a) calcined SBA-15, (b) SBA-15-EDTA-Pd (7), (c) SBA-15-EDTA-Pd(11), (d) SBA-15-EDTA-Pd(15), Figure 3.2(B). Pore size distribution of (a) calcined SBA-15, (b) SBA-15-EDTA-Pd (7), (b) SBA-15-EDTA-Pd(11), (c) SBA-15-EDTA-Pd(15).

metal Pd-EDTA (7, 11 and 15 %, respectively) complex immobilization over organo-modified SBA-15 is indicative of the grafting of metal complex, Pd-EDTA inside the channels of mesoporous SBA-15. It is clear from Table 3.1 that even though silylation procedures changed the textural properties of the mesoporous material, the decrease is more prominent after Pd-EDTA complex immobilization, since the bulkier organic moieties inside the pore channels occupies a large area of the void space. In addition the capillary condensation steps of SBA-15-EDTA-Pd(7), SBA-15-EDTA-Pd(11), and SBA-15-EDTA-Pd(15) was also get reduced in lower *P*/*P*o value due to anchoring of Pd-EDTA complexes.

Table 3.1. Textural properties of Calcined SBA-15 and SBA-15-EDTA-Pd(7), (11), (15).

S. No	Sample	N(wt. %)[a]	Pd (wt. %)[b] Input	Pd (wt. %)[b] Output	BET (m^2/g)	D_P (Å)	V_p (cm^3/g)
1.	Calcined SBA-15				739	65	1.17
2.	SBA-15-EDTA-Pd(7)	2.2	7	5.7	665	64	0.43
3.	SBA-15-EDTA-Pd(11)	2.5	11	6.2	363	56	0.47
4.	SBA-15-EDTA-Pd(15)	4.3	15	10.8	187	48	0.36

[a] Calculated based on elemental (Nitrogen) analysis value.
[b] Input (Loading) is based on the amount of Pd during synthesis reaction; output is based on the ICP-AES analysis.
(D_P) : Average pore diameter, V_p : Pore volume, S.A. : BET surface area.

3.3.3. FT-IR Spectra

The presence of isolated surface silanols, hydrogen bonded hydroxyl groups and anchored metal complex, Pd-EDTA are evidenced from the IR spectrum of the calcined SBA-15 and its modified samples. Figure 3.3 shows FT-IR spectra of (a) EDTA, (b) calcined SBA-15, (c) –OH protected NH_2-SBA-15, (d) SBA-15-EDTA-Pd(7), (e) SBA-15-EDTA-Pd(11) and (f) SBA-15-EDTA-Pd(15). In the visualized IR spectrum of calcined SBA-15 and –OH protected NH_2-SBA-15 the stretching vibrations observed between 3600 and 3400 cm^{-1} region are attributed to the hydrogen-bonded silanol groups and the sharp band at 3757 cm^{-1} corresponds to the isolated surface silanol groups (Figure 3.3.b) In the present analysis, after 3-APTMS functionalization, a sharp decrease in the intensity of peak at 3757 cm^{-1} with a peak shift to lower value is seen, demonstrating the role of surface silanols group in organo modifications of SBA-15 (Figure 3.3.c). In Figure 3.3 the peak observed near 797 cm^{-1} and 1076 cm^{-1} are due to the symmetric and asymmetric vibrations of the Si–O–Si group, respectively.[11] Two strong peaks were observed in the case of SBA-15-

EDTA-Pd(11) complexes at 1620 and 1587 cm^{-1} corresponds to the C–O stretching vibrations and N–H bending vibrations, respectively.[12]

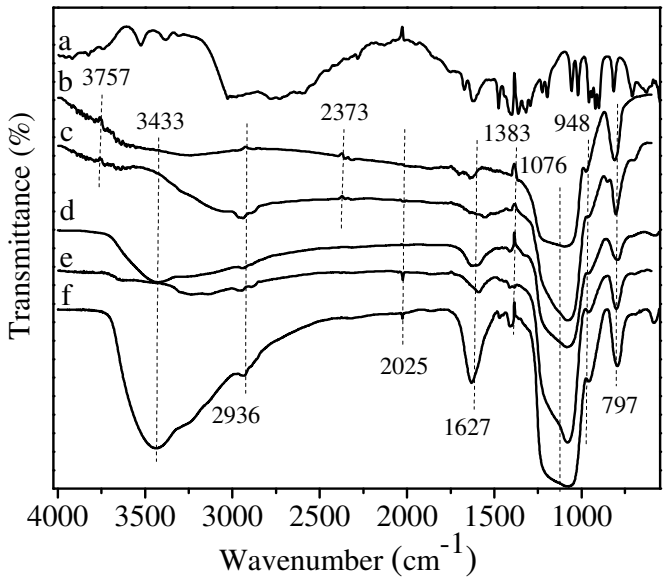

Figure 3.3. FT-IR spectrum of (a) EDTA, (b) calcined SBA-15, (c) –OH protected NH_2-SBA-15, (d) SBA-15-EDTA-Pd(7), (e) SBA-15-EDTA-Pd(11), (f) SBA-15-EDTA-Pd(15).

Further, the intensity of the C–O stretching vibrations and N–H bending vibrations increases as the loading of Pd-EDTA complex increases. Since the Pd-EDTA was anchored over the modified surface of the SBA-15, the peak at 3294 cm^{-1} ascribed to the NH_2 stretching vibrations disappeared, while a broad weak band at 3257 cm^{-1} was observed, which is attributed to the stretching vibration of $–[NH_3]+$ resulted from the EDTA modification.[13] This broad band shows much broader in case of SBA-15-EDTA-Pd(15) catalyst, which might be due to higher loading of Pd-EDTA complex. Further, new bands at 1383 and 1627 cm^{-1} were also observed for Pd-EDTA modified SBA-15 which attribute to the –COO– group symmetrical and asymmetrical stretching vibrations, respectively. These observed results indicate that all the SBA-15-EDTA-Pd complexes along with different loading are systematically synthesized.

3.3.4. ^{13}C CP MAS NMR Spectra

Figure 3.4 shows the solid state ^{13}C CP/MAS NMR spectra of (a) NH_2-SBA-15, (b) –OH protected –NH_2-SBA-15, (c) SBA-15-EDTA-Pd(11). In the solid state ^{13}C CP/MAS NMR spectra of NH_2-SBA-15, –OH protected NH_2-SBA-15 and SBA-15-EDTA-Pd(11) the peak observed at 9.3 ppm can be accounted for carbon (C1) atom bonded to the silicon. The signal at 21.3 ppm corresponding to methylene carbon (C2) and signal at 42.5 ppm can be attributed to the carbon atom attached to NH_2 group (Figure 3.4.a) of anchored 3-aminopropyltrimethoxy silane. No peak was observed for the methoxy group which confirms the successful grafting of 3-APTMS over the support (SBA-15). After –OH group protection of NH_2-SBA-15 by dimethoxydimethylsilane, along with all three peak of NH_2-SBA-15, one extra peak is clearly visible at –2.2 ppm corresponds to methyl group attached to capping agent

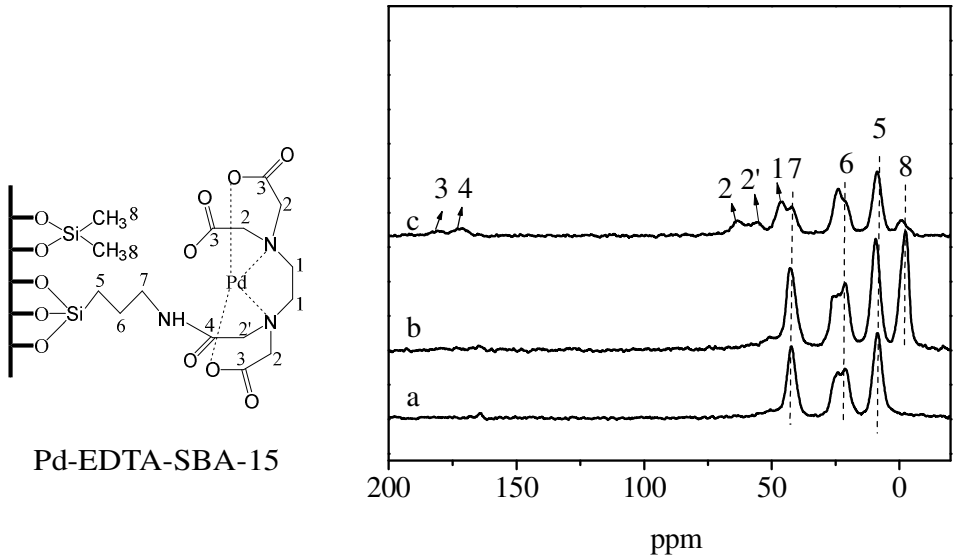

Figure 3.4. Solid state ^{13}C CP/MAS NMR spectrum of (a) NH_2-SBA-15, (b) -OH protected -NH_2-SBA-15 (c) SBA-15-EDTA-Pd(11).

dimethoxydimethylsilane (Figure 3.4.b). Two consecutive peaks observed at 171 ppm and 180.6 ppm corresponds to the carbon atoms of the amide group formation due to the anchoring of EDTA carboxylic group to the linker 3-

APTMS of the SBA-15. Furthermore, another peak observed in the case of SBA-15- EDTA-Pd(11) at 63.85 ppm corresponds to the carbon of ethylene group in EDTA, which is directly attached to the amide group and peak at 55.4 ppm is due to ethylene group which is directly attached to carboxylic acid group (Figure 3.4.c). The reason for appearance of two type peaks for ethylene might be due to all carboxylic group did not get anchored over the 3-APTMS modified surface of the SBA-15.

3.3.5. ^{29}Si CP MAS NMR Spectra

The ^{29}Si CP MAS NMR spectra of (a) Calcined SBA-15, (b) NH_2-SBA-15, (c) -OH protected NH_2-SBA-15 and (d) SBA-15-EDTA-Pd(11) exhibited in Figure 3.5. The demonstrated peaks in the spectra at –112, –102, –68 and –61 ppm which are usually assigned to Q^4 [$Si(OSi)_4$, siloxane], Q^3 [$Si(OH)(OSi)_3$, single silanol], T^3 [$SiR(OSi)_3$], and T^2 site respectively (Figure 3.5.a, b, c, d).

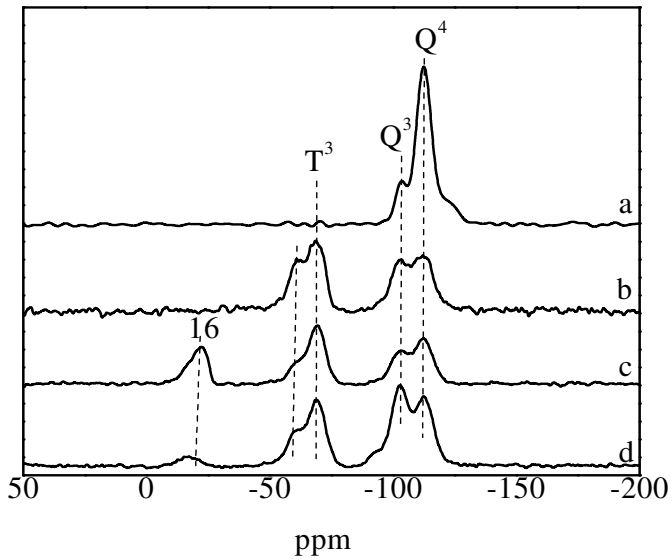

Figure 3.5. Solid state ^{29}Si CP MAS NMR spectrum of (a) Calcined SBA-15, (b) NH_2-SBA-15, (c) -OH protected -NH_2-SBA-15 (d) SBA-15-EDTA-Pd(11).

The calcined SBA-15 sample shows the presence of broad resonance peaks from -126 to -98 ppm, and it is noteworthy that the sample contains large amounts of Q^4 sites showing a high framework cross-linking.[14] In –OH protected-NH_2-SBA-15, Si spectrum shows one extra peaks at –68.48 ppm due to 3-aminopropyltrimethoxysilane, which are assigned to mixture of T^3 [$SiR(OSi)_3$] and T^2 [$Si(OH)R(OSi)_2$] organosilicon, respectively. Peak at –16.87 ppm corresponds to Si group of (dimethoxydimethylsilane) capping agent (Figure 3.5.c). After protection of –OH group in NH_2-SBA-15 by dimethoxydimethylsilane, it is clearly visible that T^2 site [$Si(OH)R(OSi)_2$] disappeared along with the appearance of new peak at -16 ppm. With these two significant changes evidently proved the free silanol group of NH_2-SBA-15 the T^2 site [$Si(OH)R(OSi)_2$] get blocked by the condensation with methoxy group of dimethoxydimethylsilane (Figure 3.5.c). The absence of T^o -Si-C-$(OH)_3$ sites confirms the EDTA-Pd complex is covalently anchored to the modified surface of the SBA-15 (Figure 3.5.d).

3.3.6. Thermal Analyses

Thermal stability of all the synthesized materials were studied by thermo gravimetric analysis under air atmosphere from ambient temperature to 1000 °C with a temperature increment of 10 °C/min. TGA plots of all synthesized and modified SBA-15 samples show approximately 5 % weight loss below 120 °C caused by the desorption of physiosorbed water molecules (Figure 3.6 A, B). In TGA plot loss of ~42 weight % from as-synthesized SBA-15 was observed between 132 °C and 500 °C; corresponds to the removal of trapped surfactant within mesopore (Figure 3.6, A, B, a). Whereas nearly no weight loss in TGA and corresponding exothermic peak in DTA was observed in the calcined SBA-15 between 132 °C and 500 °C indicate the complete removal of surfactant from SBA-15[15] (Figure 3.6, A, B, b). TGA result of -OH protected NH_2-SBA-15 sample shows weight loss in three steps. In the first step, weight loss between 70 °C and 150 °C corresponds to the loss of loosely bounded water or adsorbed molecules., In the second step weight loss was observed in the region

of 245 °C–385 °C in TGA analysis and a sharp visible exothermic peak in DTA analysis in the same temperature region (245 °C–385 °C) are attributed to 3-APTMS. TGA plot of –OH protected NH_2-SBA-15 quantitatively shows ~21.27 % weight loss, which is greater than calcined SBA-15; strongly support

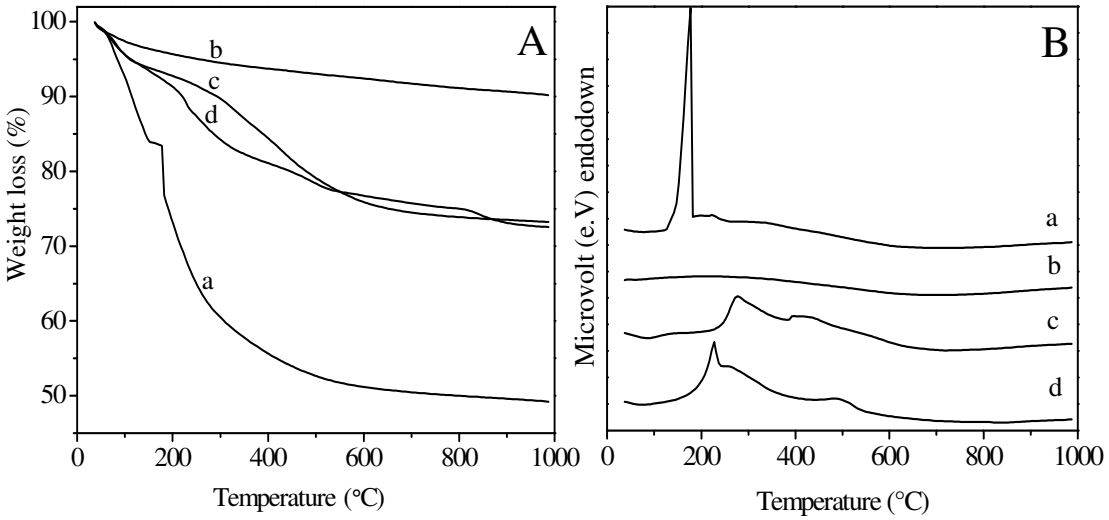

Figure 3.6. (A) TGA, (B) DTA pattern of (a) as-synthesized SBA-15, (b) calcined SBA-15, (c)-OH protected NH_2-SBA-15 and (d) SBA-15-EDTA-Pd(11).

successful anchoring of 3-A -PTMS over SBA-15. Third weight loss was observed in the range of 380 °C–480 °C corresponds to removal of dimethoxydimethylsilane [$(MeO)_2SiMe_2$] which is evidently supported by DTA analysis showing one strong exothermic peak in the same temperature range (Figure 3.6, B, c). In the case of heterogenized metal complex SBA-15-EDTA-Pd(11) one extra peak was observed along with the peaks shown in -OH protected NH_2-SBA-15, in the region of 437–556 °C assigns Pd-EDTA complex. Note that decomposition of Pd-EDTA complex occurred at elevated temperature revealing the high thermal stability of complex. Direct comparison of weight loss in the case of heterogenized SBA-15-EDTA-Pd(11) and capped

amino functionalized SBA-15 shows ~7 weight % loading of metal complex over modified SBA-15 support (Figure 3.6, A, B, d).

3.3.7. Electron Microscopy

TEM image of calcined SBA-15 and SBA-15-EDTA-Pd(11) provide structural evidence that the material organized into ordered arrays of two-dimensional hexagonal mesopores (Figure 3.7). The significant difference of the TEM patterns was not observed between the two Figures 3.7A, B. However,

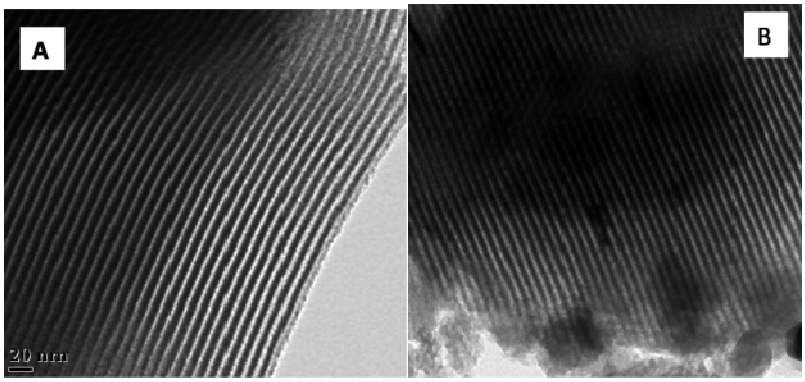

Figure 3.7. TEM Images of calcined (A) SBA-15, (B) SBA-15-EDTA-Pd(11).

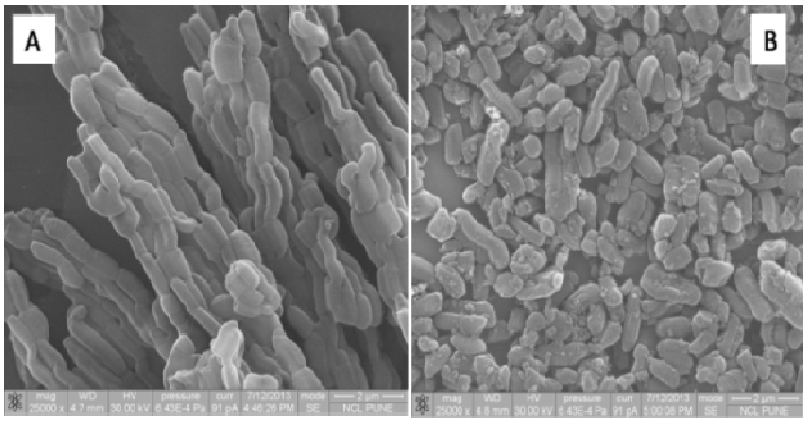

Figure 3.8. SEM Images of calcined (A) SBA-15, (B) SBA-15-EDTA-Pd(11).

after the anchoring of the EDTA-Pd complex inside the mesoporous channels of SBA-15 the images had shown distinct deep contrasting meso parallel

channels with respect to the light shaded surface. This might be interpreted as due to the presence of the EDTA-Pd complex inside the SBA-15, but not on the surface. If the EDTA-Pd complex was anchored on the surface of the functionalized SBA-15, then the high-contrast dark meso parallel channels would have appeared along the boundary of the visualized SBA-15 and not inside the porous body as observed previously by *Shephard et al.*[16] Thus, the immobilization of the Pd-complex inside the pore-channels, by anchoring to the interior walls of these porous channels may be supported by TEM. Morphologies of the calcined SBA-15 and SBA-15-EDTA-Pd(11) are shown in Figure 3.8.A, B, respectively. Calcined SBA-15 shows uniform arrays of mesochannels arrangement and clear molecular-scale periodicity in the SEM images. Further, SBA-15-EDTA-Pd(11) demonstrates molecular-based materials; the large molecular system becomes denser in comparison to the calcined SBA-15 after Pd-EDTA complex anchoring over the mesoporous surface.

3.3.8. X-ray Photoelectron Spectroscopy (XPS)

X-ray photoelectron spectroscopy (XPS) is the powerful tool to investigate the electronic properties of the species formed on the surface. In XPS electronic environment, oxidation state and or multiplicity influence the binding energy of the core electron of the metal. The synthesized material SBA-15-EDTA-Pd(11) was characterized by X-ray photoelectron spectroscopy (XPS) to ascertain the oxidation state of Pd species. In Figure 3.9 the Pd binding energy of SBA-15-EDTA-Pd(11) exhibits two strong peak centered at 336.7 eV and 341.5 eV, respectively, which are assigned to the Pd $3d_{5/2}$ and Pd $3d_{3/2}$ signal, respectively. The observed peaks correspond to the Pd^{2+} oxidation state in the synthesized SBA-15-EDTA-Pd(11). According to literature pure $PdCl_2$ metal salt binding energy for Pd $3d_{3/2}$ and Pd $3d_{5/2}$ orbital appears at 342.8 and 337.6, eV, respectively.[17] In comparison to literature value, the synthesized SBA-15-EDTA-Pd(11) show shift in binding energy of Pd towards lower value viz 341.5 Pd $3d_{3/2}$ and 336.7 eV Pd $3d_{5/2}$, respectively.[18] The shift

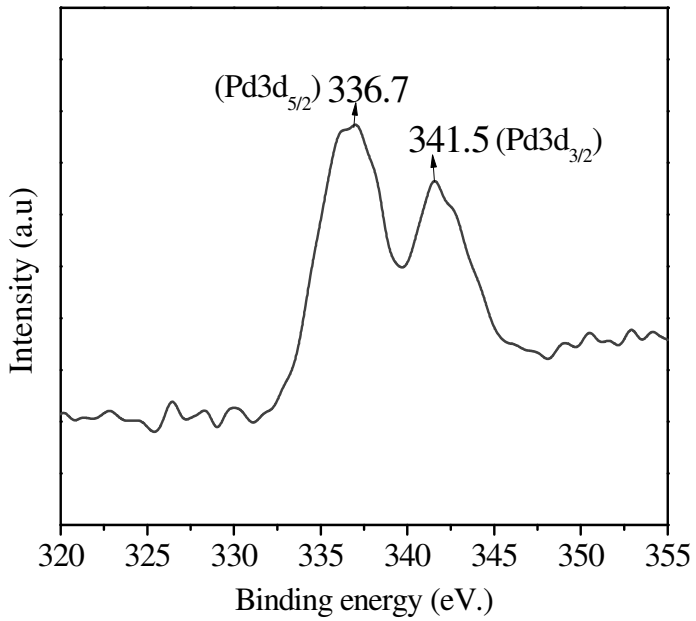

Figure 3.9. XPS of SBA-15-EDTA-Pd(11).

in the binding energy towards lower values indicated that the Pd state in SBA-15-EDTA-Pd had more electron rich state than $PdCl_2$. The reason might be possibility of electron donation from EDTA to Palladium and it suggested the strong interaction between Pd metal species and EDTA ligand was presence in SBA-15-EDTA-Pd catalyst. These results are in agreement with the UV-vis observations.

3.3.9. UV-Vis Spectra

Diffuse reflectance UV-Vis measurement is a useful technique to get information about the oxidation state of incorporated metal species. The UV-Vis spectra of (a) Calcined SBA-15, (b) SBA-15-EDTA-Pd(7), (c) SBA-15-EDTA-Pd(11), (d) SBA-15-EDTA-Pd(15) are shown in Figure 3.10. Calcined SBA-15 shows the characteristic absorption at 254 nm, which corresponds to the siliceous material (Fig.3.10, a). The diffuse reflectance spectra of SBA-15-EDTA-Pd (Pd-EDTA loading 7, 11, 15 %) catalysts display nearly identical features in absorption bands in the UV-Vis region in the range 205-680 nm with

reference to $BaSO_4$ standard. The UV visible spectra of the SBA-15-EDTA-Pd (Fig 3.10, a, b, c) show the characteristics bands at 205-290 nm and 325–362 nm and broad peak at 682 nm. The weak bands in 205-290 nm regions assigned to the weak p–p* transitions (Figure 3.10, b, c, d). Bands in 325–362 nm region

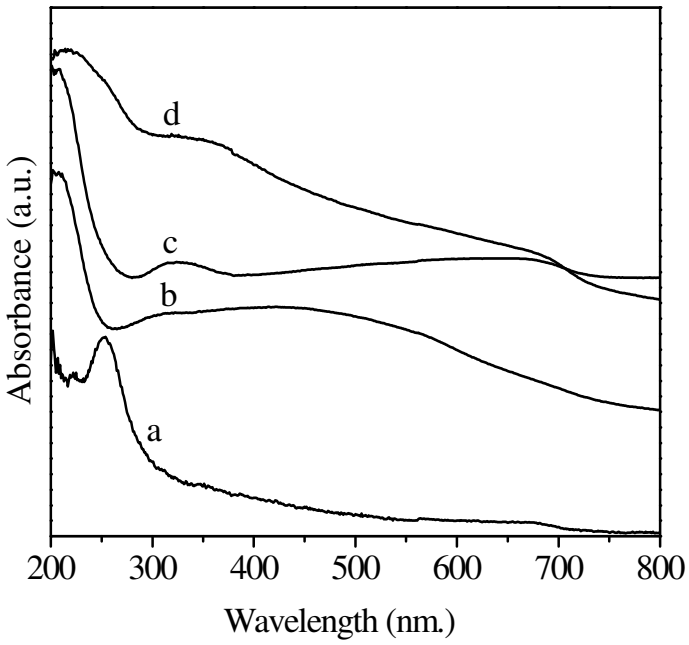

Figure 3.10. UV absorbance spectra of (a) Calcined SBA-15, (b) SBA-15-EDTA-Pd(7), (c) SBA-15-EDTA-Pd(11), (d) SBA-15-EDTA-Pd(15).

assigned to the d-d transition of the metal[19]; strongly supports the Pd(II) oxidation state. The band appears at 682 nm might be due to n–p* transition after incorporation of Pd-EDTA over the modified surface of the SBA-15[19b-d].

3.4. CATALYTIC ACTIVITY

3.4.1. Suzuki Coupling Reaction

3.4.1.1. General Procedure for Suzuki Coupling Reactions

Suzuki reaction was carried out in 25 ml oven dried two neck round bottom flask heated over temperature controlled oil bath with high stirring of 700+ rpm. In a typical run 1mmol of aryl halide, 1.15 mmol of aryl phenyl

boronic acid, 3 mmol potassium carbonate (K_2CO_3) and 15 mg of SBA-15-EDTA-Pd(11) (heterogeneous catalyst) were allowed to stir at 120 °C with solvent DMF (3.5 ml). The reaction mixture was sampled at measured time intervals and analyzed by gas chromatography. The samples were centrifuged with high rpm before analysing by gas chromatography.

3.4.1.2. Suzuki Coupling Reaction Catalytic Results

The catalyst SBA-15-EDTA-Pd with different wt.% loading of Pd-EDTA (7 %, 11 %, 15 %) were screened in the Suzuki coupling reaction using the following reaction conditions: aryl boronic acid (1.5 mmol), aryl halide (1 mmol), potassium carbonate (3 mmol), DMF (3.5 ml), SBA-15-EDTA-Pd (15 mg) at 120 °C. The conversion of iodobenzene and TON with respect to Pd loading were found to be 70 %, 99 %, 99 % and 100, 130.2 and 74.2, respectively. The reaction proceeds at the active Pd metal centre. Further the TON increases from SBA-15-EDTA-Pd(7) to SBA-15-EDTA-Pd(11) thereafter decreases.

The heterogeneous Suzuki cross-coupling of phenyl boronic acid with aryl iodide may proceed through a catalytic cycle (mechanism Step from 1 to 11) analogous to that proposed for homogeneous palladium catalysts.[20] In the first step of reaction insight, oxidative addition of aryl halide ArX (2) to the SBA-15-EDTA-Pd(11) (1) complex provides SBA-15 bound aryl palladium (II) complex (3). The leaving anion adds to the metal center to give the intermediate (3). The displacement of halide ion (X) from SBA-15-L-(Ar–Pd–X) (3) to give the more reactive organopalladium alkoxide, SBA-15-L-(Ar–Pd–CO_3K^+) or organopalladium hydroxide (R–Pd–OH) depends on the base used. Further, in second step of reaction mechanism transmetalation between SBA-15-L-(Ar–Pd–CO_3K^+) aryl palladium (II) complex (6) and bornonic acid (7) provides SBA-15-L-(Ar^1-Pd-Ar) reaction intermediate (10) with the subsequent removal of byproduct $B(OH)_2(CO3^-K^+)_2$ (9). In the last step of reaction mechanism; reductive elimination of biphenyl Ar^1-Ar (11) from the unsymmetrical Intermediate (10) regenerates the SBA-15-L-Pd (1) complex.

Since mechanism of Suzuki coupling reaction is multistep procedure and a small variation in physical and reaction parameter can change the product yield and rate of the reaction drastically. Hence the influences of solvent, reaction temperature and various bases were evaluated on the product yield using SBA-15-EDTA-Pd(11) as catalyst in iodobenzene and phenyl boronic acid.

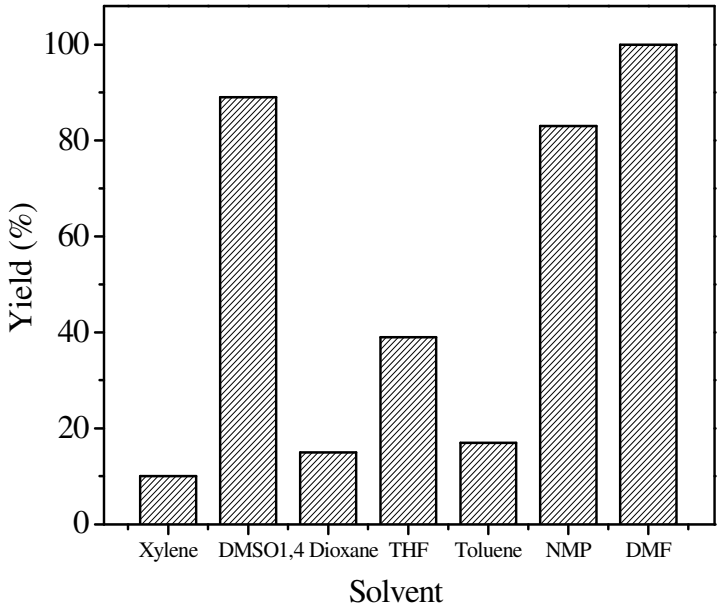

Figure 3.11. Solvent Opimization for Suzuki Coupling Reaction.

In order to probe the role of solvents in Suzuki coupling reaction, series of solvent like DMSO, DMF, HMPA, THF, 1, 4-dioxane, and toluene were used in presence of base potassium carbonate (K_2CO_3) at 120 ºC in a model reaction of Suzuki coupling between iodobenzene and phenyl boronic acid. Among all the solvents tested DMF, DMSO and NMP were able to give a significant yield (85–100 %) in 5 h reaction time period (Figure 3.11). whereas the nonpolar or less polar solvent such as THF, toluene progress with slow rate of reaction comparatively; due to strong reason of intermediate stabilization via coordinating ability to metal centre and the polarity. From the obtained results

of solvent optimization for the conversion of iodobenzene the reactivity order emerged as follows: DMF (100 %) > DMSO (89 %) > NMP (83 %) > THF (39 %) > Toluene (17 %) > 1, 4 dioxane (15 %) > Xylene (10 %), respectively (Figure 3.11). In addition, the conversion of iodobecnzene was also carried out using SBA-15-EDTA-Pd(11) in presence of water as solvent under the similar reaction conditions. The yield of the biphenyl was found to be 33 wt. % in 12 h reaction time. Since after oxidative addition of aryl halide charge separation would take place at Pd metal centre to a much greater extent. To stabilize the

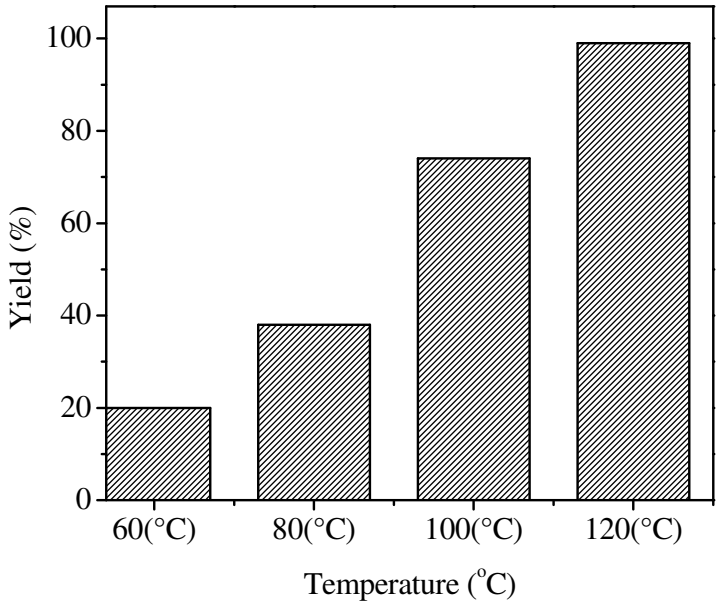

Figure 3.12. Temperature Optimization for the Suzuki Coupling Reaction.

generated high charge during the oxidative step at the Pd centre more coordination required which is possibly by the high polar solvents. Suzuki coupling reaction of iodobenzene (1 mmol) and phenyl boronic acid (1.5 mmol) in presence of K_2CO_3 using solvent DMF (3.5 ml) over SBA-15-EDTA-Pd(11) (15 mg) catalyst was examined to see the influence of temperature in the range of 60 ºC to 120 ºC on the product yield (Figure 3.12). Lower temperature does not favour the formation of product (biphenyl); however the yield of biphenyl

increased sharply with the increase in reaction temperature and reached the value of 99 % in 6 h at 120 ºC. Generally, coupling reaction favoured at high temperature since high activation energy is required to dissociate the aryl halide bond at oxidative addition step. It is noteworthy to mention here that no biphenyl product was obtained below 55 °C. Hence, the optimum reaction temperature with respect to conversion towards biphenyl product, under present reaction conditions, was found to be 120 ºC (Figure 3.12).

Various bases such as NaOH, $NaHCO_3$, K_2CO_3 and NEt_3 were screened for the reaction. Among all used bases, organic bases like triethyl amine (NEt_3)

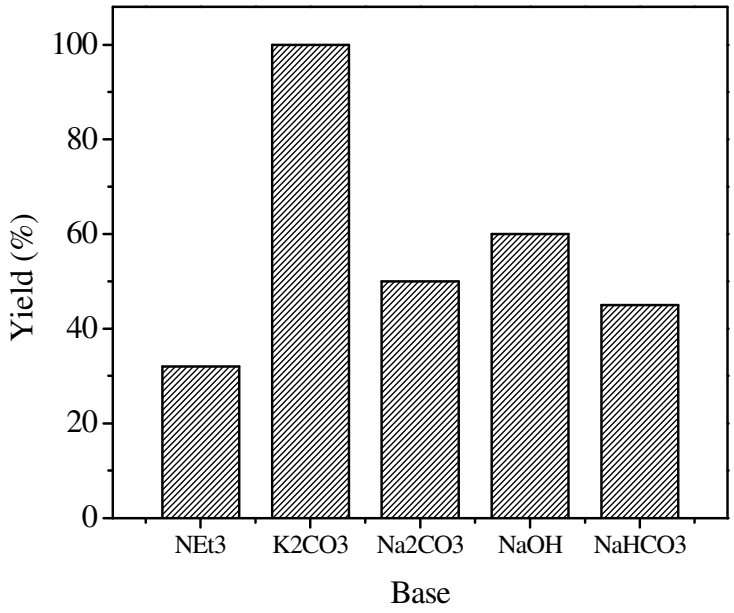

Figure 3.13. Base Optimization for the Suzuki Coupling Reaction.

was found unreactive in comparison to inorganic bases. The order of reactivity of iodobenzene in presence of various bases is arranged in the decreasing order as: K_2CO_3 (100) > NaOH (60) > $NaHCO_3$ (45) > > NEt_3 (32). It is clear that the reactivity of K_2CO_3 is found to be quite high among the used inorganic bases (Figure 3.13). Potassium carbonate is able to give 95 % yield of coupled product (biphenyl) in 5 h at 120 °C. Suzuki coupling reaction is known to be affected by salt particles, yet their mode of action has not been completely

clarified. According to the one hypothesis.[21] in the reaction, the anions at the surface of the solid salt particles acted as electron donors for Pd metal centre, which increased the electron density of Pd metal centre. This effect could promote the oxidative step to form intermediate Ar–Pd-X (3). Therefore, the reaction is accelerated because the above mentioned step is the rate determining step. In other words, the electron-donation effect could enhance the activity of the catalyst with increase in electron density of Pd.

The characteristics of organo-boron reagents (i.e., high selectivity in cross-coupling reactions, stability, nontoxic nature, and tolerance towards functional groups) often give the Suzuki coupling a practical advantage over other cross-coupling processes. After optimizing the reaction parameters of the Suzuki coupling reaction between iodobenzene and phenyl boronic acid; several substituted and non-substituted aryl halides were employed in the reaction and the results are summarized in Table 3.2. The desired corresponding products are obtained in good yields with high TONs. As shown in Table 3.2, the Suzuki coupling reaction of phenyl boronic acid with varieties of aryl halides proceeds smoothly under mild reaction conditions giving the corresponding coupled products in high yields (75 % - 99 %) (Table 3.2, entries 1-10).

Monosubstituted Aryl halides such as chlorobenzene, bromobenzene and iodobenzene with phenyl boronic acid gave 71 %, 83 %, 98 % yield of biphenyl and corresponding TON were found to be 81.2, 94.9 and 128.9, respectively (Table 3.2, entries 1, 2, 3). In the step of oxidative addition in the catalytic cycle of halogenated (X = Cl, Br, I) substrates coupling reactions involving these substrates, the activity typically decrease in the order of R–I > R–Br > R–Cl.

Table 3.2.

Reactivity of SBA-15-EDTA-Pd(11) catalyst for Suzuki reaction.

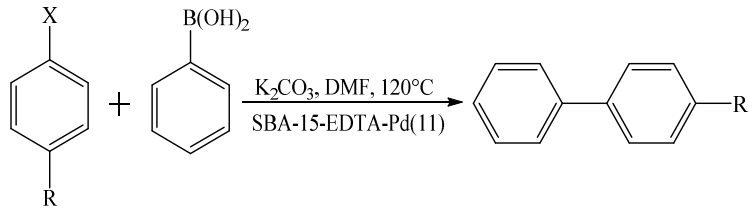

Aryl halide Phenyl boronic acid Biphenyl

S.No	Aryl halide	Product		Time (h)	Yield (%)	TON
1.	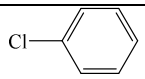	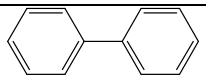	2a	30	71	81
2.	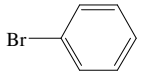	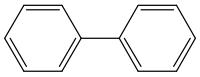	2a	8	83	94
3.	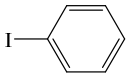	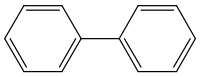	2a	5	98	128
4.	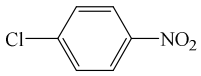	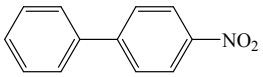	2b	6	98	128
5.	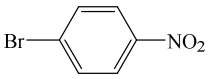	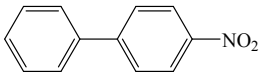	2b	6	99	130
6.	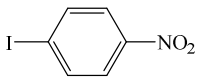	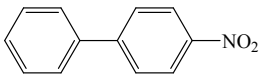	2b	3	95	125
7.	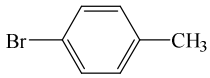	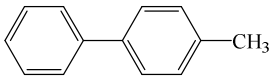	2c	9	96	109
8.	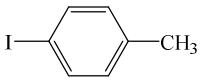	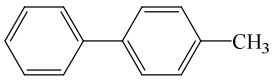	2c	7	94	107
9.	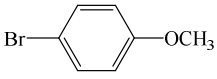	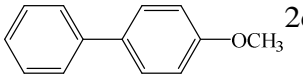	2d	9	89	101
10.	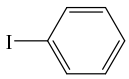	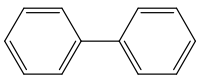	2a	1	99#	130

Reaction conditions: (1.5 mmol) arylboronic acid, (1 mmol) Aryl halide, (3 mmol) potassium carbonate (base), 3.5 ml DMF with (15 mg) Heterogeneous

SBA-15-EDTA-Pd(11) catalyst, temperature 120 °C. (See appendix for NMR detail).

[#] carried out in homogeneous catalyst EDTA-Pd. (3 mol %).

This can be explained in terms of the R–X bond dissociation enthalpies (BDE). For example, the X–Ph BDE range from X = Cl 95.5 ± 1.5 kcal/mol; X =Br 80.4 ± 1.5 kcal/mol to X= I 65.0 ± 1 kcal/mol. It is evident from the Table 3.2 that the reactivity of aryl chloride and bromides with phenyl boronic acid were found lower than aryl iodides and require comparatively longer reaction times for the completion of reaction.

Furthermore, electron rich and electron poor aryl halides react smoothly with phenyl boronic acid in the similar reaction conditions. Electron poor aryl halides like 4-chloronitrobenzene, 4-bromonitrobenzene and 4-iodonitrobenzene with phenyl boronic acid gave coupled product (4-nitro biphenyl) in 98 %, 99 %, 95 % with TON 128.9, 130.2, 125, respectively (Table 3.2, entries 4, 5, 6). The relative reactivity of aryl halide towards the metal centre decreases in the order: I > Br >> Cl. Aryl halides activated by the proximity of electron-withdrawing groups are more reactive to the oxidative addition than those with donating groups, thus allowing the use of electron deficient halides such as 4-chloronitrobenzene for the cross-coupling reaction. Further, aryl iodides are more reactive than the bromides and chlorides. The substituent effect in the aryl iodides appeared to be less significant than in the aryl chlorides and bromides.

Subsequently, the electron rich aryl halides also show moderate to excellent reactivity (89 % – 96 % yield) in the formation of corresponding products (4-methylbiphenyl, 4-methoxybiphenyl) in Suzuki coupling reaction under the similar reaction conditions. The electron rich para substituted aryl halides such as 4-bromotoluene, 4-iodotoluene and 4-bromoanisole with bornonic acid afford 96 %, 94 %, 89 % yield after 9 h, 7 h, 9 h, respectively (Table 3.2, entries 7, 8, 9). The coupling reaction of chloronapthalene with phenyl boronic acid was investigated under similar reaction condition, but no

desired coupled product was obtained even after 24 h of reaction time. In addition, the catalytic activity of SBA-15-EDTA-Pd(11) was compared with homogeneous counterpart. The product yield over SBA-15-EDTA-Pd(11) and EDTA-Pd were found to be 98 and 99 wt. % conversion in 5 h and 1 h, respectively (Table 3.2, entries 3 and 10).

3.4.2. Sonogashira Coupling Reaction

3.4.2.1. General Procedure for Sonogashira Coupling Reactions

Catalyst screening for Sonogashira coupling reaction was carried out in 25 ml oven dried two necked round bottom flask heated over reactor with high stirring 700+ rpm. In a typical run 1mmol of aryl halide, 1.5 mmol of phenylacetylene, 3 mmol triethylamine (base) and 15 mg of SBA-15-EDTA-Pd(11) (heterogeneous catalyst) were allowed to run at 120 °C with DMF as solvent. The reaction mixture was sampled at measured time intervals and analyzed by gas chromatography. The samples were centrifuged with high rpm before injecting in to the gas chromatography. The products were analyzed by GCMS and ^{1}H, ^{13}C CP MAS NMR.

3.4.2.2. Sonogashira Coupling Reactions Catalytic Results

The original Sonogashira reaction often required highly dry organic solvent, inert atmosphere, highly strong base, prolonged reaction time and phosphine containing catalyst. Generally a copper co-catalyst is needed in Sonogashira coupling reaction. However, the addition of copper, although beneficial in terms of increasing the reactivity of the system, added some shortcomings, the principal being the necessity of avoiding the presence of oxygen in order to block the undesirable formation of alkyne homocoupling through a copper mediated Hay/glasier reaction. The coppper-acetylides formed in-situ could undergo oxidative dimerization to give diaryldiacetylenes when they are exposed to air or an oxidant (a reaction known as the Glaser coupling). These by-products are generally difficult to separate from the desired products. Furthermore, the copper acetylide is a potential explosive reagent. To address

such a problem, a solution was to eliminate the copper in the so-called ‘‘copper-free’’ Sonogashira reaction.[22]

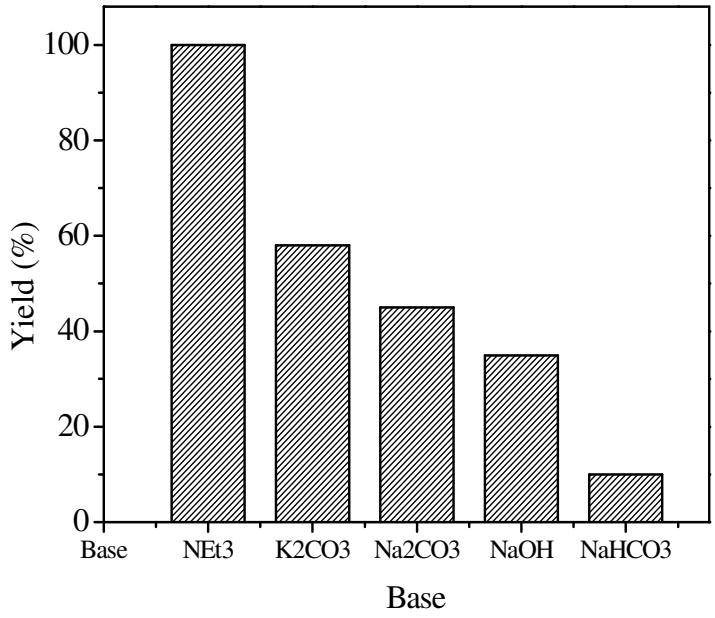

Figure 3.14. Base optimization for the Sonogashira Reaction.

Here we have shown that the synthesized catalyst SBA-15-EDTA-Pd(11) is efficient to handle in phosphine and copper free conditions for Sonogashira coupling reaction. Without the involvement of copper there are even fewer mechanistic suggestions to be found in homogeneous catalytic system.[23] The heterogeneous Sonogashira coupling of phenyl acetylene with aryl halide may proceed through a catalytic cycle analogous to that proposed for homogeneous palladium catalysts.

In the first step of the catalytic cycle (mechanism steps from 1 to 7) is initiated by oxidative addition of the aryl halide (Ar-X) to species (1), forming the oxidative addition adduct reaction intermediate (2) species. The second step is the activation of the terminal alkyne. Because no copper salt was employed, and the base must be strong enough to subtract a proton from the alkyne, a transmetalation step could be excluded.[23] The terminal alkyne C-H bond activation is accomplished by the coordination of the alkyne to SBA-15-L-(ArI-

Pd-X) (3) complex. Upon coordination, the C-H bond is weakened, and H-X is removed from SBA-15-L-(ArI-Pd-X) (3) in the presence of a base (Triethylamine) (6) to form reaction intermediate (5) with the subsequent byproduct of triethylaminehalide (7). In the last step of reaction mechanism; with reductive elimination of diphenylacetylene Ar^1-Ar (7) from the unsymmetrical Intermediate (6) regenerates the SBA-15-L-(Pd) complex.[22]

In order to probe the role of solvent in the Sonogashira coupling reactions a series of various bases such as NaOH, Na_2CO_3, K_2CO_3, NEt_3 and $NaHCO_3$ were screened for the reaction.[22] Among all used base organic base like triethylamine (NEt_3) was found most reactive in comparison to inorganic bases. The order of reactivity of Iodobenzene in presence of various bases is arranged in the decreasing order as: NEt_3 (100 %) > K_2CO_3 (58 %) > Na_2CO_3 (45 %) > NaOH (35 %) > $NaHCO_3$ (10 %). It is clear from the comparison that triethylamine plays a highly active role in Sonogashira coupling reaction (Figure 3.14). The superiority of organic base compared to inorganic base may be due to the partial inhomogeneity of inorganic bases with the organic substrate, reagent, and solvent, which lowered the conversion and increased the reaction times compared to organic bases (10-100 % in 2 h). After optimizing the reaction parameters, various substituted and non substituted aryl halide are also investigated in the Sonogashira coupling reaction between iodobenzene and phenyl acetylene in Cu free reaction conditions and results are summarized in Table 3.3. Various aryl halides were coupled with phenylacetylene in presence of SBA-15-EDTA-Pd(11), triethylamine (3 mmol) and DMF as solvent at 120 °C (Table 3.3). As evident from the Table 3.3 all substituted and non substituted aryl halides react with phenyl acetylene under mild reaction conditions to give their corresponding products (Table 3.3, entries 1-8). Mono substituted aryl halides such as chlorobenzene, bromobenzene and iodobenzene with phenyl acetylene gave coupled product (biphenyl) in 75 %, 85 %, 100 % yield with TON 85, 97, 114, respectively. As discussed earlier, chlorides show poor reactivity compared to bromides and iodides under similar reaction conditions.

Table 3.3.

Reactivity of SBA-15-EDTA-Pd(11) catalyst for Sonogashira reaction.

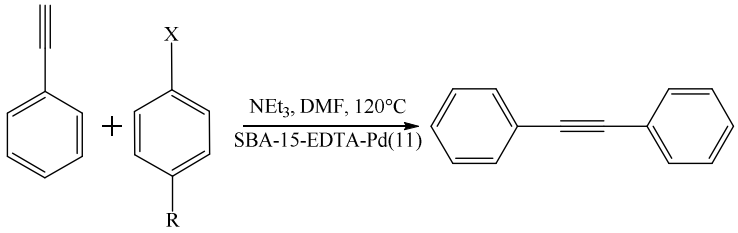

Phenylacetylene Aryl halide diphenylacetylene

S.No	Aryl halide	Product		Time (h)	Yield (%)	TON
1.	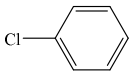	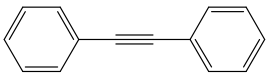	3a	24	75	85
2.	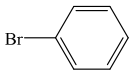	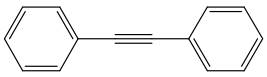	3a	8	85	97
3.	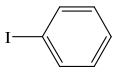	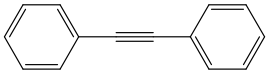	3a	6	100	114
4.	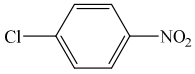	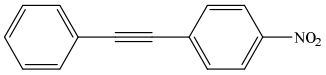	3b	1	99	113
5.	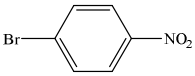	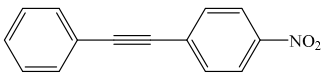	3b	7	98	112
6.	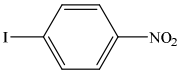	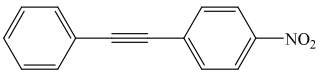	3b	1	100	114
7.	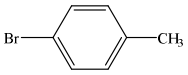	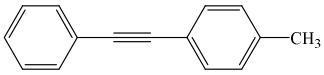	3c	9	89	101
8.	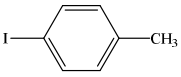	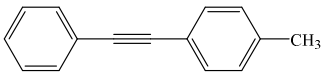	3c	7	99	113

Reaction conditions: (1.15 mmol) Phenyl acetylene, (1 mmol) aryl halide, (3 mmol) triethylamine (base), 3.5 ml DMF with (15 mg) heterogeneous SBA-15-EDTA-Pd(11) catalyst, temperature 120 °C (See appendix for NMR detail).

As clear from the Table 3.3, Sonogashira coupling reactions coupled fast with the aryl iodides and bromides in comparison to chlorides (Table 3.3, entries 1, 2, 3).

Electron withdrawing (deficient) nitro (-NO_2) bearing aryl halide such as 4-chloronitrobenzene, 4-bromonitrobenzene, 4-iodonitrobenene with phenyl acetylene gave coupled product 4-nitrobiphenyl in 99 %, 98 %, 100 % yield and 113, 112, 114 TON, respectively. From the catalytic cycle point of view in Sonogashira coupling reaction, oxidative addition of aryl halide to Pd metal centre results into transition state (3) in the first step. The relative reactivity decreases in the order of I > Br >> Cl. Aryl halides activated by the proximity of electron-withdrawing groups are more reactive to the oxidative addition than those with donating groups. Electron withdrawing groups increase the reactivity of aryl halides in coupling reaction; which is clear from the Table 3.3 (entries 4, 5, 6). However, the electron donating group such as Methyl bearing aryl halides such as 4-bromotoluene, 4-iodotoluene with phenylacetylene gave corresponding products in 89 %, 99 % yield with 101, 113 TON, respectively (Table 3.3 entries 7, 8).

Generally electron donating group bearing Aryl halides show less reactivity in coupling reaction due to increment of electron density over the Pd intermediate **(3)** results into lower feasibility for further transmetalation and reductive elimination step, respectively. It is clear from the Table 3.3 (entries 5-8) that aryl halides bearing methyl, nitro groups react with phenyl acetylene to give excellent yields of the corresponding biaryl; also the aryl chloride possessed para-substituents, give good yields. Whereas electron-rich substrates such as 4-bromotoluene and 4-iodotoluene show lower reactivity in comparison to the electron withdrawing group bearing aryl halides and take longer reaction time period for completion of the reaction (Table 3.3, entries 7, 8). The coupling reaction of sterically hindered 2-chloronapthalene with phenyl acetylene did not proceed even after longer reaction time (24 h).

3.4.3. Mizoroki-Heck Coupling Reaction

3.4.3.1. Generanl Procedure for Heck Coupling Reactions

Screening of the catalyst SBA-15-EDTA-Pd(II) for Mizoroki -Heck reaction was carried out in 25 ml two neck round bottom flask. In a typical run (1 mmol) aryl halide, (1.15 mmol) olefin, (3 mmol) triethylamine, (3.5 mL) solvent N, N´-dimethylformamide (DMF) and (15 mg) SBA-15-EDTA-Pd(II) were allowed to stir at 120 °C. The reaction mixture was analyzed by GC at measured time intervals. The products were separated by column chromatography and analyzed by GCMS, ^{1}H, and ^{13}C NMR.

3.4.3.2. Mizoroki-Heck Coupling Reactions Catalytic Results

The catalyst SBA-15-EDTA-Pd(11) was screened for the Heck C-C coupling reaction under the following reaction conditions: (1.15 mmol) styrene, (1 mmol) iodobenzene, (3 mmol) triethylamine (base), 3.5 mL DMF (solvent) and (15 mg) SBA-15-EDTA-Pd(11) catalyst. The conversion of iodobenzene and TON with respect to Pd was found to be 100 % and 128, respectively. The reaction proceeds at the active Pd metal centre. In order to optimize solvent, base and reaction temperature, Mizoroki-Heck reaction of iodobenzene with styrene using SBA-15-EDTA-Pd(11) catalyst under different reaction conditions was initially examined. A controlled experiment indicated that no cross-coupling product was observed in the absence of the catalyst SBA-15-EDTA-Pd(11) or base.

The heterogeneous Heck coupling of a styrene with an aryl iodide may proceed through a catalytic cycle, analogous to that proposed for homogeneous palladium catalysts.[24] In the first step of the reaction insight, an oxidative addition of the aryl halide ArX (2) to the SBA-15-EDTA-Pd (1) complex provides an SBA-15 bound aryl palladium (II) complex (3) intermediate. Further, in the next step of the reaction mechanism, olefin group reacted over SBA-15-L-(Ar-Pd-X)(3) intermediate resulting into aryl palladium(II) complex (5) followed by α, β migratory insertion step gives the SBA-15-L-[Arl-(H)-Pd–(X)-Ar] reaction intermediate (7), with the subsequent formation of trans

stilbene (8) product and removal of the byproduct HX(10). In the last step of the reaction mechanism, the reductive elimination from the unsymmetrical intermediate (9) regenerates the SBA-15-L-Pd (1) complex. Since the mechanism of the Heck coupling reaction is a multistep procedure, a small variation in the physical and reaction parameters can change the product yield and rate of the reaction drastically. Hence, the influences of the solvent, reaction temperature and various bases were evaluated using SBA-15-EDTA-Pd(11) catalyst with iodobenzene and styrene.

In an initial study, the screening of base for a standard Mizoroki-Heck reaction under the following reaction conditions was performed; iodobenzene (1 mmol) and styrene (1.15 mmol) in presence of solvent DMF (3.5 ml) over heterogeneous SBA-15-EDTA-Pd(11) (15 mg) catalyst with various organic and inorganic bases (Table 3.4, entries 1-5) was carried out. Tri-ethylamine (NEt_3) was found to be the most effective base in terms of yield (100 %). The order of reactivity of bases follow the order $NaHCO_3$ (29 %) < K_2CO_3 (37 %) < Na_2CO_3 (40 %) < NaOH (41 %) < NEt_3 (100 %). It is clear from the comparison that the tri-ethylamine plays a highly active role in the Heck coupling reaction

Table 3.4.

Optimization of base in Mizoroki-Heck C-C coupling reaction.

S. No.	Base	Yield (%)
1.	NEt_3	100
2.	K_2CO_3	37
3.	Na_2CO_3	40
4.	NaOH	41
5.	$NaHCO_3$	29

Reaction conditions: (1.15 mmol) styrene, (1 mmol) iodobenzene, (3 mmol) base, 3.5 ml (DMF) Solvent, with (15 mg) SBA-15-EDTA-Pd(11) catalyst. Isolated yields (product) were analyzed by GCMS and ^{1}H, ^{13}C CP MAS NMR.

(Table 3.4). These organic bases were superior to inorganic bases in terms of reactivity. This may be due to the partial in-homogeneity of the inorganic bases with the organic substrate, reagent and solvent, which lowered the conversion and increased the reaction times compared to the organic bases (20–100 % in 5 h). Furthermore, for the effect of temperature on catalytic activity, standard Mizoroki-Heck reaction of iodobenzene and styrene was performed. Lower temperature does not favour the formation of product; however, the yield of trans stilbene increased sharply with the increase in reaction temperature and reached the value of 99 % in 6 h at 120 ºC. It is noteworthy to mention here that no trans stilbene product was obtained below 55 °C. Hence, the optimum reaction temperature with respect to conversion towards trans stilbene product, under present reaction conditions, was found to be 120 ºC.

Table 3.5.

Optimization of solvent in Mizoroki-Heck C-C coupling reaction.

S. No.	Solvent	Yield (%)
1.	Xylene	8
2.	DMSO	89
3.	1,4 Dioxane	10
4.	THF	39
5.	Toluene	15
6.	NMP	75
7.	DMF	100

Reaction conditions: (1.15 mmol) styrene, (1 mmol) iodobenzene, (3 mmol) triethylamine base, 3.5 ml Solvent, with (15 mg) SBA-15-EDTA-Pd(11) catalyst. Isolated yields (product) were analyzed by GCMS and ^{1}H, ^{13}C CP MAS NMR.

In order to probe the role of solvent in Mizoroki-Heck coupling reaction, series of solvent like DMSO, DMF, NMP, THF, 1, 4 dioxane, Xylene and Toluene

were used in presence of base triethylamine ((NEt_3) at 120 ºC in a model reaction of Mizoroki-Heck coupling between iodobenzene and styrene. Among all the solvents used DMF and DMSO were able to give a significant yield (89-100 %) in 5 h reaction time period (Table 3.5) whereas the nonpolar or less polar solvent progress less comparatively with the strong reason of intermediate stabilization via coordinating ability and polarity. From the obtained results of solvent optimization for the conversion of iodobenzene the reactivity order emerged as follows: DMF (100 %) > DMSO (89 %) > NMP (75 %) > THF (39 %) > Toluene (15 %) > 1, 4 dioxane (10 %) > Xylene (8 %), respectively.

After optimizing the reaction parameters for the Mizoroki-Heck coupling reaction between iodobenzene and styrene; several substituted and non-substituted aryl halides with various olefins were employed in the Heck coupling reaction and the results are summarized in Table 3.6. The desired corresponding products are obtained in good yields with high turnover number (TONs). As shown in Table 3.6, the Mizoroki-Heck coupling reaction with varieties of aryl halides and olefins proceeds smoothly under mild reaction conditions giving the corresponding coupled products in high yields (20 % – 99 %) (Table 3.6, entries 1-28). It is noteworthy to mention here that only trans products were obtained selectively in all the reaction.

Monosubstituted Aryl halides such as chlorobenzene, bromobenzene and iodobenzene with styrene gave 39 %, 91 %, 98 % yield of trans stilbene and corresponding TON were found to be 51, 130 and 128, respectively (Table 3.6, entries 1, 2, 3). In the step of oxidative addition of the catalytic cycle of the halogenated (X = Cl, Br, I) substrates, coupling reactions involving these substrates typically decrease in the order R-I > R-Br > R-Cl. This can be explained in terms of the R-X bond dissociation enthalpies (BDE). For example, the X-Ph BDE ranges from X = Cl 95.5 ±1.5 kcal mol^{-1}; X = Br 80.4 ± 1.5 kcal mol^{-1} to X = I 65.0 ±1 kcal mol^{-1}. It is evident from Table 3.6 that the reactivity of the aryl chloride and bromides with styrene were found to be lower than aryl iodides and require comparatively longer reaction times for the completion of the reaction (Table 3.6, entries 1-18).

Table 3.6.

SBA-15-EDTA-Pd(11) catalyst for Mizoroki-Heck reaction.

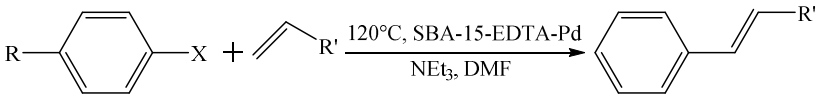

Aryl halide Olefin Product

X = Cl, Br, I. R = H, NO_2. R´ = Ph, Acrylate, C≡N.

S.No.	Aryl halide	Olefins	Product	Time (h)	Yield (%)	TON
1.	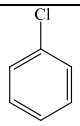	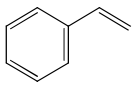	6a 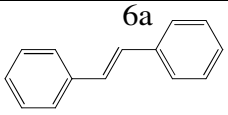	12	39	51
2.	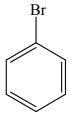	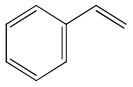	6a 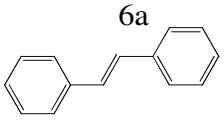	10	91	130
3.	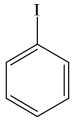	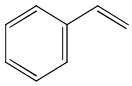	6a 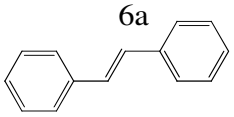	6	98	128
4.	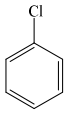	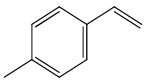	6k 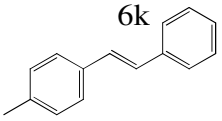	24	20	26
5.	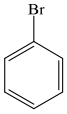	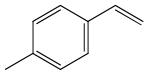	6k 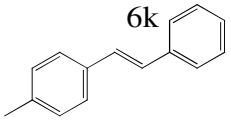	12	75	98
6.	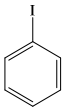	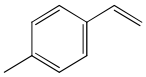	6k 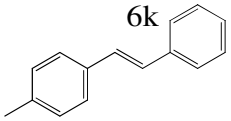	10	97	127
7.	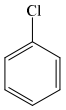	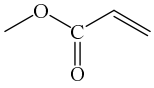	6b 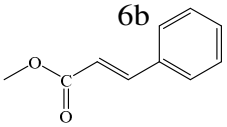	5	79	103
8.	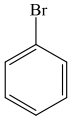	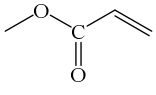	6b 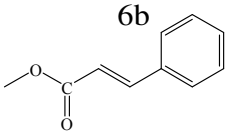	3	99	130

9.	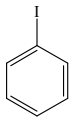	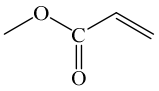	6b 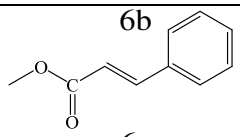	2	99	130
10.	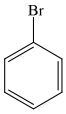	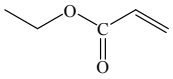	6c 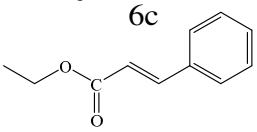	3.5	97	127
11.	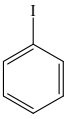	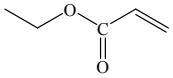	6c 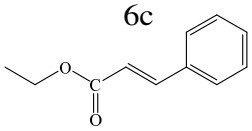	2	99	130
12.	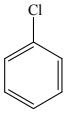	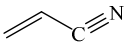	6l 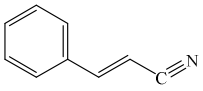	12	75	98
13.	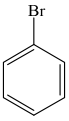	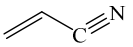	6l 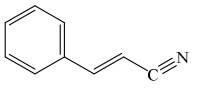	3	99	130
14.	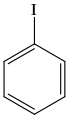	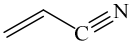	6l 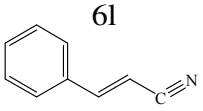	2	100	131
15.	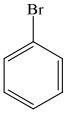	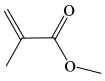	6d 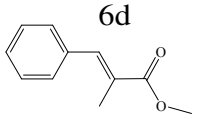	5	97	127
16.	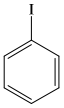	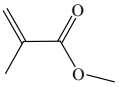	6d 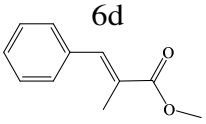	4.5	95	125
17.	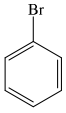	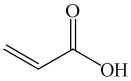	6i 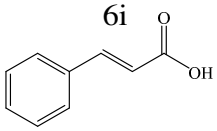	2	100	131
18.	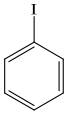	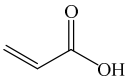	6i 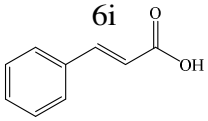	1	99	130
19.	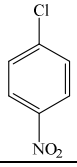	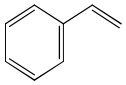	6g 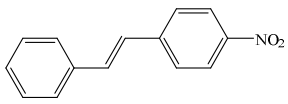	6	100	131

20.	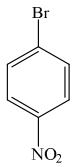	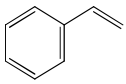	6g 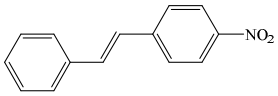	5	92	121
21.	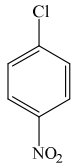	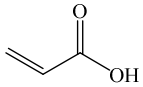	6h 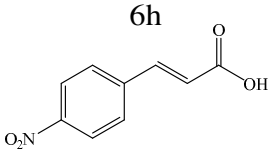	2.5	92	121
22.	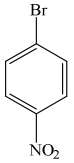	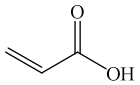	6h 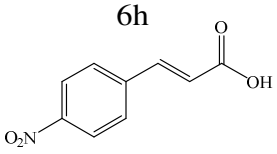	2.5	95	125
23.	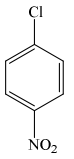	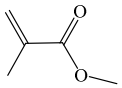	6j 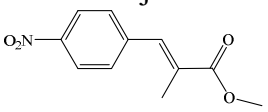	1.5	100	131
24.	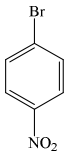	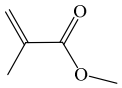	6j 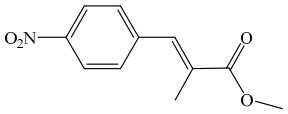	2	99	130
25.	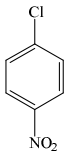	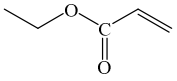	6f 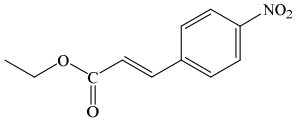	2	98	128
26.	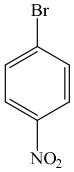	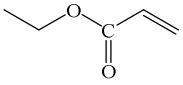	6f 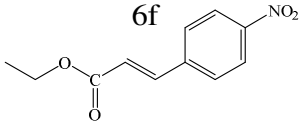	1.5	99	130
27.	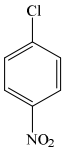	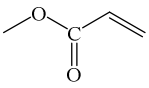	6e 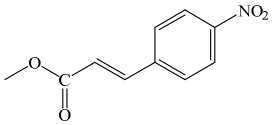	2	100	131
28.	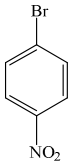	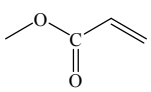	6e 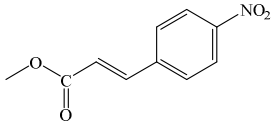	2	95	119

Reaction conditions: (1.15 mmol) olefin, (1 mmol) aryl halide, (3 mmol) triethyl amine base, 3.5 ml DMF with (15 mg) heterogeneous SBA-15-EDTA Pd(11) catalyst, Temperature 120 °C. Isolated yields (product) were analyzed by GCMS and ^{1}H, ^{13}C CP MAS NMR (See appendix for NMR detail).

In the described Heck C-C coupling reaction non aromatic olefins react with aryl iodide to give respective coupled products under similar reaction conditions with higher rate of reaction. Non aromatic olefins *viz;* acrylic acid, acrylonitrile, methyl acrylate, ethyl acrylate, methyl metha acrylate react with aryl iodide to give the respective cross coupled product in 99 %(1 h), 100 % (2 h), 99 %(2 h), 99 %(2 h), 95 %(4.5 h) yield with TON 130, 131, 130, 130, 125, respectively (Table 3.6, entries 9, 11, 14, 16, 18). As it is evident from the Table 3.6, in case of non aromatic olefins, as the steric hindrance increases (in terms of carbon atom) on the olefin substituents; the time of reaction completion increases. Furthermore, the similar mode of reactivity was also observed for the non aromatic olefins (acrylic acid, acrylonitrile, methyl acrylate, ethyl acrylate, methyl metha acrylate) with other aryl halides (bromobenzene) (Table 3.6, entries 3, 10, 12, 13, 15, 17). Whereas, aromatic olefin styrene with aryl iodide gives trans stilbene product in 6 h; which is longer time period than non aromatic olefins (acrylates) for the same reaction condition (Table 3.6, entry 1). Furthermore, α methyl styrene gave slightly lower yield (Table 3.6, entry 6) compared to styrene for the same reaction. The reason for the longer reaction time period might be due to olefin group faces steric hindrance in aromatic group than in the non-aromatic acrylate reactants.

Furthermore, electron poor aryl halides such as 4-chloronitrobenzene and 4-bromonitrobenzene show high rate of reaction with styrene under similar reaction conditions. The corresponding yield of the coupled product (4 nitro stilbene) were 100% and 92% with TON of 131, 121, respectively. The relative reactivity of aryl halide towards the metal centre decreases in the order: I > Br ≫ Cl. Furthermore, electron poor aryl halides such as chloro nitrobenzene reacts, with acrylates *viz:* acrylic acid, methyl acrylate, ethyl acrylate, methyl

metha acrylate with good yield 92 % (2.5 h), 95 % (2 h), 99 % (1.5 h), 100 % (1.5 h) and high TON 121, 131, 130, 131, respectively under similar reaction conditions with higher rate of reaction than non electron deficient halides. The steric hindrance in terms of carbon atom in acrylates is less significant with the activated electron poor aryl halides.

3.4.4. Heterogeneity and Recycling studies of the Catalyst SBA-15-EDTA-Pd(11)

To test if metal was leached out from the solid catalyst during reaction; the hot filtration test was performed. In this process the Sonogashira coupling reaction mixture was collected by filtration at the reaction temperature (120 °C) after a reaction time of 1 h which gave 58 % conversions of iodobenzene. The residual activity of the supernatant solution was studied. It was noticed that

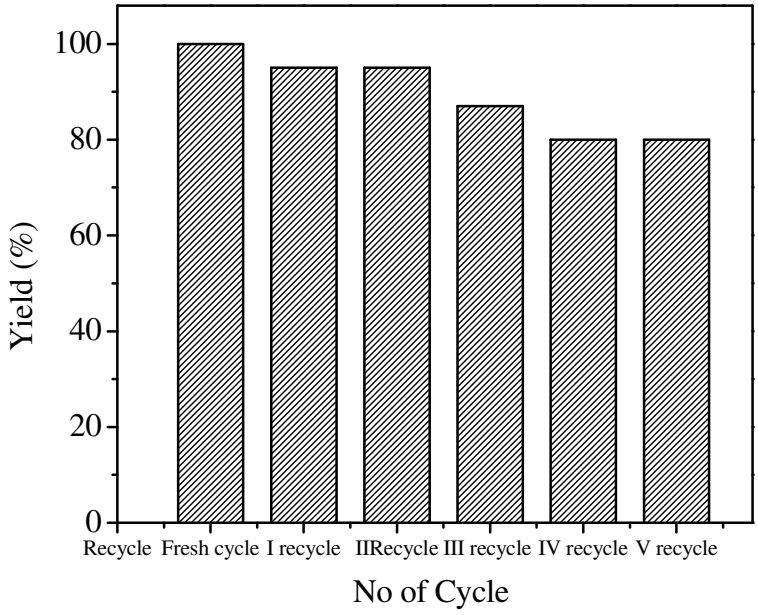

Figure 3.15. Recycling study of SBA-15-EDTA-Pd(11) catalyst.

after filtration of the SBA-15-EDTA-Pd(11) catalyst from the reaction mixture at the elevated reaction temperature (120 °C) (in order to avoid possible recor-ination or precipitation of soluble palladium upon cooling) coupling reactions

did not proceed further. Thus results of the hot filtration test suggest that Pd was not being leached out from the solid catalyst during the coupling reactions. These results confirm that the palladium catalyst remains on the support even at elevated temperatures during the reaction. Further, to evaluate the reusability, after carrying out the reaction, the mixture was filtered using a sintered glass funnel, and the residue was washed with DMF (3–5 ml), dichloromethane (2–5 ml) and acetone (2–5 ml). After being dried in an oven (overnight), the catalyst could be reused directly without further purification (Figure 3.15). The amounts of Pd leaching into solution for the Suzuki reactions were detected through ICP. The loss of Pd amount for reaction was less than 1.0 weight % of total Pd content. Even though a small amount of Pd loss could be detected, catalyst still showed relatively high reusability and stabilities for Sonogashira coupling reactions. The present study indicates that the catalyst can be recycled in a number of times without losing its activity to a greater extent.

3.5. REFERENCES

[1] a) A. Dahan, M. Portnoy, *Org. Lett.* **2003**, 5, 1197.; b) F.X. Felpin, T. Ayad, S. Mitra, Eur. *J. Org. Chem.* **2006**, 12, 2679.; c) A. Cwik, Z. Hell, F. Figueras, *Adv. Synth. Catal.* **2006,** 348, 523.; d) B. M. Choudary, S. Madhi, N. S. Chowdari, M. L. Kantam, B. Sreedhar, *J. Am. Chem. Soc.* **2002,** 124, 14127.

[2] a) J. Y. Ying, C. P. Mehnert, M. S. Wong, *Angew. Chem. Int. Ed.* **1999,** 38, 56.; b) D. Zhao, J. Feng, Q. Huo, N. Melosh, G. H. Fredrickson, B. F. Chmelka, G. D. Stucky, *Science*. **1998,** 279, 548.; c) R. I. Kureshy, A. H. Khan, K. Pathak, V. Jasra, *Tetrahedron: Asymm.* **2005,** 16, 3562.

[3] a) C. Amatore, A. Jutand, M. Amine, M. Barki, *Organometallics* **1992,** 11, 3009.; b) H. A. Dieck, R. F. Heck, *J. Org. Chem* **1975,** 40, 1083.; c) C. A. Fleckenstein and H. Plenio, *Chem. Soc. Rev*. **2010** 39, 694.

[4] a) A. Zapf, M. Beller, *Top. Catal.* **2002,** 19, 101.; b) L. X. Yin, J. Liebscher, *Chem. Rev.* **2007,** 107, 133.

[5] a) V. P. W. Bohm, C. W. K. Gstottmayr, T. Weskamp, W. Herrmann, *J. Organomet. Chem*. **2000,** 595, 186.; b) B. Tao, D. W. Boykin, *Tetrahedron Lett.* **2002,** 43, 4955.; c) D. A. Alonso, C. Najera, M. C. Pacheco, *Org. Lett*. **2000,** 2, 1823.; d) B. Bedford, C. S. Cazin, *Chem. Comm*. **2001,** 17, 1540; e) G. A. Grasa, A. C. Hillier, S. P. Nolan, *Org. Lett.* **2001,** 3, 1077.; f) S. R. Borhade, S. B. Waghmode, *Tetra. Lett.* **2008,** 49, 3423.

[6] a) I. P. Beletskaya, V. Andrei, Cheprakov, *Chem. Rev*. **2000,** 100, 3009.; b) V. Polshettiwar, A. Molnar, *Tetra.* **2007**, 63, 6949.; c) S. P. Stanforth, *Tetrahedron.* **1998**, 54, 263.

[7] a) C. M. Crawforth, I. J. S. Fairlamb, A. R. Kapdi, J. L. Serrano, R. J. K. Taylor, G. Sanchez, *Adv. Synth. Catal.* **2006,** 348, 405.; b) M. Lamblin, L. N. Hardy, J. C. Hierso, E. Fouquet, F. X. Felpin, *Adv. Synth. Catal.* **2010**, 352, 33.; c) X. F. Wu, H. Neumann, M. Beller, *Chem. Commun*. **2011,** 47, 7959.; d) M. Lamblin, L. N. Hardy, J. C Hierso, E. Fouquet, F. X. Felpinb, *Adv. Synth. Catal.* 352, **2010**, 33.; e) T. N. Glasnov, S. Findenig, C. O. Kappe. *Chem. Eur. J.*, 1001, **2009,** 15.; f) E. Chorell, P. Das, F. Almqvist, *J. Org. Chem.* 72**, 2007,** 4917.

[8] a) I. P. Beletskaya, V. Andrei, Cheprakov, *Chem. Rev*. 2000**, 100**, 3009.; b) V. Polshettiwar, A. Molnar, *Tetrahedron.* **63,** 2007, 6949; c) S. P. Stanforth, *Tetra.* 54, **1998**, 263.

[9] a) N. Dmitri, Korolev, N. A. Bumagin, *Tetra. Lett.* **2005,** 46, 5751.; b) D. Zhao, J. Feng, Q. Huo, N. Melosh, G. Fredrickson, B. Chmelka, G. Stucky*, Science* **1998,** 279, 548.

[10] a) C. Yu, B. Tian, J. Fan, G. D. Stucky, D. Zhao, *J. Am. Chem. Soc.* **2002,** 124, 4556.; b) J. D. Galo, A. A. S. Illia, C. Sanchez, B. Lebeau, J. Patarin*, Chem. Rev.* **2002,** 102, 4093.

[11] a) M. D. Alba, Z. Luan, J. Klinowski, *J. Phys. Chem*. **1996,** 100, 2178.; b) A. B. Bourlinos, T. Karakoatas, D. Petridis*, J. Phys. Chem. B.* **2003,** 107, 920.

[12] Y. Jiang, Q. Gao, H. Yu, Y. Chen, F. Deng. *Micro. Meso. Mat*. **2007,** 103, 316.

[13] M. Kaplun, A. Nordin, P. Persson, *Langmuir.* **2008,** 24, 483.

[14] H. Yoshitake, T. Yokoi,T. Tatsumi, *Chem. Mater.* **2002,** 14, 4603.

[15] M. Chidambaram, A. P. Singh, *App. Cat. A: Gen*. **2006,** 310, 79.

[16] D. S. Shephard, W. Zhou, T. Maschmeyer, J. M. Matters, C. L. Roper, S. Parsons, B. F. G. Johnson, M. J. Duer, *Angew. Chem. Int. Ed.* **1998,** 37, 2719.

[17] Gniewek, A. M. Trzeciak, J. J. Ziółkowski, L. K. epinski, J. Wrzyszcz, W. Tylus, *J. Catal*. **2005,** 229, 332.

[18] Z. Gao, Y. Feng, F. Cui, Z. Hua, J. Zhou, Y. Zhu, J. Shi, *J. Mol. Cat. A: Chem.* **2011,** 336, 51.

[19] a) D. S. Martin, R.M. Rush, G.A. Robin, *Inorg. Chem.* **1980,** 19, 1705; b) A. O. Adeloye, P. A. Ajibade. *Molecules* **2011**, *16*, 4615.; c) B. Vlckov, V. Baumrukb, J. Mosinger *Journal of Molecular Structure,* **1992**, 265, 9.; d) A. Modak, J. Mondal, M. Sasidharan, A. Bhaumik. *Green Chem*. **2011**, 13, 1317.

[20] a) M. M. Manas, M. Perez, R. Pleixats, *J. Org. Chem.* **1996**, 61, 2346.; b) N. Miyaura, K. Yamada, H. Suginome, A. Suzuki *J. Am. Chem. Soc.* **1985,** 107, 972.

[21] Zhang, J. Song, H. Liu, J. Shi, J. Ma, H. Fan, W. Wang, P. Zhang, B. Han. *Green chem.* **2014,** 16, 1198.

[22] a) T. Ljungdahl, T. Bennur, A. Dallas, H. Emtenas, J. Mårtensson. *Organometallics*. **2008,** 27, 2490.; b) T. Ljungdahl, K. Pettersson, B. Albinsson, J. Mårtensson, *J. Org. Chem*. **2006,** 71, 1677.

[23] a) J. Cheng, Y. Sun, F. Wang, M. Guo, J. H. Xu, Y. Pan, Z. Zhang. *J. Org. Chem.* **2004,** 69, 5428.; b) B. H. Lipshutz, D. W. Chung, B. Rich. *Org. lett*. **2008,** 10, 3793.

[24] R. F. Heck , J. P. Nolley, J. Org. Chem. **1972,** 37, 2320.

CHAPTER-4

A Recyclable and Efficient Pd(II) 4-(2-Pyridyl)-1, 2, 3-Triazole Complex over the Solid Periodic Mesoporous Organosilica (PMO) Support by "Click Reactions"

4.1. INTRODUCTION

After the discovery of silica-based mesoporous materials extensive research has been devoted to the synthesis of siliceous and non-siliceous mesoporous materials.[1] Further, a new class of organic-inorganic hybrid mesoporous material with integrating organic groups in the wall channel is reported; in which organic molecules reside on the pore surfaces, this new class of materials incorporates organic groups (like ethane, ethene, benzene, biphenyl, etc.) into the framework as molecularly bridging ligands.[2] These unique hybrid materials known as periodic mesoporous organosilicas (PMO); were obtained by the hydrolysis and condensation reactions of silsesquioxane precursors in presence of surfactant species. A wide variety of organo-bridged hybrid mesoporous materials are prepared by a suitable choice of the organo siloxane precursor, $(R_0O)_3$-SiR-Si$(OR_0)_3$, where R = –(CH_2)x–, –C_6H_4–, –CH≡CH–, because the nature of organic groups in the hybrid materials controls properties like the ion exchange capacity, dielectric as well as mechanical properties, surface hydrophobicity, hydrothermal stability.[3] Thus novel concept of the introduction of organic functionalities in the silica framework is to modify the physical and chemical properties of the mesoporous materials, while the inorganic features makes the material thermally and structurally more stable. In addition, the nature of the organic groups integrated inside the frame wall channels of mesoporous materials can change the nature of interactions of the surfactant-silicate assembly and thereby the structure of the finally developed materials.[4]

Sustained development of homogeneous catalysts for fine chemical production has led to the opinion for the heterogenization these catalysts. Till today several methods for heterogenization of homogeneous catalysts have been explored.[5] Immobilization of metal complexes onto the surfaces of solid supports is highly desirable in the development of reusable catalysts. Recently, the Cu(I)-catalyzed azide–alkyne reaction **"click chemistry"** has become emerging field, owing to its simplicity, mild reaction conditions, quantitative conversions and high tolerance of functional groups proved to be one of the best tools for covalent attachment between appropriately functionalized molecules and to solid supports via 1, 2, 3-triazole linkage.[6] The 1, 3-dipolar cycloaddition reactions between organic azides and

terminal alkynes were first systematically studied by *Huisgen* several decades ago.[7] These reactions demonstrate high regioselectivity to give the 1, 4-linked triazoles (click triazole) in excellent yields, has high atom efficiency and low byproduct. After the discovery of the click reaction, is applicable in diverse areas of chemistry such as dendrimers and polymers, drug discovery, material science and bioconjugation.[8] The triazole ligands have the potential to act as nitrogen-donor ligands and from long time known for their coordination with a variety of transition metals.[9] The "**click method**" provides an extremely convenient route for the synthesis of (2-pyridyl)-substituted 1, 2, 3-triazoles; which could be potentially used as the 2, 2´-bipyridine analogues.[10]

Palladium catalyzed cross-coupling reactions of aryl halides or halide equivalents with various nucleophiles have been shown to be highly effective and practical methods for the formation of C–C bonds. These coupling reactions make use of a variety of trans metalating agents such as organoboron, organomagnesium, organosilicon, organostannane and organozinc reagents.[11-15] Among all the Stille reaction involves coupling of an organotin compound with a sp^2-hybridized organic halide catalyzed by palladium. Stille reaction popularity is usually attributed to the stability in air and functional group tolerance of stannanes, as well as their chemo selectivity and broad scope in terms of reaction. This transformation has become a useful synthetic tool for carbon-carbon bond formation and can also be extended to numerous organic electrophiles.[16] Similarly in the class of the C-C coupling reactions the organo magnesium compounds are generally more readily available than any alternative organometallic nucleophile. The improvement of the functional group tolerance of the Kumada-Corriu-Tamao coupling has become a very important and practical impact on the current scenario of metal-catalyzed C-C coupling reactions in organic synthesis.[17]

Accordingly, in the present chapter we report our attempt to graft Pd metal complexes of 4-(2-pyridyl)-1, 2, 3 triazole, a version of "**click reaction**" product, and its derivatives into B-PMO phases and their catalytic properties on Stille and Kumada C-C coupling reactions. The immediate goals of our study were (i) to evaluate the heterogenization method of the 4-(2-pyridyl)-1, 2, 3 triazole Pd(II) complex over organo-hybrid mesoporous B-PMO support, (ii) to characterize the heterogenized B-

PMO-TZ-Pd(II) by various physiochemical techniques (iii) to measure the catalytic properties in Stille and Kumada C-C coupling reaction (iv) to optimize the reaction parameter such as temperature, solvent and base in the both coupling reactions, (v) to determine the extent of stability of the catalysts as well as their recycling properties.

4.2. EXPERIMENTAL

4.2.1. Material

Hybrid mesoporous materials were synthesized using C16–TMABr as surfactant and 1, 2-Bis (triethoxysilyl) benzene (BTEB) and Tetraethyl orthosilicate (TEOS) as the silica sources. 3-Chloropropyl trimethoxysilane (3-ClPTMS), 2-Ethynylpyridine, Copper iodide, Sodium azide, Olefins and Aryl halide purchased from Aldrich. All solvents used in these experiments were obtained from Merck (India) and dried before use according to standard methods. All chemicals were purchased from Aldrich Chemicals and used as received.

4.2.2. Synthesis Procedure of Catalyst

4.2.2.1. Synthesis of hybrid mesoporous Benzene-PMO materials

In a typical synthesis procedure for BTEB- **C16–TMABr** system, 5 g of BTEB was added slowly, but with vigorous stirring to an aqueous solution mixture of C16-TMABr surfactant (3.4 g) in sodium hydroxide (1.8 g). The gel having a molar composition of

1 BTEB : 0.67 C16–TMABr : 3.20 NaOH : 450H_2O.

was stirred for another 20 h at ambient temperature and then allowed to reflux for an additional 48 h at 95 ºC. The white precipitate obtained by above method was then collected by vacuum filtration, washed well with deionized water, and finally dried at 353 K for 2 h. The surfactant occluded inside the pores of the hybrid materials was removed by stirring the as-synthesized material in an EtOH–HCl mixture at 60 ºC for 6 h. The solvent extraction was repeated twice to ensure a complete removal of the surfactant groups. The synthesized material is abbreviated as B-PMO.

4.2.2.2. Azide functionalization over benzene PMO (B-PMO-N_3)

Surface modification of benzene containing periodic organosilica material (B-PMO) with 3-azidopropyltrimethoxysilane (Az-PTMS) was achieved by a post grafting method.[18] To a suspension of 1 g of B-PMO in 50 ml of toluene, 2 ml 3-azidopropyl trimethoxysilane (Az-PTMS) was added, and the mixture was stirred for 18 h at 90 ºC under nitrogen atmosphere. After the completion of reaction, the contents were cooled, filtered and washed with toluene to remove extra unreacted 3-Az-PTMS. The sample was then dried at 80 °C for 8 h in a vacuum oven and preserved under argon atmosphere for further use [Scheme 4.1(B)]. The obtained material is abbreviated as B-PMO-N_3. Yield: 1.15 g (solid). ^{13}C NMR: 11.49, 24, 55, 135.

4.2.2.3. Click chemistry between 2-ethynylpyridine and B-PMO-N_3

In a 20 ml capped vial with a magnetic stirr bar, copper iodide (1 mg) and vacuum distilled N, N-di-isopropylethylamine (DIPEA) (2 mg) were charged with anhydrous, nitrogen-purged dimethylformamide (DMF) (2.5 ml). The mixture was stirred until the solution turned green and transferred to an anhydrous, nitrogen-purged tetrahydrofuran (THF) reaction mixture (7.5 ml) containing 3-azidopropyltrimethoxysilane mesoporous organosilica material (PMO-N_3) (500 mg). The reaction mixture was stirred for additional 20 min before the 2-ethynylpyridine (10 mmol) were added and stirred at 50 °C for 24 h. After cooling down to room temperature, the obtained sample was ultrasonicated for 10 min, rinsed with THF, and dried with nitrogen. The sample was kept in desiccators in the absence of light for further characterization and modification [Scheme 4.1(C)]. The obtained material is designated as B-PMO-TZ. ^{13}C NMR: 11, 24, 55, 124, 135, 149, 156.

4.2.2.4. Metalation over the B-PMO-TZ surface by $PdCl_2$

A solution of $PdCl_2$ (0.216 g, 1.22 mmol) in DMSO (50 ml) was added to the (2.01 g) of 4-(2-pyridyl)-1, 2, 3 triazole ligand benzene PMO material (B-PMO-TZ).[19] The reaction mixture was refluxed under argon for 24 h. The product was allowed to cool and filtered. The yellow solid was washed with DMSO (30 ml) and acetone (30

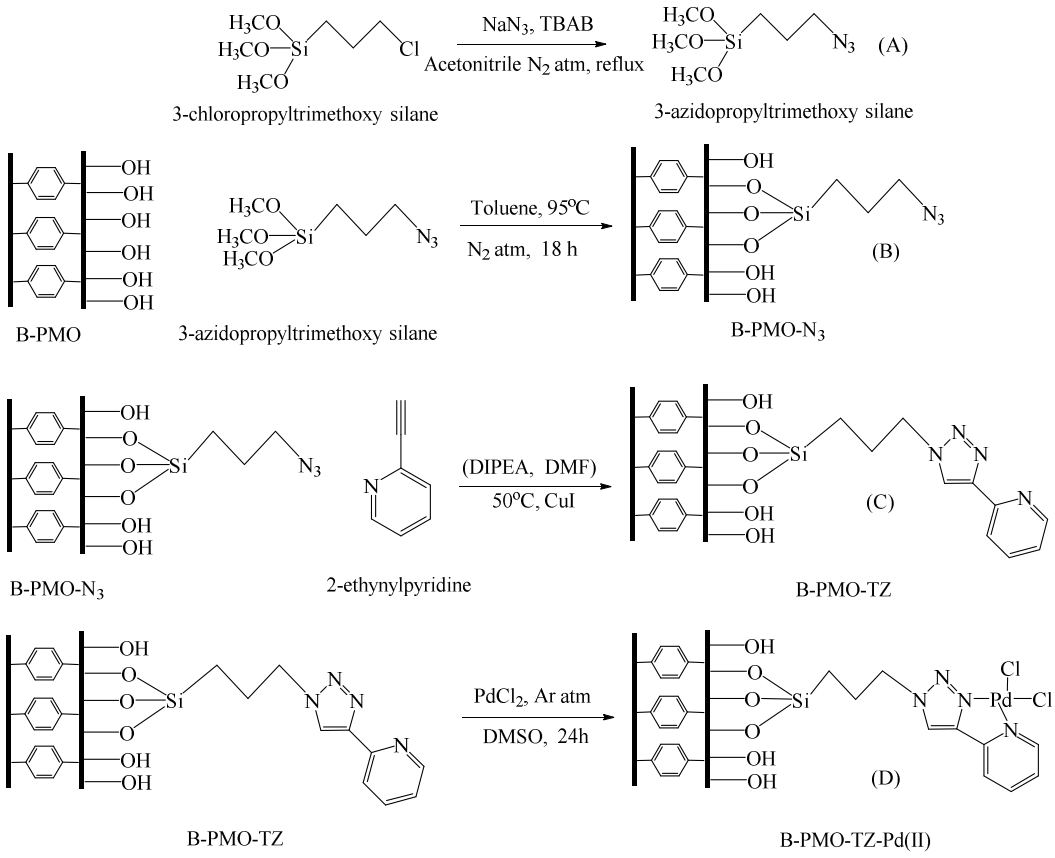

Scheme 4.1. Schematic diagram of (A) Synthesis of 3-azidopropyltrimethoxysilane, (B) Functionalization of azide over benzene PMO, (C) B-PMO modification via 4-(2-pyridyl)-1, 2, 3-triazole ligand, (D) Pd metalation over B-PMO-TZ.

mL). Further, product was Soxhlet-extracted with dichloromethane (CH_2Cl_2) for 24 h to remove physically adsorbed $PdCl_2$ and organic moieties. The resulting product was dried under vacuum at 60 °C to give 1.93 g of the grey colour B-PMO-TZ-Pd(II) [Scheme 4.1(D)].

4.2.3. Instruments for Characterization

Powder X-ray diffractograms (XRD) of the materials were recorded using a PANalytical X'pert Pro dual goniometer diffractometer. The radiation used was Cu Kα (1.5418 Å) with a Ni filter and the data collection was carried out using a flat holder in Bragg-Brentano geometry (0.5 to 5 °; 0.2 °/min).

N_2 adsorption–desorption isotherms, pore size distributions as well as the textural properties of the hybrid materials were determined by using a Micromeritics ASAP 2020 instrument and Autosorb 1C Quantachrome USA. Pore size distribution curves were obtained via the NLDFT model assuming cylindrical pore geometry and the micropore volume calculated via t–plot analyses as a function of relative pressure using the Broekhoff de Boer model for thickness curve measured between 3.5–5.0 Å.

A JEOL JEM–3010 and Tecnai (Model F30) both operating at 300 KV were used for HRTEM samples observation. Chemical analysis was carried out in a Lab Tam 8440 Plasma lab sequential mode ICP–OES Spectrometer and a Spectro Arcos ICP-OES instrument. The scanning electron micrographs of the samples were obtained in dual beam scanning electron microscope (FEI company, model Quanta 200 3D) operating at 30 kV. The samples were loaded on stubs and sputtered with thin gold film to prevent surface charging and also to protect from thermal damage due to electron beam.

^{1}H NMR spectra were recorded on Bruker AC–200 instruments using deuteriated solvent. Chemical shifts are reported in ppm. Liquid ^{13}C NMR spectra were recorded on Bruker AC–200 instruments operating at 50 MHz. ^{13}C NMR chemical shifts are reported in ppm relative to the central line of $CDCl_3$ (d 77.0). Solid-state ^{13}C CP MAS NMR and ^{29}Si MAS NMR spectra were recorded on a Bruker MSL 300 NMR spectrometer with a resonance frequency of 75.5 MHz and 59.6 MHz for ^{13}C and ^{29}Si, and the chemical shifts were referenced to glycine and TMS respectively. Infrared spectra were recorded using a Perkin Elmer, Spectrum one FTIR spectrophotometer. The liquid samples or dilute solution of the solid samples in THF were spread over KBr plates, and their spectra were recorded. Thermal analysis (TG–DTA) of the samples was conducted using a Pyris Diamond TGA analyzer with a heating rate of 10 ºC min^{-1} under air atmosphere.

4.3. CHARACTERIZATION

4.3.1. Powder X-Ray Diffraction

Small-angle X-ray diffraction (XRD) patterns of (a) As-synthesized B-PMO, (b) surfactant extracted B-PMO, (c) B-PMO-N_3 and (d) B-PMO-TZ-Pd(II) are shown in the Figure 4.1. The as-synthesized B-PMO sample exhibit one intense peak at 2.1 and broad peak at 3.4 *2θ* value. After solvent extraction of as-synthesized B-PMO, well resolved and increase in intensity of all the peaks were observed which clearly demonstrates the removal of surfactant molecules from the meso-channels of the B-PMO. In all the samples three well resolved peaks at 2.1, 3.4 and 3.9 2θ value were observed and indexed as the (100), (110), (200), reflections of *p6mm* hexagonal symmetry.[20] In the case of 3-azidopropyltrimethoxysilane (3-Az-PTMS) immobilized B-PMO, B-PMO-N_3 and B-PMO-TZ-Pd(II) (Figure 4.1.c, d), the two dimensional hexagonal pore structures are preserved, however we observed a continuous decrease in intensity after each modification.

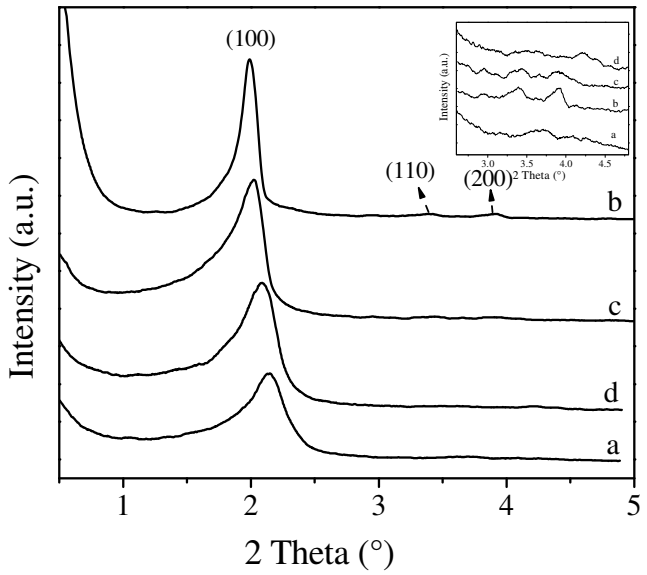

Figure 4.1. Small angle XRD (a) As-synthesized B-PMO, (b) Surfactant extracted B-PMO, (c) B-PMO-N_3 and (d) B-PMO-TZ-Pd(II). Inset shows the enlarged image of higher order diffraction.

This decrease in the peak intensity implied that the azide modification and Pd complex immobilization might disturb the orderedness of mesoporous structure to a certain degree.

4.3.2. FT-IR Spectra

Removal of surfactant groups from the pore channels of the hybrid materials as well as the presence of benzene fragments in the framework and further modification via triazole ligand (click reaction) over the mesoporous framework were analyzed by FT–IR studies. Figure 4.2(a-d) shows the infrared spectra of the as-synthesized B-PMO, surfactant-extracted B-PMO, B-PMO-N_3, B-PMO-TZ-Pd(II). In the as-synthesized B-PMO strong bands are present at 2921, 2851 and 1471; the first two bands correspond to C–H stretching vibration of the surfactant C16-TMABr. The band at 1471 cm^{-1} is due to C–H bending vibration. The absence of peaks at 2921 cm^{-1} and 2851 cm^{-1} in surfactant extracted B-PMO [Figure 4.2.b] suggests complete re-

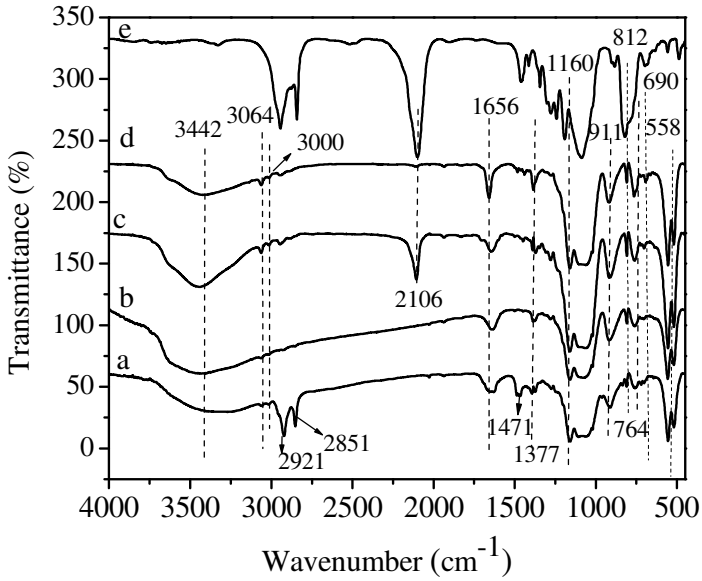

Figure 4.2. FT-IR spectrum of (a) As-synthesized B-PMO, (b) Surfactant extracted B-PMO, (c) B-PMO-N_3 (d) B-PMO-TZ-Pd(II) and (e) 3-AZPTMS.

-moval of the template during the solvent extraction process.[21] While the presence of

aromatic C–H stretching vibration in all the samples as-synthesized B-PMO, surfactant-extracted B-PMO, B-PMO-N_3, B-PMO-TZ-Pd(II) at 3000 and 3064 suggests the retention of organic fragments (–C_6H_4–) unit in the framework positions (BTEB). The as-synthesized and solvent-extracted B-PMO, B-PMO-N_3 and B-PMO-TZ-Pd(II) show strong bands at 812, 690 (aromatic C–H bending) and at 1656 cm^{-1} corresponds to the aromatic C=C bending of the fragments of 1, 2-bis (triethoxysilyl) benzene (BTEB). The asymmetric and symmetric stretching vibrations of the Si–O bands were observed at 1160 and at 911cm^{-1} which relate to the presence of residual silanol Si–OH group.[22] In addition, the presence of intense bands at 1050 cm^{-1} and at 690 cm^{-1}, assigned to the C–Si aromatic stretching vibrations, proves well that the organic bridge was not cleaved during the extraction and further modifications [Figure 4.2. b, c, d]. Furthermore, B-PMO-N_3 shows sharp absorbance at 2106 cm^{-1}; which is a characteristic stretching vibration of any organic azide (N_3).[23] The absence of this peak at 2106 cm^{-1} in B-PMO-TZ-Pd(II) show that the azidopropyl group successfully incorporated to the 2-ethynylpyridine via click reaction.

4.3.3. ^{13}C CP MAS NMR Spectra

Figure 4.3 shows ^{13}C CP MAS NMR of (a) As-synthesized B-PMO (b) surfactant extracted B-PMO, (c) B-PMO-N_3, (d) B-PMO-TZ-Pd(II). All the samples show an intense peak at 135 ppm along with sidebands (denoted with stars) correspond to framework benzene carbon atom of the BTEB precursor. In addition, the appearance of intense peaks at 32 and 67 ppm in the case of as-synthesized B-PMO (Figure 4.3.a) correspond to the carbon atom from surfactant molecules, Moreover; carbon NMR of surfactant extracted B-PMO shows the absence of peaks in the same range 32 and 67 ppm (Figure 4.3.b). This result indicates that the surfactant groups are removed from the pores of the hybrid sample by employing ethanol extraction procedures (Figure 4.3.b).[22] In case of B-PMO-N_3, three peaks at, 12, 24, and 56 ppm were observed correspond to the carbon (C1) attached to Si, middle carbon (C2) and carbon (C3) attached to the azide (N_3), respectively.[23] The appearance of smaller peaks at 125, 136, 149 and 166 ppm clearly demonstrate the functionalization of 4-(2-pyridyl)-1, 2, 3-triazole Pd(II) complex over B-PMO. All

these results prove the proper 4-(2-pyridyl)-1, 2, 3 traizole Pd(II) complex over the mesoporous B-PMO.

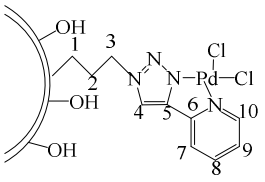

B-PMO-TZ-Pd(II)

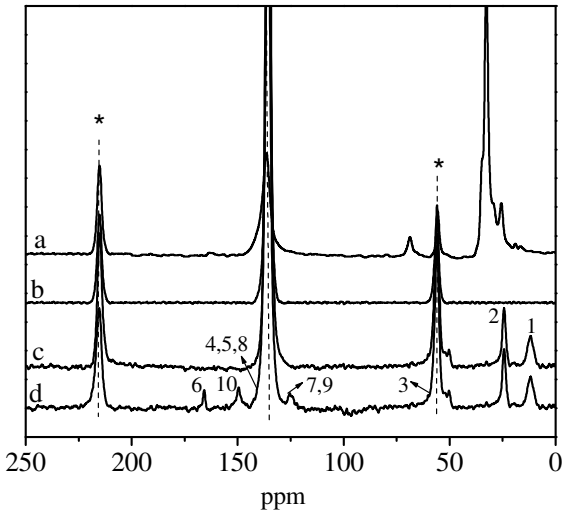

Figure 4.3. Solid state ^{13}C CP MAS NMR spectrum (a) As-synthesized B-PMO (b) Surfactant extracted B-PMO, (c) B-PMO-N_3 and (d) B-PMO-TZ-Pd(II).

4.3.4. ^{29}Si CP MAS NMR Spectra

Solid state ^{29}Si CP MAS NMR spectra of (a) As-synthesized B-PMO, (b) Surfactant extracted B-PMO, (c) B-PMO-N_3 and (d) B-PMO-TZ-Pd(II) are shown in the Figure 4.4 a-d. Silicon NMR spectra of the Surfactant extracted B-PMO sample shows an intense peak at –57 ppm, corresponding to T^2 sites [R-Si-$(OSi)_2$-OH], and at –68 ppm for the T^3 sites, [R-Si-$(OSi)_3$]. The absence of Q units [Q*n* Si(OSi)*n*$(OH)_{4-n}$] below –100 ppm confirms that there is negligible hydrolytic Si–C bond cleavage and the bridge-bonded organic group is intact in the silica framework under the synthetic conditions. After solvent extraction and modification, all the prepared samples show the presence of only T^n sites, indicates that the solvent extraction treatments had removed the organic groups of surfactant from the wall positions.[24] Organosilica samples (Figure 4.4.b, c, d) also show decrease in the percentage of T^2 sites after grafting with 4-(2-pyridyl)-1, 2, 3-triazole Pd(II) complex with a corresponding increase in the T^3 sites which shows more intense anchoring of the 3-azidopropyltrimethoxysilane (3-Az-PTMS) in addition a small peak of T^1 is also

visible. The silicon resonances of partially condensed T^2 [$(SiO)_2(OH)SiC$] and compl-

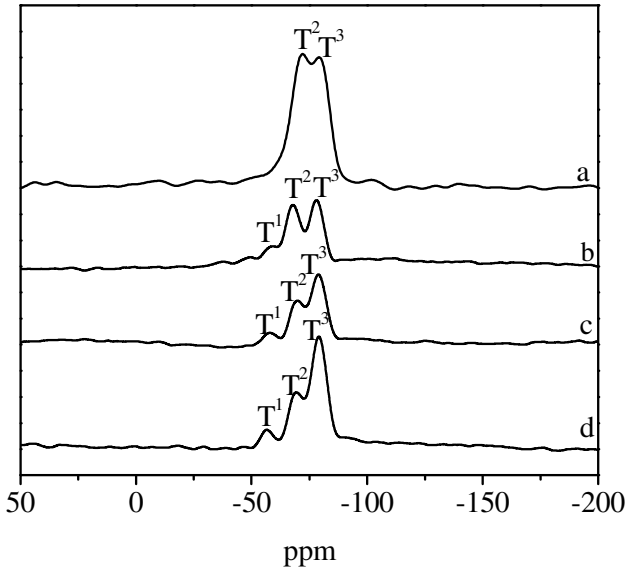

Figure 4.4. Solid state ^{29}Si CP MAS NMR spectrum (a) As-synthesized B-PMO, (b) Surfactant extracted B-PMO, (c) B-PMO-N_3 and (d) B-PMO-TZ-Pd(II).

-ete condensed T^3 [$(SiO)_3SiC$] sites, are highly intense in comparison to T^1 [-$(SiO)(OH)_2$-Si-C] site, indicating the presence of organic moieties inside the framework and the high degree condensation of the silanol groups.

4.3.5. Thermal Analyses

Thermal analyses (TGA and DTA) of (a) As-synthesized B-PMO, (b) Surfactant extracted B-PMO, (c) B-PMO-TZ and (d) B-PMO-TZ-Pd(II) was carried out in air atmospheres to investigate the thermal stability of the synthesized hybrid materials, and the results are shown in Figure 4.5. TGA plots of all synthesized and modified B-PMO samples show approximately 5 % weight loss below 120 °C caused by the desorption of physisorbed water molecules. A loss of ~12 weight % was observed between 200 °C and 370 °C for the as-synthesized B-PMO corresponds to the removal of trapped surfactant within closed pore (Figure 4.5.A, B.a). Whereas no weight loss in TGA and DTA was observed in the surfactant extracted B-PMO between 200 °C and 370 °C (Figure 4.5.A, B.b) indicate the complete removal of

surfactant from B-PMO. The matrix decomposition i.e. loss of benzene [1, 2-bis (triethoxysilyl) benzene (BTEB)] fragments bonded in the mesopore frame wall channels is observed in the range of 600-650 °C in all the samples (Figure 4.5.A, B) attributes that the present mesoporous host materials (B-PMO) are thermally stable up to a temperature of 600 °C.[25] DTA plot of B-PMO-TZ (Figure 4.5. B, c) except the benzene fragments exothermic peak at 611 °C; shows two distinct exothermic peaks between 223 °C–273°C and 318 °C–338 °C due to propyltrimethoxysilane linker group and 1, 2, 3 triozole ring, respectively (Figure 4.5.A,c). Exothermic peak of 1, 2,

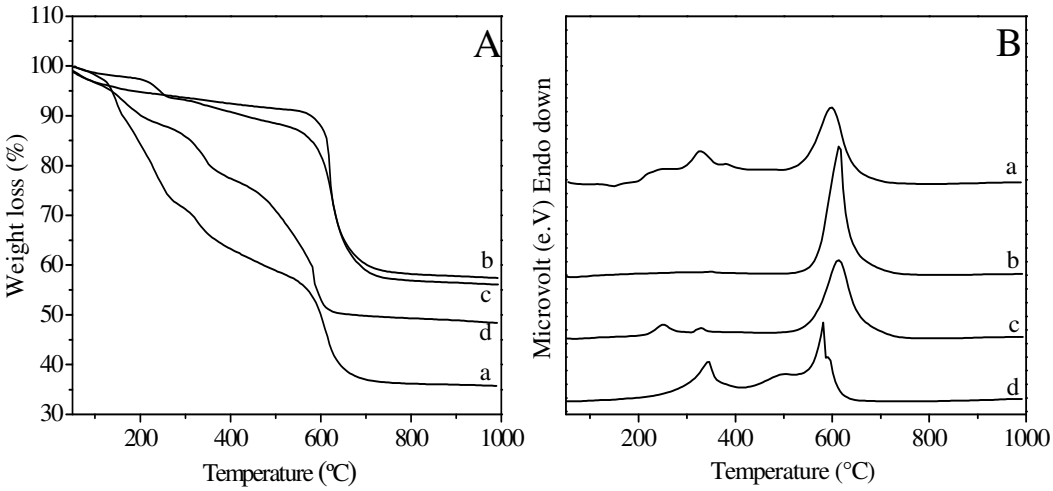

Figure 4.5. (A) TGA, (B) DTA Graph, (a) As-synthesized B-PMO, (b) Surfactant extracted B-PMO, (c) B-PMO-TZ and (d) B-PMO-TZ-Pd(II).

3 triozole in B-PMO-TZ is visible at higher temperature (318 °C–338 °C) might be due to the aromatic character of the ring (Figure 4.5.A, B.c) than the peak of propyltrimethoxysilane linker group (223 °C–273 °C). Further B-PMO-TZ-Pd(II) shows two broad peaks between 250 °C and 400 °C and between 450 °C and 600 °C; the former weight loss may be due to the decomposition of 1, 2, 3-triaozole Pd complex occluded in the mesoporous benzene-PMO and latter weight loss may be assigned to the decomposition of matrix benzene moiety, respectively.

4.3.6. UV-Vis Spectra

The UV-Vis spectra of (a) As-synthesized B-PMO (b) Surfactant extracted B-PMO, (c) B-PMO-N_3, (d) B-PMO-TZ and (e) B-PMO-TZ-Pd(II) are shown in Figure 4.6. All B-PMO samples in Figure 4.6 show two sharp typical absorption peaks at 220 and at 275 nm. The absorption peaks at 220 nm and 275 nm correspond to the π-π^* interaction between the phenylene groups present in the B-PMO network. After surfactant extraction process, an increase in absorption intensity of 220 and 275 nm peaks was noticed in B-PMO which may be due to increase in π electron interaction in phenylene ring without surfactant molecule. In the case of B-PMO-TZ, π-π^* transit-

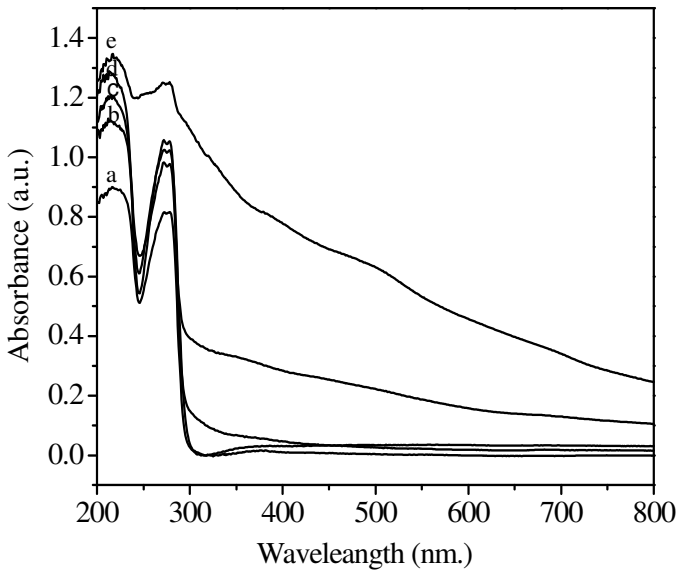

Figure 4.6. DRS-UV Visible Spectra of (a) As-synthesized B-PMO, (b) Surfactant extracted B-PMO, (c) B-PMO-N_3, (d) B-PMO-TZ and (e) B-PMO-TZ-Pd(II).

-ion between 275 and 288 nm is well matched with the reported value.[26] At the same time, palladium loaded complex B-PMO-TZ-Pd(II) show a broad absorption bands between 275 and 288 nm (Figure 4.6.e) than the B-PMO-TZ (Figure 4.6.d). The B-PMO-TZ-Pd(II) shows two broad band observed at around 379 nm and 424 nm tentatively assigned to metal to ligand charge transfer transition (MLCT). According to literature, these two bands can be assigned to metal to ligand charge transfer

transition (MLCT) and Pd^{+2} d-d transition, respectively.[27] The broad absorption up to 600 nm in B-PMO-TZ-Pd(II) may be due to the strong stabilization of the $PdCl_2$ complex over modified B-PMO surfaces.

4.3.7. Nitrogen Adsorption-Desorption

The nitrogen adsorption-desorption results of B-PMO and B-PMO-TZ-Pd(II) and their corresponding pore size distribution curves are plotted in Figure 4.7. The surface area, average pore diameter (Dp) and the pore volume (Vp) observed for the B-PMO and B-PMO-TZ-Pd(II) samples are summarized in Table 4.1. All samples show type IV adsorption isotherms, according to the IUPAC classification, indicating the uniformity of the mesopores due to capillary condensation of N_2 within the meso-

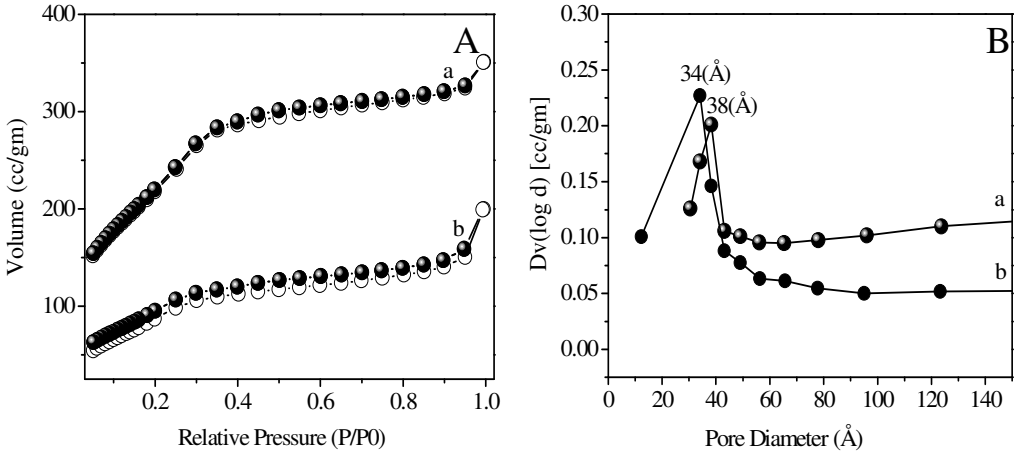

Figure 4.7. Nitrogen adsorption-desorption isotherm and (BJH) pore size distribution (A) B-PMO, (B) B-PMO-TZ-Pd(II).

-pores with completely reversible nature, uniformly sized mesopores, with a capillary condensation step at *P*/*P*o = 0.3–0.4, according to the IUPAC classification mesoporous materials having uniform mesopore structure. The total surface area, average pore diameter and pore volume observed for the B-PMO and B-PMO-TZ-Pd(II) were found to be 796 m^2g^{-1}, 38 Å, 0.49 cm^3g^{-1} and 412 cm^3g^{-1}, 33 Å, 0.21 cm^3g^{-1}, respectively. The decrease in total mesoporous pore volume (58 %), surface area (49 %) and pore diameter (14 %) after metal complex immobilization over B-

PMO is indicative of the grafting of complex inside the channels of mesoporous B-PMO. It is clear from Table 4.1 that even though silylation procedures changed the textural properties of the mesoporous material, the decrease is more prominent after complex immobilization since the bulkier organic moieties inside the pore channels

Table 4.1.

Textural properties of Surfactant extracted B-PMO & B-PMO-TZ-Pd(II) samples.

Sample	N(wt.%) [a]	Loading of Pd (wt. %) [b]		S.A (m^2/g)	(D_P) (Å)	(Vp) cm^3/g
		Input	Output			
B-PMO				796	38	0.49
B-PMO-TZ-Pd(II)	1.5	4	2.2	412	33	0.21

[a] Calculated based on elemental (Nitrogen) analysis value.
[b] Input is based on the amount of Pd during synthesis reaction; output is based on the ICP–OES analysis.
S.A : BET surface area (D_P) : Average pore diameter, Vp : Pore volume.

occupy a large area of the void space. The capillary condensation steps of B-PMO-TZ-Pd(II) due to anchoring of 4-(2-pyridyl)-1, 2, 3-triazole Pd(II) complex get reduced to lower *P*/*P*o values. The shift to slightly lower partial pressures, showing a possible reduction in the pore size and a partial distortion in pore arrangement, consistent with the XRD results. It is known that the inflection position in N_2 sorption isotherms depends on the diameter of the mesopores and the sharpness usually indicates the uniformity of the mesopores, due to capillary condensation of N_2 within the mesopores.

4.3.8. Electron Microscopy

The morphology and structural ordering of the hybrid catalysts were investigated by SEM and TEM. Morphologies of the surfactant extracted B-PMO and B-PMO-TZ-Pd(II) are shown in Figure 4.8 A, B, respectively. B-PMO shows uniform

arrays of mesochannals arrangement and clearly shows molecular-scale periodicity in the SEM images. Further, B-PMO-TZ-Pd(II) demonstrates molecular-based materials, the large molecular system becomes more denser in comparison to the B-PMO after 4-(2-pyridyl)-1, 2, 3 triazole Pd(II) complex anchoring over the mesoporous surface. Transmission electron microscopic image (TEM) of the B-PMO and B-PMO-TZ-

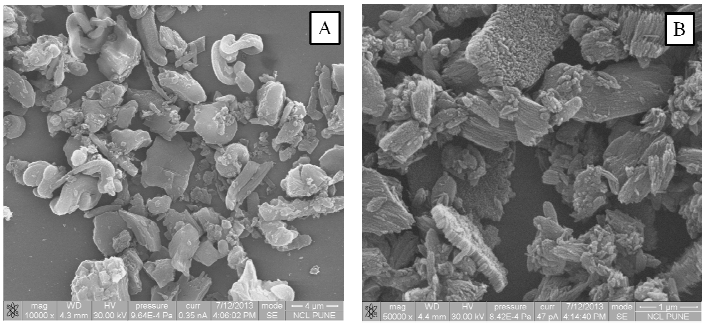

Figure 4.8. SEM images of (A) Surfactant extracted B-PMO, (B) B-PMO-TZ-Pd(II).

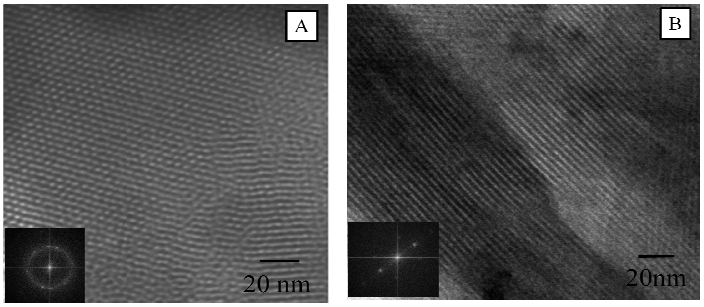

Figure 4.9. TEM images of (A) Surfactant extracted B-PMO and (B) B-PMO-TZ-Pd(II).

-Pd(II) are shown in Figure 4.9.A, B. TEM image of B-PMO and B-PMO-TZ-Pd(II) provide structural evidence that the material organized into ordered arrays of two-dimensional hexagonal mesopores [Figure 4.9.A & B]. The highly uniform mesopores are clearly evident from the TEM image of B-PMO [Figure 4.9.A]. At the same time the formation of uniformly distributed 4-(2-pyridyl)-1, 2, 3-triazole Pd(II) complex inside the meso channels was noticed as a dispersed dark spots in the B-PMO-TZ-Pd(II) [Figure 4.9.B]. All these results clearly indicate the maintenance of mesopore

in B-PMO even after repeated treatment for anchoring 4-(2-pyridyl)-1, 2, 3 triazole Pd(II) complex over B-PMO.

4.3.9. X-ray Photoelectron Spectroscopy (XPS)

X-ray photoelectron spectroscopy (XPS) is the powerful tool to investigate the electronic properties of the species formed on the surface, such as the electronic environment, e.g. oxidation state and or/multiplicity influences, the binding energy of the core electron of the metal. The synthesized heterogeneous catalyst B-PMO-TZ-Pd(II) was characterized by XPS analysis. The accuracy of the measured binding energy (BE) was ±0.3 eV. The spectrum in Figure 4.10. Display the Pd binding energy in B-PMO-TZ-Pd(II) which exhibits two well resolved peaks centered at 342 and 336.2 eV, which are assigned to Pd $3d_{3/2}$ and Pd $3d_{5/2}$, respectively. The observed peaks correspond to the Pd^{2+} oxidation state in the synthesized B-PMO-TZ-Pd(II).[28]

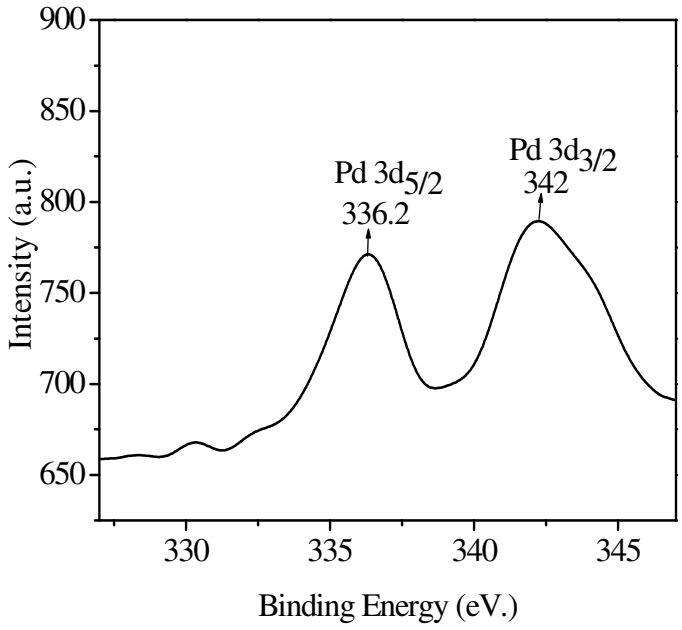

Figure 4.10. XPS Spectra of B-PMO-TZ-Pd(II).

According to literature pure $PdCl_2$ metal salt binding energy for Pd $3d_{3/2}$ and Pd $3d_{5/2}$ orbital appears at 342.8 and 337.6, respectively.[29] In comparison to literature value, the synthesized B-MO-TZ-Pd(II) show shift in binding energy of Pd towards

lower value viz 342 Pd $3d_{3/2}$ and 336.2 eV Pd $3d_{5/2}$ respectively. The remarkable decrease of Pd binding energy in B-PMO-TZ-Pd(II) implies that there is a strong coordination interaction between Pd metal species and 4-(2-pyridyl)-1, 2, 3 triazole ligand. These results are in agreement with the UV-vis observations.

4.4. CATALYTIC ACTIVITY

4.4.1. Stille Coupling Reaction

4.4.1.1. General Procedure for Stille Coupling Reactions

Screening of the catalyst for reaction was carried out in 25 ml two neck round bottom flask. In a typical run of aryl halide (1 mmol), of phenyltributyltin (1.15 mmol), cesium fluoride (CsF) (3 mmol), dimethylsulfoxide (DMSO) (3.5 ml) and B-PMO-TZ-Pd(II) (30 mg) catalyst under argon were allowed to stir at 120°C temperature. The reaction mixture was analyzed by GC at measured time intervals. The products were separated by column chromatography and analyzed by GCMS, ^{1}H, and ^{13}C NMR.

4.4.1.2. Stille Coupling Reaction Catalytic Results

Stille coupling is an important reaction for the synthesis of unsymmetrical and symmetrical biaryls using aryl halides. One of the reasons for the popularity of the Stille reaction in modern organic synthesis is the fact that triaryl organotin species are readily available, quite air and moisture stable, and tolerate many functional groups. These properties are mostly due to the low polarity of the Sn-C bond. The original Stille coupling reaction often requires highly dry organic solvent, inert atmosphere, prolonged reaction time and phosphine containing catalyst. The catalytic Screening of the synthesized B-PPMO-TZ-Pd(II) catalyst was carried out by reacting iodobenzene with phenyltributyltin in dimethylsulfoxide (DMSO) at 120 °C in presence of cesium fluoride (CsF) to afford 95% yield of biphenyl and 239 turn over number (TON).

The heterogeneous Stille cross-coupling of organostannanes with aryl iodide may proceed through a catalytic cycle analogous to that proposed for homogeneous palladium catalysts.[30] In the first step of reaction, oxidative addition of aryl halide ArX (2) to the B-PMO-Pd complex provides B-PMO bound aryl palladium complex

(3). The leaving anion adds to the metal center to give the intermediate (3). Further in second step of reaction mechanism transmetalation between B-PMO aryl palladium complex (3) and organostannanes (4) provides B-PMO-Ar^1-Pd-Ar reaction intermediate (6) with the subsequent removal of byproduct Bu_3SnX (5). It is suggested that fluorides were used to activate the stannane and to enhance the tin reactivity towards transmetalation. In the last step of reaction mechanism; with reductive elimination of biphenyl Ar^1-Ar (7) from the unsymmetrical Intermediate (6) regenerates the B-PMO-TZ-Pd(0) complex. Furthermore, 3 is a common intermediate for the reaction mechanism and the direct coupling of aryl halide and tributyltin gives biaryl (7), in large amount. Ar^1-Ar (7) from the unsymmetrical Intermediate (6) regenerates the B-PMO-TZ-Pd(0) complex. Furthermore, 3 is a common intermediate for the reaction mechanism and the direct coupling of aryl halide and tributyltin gives biaryl (7), in large amount.

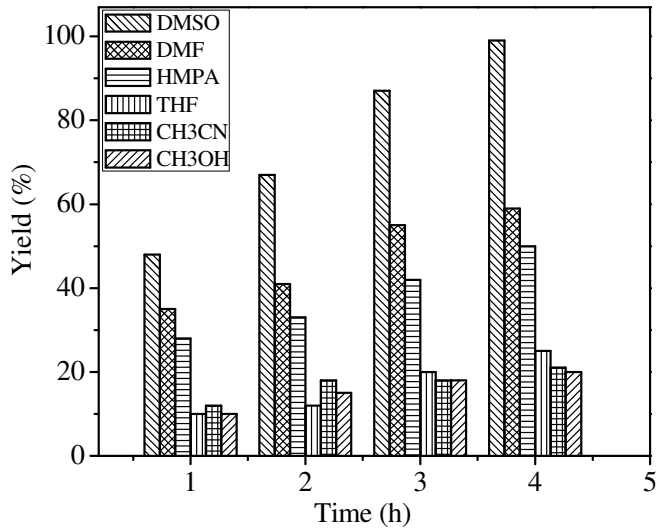

Figure 4.11. Solvent optimization for the Stille Coupling Reaction.

Reaction conditions: iodobenzene (1mmol), tributyltinphenyl (1.15mmol), base Cesium fluoride (CsF) (3mmol), solvent (3 ml), B-PMO-TZ-Pd(II) catalyst ((30 mg),Temperature 120 ºC.

Since mechanism of Stille coupling reaction is multistep procedure and a small variation in physical and reaction parameter such as solvent, temperature and base can change the product yield and rate of the reaction drastically. Hence the influences of solvent, reaction temperature and various bases were evaluated on the product yield using B-PMO-TZ-Pd(II) as catalyst in the reaction of iodobenzene and phenyltributyltin. In order to probe the role of solvents in Stille coupling reaction, series of solvents like DMSO, DMF, HMPA, THF, ethanol, and CH_3CN were used in presence of base cesium fluoride (CsF) at 120 ºC in a model reaction of Stille coupling between iodobenzene and phenyltributyltin. Among all the used solvents DMSO, DMF and HMPA were able to give significant yield (50-99 %) in 5 h reaction time period. Whereas the nonpolar or less polar solvents such as THF, CH_3CN and CH_3OH were not found much effective in the coupling reaction. The reactivity order of iodobenzene conversion in presence of various solvents follows the order: DMSO (99 %) > DMF (59 %) > HMPA (50 %) > THF (25 %) > CH_3CN (21 %) > CH_3OH (10 %), respectively (Figure 4.11.). Since after oxidative addition of aryl halide charge separation would take place at Pd metal centre to a much greater extent, therefore, it is suggested that the highly polar solvent helps in stabilizing the intermediate state (3).[30] To stabilize the high charge during the oxidative step at the Pd centre more coordination is required which is possibly generates by the high polar solvents. Whereas, the non polar solvents are not able to stabilize the intermediate state (3). Hence, solvents play an important role in reaction progress with strong reason of intermediate stabilization via coordinating ability and the polarity.

Stille coupling reaction of iodobenzene (1mmol) and phenyltributyltin (1.5mmol) in presence of CsF using solvent DMSO (3.5 ml) over B-PMO-TZ-Pd(II) catalyst was examined to see the influence of temperature in the range of 60 ºC to 120 ºC on the product yield. The obtained results are summarized in (Figure 4.12). Lower temperature does not favor the formation of product (biphenyl); however the yield of biphenyl increased sharply with the increase in reaction temperature and reached the value of 99 % in 6 h time reaction time period at 120 ºC. Generally coupling reaction favored at high temperature since high activation energy is required to dissociate the aryl halide bond at oxidative addition step. It is noteworthy to mention here that no

product was obtained below 50 °C. Hence, the optimum reaction temperature with respect to conversion towards biphenyl product, under present reaction conditions, was found to be 120 ºC.

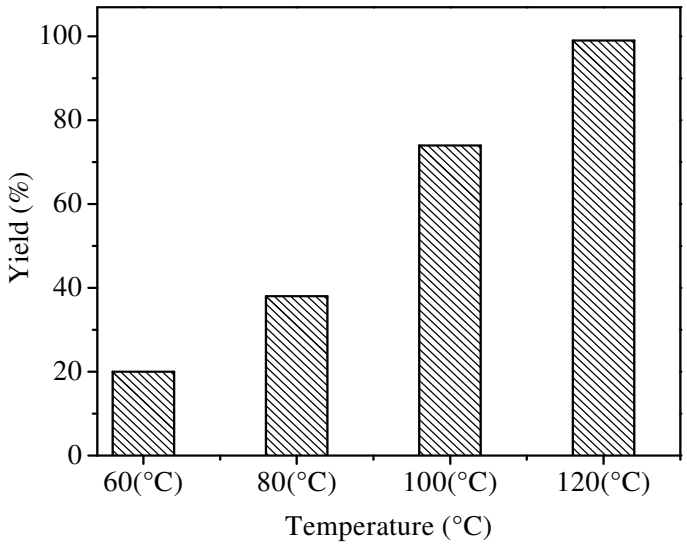

Figure 4.12. Temperature Optimization for Stille Coupling Reaction.

Reaction conditions: iodobenzene (1mmol), tributyltinphenyl (1.15mmol), base Cesium fluoride (CsF) (3mmol), DMSO solvent (3 ml), with heterogeneous B-PMO-TZ-Pd(II) catalyst (30 mg), Temperature 120 ºC.

The role of base in Stille coupling reaction is to activate the phenyltributyltin compound for reaction. Various bases such as NaOH, Na_2CO_3, K_2CO_3, NEt_3 and CsF were screened for the reaction. Among all used bases organic bases like triethyl amine (NEt_3) was found unreactive in comparison to inorganic bases. The order of reactivity of iodobenzene in presence of various bases are arranged in the decreasing order as: CsF (95 %) > K_2CO_3 (56 %) > Na_2CO_3 (45 %) > NaOH (20 %) > NEt_3 (2 %). It is clear that the reactivity of CsF is found to be quite high among the used inorganic bases. Cesium fluoride is able to give 95 % yield of coupled product (biphenyl) in 5 h at 120 °C. The Stille reaction is known to be affected by fluoride salts, yet their mode of action has not been completely clarified.[31] One of the hypotheses attributes to

Table 4.2.

Reactivity of B-PMO-TZ-Pd(II) catalyst for Stille Coupling Reaction.

Aryl halide Phenyltributyltin Biphenyl

X = Cl, Br, I. R' = H, NO_2, CH_3, OCH_3.

S.No	Aryl halide	Product		Time (h)	Yield (%)	TON
1.	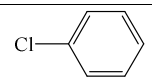	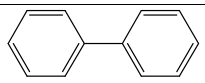	4a	24	35	84.6
2.	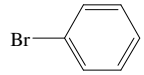	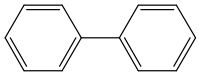	4a	10	75	181
3.	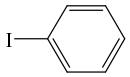	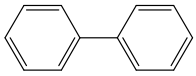	4a	5	99	239
4.	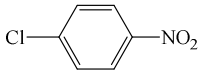	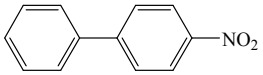	4b	5	95	229
5.	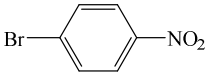	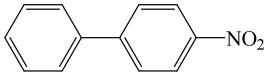	4b	8	95	229
6.	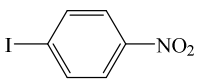	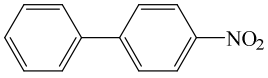	4b	4	99	239
7.	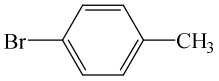	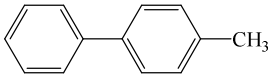	4c	12	96	232
8.	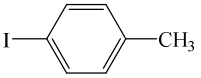	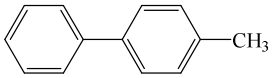	4c	5	99	239
9.	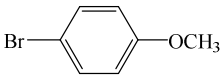	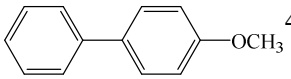	4d	9	89	215

Reaction conditions: iodobenzene (1mmol), phenyltributyltin (1.15mmol), base Cesium fluoride (CsF) (3mmol), DMSO solvent (3 ml), with heterogeneous B-PMO-TZ-Pd(II) catalyst (30 mg), Temperature 120 ºC. Isolated yields (product) were analyzed by GCMS and ^{1}H, ^{13}C CP MAS NMR. TON (turnover number) = moles of product converted per mole of Pd (See appendix for NMR detail).

achieve higher yield of biphenyl is that in the presence of fluoride reagents the formation of insoluble organotin (5) fluorides takes place, which helps in shifting the reaction equilibrium toward the coupled products in transmetalation step of the reaction mechanism.[30] Finally, it is noteworthy that all the products are obtained free of organotin contamination, since the organotin fluorides (5) side product is easily removed. A major drawback of the use of organotins reagents in Pd catalyzed coupling reactions is solved. Another explanation takes into the account that the fluoride anion coordinates to tin to afford a pentacoordinated tin species with enhanced reactivity of the Sn-C bond towards transmetalation step of the reaction mechanism. After optimizing the reaction parameters of the Stille coupling reaction between iodobenzene and phenyltributyltin; several substituted and non-substituted aryl halides are also employed in the reaction and the results are shown in Table 4.2. The desired corresponding products are obtained in good yields with high TONs. To examine the scope of this coupling reaction, a variety of aryl halides were coupled with phenyltributyltin in the presence of a catalytic amount of B-PMO-TZ-Pd(II) (30 mg) at 120 ºC in presence of CsF base and DMSO solvent (Table 4.2). As shown in Table 4.2, the Stille coupling reaction of phenyltributyltin with variety of aryl halide proceed smoothly under mild reaction conditions giving the corresponding coupled products in high yields (75 % - 99 %) (Table 4.2, entries 1-10).

Monosubstituted Aryl halides such as chlorobenzene, bromobenzene and iodobenzene with phenyltributyltin gave 35 %, 75 %, 99 % yield of biphenyl and corresponding TON were found to be 84.6, 181.4, 239.4, respectively (Table 4.2, entries 1, 2, 3). The low reactivity of chlorides is usually attributed to the strength of the C-Cl bond (*bond dissociation energies for Ph–X where X=Cl: 96 kcal/mol; Br: 81 kcal/mol; I: 65 kcal/mol*). It is evident from the Table 4.2 that the reactivity of aryl chloride and bromides with arylstannanes (phenyltributyltin) found lower than aryl iodides and requires comparatively longer reaction times for the completion of reaction.

Furthermore, electron rich and electron poor aryl halides react smoothly with phenyltributyltin in the similar reaction conditions. Electron poor aryl halides like 4-chloronitrobenzene, 4-bromonitrobenzene and 4-iodonitrobenzene with

phenyltributyltin gave coupled product (4-nitrobiphenyl) in 95 %, 95 %, 99 % with TON 229.7, 229.7, 239.4, respectively (Table 4.2, entries 4, 5, 6). Since in the first step of Stille mechanism oxidative addition of aryl halide to Pd metal centre results into Pd(II) transition state (3), oxidative addition is often the rate-determining step in a catalytic cycle. The relative reactivity of aryl halide towards the metal centre decreases in the order: I > Br >> C1. Aryl halides activated by the proximity of electron-withdrawing groups are more reactive to the oxidative addition than those with donating groups, thus allowing the use of electron deficient halides such as 4-chloronitrobenzene for the cross-coupling reaction. Further, aryl iodides are more reactive than the bromides and chlorides. The substituent effect in the aryl iodides appeared to be less significant than in the aryl chlorides and bromides.

Subsequently, the electron rich aryl halides also show moderate to excellent reactivity (89 % - 99 % yield) in the formation of corresponding products (4-methylbiphenyl, 4-methoxybiphenyl) in Stille coupling reaction under the similar reaction conditions. The electron rich para substituted aryl halides such as 4-bromotoluene, 4-iodotoluene 4-bromoanisole with phenyltributyltin afford 96 %, 99 %, 89 % yield after 12 h, 5 h, 9 h, respectively (Table 4.2, entries 7, 8). The coupling reaction of chloronaphthalene with phenyltributyltin was investigated under similar reaction condition, but no desired coupled product was obtained even after 24 h of reaction time.

4.4.2. Kumada Coupling Reactions

4.4.2.1. General procedure for Kumada Coupling Reactions

A round bottom flask was charged with aryl halide (1.0 mmol), B-PMO-TZ-Pd(II) (30 mg), and tetrahydrofuran (THF) (2 mL) solution (solution A), solution of phenyl magnesium bromide (ArMgBr) (2 mmol) was added drop wise into solution A at room temperature with constant stirring. The reaction mixture was stirred at 55 °C for the specified period of time. The reaction mixture was cooled to room temperature and small amount (0.5 ml) of the resulting solution was taken, filtered and analyzed by GC. Solvent was then removed under reduced pressure and column chromatography on silica gel gave the purified products; which were analyzed by

GCMS, ^{1}H, and ^{13}C NMR.

4.4.2.2. Kumada coupling reactions Catalytic Results

Corriu-Tamao-Kumada coupling metal-catalyzed cross-coupling of carbon-carbon bond is one of the most powerful tools in organic synthesis. In order to screen B-PMO-TZ-Pd(II) catalyst, the reaction between iodobenzene and phenyl magnesium bromide was carried out in tetrahydrofuran (THF) solvent at 50 ºC. The final product biphenyl was obtained in 99 % yield with TON 229. Further, influence of solvents was investigated to optimize the reaction conditions. The present heterogenized palladium-catalyzed Kumada coupling could be well understood by analogous to the widely accepted mechanism for homogeneous Kumada coupling reaction. Initially in the first step of reaction, oxidative addition of aryl halide ArX (2) to the B-PMO-Pd(0) complex, provides B-PMO bound aryl palladium complex (3). The oxidative addition of C(sp3)-X to Pd(0) complex usually follows an associative bimolecular process (S_N2 reaction), similar to the other coupling reaction mechanism.[30] Consequently in next step of reaction mechanism, transmetalation between B-PMO aryl palladium complex (3) and aryl magnesium bromide (4) provides B-PMO-Ar^1 -Pd-Ar reaction intermediate (6) with the subsequent removal of byproduct MgBrX (5) salt and the catalyst B-PMO-TZ-Pd is regenerated again. Since Grignard reagent itself is highly basic in nature; no organic or inorganic base is required to be added to initiate the reaction. In the last step of reaction mechanism, the reductive elimination of biphenyl Ar^1-Ar (7) from the unsymmetrical intermediate (6) regenerates the B-PMO-TZ-Pd complex.[32] The influence of solvent and reaction temperature was evaluated on the product yield using B-PMO-TZ-Pd as a catalyst in Kumada coupling reaction by reacting iodobenzene and phenyl magnesium bromide.

To evaluate the role of solvent in Corriu-Tamao-Kumada coupling reaction various solvents; such as THF, DMSO, CH_3OH, DMF, Toluene, acetonitrile were screened by reacting iodobenzene with phenyl magnesium bromide at 50 °C in presence of synthesized heterogeneous B-PMO-TZ-Pd(II) catalyst. The reaction proceeds smoothly in the order THF > acetonitrile > toluene > CH_3OH > DMSO > DMF. From the Figure 4.13. it is clear that reaction proceed smoothly in THF and

acetonitrile solvents in comparison to DMSO and DMF. Grignard reagent (RMgX) is very polar and consequently requires a coordinating solvent to keep it in solution. Ethers are most suitable owing to the availability of lone-pair electrons for coordination to the magnesium ion and solubilization in organic media. Solvents with electrophilic sites such as acetonitrile, DMF, acetone, and ethyl acetate are not suitable owing to their great (irreversible) reactivity with Grignard reagent (RMgX). On the basis of above results nonpolar solvents were suggested to increase the reactivity of Corriu-Tamao-Kumada coupling reaction. Corriu-Tamao-Kumada coupling between iodobenzene and phenyl magnesium bromide was examined in the

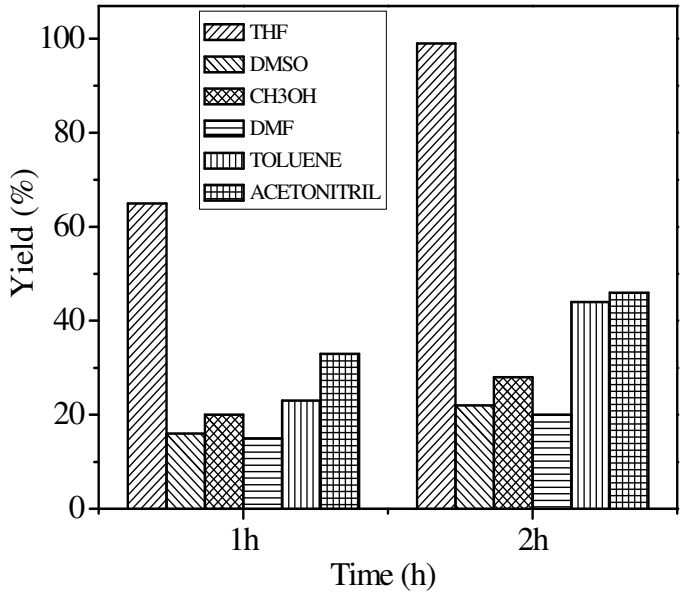

Figure 4.13. Solvent optimization for Corriu-Tamao-Kumada Coupling Reaction.

Reaction conditions: (1 mmol) iodobenzene, (1.5 mmol) phenyl magnesium bromide, 3.5 ml solvent, with Temperature = 50 ºC, heterogeneous B-PMO-TZ-Pd(II) catalyst (30 mg).

temperature range between 30 °C and 50 °C. Reaction does not favor the formation of product at room temperature (30 °C). However, the reaction proceeds smoothly at temperature 50 °C with 99 % yield within 2 h of reaction time period. Since the phenyl magnesium bromide is highly basic in nature; the predominant characteristic

Table 4.3.

B-PMO-TZ-Pd(II) catalyst for Corriu-Tamao-Kumada Coupling Reaction.

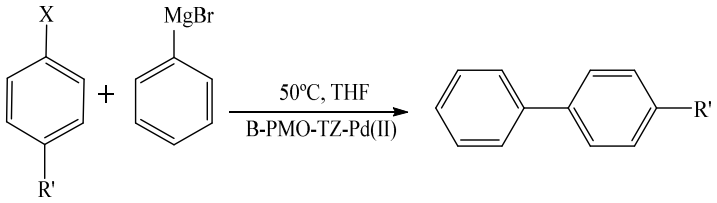

Aryl halide Phenyl magnesium Bromide Biphenyl

X = Cl, Br, I. R' = H, NO_2, CH_3, OCH_3

S.No	Aryl halide	Product		Time (h)	Yield (%)	TON
1.	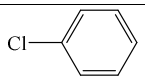	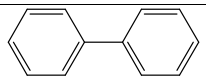	4a	12	40	96
2.	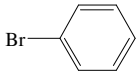	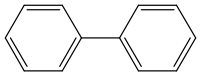	4a	7	92	222
3.	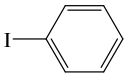	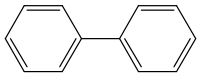	4a	2	95	229
4.	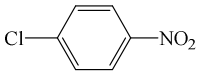	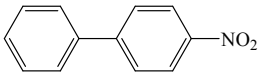	4b	2	99	239
5.	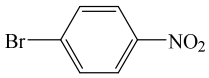	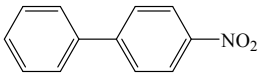	4b	4	96	232
6.	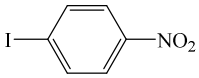	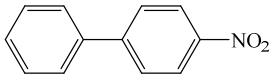	4b	3	98	237
7.	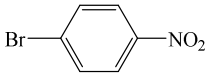	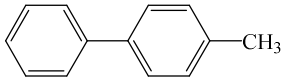	4c	6	83	200
8.	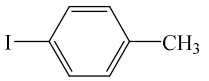	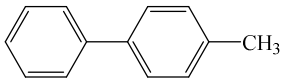	4c	2	95	229
9.	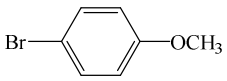	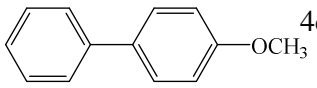	4d	5	90	217

Reaction conditions: (1 mmol) iodobenzene, (1.5 mmol) phenyl magnesium bromide, 3.5 ml (THF) solvent, with (30 mg), Temperature = 50 ºC, heterogeneous B-PMO-TZ-Pd(II) catalyst. Isolated yields (product) were analyzed by GCMS and ^{1}H, ^{13}C CP MAS NMR. TON (turnover number) = moles of product converted per mole of Pd. (See appendix for NMR detail)

magnesium ion of a Grignard Reagent is the anionic aspect of the carbon attached directly to the Grignard reagent is nucleophilic and usually quite basic in nature. Quite small excess of phenyl magnesium bromide (PhMgBr) (1.8 equivalents) was utilized to deprotonate, rather than adding a base. The efficiency of this catalytic system was tested with various Para substituted halides (Table 4.3 entries 1-9). After optimizing the reaction parameters, various substituted and non substituted aryl halide are also investigated in the Corriu-Tamao-Kumada coupling reaction between iodobenzene and phenyl magnesium bromide and results are summarized in Table 4.3.

Various aryl halides were coupled with phenyl magnesium bromide in presence of B-PMO-TZ-Pd(II) and THF as solvent at 50 °C (Table 4.3). As evident from the Table 4.3 all substituted and non substituted aryl halides react with phenyl magnesium bromide under mild reaction conditions to give their corresponding products. (Table 4.3, entries 1-9). Mono substituted aryl halides such as chlorobenzene, bromobenzene and iodobenzene with phenyl magnesium bromide gave coupled product (biphenyl) in 40 %, 92 %, 95 % yield with TON 96, 222, 229, respectively. As discussed earlier, chlorides show poor reactivity compared to bromides and iodides under similar reaction conditions. The low reactivity of chlorides is usually attributed to the strength of the C-Cl bond. As clear from the Table 4.3, Corriu-Tamao-Kumada coupling reactions coupled fast with the aryl iodides and bromides in comparison to chlorides (Table 4.3, entries 1, 2, 3). Electron withdrawing (deficient) nitro (-NO_2) bearing aryl halide such as 4-chloronitrobenzene, 4-bromonitrobenzene, 4-iodonitrobenene with phenyl magnesium bromide gave coupled product 4-nitrobiphenyl in 99 %, 96 %, 98 % yield and 239, 232, 237 TON, respectively. From the catalytic cycle point of view in Kumada coupling reaction, oxidative addition of aryl halide to Pd metal centre results into Ar-Pd-X transition state (3) in the first step. Similar to the other coupling reaction mechanism, oxidative addition is often the rate-determining step in a catalytic cycle. The relative reactivity decreases in the order of I > Br >> C1. Aryl halides activated by the proximity of electron-withdrawing groups are more reactive to the oxidative addition than those with donating groups. Electron withdrawing groups increase the reactivity of aryl halides in coupling reaction; which is clear from the Table 4.3 (entries 4, 5, 6). However, the electron donating group such as Methyl and

methoxy bearing aryl halides such as 4-bromotoluene, 4-iodotoluene, 4-bromoanisole with phenyl magnesium bromide gave corresponding products in 83 %, 95 %, 90 % yield and 207, 229, 217, TON, respectively.

Generally, electron donating bearing Aryl halides show less reactivity in coupling reaction as the electron density increases over the Pd intermediate (3) results in to lower feasibility for further transmetalation and reductive elimination step, respectively. It is clear from the Table 4.3 (entries 5-9) that aryl halides bearing methyl, nitro, methoxy groups react with aryl Grignard to give excellent yields of the corresponding biaryl; whereas the aryl chloride possessed perasubstituents, give good yields in the presence of slightly larger excess of the Grignard reagent (1.8 mmol). Electron-rich substrates such as 4-bromotoluene and 4-iodotoluene show lower reactivity in comparison to the electron withdrawing bearing aryl halides and take longer reaction time period for completion of the reaction (Table 4.3, entries 7, 8). The coupling reaction of sterically hindered 2-chloronapthalene with phenyl magnesium bromide did not proceed even after longer reaction time (4 h).

Furthermore, it is concluded that the nature of the support is responsible for the enhancement of the catalytic activity. This effect in our opinion can be assigned to the increased hydrophobicity of the framework walls of B-PMO due to the presence of phenylene bridges in defined positions. The unique hydrophobic pores facilitate the adsorption of organomettlic neucleophiles and aryl halides close to the active sites, and/or reduce the adsorption of the by-products such as Bu_3SnX and MgBrX. Moreover, the heterogenized B-PMO-TZ-Pd(II) catalyst offers further advantages like the easy catalyst and product recovery as well as possible reuse of the catalyst systems in the reaction.

4.4.3. Heterogeneity and Recycling Studies of Catalyst B-PMO-TZ-Pd(II)

To test if metal was leached out from the solid catalyst during reaction; the hot filtration test was performed. In this process the Stille coupling reaction mixture was collected by filtration at the reaction temperature (120 °C) after a reaction time of 1 h which gave 43% conversions of iodobenzene. The residual activity of the supernatant solution was studied. It was noticed that after filtration of the B-PMO-TZ-Pd(II)

catalyst from the reaction mixture at the elevated reaction temperature (120 °C) (in order to avoid possible recoordination or precipitation of soluble palladium upon cooling) coupling reactions did not proceed further. Thus results of the hot filtration test suggest that Pd was not being leached out from the solid catalyst during the coupling reactions. These results confirm that the palladium catalyst remains on the support even at elevated temperatures during the reaction.

To check the recyclability of the optimized catalyst, B-PMO-TZ-Pd(II) Kumada coupling between iodobenzene and phenyl magnesium bromide was carried out in presence of THF (3.5 ml) at 50 °C which gave 99 % yield of biphenyl within 2 h. Generally, it has been found that precipitate of $MgBr_2$ are generated in the Kumada coupling reaction which may be deposited on the pore walls of BPMO-TZ-Pd(II), causing a decrease in catalytic activity. In present system, the $MgBr_2$ salt did not slow

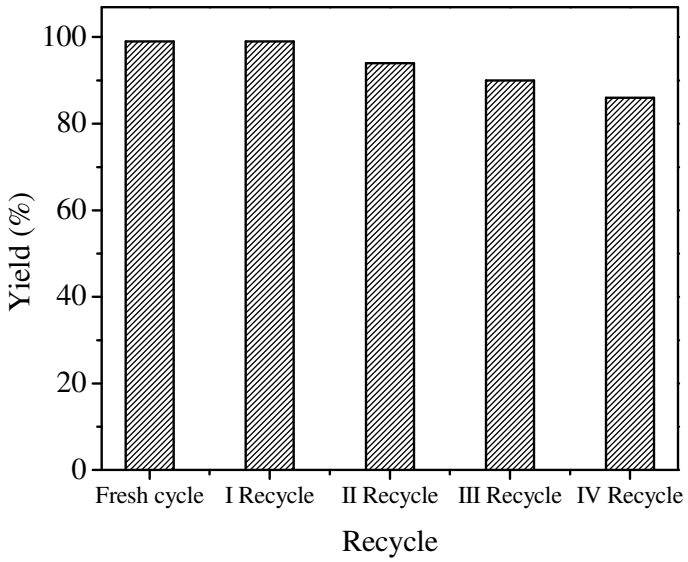

Figure 4.14. Recycling of catalyst B-PMO-TZ-Pd(II).

Reaction conditions: (1 mmol) iodobenzene, (1.5 mmol) phenyl magnesium bromide, 3.5 mL (THF) solvent, Temperature = 50 ºC, heterogeneous B-PMO-TZ-Pd(II) catalyst (30 mg)

down the reaction, presumably due to the short and highly connective channels in the

mesostructures of organosilica B-PMO-TZ-Pd(II) material, which provides good transport of the reactants and products. After the reaction, the catalyst was recovered by centrifugation, washed with DMSO latter with dichloromethane and finally sonicated in acetone and dried under vacuum overnight. The recovered B-PMO-TZ-Pd(II) was re-used for the same reaction for four times; the catalyst retained almost similar level of active indicating the stability of the catalyst (Figure 4.14). The present study indicates that the catalyst can be recycled a number of times without losing its activity to a greater extent.

4.5. REFERENCES

[1] a) S. Inagaki, Y. Fukushima, K. Kuroda, *J. Chem. Soc.,Chem.Commun*. 1993, **8**, 680.; b) T. C. Kresge, E. M. Leonowicz, W. J. Roth, C. J. Vartuli, J. S. Beck, *Nature*. **1992**, 359, 710.; c) H. J. Clark, J. D. Macquarrie, *Chem. Comm*. **1998**, 8, 853.; d) D. Vos, E. De, M. Dams, B. F. Sels, P. A. Jacobs, *Chem. Rev*. **2002,** 102, 3615.

[2] a) F. Hoffmann, M. Cornelius, J. Morell, M. Froba, *Angew. Chem. Int. Ed.* **2006,** 45, 3216.; b) S. Hamoudi, Y. Yang, I. L. Moudrakovski, S. Lang, A. Sayari, *J. Phys. Chem. B.* **2001**, 105, 9118.; c) S. Hamoudi, S. Kaliaguine, *Chem. Comm.* **2002,** 18, 2118.

[3] a) M. P. Kapoor, A. K. Sinha, S. Seelan, S. Inagaki, S. Tsubota, H. Yoshida, M. Haruta, *Chem. Comm*. **2002**, 23, 2902.; b) A. Bhaumik, M. P. Kapoor, S. Inagaki, *Chem. Comm*. **2003,** 4, 470.; c) S. Shylesh, M. P. Kapoor, L. R. Juneja, P. P. Samuel, C. Srilakshmi, A. P. Singh, *J. of Mol. Catal. A: Chemical.* **2009**, 103, 118.

[4] a) W. Guo, X. M. Zhao, *Micropor. Mesopor. Mater*. **2005**, 85, 32.; b) M. P. Kapoor, A. Bhaumik, S. Inagaki, K. Kuraoka, T. Yazawa, *J. Mater. Chem*. **2002,** 12, 3078.

[5] a) S. H. Cho, T. Gadzikwa, M. Afshari, S. T. Nguyen, J. T Hupp, *Eur. J. Inorg. Chem.* **2007,** 31, 4863.; b) A. Sakthivel, S. Syukri, A. K. Hijazi, F. E. Kuhn, *Catal. Lett.* **2006,** 111, 43.

[6] H. C. Kolb, M. G. Finn, K. B. Sharpless, *Angew. Chem., Int. Ed.* **2001,** 40, 2004.

[7] R. Huisgen, G. Szeimies, L. Mobius, *Chem. Ber.* **1967,** 100, 2494.

[8] a) R. A. Evans, Aust. *J. Chem*. **2007**, 60, 384.; b) H. C. Kolb, K. B. Sharpless, *Drug. Dis. Today*. **2003,** 8, 1128.; c) H. N. Gopi, K. C. Tirupula, S. Baxter, S. Ajith, I. M. Chaiken, *Chem.Med.Chem.* **2006,** 1, 54.

[9] a) H. Struthers, T. L. Mindt, R. Schibli, *Dalton Trans.* **2010,** 39, 675.; b) T. Romero, R. A. Orenes, A. Espinosa, A. Tarraga, P. Molina, *Inorg. Chem.* **2011,** 50, 8214.

[10] a) J. T. Fletcher, B. J. Bumgarner, N. D. Engels, D. A. Skoglund, *Organometallics.* **2008,** 27, 5430.; b) Y. Li, J. C. Huffman, A. H. Flood, *Chem. Comm.* **2007**, 26, 2692.

[11] N. S. Miyaura, *A. Chem. Rev*. **1995,** 95, 2457.

[12] K. Tamao, K. Sumitani, M. Kumada, *J. Am. Chem. Soc*. **1972,** 94, 4374.

[13] T. Hiyama, *J. Organomet. Chem.* **2002**, 653, 58.

[14] J. K. Stille, *Angew. Chem, Int. Ed.* **1986,** 25, 508.

[15] E. Negishi, *Acc. Chem. Res*.**1982,** 15, 340.

[16] a) G. Lu, C. Caib, B. H. Lipshutz, *Green Chem.* **2013,** 15, 105.; b) C. Chiappe, G. Imperato, E. Napolitanob, D. Pieraccini, *Green Chem*. **2004**, 6, 33.

[17] a) C. A. Hillier, A. G. Grasa. S. M. Viciu, H. M. Lee, Y. Chuluo, A. C. Nolan. J. O*rgano. Chem.* **2002,** 653, 69.; b) P. Knochel, A. Krasovskiy, I. Sapountzis, *Handbook of Functionalized Organometallics, Vol. 1 (Ed.: P. Knochel), Wiley-VCH, Weinheim.* **2005**, 109.

[18] a) P. Paoprasert, J. W. Spalenka, D. L. Peterson, R. E. Ruther, R. J. Hamers, P. G. Evans, P. Gopalan, *J. Mater. Chem.* **2010,** 20, 2651.; b) B. S. Rana, S. L. Jain, B. Singh, A. Bhaumik, B. Sain, A. K. Sinha. *Dalton Trans.*, **2010,** 39, 7760.

[19] D. Urankar, B. Pinter, A. Pevec, F. D. Proft, I. Turel, J. Kosmrlj. *Inorg. Chem***. 2010**, 49, 4820.

[20] N. Hao, Y. Yang, Y. Wang, P. A. Webley, D. Zhao, *J. of Coll. and Inter. Sci.* **2010,** 346, 429.

[21] a) M. A. Wahab, Kim, C. S. Ha, *Micropor. Mesopor. Mater*. **2004,** 69, 19.; b) M. C. Burleigh, M. A. Markowitz, M. S. Spector, B. P. Gaber, *J. Phys. Chem. B.* **2001,** 105, 9935.

[22] S. Shylesh, C. Srilakshmi, A. P. Singh, B. G. Anderson, *Micropor. Mesopor. Mater***. 2007,** 99, 334.

[23] M. Kar, B. Malvi, A. Das, S. Panneri, S. S. Gupta, *J. Mater. Chem*, **2011,** 21, 6690.

[24] S. Y. Wu, H. S. Hsueh, M. H. Huang, *Chem. Mater*. **2007,** 19, 5986.

[25] W. J. Hunks, G. A. Ozin, *Chem. Mater.* **2004,** 16, 5465.

[26] B. Camarota, Y. Goto, S. Inagaki, E. Garrone, B. Onida, *J. Phys. Chem. C.* **2009,** 113, 20396.

[27] a) L. E. Alonso, K. P. D. Jong, B. M. Weckhuysen, *Phys. Chem. Chem. Phys*. **2010,** 12, 97.; b) H. Yang, X. Han, Z. Ma, R. Wang, J. Liu, X. Ji, *Green Chem*. **2010**, 12, 441.

[28] H. Yang, Y. Wang, Y. Qin, Y. Chong, Q. Yang, G. Li, *Green Chem*. **2011,** 13, 1352.

[29] A. Gniewek, A. M. Trzeciak, J. J. Ziółkowski, L. K. epinski, J. Wrzyszcz, W. Tylus, *J. of Cat*. **2005,** 229, 332.

[30] P. Espinet, A. M. Echavarren, *Angew. Chem. Int. Ed.* **2004,** 43, 4704.; b) L. Yin, J. Liebscher, *Chem. Rev***. 2007,** 107, 133.

[31] S. P. H. Mee, V. Lee, J. E. Baldwin, *Angew. Chem. Int. Ed.* **2004,** 43, 1132.

[32] a) E. Fouquet, M. Pereyre, A. L. Rodriguez, *J. Org. Chem.* **1997,** 62, 5242.; b) Y. S. Cho, B. R. Yoo, S. Ahn, N. Jung, *Bull. Korean Chem. Soc.* **1999,** 20, 422.

CHAPTER-5

Covalently Anchored 2, 4, 6-Triallyloxy-1, 3, 5-Triazine Pd(II) Complex Over Modified Surface of SBA-15

5.1 . INTRODUCTION

Liquid-phase hydrogenation of olefins using heterogeneous catalysts is an industrially relevant process.[1-3] Along with olefin, hydrogenation of nitro compounds to amines has become one of the most important chemical reactions since organic amines are essential materials for the production of agrochemicals, dyes, pharmaceuticals, polymers and rubbers.[4,5] For more than 100 years chemists have used heterogeneous catalysts based on noble metals on various supports.[6,7] Homogeneous hydrogenation catalysis was developed in the 1960's and is reviewed frequently.[8] It is well known that Pd-catalyzed reactions are of significant importance in modern chemical transformations.[9-11] There is a growing demand for organo-metallic reagents that exhibit favorable chemoselectivity and stereoselectivity in hydrogenation reactions. Generally reaction proceeds using N-ligand based palladium catalysts. However, most of these ligands are expensive and significantly limited to their industrial applications.[12-14] Also some of these new ligands are not easily available and contain tedious and expensive synthesis processes and hardly stable in catalytic systems. Therefore, simple easily accessible stable catalyst is desired for heterogeneous reactions. Unfortunately, the efficient separation and subsequent recycling of homogeneous Pd catalysts remain a scientific challenge. Therefore, developing a facile and expedient approach to separate and recycle homogeneous catalysts is highly desirable.

Since the discovery of ordered mesoporous silicas,[15] these materials have attracted wide spread attention in both academics and industry due to their huge potential applications.[16,17] Today mesoporous materials have been employed successfully in gas adsorption and storage,[18] sensing,[19] catalysis,[20] optical device[21] and ion exchange.[22] Since the synthesis of ordered mesoporous materials in 1992 sparked worldwide interest in the field of heterogeneous catalysis and separation science; SBA-15 has become the most popular member of the group and possessed extremely high surface area, easily accessible, uniform pore sizes and stability. [23-25] SBA-15 can carry suitable functional groups at their surface, which can effectively interact with relevant metal ion/molecules, which makes them a potential candidate for heterogeneous catalysts. Furthermore, the leaching of the active site can also be

avoided as the organic moieties are covalently attached to the inorganic support. Various homogenous complexes were widely used for this transformation via covalent attachment.[26-28]

Accordingly, in the present chapter we report our attempt to graft Pd metal complex of 2, 4, 6-triallyloxy-1, 3, 5-triazine (TAT), derivatives over SBA-15 phases and their catalytic properties in hydrogenation reactions. The immediate goals of our study were (i) to evaluate the heterogenization method of the 2, 4, 6-triallyloxy-1, 3, 5-triazine Pd(II) complex over organic modified SBA-15 support, (ii) to characterize the heterogenized SBA-15-TAT-Pd(II) complexes by various physiochemical techniques (iii) to measure the catalytic properties in hydrogenation reaction and (iv) to determine the extent stability of the catalyst as well as their recycling properties.

5.2. EXPERIMENTAL

5.2.1. Materials

Tetraethylorthosilicate (TEOS), Pluronic 123 (P_{123}, Average Mol. wt. = 5800), 3-Mercaptopropyl trimethoxysilane (3-MPTMS), 2, 4, 6-triallyloxy-1, 3, 5-triazine, Azo-bisisobutyronitrile, Palladium acetate, Olefin, Aromatic olefins, Nitrobenzene were purchased from Aldrich. All solvents used in experiments were obtained from Merck (India) and dried before use according to standard methods.

5.2.2. Synthesis Procedure of Catalyst

5.2.2.1. Synthesis of SBA-15 and Surface Modifications

The synthesis of mesoporous SBA-15 was carried out hydrothermally under the autogeneous pressure of an autoclave. The polymer surfactant P_{123} was used as a template and hydrochloric acid served as a mineralizer. The following gel composition was used for the synthesis.

0.043 TEOS: 4.4 g P_{123} M_{avg}= 5800 = [EO_{20}-PO_{70}-EO_{20}]: 8.33 H_2O: 0.24 HCl.

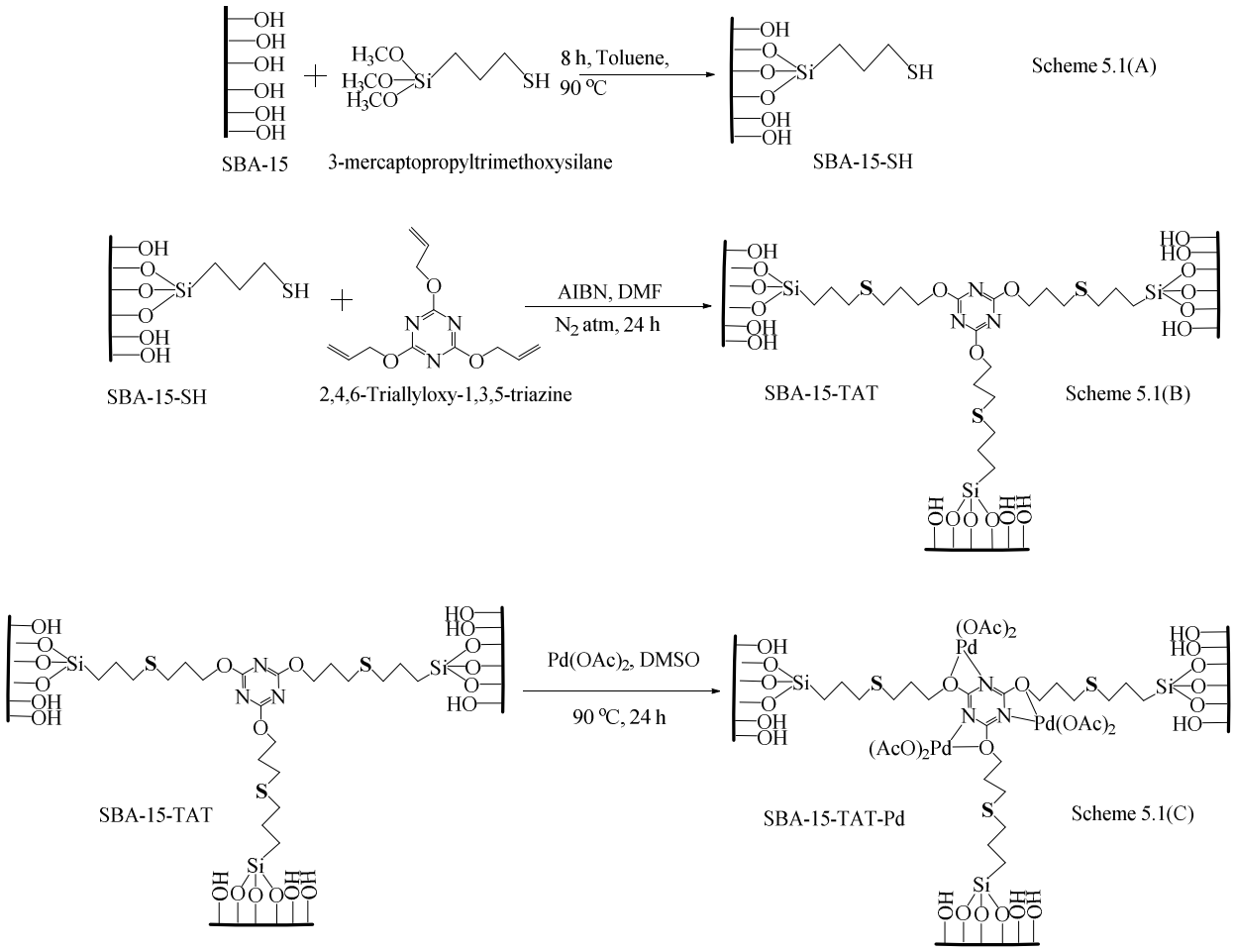

Scheme 5.1. Schematic diagram of heterogeneous SBA-15-TAT-Pd(II) synthesis. 5.1(A) Surface Modification via 3-MPTMS (3-mercaptopropyl trimethoxysilane) of SBA-15, Scheme 5.1(B). Anchoring of 2, 4, 6-triallyloxy-1, 3, 5-triazine (TAT) complex over modified surface of SBA-15, Scheme 5.1(C). Metalation by Pd acetate.

Typically, 4.4 g of tri block co-polymer dispersed in 30 g of distilled water was stirred for 1.5 h. To the resultant solution, 120 g of 2 M HCl was added under stirring and the stirring was continued for 2 h. Finally, 9 g of TEOS was added drop wise and the mixture was maintained at 40 °C for 24 h with continuous stirring. The mass was submitted to a hydrothermal treatment (100 °C, 48 h) under static condition. The precipitate was filtered, washed with distilled water, dried in an oven (90 °C, 12 h) and then calcined in air (500 °C, 6 h) to remove the template. The calcined SBA-15 was characterized by powder XRD.[29]

Surface modification of SBA-15 was achieved by a post grafting method [Scheme 5.1(A)]. One gram of SBA-15 was suspended in a 100 mL of dry toluene and refluxed with 2.5 mmol of 3-Mercaptopropyl trimethoxysilane (3-MPTMS) for 12 h under N_2 atmosphere. The material was filtered after cooling to ambient temperature, washed with dry toluene and dichloromethane, respectively. Soxhlet extraction was carried out for 24 h in dichloromethane (DCM) to remove occluded organosilane. The sample was dried in vacuum for 10 h. The percentage loading of the 3-mercaptopropyl trimethoxysilane groups anchored on the SBA-15 was estimated from chemical analysis. The obtained material is designated as SBA-15-SH.

5.2.2.2. Synthesis of 2, 4, 6 -triallyloxy-1, 3, 5-triazine anchored SBA-15 and Pd metalation

In a typical synthesis, 1 g of organofunctionalized SBA-15, (3-Mercaptopropyl trimethoxysilane) was added to the solution containing 1.06 g solution of 2, 4, 6 -triallyloxy-1, 3, 5-triazine and 0.1 g of azobisisobutyronitrile (AIBN) (initiator) in 20 mL of DMF and refluxed at 100 °C for 24 h under nitrogen atmosphere. The solid was filtered and soxhlet-extracted with dichloromethane for 24 h. The resultant material was dried in vacuum for 2 h. Pd acetate (0.157 mmol) in 20 mL distilled DMSO (Dimethyl sulfoxide) was added in triazene modified SBA-15-SH solution and stirred at 85 °C for 12 h [Scheme 5.1(B, C)]. The resultant material was washed with THF and soxhlet extracted with dichloromethane (DCM) to remove the unanchored metal complex from the SBA-15 surface.[30]

5.2.3. Instruments for Characterization

Powder X-ray diffractograms (XRD) of the materials were recorded using a PAN analytical X'pert Pro dual goniometer diffractometer. A proportional counter detector was used for low angle experiments. The radiation used was Cu Kα (1.5418 Å) with a Ni filter and the data collection was carried out using a flat holder in Bragg-Brentano geometry (0.5–5 °; 0.2 °/min). Care was taken to avoid sample displacement effects. N_2 adsorption–desorption isotherms, pore size distributions as well as the textural properties of the hybrid materials were determined by using a Micromeritics ASAP 2020 instrument and Autosorb 1C Quantachrome USA. The program consisting of both an adsorption and desorption branch and typically ran at –196 °C after samples were degassed at 250 °C for 2 h. Specific surface areas were calculated via the BET model at relative pressures of P/Po = 0.06–0.3. The total pore volume was estimated from the uptake of adsorbate at a relative pressure of P/Po = 0.99. A JEOL JEM-3010 and Tecnai (Model F30) both operating at 300 KV were used for HRTEM samples observation. Samples were crushed and dispersed in isopropanol with low power sonication before putting a drop over carbon coated Cu grid for observation. Chemical analysis was carried out in a Lab Tam 8440 Plasma lab sequential mode ICP–OES Spectrometer and a Spectro Arcos ICP-OES instrument. Standard solution was used for calibration purpose. The scanning electron micrographs of the samples were obtained in dual beam scanning electron microscope (FEI company, model Quanta 200 3D) operating at 30 kV. The samples were loaded on stubs and sputtered with thin gold film to prevent surface charging and also to protect from thermal damage due to electron beam. ^{1}H NMR spectra were recorded on Bruker AC–200 instruments using deuteriated solvent. Liquid ^{13}C NMR spectra were recorded on Bruker AC–200 instruments operating at 50 MHz. ^{13}C NMR chemical shifts are reported in ppm relative to the central line of $CDCl_3$ (d 77.0). Solid-state ^{13}C CP MAS NMR and ^{29}Si MAS NMR spectra were recorded on a Bruker MSL 300 NMR spectrometer with a resonance frequency of 75.5 MHz and 59.6 MHz, respectively for ^{13}C and ^{29}Si, and the chemical shifts were referenced to glycine and TMS respectively. Infrared spectra were recorded using a Perkin Elmer Spectrum one FTIR spectrophotometer. IR spectra were recorded in the range of 4000–400 cm^{-1}.

Thermal analysis (TG-DTA) of the samples was conducted using a Pyris Diamond TGA analyzer with a heating rate of 10 ºC min^{-1} under air atmosphere. Palladium core levels were studied using an ambient pressure photoelectron spectrometer and more details of the instrument are available in reference 31.

5.3. RESULTS AND DISCUSSIONS

5.3.1. Powder X-ray Diffraction

The uniqueness of mesoporous structure, phase purity, degree of orderdness and unit cell parameters of all mesoporous materials were determined by powder X-ray diffraction (XRD). XRD pattern of as-synthesized SBA-15, calcined SBA-15, SBA-15-SH, SBA-15-TAT and heterogenized SBA-15-TAT-Pd(II) complexes are visualized in Figure 5.1. The small-angle XRD pattern in all synthesized samples shows three well-resolved peaks; indexable as (100), (110), (200) reflections associated with *p6mm* hexagonal symmetry. After calcination, the peak intensity of (100) plane increases compared to as-synthesized SBA-15 due to the removal of surf-

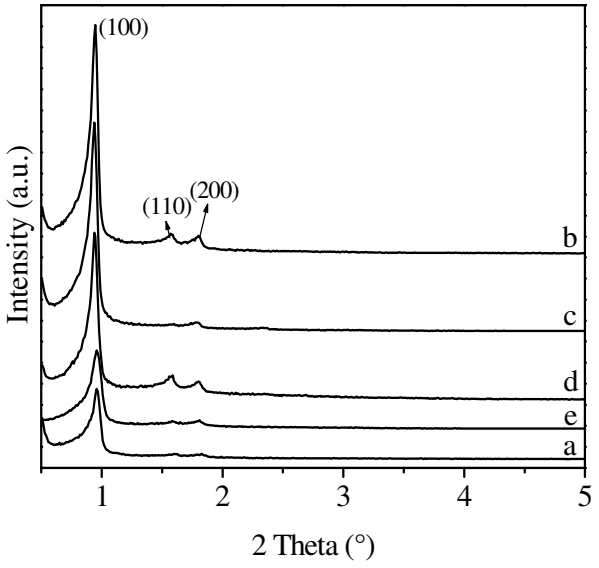

Figure 5.1. XRD pattern of (a) As-synthesized SBA-15, (b) Calcined SBA-15, (c) SBA-15-SH, (d) SBA-15-TAT and (e) SBA-15-TAT-Pd(II).

-actant molecules. (Figure 5.1.a, b). It is evident from Figure 5.1 that XRD patterns of the modified SBA-15 materials are almost similar to the parent SBA-15 with small decrease in overall intensity of (100), (110) and (200) reflections as the organic moieties (-TAT & -SH) get anchored one by one over the mesoporous SBA-15 wall. After organic group modification over SBA-15 by post grafting method, the XRD pattern (Figure 5.1.b-e) shows that the *p6mm* morphology is preserved.[32] This perseverance of peak positions indicates that partial filling of 2, 4, 6 -triallyloxy-1, 3, 5-triazine Pd(II) complex inside the mesopores is less detrimental to the quality of the SBA-15. The persistence of the (100), (110) and (200) reflections (Figure 5.1.b-e) not only proved the structural stability of the support but also the existence of long range order even after a number of treatments with organic molecules in solvents. All these observations clearly show that the ordered mesoporosity and structural stability retained even after incorporation of 2, 4, 6-triallyloxy-1, 3, 5-triazine Pd(II) complexes.

5.3.2. FT-IR Spectra

The presence of isolated surface silanols, hydrogen bonded hydroxyl group and anchored complex, 2, 4, 6 -triallyloxy-1, 3, 5-triazine Pd(II) are evident from the IR spectrum of calcined SBA-15, SBA-15-SH, SBA-15-TAT and SBA-15-TAT-Pd(II) in Figure 5.2. The bands observed in the range of 850–770 cm^{-1} account for the symmetric stretching vibrations of the Si-O-Si bonds, while the band at 1090 cm^{-1} is assigned to the asymmetric (Si–O–Si) vibrations.[33] In the hydroxyl region (3200–3600 cm^{-1})[34], a broad, typical peak of Si–O–H and S–H of thiol functionalized SBA-15 were observed at around 3436 cm^{-1} and 468 cm^{-1}, respectively. Propyl thiol-functionalized SBA-15 shows a characteristic peak at 2934 cm^{-1} corresponds to C–H stretching vibrations. The weak bands at 1340 cm^{-1}, 1381 cm^{-1}, 1468 cm^{-1} are assigned to bending vibrations of methylene groups. Whereas, the band at 705 cm^{-1} relates to the C–S stretching vibrations.[35]

Except the calcined SBA-15, other samples show distinct C–H vibrations at 2934 cm^{-1}, corresponding to C–H bond in the modified samples (Figure 5.2. b, c, d). Furthermore, SBA-15 modified samples (Figure 5.2.b, c, d) exhibit strong and broad

absorption band at 3435 cm^{-1}, due to N–H stretching vibration which overlap with the –OH stretching frequency. All the modified SBA-15-SH, SBA-15-SH-TAT and SBA-15-SH-TAT-Pd(II) exhibit strong band at 1571 cm^{-1}, due to ring >C-N stretching vibration and additional peak at 1168 cm^{-1} (C–N) gets overlap with the symmetric stretching vibrations of the Si–O–Si bonds (1088 cm^{-1}).[36]

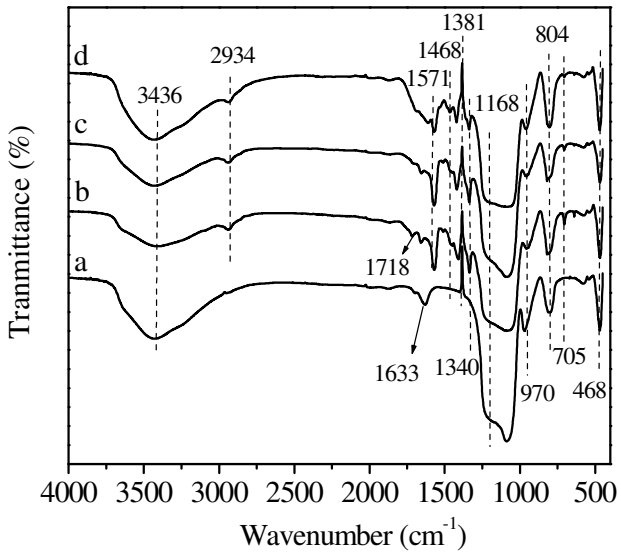

Figure 5.2. FT-IR spectrum of (a) Calcined SBA-15, (b) SBA-15-SH, (c) SBA-15 TAT and (d) SBA-15-TAT-Pd(II).

The above mode of vibrations clearly indicate that 2, 4, 6-triallyloxy-1, 3, 5-triazine Pd(II) complex and organic modifiers were incorporated successfully over the surface modified SBA-15.

5.3.3. Diffuse reflectance UV–Vis Spectroscopy

The diffuse reflectance spectra (200–800 nm) of calcined SBA-15 and SBA-15-TAT-Pd(II) show the characteristic absorption at 254 nm, corresponds to typical siliceous material (Figure 5.3.a).[37] SBA-15-TAT-Pd(II) shows characteristic absorption band at 260 nm corresponding to a metal-ligand charge transfer (MLCT).

The shift towards higher energy values result from the metallation by Pd acetate. The presence of high coordinating ligand like 2, 4, 6-triallyloxy-1, 3, 5-triazine (TAT), the Pd(II) shifts the absorbance band towards the higher frequency region resulting in a slight deviation from theoretical values. Another strong absorbance at 380 nm *i.e.* in the visible region may be due to a change in $\pi \rightarrow \pi^*$ and at 682 nm corresponds to

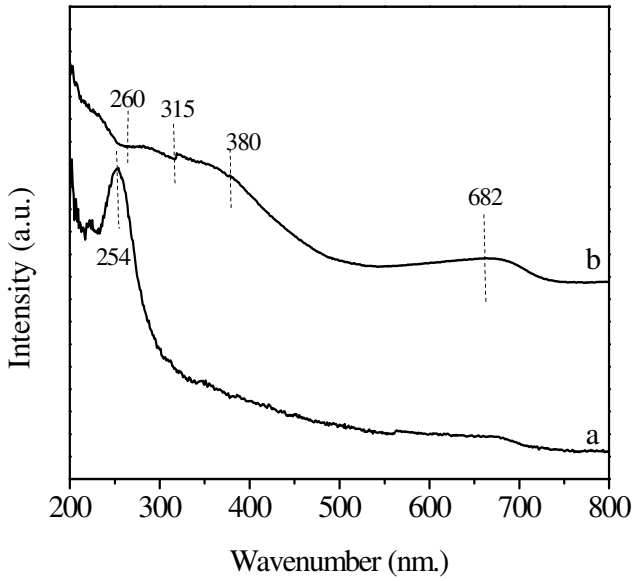

Figure 5.3. UV-vis spectra of (a) Calcined SBA-15 and (b) SBA-15-TAT–Pd(II).

$n \rightarrow \pi^*$ transitions after Pd grafting over organo-modified SBA-15-TAT complex[35] (Figure 5.3.b). These results are in agreement with XPS results.

5.3.4. ^{13}C CP MAS NMR Spectra

The organic moiety 2, 4, 6-triallyloxy-1, 3, 5-triazine anchored over the modified (–SH) surface of SBA-15 is further demonstrated by ^{13}C NMR techniques. ^{13}C Liquid NMR of 2, 4, 6-triallyloxy-1, 3, 5-triazine (TAT) and ^{13}C solid state NMR spectrum of SBA-15-TAT-Pd(II) are depicted in Figure 5.4. a, b. The peaks at 8, 20 and 34 ppm, present in SBA-15-TAT-Pd(II) catalyst are assigned to the carbon atoms (C1–C3) of the propyl chain in organic modifier (3-MPTMS), indicate the successful

3-Mercaptopropyl trimethoxysilane functionalization over SBA-15 (Figure 5.4.b). The presence of new resonance in the ^{13}C CP MAS NMR spectrum and also in ^{13}C Liquid NMR of 2, 4, 6-triallyloxy-1, 3, 5-triazine (TAT), at 72 ppm corresponds to carbon attached to the oxygen atom in the allylic chain of triazene ligand (Figure 5.4. a, b). Furthermore, peak present in both TAT and SBA-15-TAT-Pd(II) at 169 ppm corresponds to the carbon present in the ring of triazene ligand (TAT). In additon, low

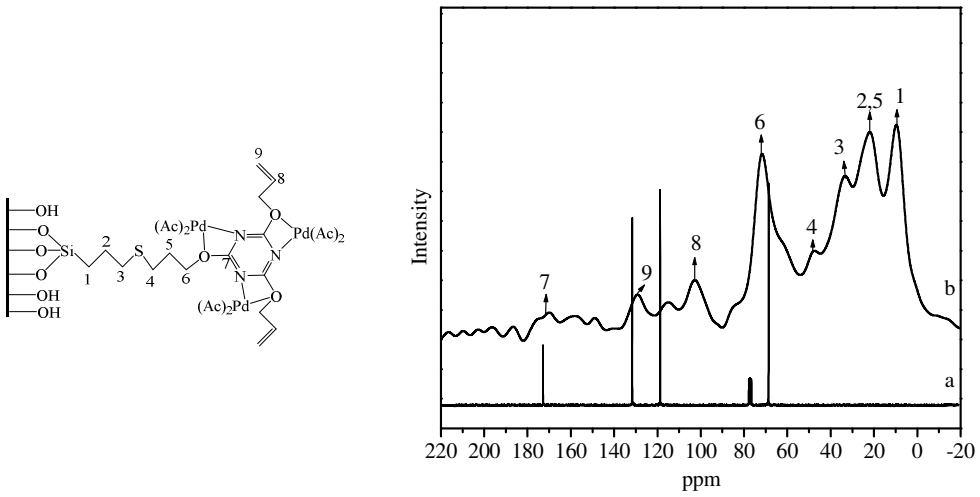

Figure 5.4. Liquid ^{13}C NMR of (a) 2, 4, 6-triallyloxy-1, 3, 5-triazine (TAT) and (b) Solid state ^{13}C CP MAS NMR of SBA-15-TAT-Pd(II).

intensity extra peaks in the range of 103–130 ppm corresponds to the unmodified allylic group of triazene ligand (Figure 5.4, a, b), which might be due to the unreacted portion of the allylic group of 2, 4, 6-triallyloxy-1, 3, 5-triazine ligand. Since the intensity of the un-reacted carbon peak is lower, it is confirmed that the maximum amount of anchoring of TAT over 3-MPTMS modified SBA-15. All the resonance peaks of ^{13}C NMR support the successful anchoring of 2, 4, 6-triallyloxy-1, 3, 5-triazine over the 3-MPTMS modified SBA-15 surface.

5.3.5. Solid state ^{29}Si MAS NMR Studies

The degree of functionalization of surface silanol groups of SBA-15 with organic moiety can be monitored by ^{29}Si CP MAS NMR spectroscopy. ^{29}Si CP–MAS

NMR spectra of calcined SBA-15 and SBA-15-TAT-Pd(II) are depicted in Figure 5.5. The spectrum shows broad resonance peaks from –90 to –120 ppm, indicative for a range of Si–O–Si bond and the bands are centered at –93 ppm, –102 ppm and –111 ppm assigned to Q^2 [germinal silanol, $(SiO)_2Si(OH)_2$], Q^3 [single silanol, $(SiO)_3Si(OH)$] and Q^4 [siloxane, $(SiO)_4Si$] sites of the silica framework, respectively (Fig.5.5. a, b). The calcined SBA-15 shows the presence of broad resonance peaks

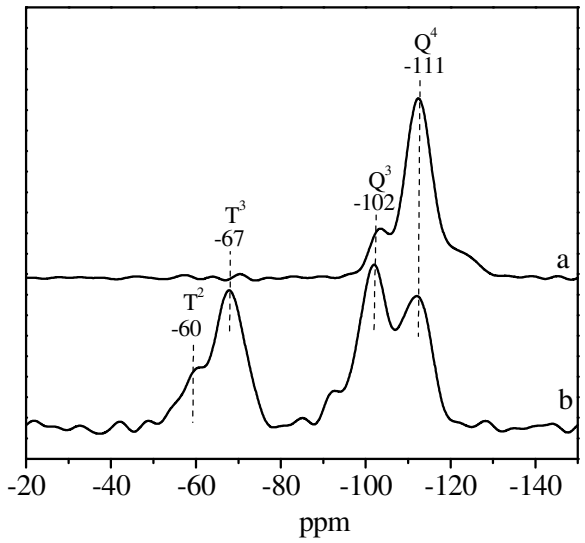

Figure 5.5. Solid state ^{29}Si CP MAS NMR spectrum of (a) Calcined SBA-15 and (b) SBA-15-TAT-Pd(II).

from –98 to –126 ppm, indicative for a range of Si–O–Si bond, and it is noteworthy that the sample contains large amounts of Q^4 sites showing a high framework cross-linking. In general, the Q^3 sites are considered to be rich with isolated Si–OH groups, which may be free or hydrogen-bonded. Spectrum of SBA-15-TAT-Pd(II) show two peaks at –67 ppm and at –60 ppm which are assigned to T^3 [$SiR(OSi)_3$] and T^2 [$Si(OH)R(OSi)_2$], respectively. The presence of major T^3 peak indicate that the proper heterogenization of 3-mercaptopropyltrimethoxy silane over SBA-15.[38] ^{29}Si CP MAS NMR spectra provide direct evidence for the formation of a highly condensed siloxane network with organic group covalently bonded to the mesoporous silica.[39]

5.3.6. Electron Microscopy

TEM images of calcined SBA-15 and SBA-15-TAT-Pd(II) provide structural evidence that the material is organized into ordered arrays of two-dimensional hexagonal mesopores (Figure 5.6.A.B). The significant difference of the TEM patterns was not observed between the two Figures 5.6.A, B. However, after the anchoring of TAT-Pd(II) complex inside the mesoporous channels of SBA-15, the

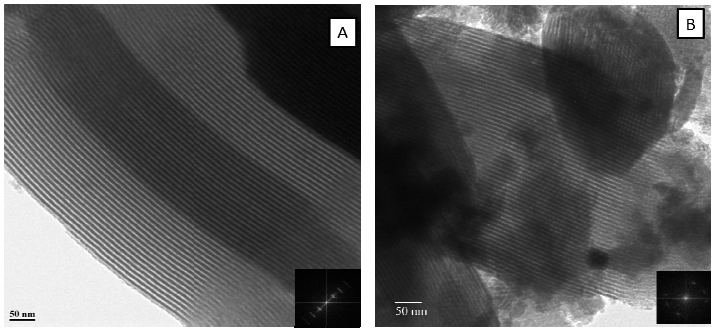

Figure 5.6. TEM Images (A) Calcined SBA-15 and (B) SBA-15-TAT-Pd(II).

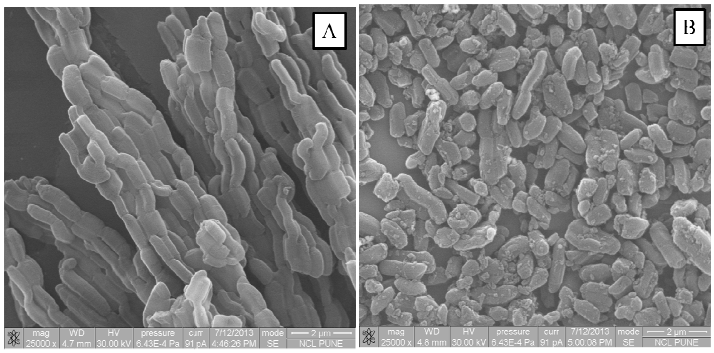

Figure 5.7. SEM images of (A) Calcined SBA-15 and (B) SBA-15-TAT-Pd(II).

image had shown distinct deep contrasting meso parallel channels with respect to the light shaded surface. This might be interpreted as due to the presence of the TAT-Pd(II) complex inside the mesopores of the SBA-15, but not on the surface. If the TAT-Pd(II) complex was anchored on the surface of the functionalized SBA-15, then

the high-contrast dark meso parallel channels would have appeared along the boundary of the visualized SBA-15 and not inside the porous body as observed previously by *Shephard et al.*[40] From this results it is very clear that the Pd-complex was immobilized inside the pore channels of modified SBA-15. SEM image of the calcined SBA-15 and SBA-15-TAT-Pd(II) are shown in Figure 5.7 A, B, respectively. Calcined SBA-15 shows uniform arrays of small agglomerate particle meso channals arrangement and clear molecular-scale periodicity in the SEM images. Furthermore, SBA-15-TAT-Pd(II) demonstrates molecular-based materials; the particle morphology in the large molecular system does not change and becomes denser after TAT-Pd(II) complex anchoring over the mesoporous surface in comparison to the calcined SBA-15.

5.3.7. Thermal Analysis

Thermal stability of all the synthesized materials were studied by thermo gravimetric analysis (TGA) under air atmosphere from ambient temperature to 1000 °C with a temperature increment of 10 °C/min. TGA and DTA of (a) As-synthesized SBA-15, (b) Calcined SBA-15, (c) SBA-15-SH and (d) SBA-15-TAT are shown in the Figure 5.8.A, B. TGA plots of calcined SBA-15 and modified SBA-15 samples show approximately 5 % weight loss below 120 °C caused due to the desorption of physiosorbed water molecules (Figure 5.8.A, a-d).[41–43] A loss of ~56 weight % was observed between 132 °C and 400 °C for the as-synthesized SBA-15 corresponds to the removal of trapped surfactant within closed pores (Figure 5.8.A, a). Whereas, nearly no weight loss in TGA was observed in the calcined SBA-15 between 132 °C and 400 °C indicates the complete removal of surfactant from SBA-15. Moreover a total weight loss of ~ 7% was noticed for calcined SBA-15 and this may be due to removal of surface silanol groups at very high temperature (Figure 5.8, A, b). TGA result of SBA-15-SH samples shows weight loss in two steps. In the first step, weight loss was occurred between 70 °C and 150 °C corresponds to the loss of loosely bounded water and adsorbed moisture. In the second step, weight loss was observed in the region of 245 °C-385 °C in TGA analysis and a sharp exothermic peak visible in DTA analysis is attributed to decomposition of 3-MPTMS (Figure 5.8.A, B, c).

TGA result of SBA-15-SH material shows quantitatively 14.27 % weight loss, which is greater than calcined SBA-15; strongly supports successful anchoring of 3-MPTMS over SBA-15 (Figure 5.8.A, b, c). In the case of SBA-15-TAT samples, a total weight loss of ~35 % was noticed, is due to the complete decomposition of organic moieties heterogenized over SBA-15, which is supported by the exothermic peak in the DTA spectrum of the same sample (Figure 5.8.B.d).

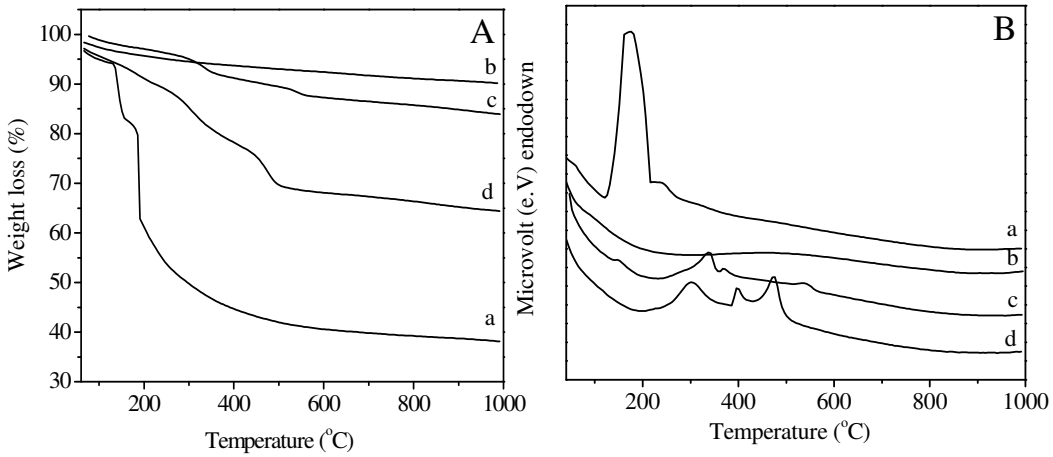

Figure 5.8. (A) TGA, (B) DTA of (a) As-synthesized SBA-15, (b) Calcined SBA-15, (c) SBA-15-SH and (d) SBA-15-TAT.

All the TGA and DTA results clearly indicate that 2, 4, 6 -triallyloxy-1, 3, 5-triazine is well anchored over the modified surface of calcined SBA-15.

5.3.8. Nitrogen Sorption Studies

The nitrogen adsorption–desorption results of calcined SBA-15, SBA-15-TAT-Pd(II) and their corresponding pore size distribution curves are plotted in Figure 5.9. The surface area, average pore diameter and pore volume determined for the calcined

Table 5.1.

Textural properties of mesoporous calcined SBA-15 & SBA-15-TAT-Pd(II).

S.No.	Sample	N[a] (wt. %)	Loading of Pd (wt. %)[b] Input	Output	S.A (m^2/g)	D_P (Å)	Vp (cm^3/g)
1.	Calcined SBA-15				830	65	1.13
2.	SBA-15-TAT-Pd(II)	1.85	4	2.2	285	55	0.46

[a] Calculated based on elemental (Nitrogen) analysis value.

[b] Input is based on the amount of Pd during synthesis reaction; output is based on the ICP-OES analysis.

S.A : BET surface area (D_P) : Average pore diameter, (Vp) : Pore volume.

SBA-15 and SBA-15-TAT-Pd(II) are summarized in the Table 5.1. All the samples show type IV adsorption isotherms, according to the IUPAC classification, indicating mesopores with completely reversible nature, uniformly sized, with a capillary condensation step at *P*/*P*o = 0.3–0.4. The total surface area, average pore diameter and pore volume observed for the calcined SBA-15 and SBA-15-TAT-Pd(II), were found to be 830 m^2/g, 65 Å, 1.13 cm^3/g and 285 m^2/g, 55 Å, 0.46 cm^3/g, respectively. The decrease in total mesoporous surface area (65 %), pore diameter (15 %) and pore volume (59 %) after 2, 4, 6 -triallyloxy-1, 3, 5-triazine Pd(II) complex immobilization over organo-modified SBA-15 is indicative of the grafting of TAT-Pd(II) complex over the mesoporous SBA-15 (Table 5.1).

It is clear from Table 5.1 that even though silylation procedures changed the textural properties of the mesoporous material, the decrease is more prominent after 2, 4, 6 -triallyloxy-1, 3, 5-triazine Pd(II) complex immobilization over SBA-15 since the bulkier organic moieties inside the pore channels occupy more area of the void space (Figure 5.9 inset a, b). The capillary condensation steps of SBA-15-TAT-Pd(II) get reduced to lower *P*/*P*o values compared to calcined SBA-15 (Figure 5.9.a, b). This shift towards slightly lower partial pressure shows a possible reduction in the pore size and a partial distortion in pore arrangement, consistent with the XRD results. It is

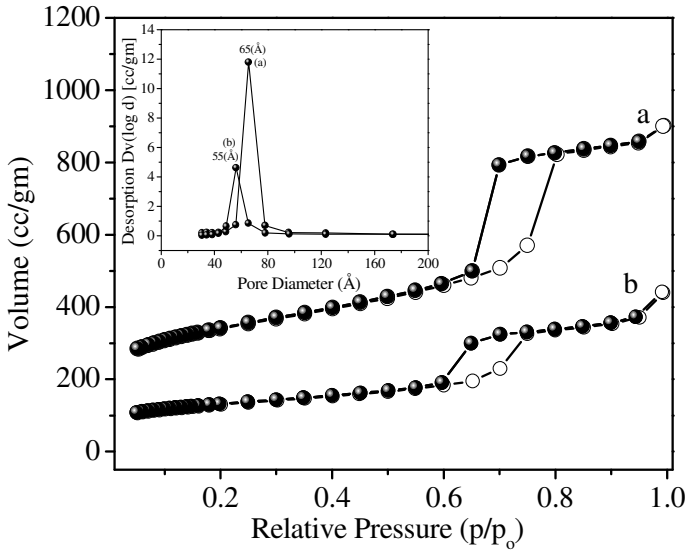

Figure 5.9. Nitrogen adsorption-desorption isotherm and inset (BJH) pore size distribution of (a) calcined SBA-15 and (b) SBA-15-TAT-Pd(II).

also known that the inflection position in N_2 sorption isotherms depends on the diameter of the mesopores and the sharpness usually indicates the uniformity of the mesopores, due to capillary condensation of nitrogen molecule. These results directly supporting the previous results of proper heterogenization of metal complex inside the mesoporous channels of the SBA-15.

5.3.9. X-ray photoelectron Spectroscopy (XPS*)*

X-ray photoelectron spectroscopy (XPS) is the powerful tool to investigate the electronic properties of the species formed on the surface of the materials. XPS is highly sensitive to electronic environment, e.g. oxidation state and or multiplicity influences in the binding energy of the core electron of the metal. The synthesized material SBA-15-TAT-Pd(II) was characterized by X-ray photoelectron spectroscopy (XPS) to ascertain the oxidation state of Pd species. In Figure 5.10 the Pd binding energy of SBA-15-TAT-Pd(II) exhibits two strong peaks centered at 337.9 eV. and 344 eV., respectively, which are assigned to the Pd $3d_{5/2}$ and Pd $3d_{3/2}$, respectively. The observed peaks indicate that palladium is present in the Pd^{2+} oxidation state in the synthesized SBA-15-TAT-Pd(II). According to literature report pure Pd acetate metal

salt binding energy for Pd $3d_{5/2}$ and Pd $3d_{3/2}$ orbital appears at 338.2 eV. and 345.3 eV., respectively.[44] In comparison to literature value, the synthesized SBA-15-TAT-

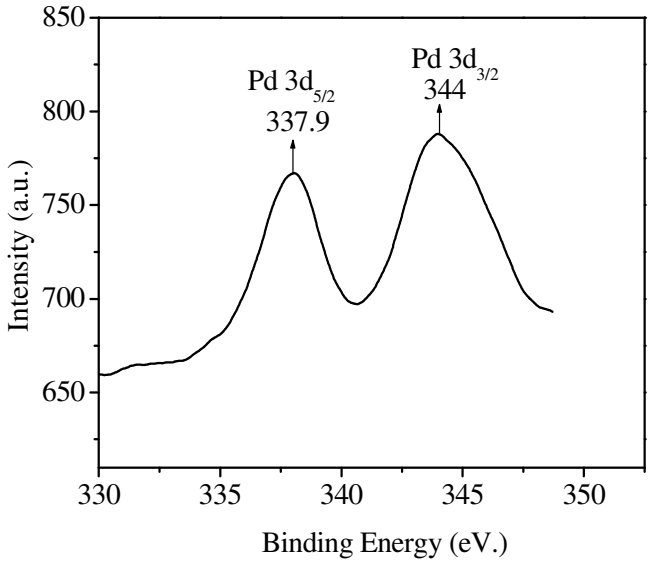

Figure 5.10. XPS spectra of SBA-15-TAT-Pd(II).

Pd(II) show shift in binding energy of Pd towards lower value *viz* 337.9 eV. Pd $3d_{5/2}$ and 344 eV. Pd $3d_{3/2}$, respectively. The decrease of Pd binding energy in 2, 4, 6 -triallyloxy-1, 3, 5-triazine complex functionalized SBA-15 implies that there is a strong coordination interaction between Pd metal species and 2, 4, 6 -triallyloxy- 1, 3, 5-triazine ligand.[45] These results are in agreement with the UV-vis observations.

5.4. CATALYTIC REACTIVITY

5.4.1. Procedure for Hydrogenation Reaction

In a typical liquid-phase hydrogenation reaction, 1.0 g of olefin, 50 mL of methanol and 0.025 g of SBA-15-TAT-Pd(II) catalyst were placed in a 100 mL Parr autoclave (Parr Inst. Co. Mod. 3911), pressurized with hydrogen (150 psi) and stirred at room temperature for a specific time. Samples were periodically withdrawn from the reaction mixture, filtered off and analyzed. Olefin conversion and selectivity were

determined by using gas chromatography equipped with a flame ionization detector (FID) and a capillary column. Before GC analysis, the samples were centrifuged for 5 min at 4000 rpm. At the end of specified time, the contents were analyzed by GC. Control experiments in the absence of catalyst showed practically no (<0.1 %) reduction of substrate. Peak positions of various reaction products were compared and matched with the retention times of authentic samples. Identity of the products was also confirmed by GC–MS.

5.4.2. Catalyst SBA-15-TAT-Pd(II) for Hydrogenation Reactions

Hydrogenation is one of the most basic chemical transformations of organic substances. Olefin and nitro compounds hydrogenation is an industrially important reaction. The catalytic activity of SBA-15-TAT-Pd(II) was tested in the hydrogenation of a variety of unsaturated olefin and aromatic nitro compounds to their corresponding products. The catalytic performance of the heterogenized catalyst SBA-15-TAT-Pd(II) in olefin hydrogenation was initially studied with styrene as the substrate under mild reaction conditions (Pressure H_2 = 150 psi, T = 40 °C). The reactions were carried out in methanol solvent at room temperature and under 100 psi hydrogen pressure. Detailed observations of all the reactions are given in Table 5.2. It is evident from the Table 5.2 that the SBA-15-TAT-Pd(II) is quite active for the hydrogenation reaction under mild reaction conditions. In the case of styrene and α-methyl styrene, the hydrogenated products (ethylbenzene & cumene) were obtained within 15 min, 45 min with 2320, 2320 TON, respectively (Table 5.2, entries 1, 5). The reason for longer reaction time period for α-methyl styrene might be due to the steric hindrance produced by the methyl group next to the olefin group. In the absence of SBA-15-TAT-Pd(II) catalyst, negligible styrene conversion was observed (~7 %). It is noteworthy to mention that no ring hydrogenated products were observed with styrene, and α-methyl styrene.

Table 5.2. SBA-15-TAT-Pd(II) catalyst for Hydrogenation Reaction.

S. No.	Reactant	Product	Time (min.)	Yield (%)	TON
1.	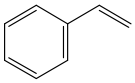	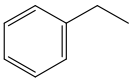	15	100	2320
2.			60	100	2320
3.			90	80	1850
4.	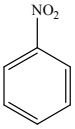	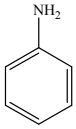	60	95	2200
5.	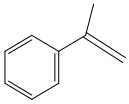	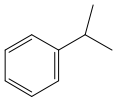	45	100	2320
6.	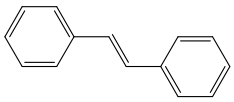	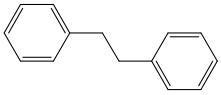	480	---	---
7.			30	96	2230
8.			15	100	2320

Reaction conditions: of substrate (10 mmol), SBA-15-TAT-Pd(II) catalyst (0.025 g), H_2 Pressure = 150 psi, Reaction Temperature = 40 °C, solvent = 50 mL methanol.

Non-aromatic cyclic olefin group containing substrates cyclopentene, cyclohexene and cyclooctene gave hydrogenated products in 30 min, 60 min, 90 min with 2320, 2320, 1850 TON, respectively (Table 5.2, entries 7, 2, 3). The increase in reaction time for non-aromatic cyclic olefin containing substrates may be due to the increase in size of ring in term of carbon atoms. Whereas 1-hexene affords 100 % conversion to the corresponding hydrogenated product hexane in 15 min with 2320 TON. It is clear from the Table 5.2 that acyclic olefins afford higher rate of reaction in

comparison to the cyclic olefin in presence of SBA-15-TAT-Pd(II); the reason might be that the olefin group faces steric hindrance in cyclic structure of aromatic or non-aromatic compounds. Furthermore, the SBA-15-TAT-Pd(II) catalyst affords 100 % conversion of the aromatic nitro (nitrobenzene) in 1 h with 2200 TON without the ring hydrogenation (Table 5.2, entry 4). The *trans*-stilbene, did not give any product under the specified time period. This is probably due to the relatively large steric hindrance (Table 5.2, entry 6) of the reactant molecule.

5.4.3. Heterogeneity and Recycling Studies of Catalyst SBA-15-TAT-Pd(II)

In order to understand whether the observed catalytic activity arises from truly heterogeneous catalyst systems, a series of leaching experiments was conducted. To test if metal is leached out from the solid catalyst during a reaction; the hot filtration test and recycling study of heterogeneous catalyst SBA-15-TAT-Pd(II) under the reaction conditions; 10 mmol of styrene, 150 psi of H_2 pressure, 0.025 g of catalyst SBA-15-TAT-Pd(II), 50 mL methanol, T = 40 °C was performed. Hydrogenation reaction mixture was collected by filtration at temperature (40 °C) after a reaction time of 5 min which give 58 % conversions of styrene. The residual activity of the supernatant solution was studied. It was observed that after filtration of SBA-15-TAT-Pd(II) catalyst from the reaction mixture at the elevated reaction temperature (40 °C) (in order to avoid possible re-coordination or precipitation of soluble palladium upon cooling) hydrogenation reactions did not proceed further. Thus, results of the hot filtration test suggest that Pd was not being leached out from the solid catalyst during the reaction. These results confirm that the palladium catalyst remains on the support. This clearly demonstrate that the reaction ceased after the removal of SBA-15-TAT-Pd(II) catalyst from the reaction mixture.

Reusability is an important feature to be monitored for application of heterogenized single-site catalysts. Reusability of heterogeneous catalyst SBA-15-TAT-Pd(II) was performed under the reaction conditions; 10 mmol of styrene, 150 psi of H_2 pressure, 0.025 g of catalyst SBA-15-TAT-Pd(II), 50 mL methanol solvent, T = 40 °C. Hydrogenation reaction mixture was filtered using a sintered glass funnel, and the residue extensively washed with, 1, 2 dichloromethane (DCM) (2-5 mL) and

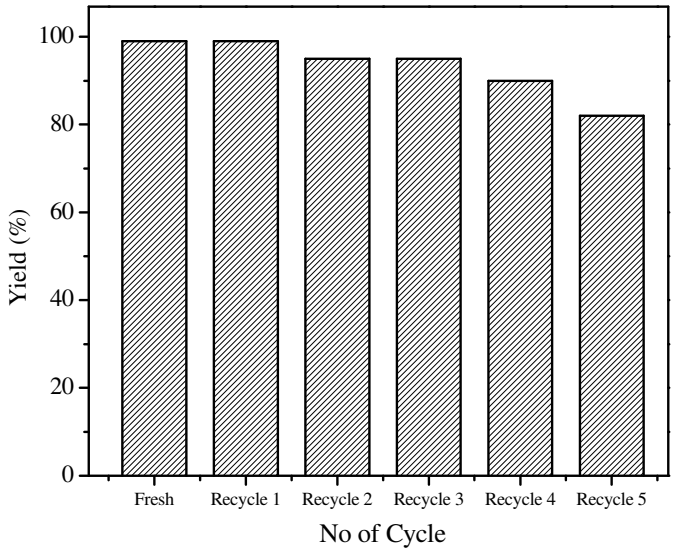

Figure 5.11. Recycling study of heterogeneous catalyst SBA-15-TAT-Pd(II).

Reaction Conditions: 10 mmol of styrene, 150 psi of H_2 pressure, 0.025 g of catalyst SBA-15-TAT-Pd(II), 50 mL methanol, T = 40 °C.

further with methanol. The gas chromatography analysis of the filtrate shows no detectable amounts of reagents and products. The catalyst was dried under vacuum overnight before performing the reusability test. The catalyst could be reused directly without further purification and was reused up to five cycles (Figure 5.11). The amounts of Pd leaching into solution for the hydrogenation reactions were detected through ICP. The loss of Pd amount for the hydrogenation reaction was less than 1.0 weight percentage of total Pd content. Even though a small amount of Pd loss could be detected, catalyst still shows high reusability and stability for hydrogenation reactions. Nearly similar conversion was found even after five cycles by using SBA-15-TAT-Pd(II) catalyst in the hydrogenation reaction.

5.5. REFERENCES

[1] O. Schmidt, *Chem. Re*v. **1933**, 12, 363.

[2] R. A. W. Johnstone, A. H. Wilby, I. D. Entwistle, *Chem. Rev.* **1985**, 85, 129.

[3] C. M. Crudden, D. Allen, M. D. Mikoluk, J. Sun, *Chem. Comm.* **2001**, 1154.

[4] B. Chen, U. Dingerdissen, J. G. E. Krauter, H. G. J. Lansink Rotgerink, K. M¨obus, D. J. Ostgard, P. Panster, T. H. Riermeier, S. Seebald, T. Tacke, H. Trauthwein, *Appl. Catal: A*, **2005**, 280, 17.

[5] K. Nomura, *J. Mol. Catal. A: Chem.*, **1998,** 130, 1.

[6] H. U. Blaser, C. Malan, B. Pugin, F. Spindler, H. Steiner, M. Studer, *Adv. Synth. Catal.* **2003,** 345, 103.

[7] R. M. Magdalene, E. G. Leelamani, N. M. N. Gowda, *J. Mol. Catal. A: Chem.* **2004,** 223, 17.

[8] a) *The Handbook of Homogeneous Hydrogenation* (Eds.: J. G. de Vries, C. J. Elsevier), Wiley-VCH, Weinheim, **2007.**; b) P. W. N. M: van Leeuwen, *Homogeneous Catalysis—Understanding the Art, Kluwer Academic Publ.,* Dordrecht, **2004,** chap. 4.; c) S. Bhaduri, D. Mukesh, Hydrogenation of Alkenes, Wiley, NY, **2000;** d) A Bçrner, J. Holz, *Homogeneous Hydrogenations, in Transition Metals for Organic Synthesis,* Vol. 2, 2nd ed. (Eds.: M. Beller, C. Bolm), Wiley-VCH, Weinheim, **2004**.

[9] *a*) M. M. Dell'Anna, M. Gagliardi, P. Mastrorilli, G. P. Suranna, C. F. Nobile, *J. Mol. Catal. A: Chem.* **2000,** 158, 515.; b) Y. Zheng, K. Ma, H. Wang, X. Sun, J. Jiang, C. Wang, R. Li, J. Ma, *Catal. Lett.* **2008,** 124, 268.; *c*) A. J. Amali, R. K. Rana, *Chem. Commun.*, **2008,** 4165.

[10] *a*) N. Erathodiyil, S. Ooi, A. M. Seayad, Y. Han, S. S. Lee, J. Y. Ying, *Chem.–Eur. J.*, **2008**, 14, 3118.; b) K. C. Nicolaou, A. L. Nold, R. R. Milburn, C. S. Schindler, K. P. Cole, J. Yamaguchi, *J. Am. Chem. Soc.*, **2007,** 129, 1760.; c) F. Zhao, K. Murakami, M. Shirai, M. Arai, *J. Catal.*, **2000,** 194, 479.

[11] *a*) A. Biffis, M. Zecca, M. Basato, *J. Mol. Catal. A: Chem.*, **2001,** 173, 249.; b) L. Yin and J. Liebscher, *Chem. Rev.*, **2007**, 107, 133.

[12] D. H. Lee, J. Y. Jung, M. J. Jin. *Chem. Commun.* **2010,** 46, 9046.

[13] J. Yang, L. Wang. *Dalton Trans.* **2012,** 41, 12031.

[14] I. Blaszczyk, A. M. Trzeciak. *Tetra.* **2010,** 66, 9502.

[15] C. T. Kresge, M. E. Leonowicz, W. J. Roth, J. C. Vartuli, J. S. Beck. *Nature.* **1992,** 359, 710.

[16] Y. Jackie, Ying, P. Christian, S. Mehnert, S. Michael, Wong. *Angew. Chem. Int. Ed.* **1999,** 38, 56.

[17] G. J. de A. A. Soler-Illia, C. Sanchez, B. Lebeau, J. Patarin. *Chem. Rev.* **2002,** 102, 4093.

[18] A. Walcarius, L. Mercier. *J. Mater. Chem.* **2010,** 20, 4478.

[19] L. Nicole, C. Boissiere, D. Grosso, P. Hesemann, J. Moreau, C. M. Sanchez. *Chem. Commun.* **2004,** 2312.

[20] A. Corma. *Chem. Rev.* **1997,** 97, 2373.

[21] Quach, V. Escax, L. Nicole, P. Goldner, O. Guillot-Noel, P. Aschehoug, P. Hesemann, J. Moreau, D. Gourier, C. Sanchez. *J. Mater. Chem.* **2007,** 17, 2552.

[22] Z. Luan, M. Hartmann, D. Zhao, W. Zhou, L. Kevan. *Chem. Mater.* **1999,** 11, 1621.

[23] A. Quach, V. Escax, L. Nicole, P. Goldner, O. Guillot-Noel, P. Aschehoug, P. Hesemann, J. Moreau, D. Gourier, C. Sanchez. *J. Mater. Chem.* **2007,** 17, 2552.

[24] J. S. Beck, J. C. Vartuli, W. J. Roth, M. E. Leonowicz, C. T. Kresge, K. D. Schmitt, C. T-W. Chu, D. H. Olson, E. W. Sheppard, S. B. Mc Cullen, J. B. Higgins, J. L. Schlenker. *J. Am. Chem. Soc.* **1992,** 114, 10834.

[25] D. Zhao, J. Feng, Q. Huo, N. Melosh, G. H. Fredrickson, B. F. Chmelka, G. D. Stucky. *Science.* **1998,** 279, 548.

[26] S. Sisodiya, A. Lazar, S. Shylesh, L. Wang, W. R. Thiel, A. P. Singh, *Catal. Comm.* **2012,** 25, 22.

[27] P. Sharma, A. P. Singh, *Cat. Today.* **2012,** 198, 184.

[28] H. Wang, K. Schaefer, A. Pich, M. Moeller, *Chem. Mater.* **2011,** 23, 4748.

[29] C. Z. Yu, B. Tian, J. Fan, G. D. Stucky, D. Zhao, *J. of Am. Chem. Soc.* **2002,** 124, 4556.

[30] Baleizao, B. Gigante, H. Garcia, A. Corma. *J. Cat.* **2003,** 215, 199.

[31] K. Roy, C. P. Vinod, C. S. Gopinath, *J. Phys. Chem. C*, **2013**, 117, 4717.

[32] J. Galo, A. A. de, C. Soler-Illia, B. Sanchez, J. Lebeau, Patarin, *Chem. Rev.* **2002,** 102, 4093.

[33] T. W. Dijkstra, R. Duchateau, R. A. van Santen, A. Meetsma, G. P. A. Yap, J. *Am. Chem.* Soc. **2002,** 124, 9856.

[34] N. H. Jentys, H. Pham, Vinek, J. *Chem. Soc. Faraday Trans.* **1996,** 92, 3287.

[35] a) S. Srinivas, P. Ratnasamy. *Micro. Meso. Mat.* **2007,** 105, 170.; b) A. O. Adeloye, P. A. Ajibade. *Molecules* **2011**, *16*, 4615-4631.; c) B. Vlckov, V. Baumrukb, J. Mosinger *Journal of Molecular Structure,* **1992**, 265, 9-16.; d) A. Modak, J. Mondal, M. Sasidharan, A. Bhaumik. *Green Chem.* **2011**, 13, 1317.

[36] A. Modak, J. Mondal, M. Sasidharan, A. Bhaumik, *Green Chem.* **2011,** 13, 1317.

[37] T. Soundiressane, S. Selvakumar, S. Menage, O. Hamelin, M. Fontecave, A. P. Singh, *J. of Mol. Catal. A: Chem*. **2007,** 270, 132.

[38] H. Yoshitake, T. Yokoi, T. Tatsumi, *Chem. Mater.* **2002,** 14, 4603.

[39] P. Sharma, A. P. Singh. *Catal. Sci. Technol.* **2014,** 4**,** 2978.

[40] D. S. Shephard, W. Zhou, T. Maschmeyer, J. M. Matters, C. L. Roper, S. Parsons, B. F. G. Johnson, M. J. Duer, *Angew Chem. Int. Ed*. 37, **1998,** 37, 2719.

[41] M. Chidambaram, A. P. Singh, *Appl. Catal: A Gen.* **2s006,** 310, 79.

[42] S. Shylesh, A. P. Singh, *J. Catal.* **2004,** 228, 333.

[43] S. C. Laha, P. Mukherjee, S. R. Sainkar, R. Kumar, *J. Catal.* **2002,** 207, 213.

[44] H. Yang, Y. Wang, Y. Qin, Y. Chong, Q. Yang, G. Li, Li, Zhang, W. Li, *Green Chem.* **2011,** 13, 1352.

[45] R. Venkatesan, M. H. G. Prechtl, J. D. Scholten, R. P. Pezzi, G. Machado, J. Dupont. *J. Mater. Chem.* **2011,** 21, 3030.

CHAPTER-6

Summary and Conclusions

6.1. SUMMARY

The present thesis gives an account of (i) the synthesis of organic-inorganic hybrid mesoporous materials by immobilization of several metal complexes on organically modified SBA-15 and periodic mesoporous organosilicas (PMO) having benzene groups in the frame wall positions, (ii) in-depth characterization of metal complex immobilized mesoporous materials and (iii) application of these materials as catalysts in oxidation, hydrogenation and C-C coupling reactions.

The present thesis is divided into six chapters including the current one as follows:

Chapter 1 Gives an idea about current scenario in the field of mesoporous molecular sieve materials, particularly transition metal complex based mesoporous materials, more precisely Pd and Mn transition metal catalysed oxidation, hydrogenation and C-C coupling reactions. The different characteristic properties of these materials include shape selectivity, formation mechanisms etc., and further more literature survey over synthesis aspects, characterization techniques, and different catalytic applications has been discussed. The scopes and objectives of the present work were outlined at the end of this chapter.

Chapter 2 Includes detailed synthesis and characterization of Chloro (S, S)(−)[N-3-tert-butyl-5-chloromethyl salicylidene]-N-[3,5-di tert-butylsalicylidene] 1,1-binaphthyl-2, 2-diamine manganese(III) (homogeneous system) complex on modified SBA-15 by using 3-aminopropyl trimethoxysilane as a reactive surface modifier to give supported catalyst. The surface properties of the functionalized catalyst were analyzed by a series of characterization techniques such as elemental analysis, XRD, N_2 sorption measurement isotherm, FT–IR, TGA–DTA, XPS, and solid state ^{13}C NMR. The XRD and N_2 sorption measurement, UV reflectance and CP MAS NMR spectroscopy (^{13}C and ^{29}Si) of the catalyst confirmed the structural integrity of the mesoporous hosts and the spectroscopic characterization technique proved the successful anchoring of the metal complex over the modified mesoporous support.

The screening of the catalyst Mn(III)-L-SBA-15 and neat Mn(III)- L complexes was done in the oxidation reaction of thioanisole (methyl phenyl sulfide) by using TBHP as an oxidant. Mn(III)-L-SBA-15 catalyst shows higher activities and turnover number (TON) and exhibit enhanced enantiomeric excess comparable to homogeneous catalyst Mn(III)-L. Moreover; bulkier alkene like 1, 2-dihydronaphthalene was also efficiently epoxidized with the synthesized supported catalyst Mn(III)-L-SBA-15.

Chapter 3 Includes synthesis of phosphine obstructed highly efficient and reusable SBA-15-EDTA-Pd catalyst by anchoring Pd−EDTA complex over the surface of organo-functionalized SBA-15. The physiochemical properties of the organo-functionalized catalyst were analyzed by elemental analysis, ICP−OES, XRD, N_2 sorption measurement isotherm, TGA & DTA, solid state ^{13}C, ^{29}Si NMR spectra FT-IR, XPS DRS UV−Visible, SEM and TEM. XRD and N_2 sorption analyses of synthesized catalyst confirm that ordered mesoporous channel structure was retained even after the multistep synthetic procedures. The (100), (110) and (200) reflections in SBA-15 provide good structural stability, existence of long range order and high pore wall thickness. The organic moieties anchored over the surface of SBA-15 and inside the pore wall were demonstrated by solid state ^{13}C NMR and FT−IR spectroscopy. Further, solid state ^{29}Si NMR spectroscopy provides the information about degree of functionalization of SBA-15 surface silanol groups. The electronic environment and oxidation state of Pd metal in SBA-15-EDTA-Pd(11) were monitored by XPS, DRS UV-visible techniques. Moreover, the morphologies and topographic information of synthesized catalyst were confirmed by SEM and TEM analysis. The synthesized catalyst SBA-15-EDTA-Pd(11) was screened for the Heck, Suzuki and Sonogashira coupling reactions and show higher catalytic activity with higher TON (turn over number). The anchored solid catalyst can be recycled efficiently and reused several times without major loss in reactivity.

Chapter 4 An efficient and highly reusable B-PMO-TZ-Pd(II) has been synthesized by anchoring 4-(2-pyridyl)-1, 2, 3-triazole ligand over the inner surface of organo-

functionalized benzene containing periodic mesoporous organosilica (B-PMO) via "**Click reaction**" and subsequent complexation with $PdCl_2$. B-PMO with uniform hexagonal arrangement were prepared using C16 alkyl trimethyl ammonium bromide [CTAB] surfactant under basic conditions. The physiochemical properties of the functionalized catalyst were analyzed by elemental analysis, ICP-OES, XRD, N_2 sorption measurement isotherm, TGA & DTA, solid state ^{13}C, ^{29}Si NMR spectra FT-IR, XPS, DRS UV-Vis, SEM and TEM. The (100), (110) and (200) reflections in B-PMO provide good structural stability, existence of long range order and high pore wall thickness. TGA-DTA results revealed the high thermal stability of synthesized catalyst, B-PMO-TZ-Pd(II). Furthermore, B-PMO-N_3 shows sharp absorbance at 2106 cm^{-1}; which is a characteristic stretching vibration of any organic azide (N_3). The absence of this peak at 2106 cm^{-1} in B-PMO-TZ-Pd(II) shows that the azidopropyl group successfully incorporated to the 2-ethynylpyridine via click reaction. The electronic environment and oxidation state of Pd metal in B-PMO-TZ-Pd(II) were monitored by XPS, DRS UV-visible techniques. The synthesized B-PMO-TZ-Pd(II) catalyst was screened in the Stille and Kumada coupling reactions and show higher catalytic activities with high TONs. The anchored solid B-PMO-TZ-Pd(II) catalyst can be recycled efficiently and reused several time (four times) without major loss in reactivity.

Chapter 5 Describe the synthesis of SBA-15-TAT-Pd(II) by anchoring of 2, 4, 6-triallyloxy-1, 3, 5-triazine (TAT) complex over the surface of organo-functionalized SBA-15. The physiochemical properties of the organo-functionalized catalyst were analyzed by various characterizations techniques. XRD and N_2 sorption analyses were done to find out textural properties of synthesized catalyst and confirm that ordered mesoporous channel structure was retained even after the multistep synthetic procedures. The organic moieties anchored over the surface of SBA-15 and inside the pore wall were demonstrated by solid state ^{13}C NMR and FT-IR spectroscopy. The electronic environment and oxidation state of Pd metal in SBA-15-TAT-Pd(II) were monitored by XPS, DRS UV-visible techniques. The synthesized catalyst SBA-15-TAT-Pd(II) was screened for the hydrogenation reactions and show higher catalytic

activity with high TON. The anchored solid catalyst can be recycled efficiently and reused several time (five times) without major loss in reactivity.

Chapter 6 This chapter gives an overall summary of major conclusions of the present study with respect to the synthesis and characterization of immobilized catalysts and the successful attempt in using the catalytic properties of the catalyst for oxidation, hydrogenation and C-C coupling reactions.

6.2. CONCLUSIONS

Chapter 2: Mn(III) based binaphthyl schiff base complex heterogenized over organo-modified SBA-15.

- Highly ordered SBA-15 was synthesized by hydrothermal method.
- The covalent functionalization of Mn(III)-L complex over modified surface of SBA-15 was successfully achieved by multiple step synthetic procedures.
- The presence of (100) (110) and (200) reflection in the XRD pattern confirms the retention of hexagonal ordering of SBA-15 even after organo functionalization and metal complex [Mn(III)-L] anchoring.
- The effect of neat Mn(III)-L complex loading on the physical properties of SBA-15 (surface area and pore size parameter) was explored by nitrogen sorption study.
- Appearance of characteristic C=N peak at 1629 cm^{-1} in the FT-IR spectrum of metal complex immobilized SBA-15 clearly indicate the anchoring of homogeneous complex over modified SBA-15 support.
- TGA-DTA analysis show a total weight loss of 35.6 % and 21.2 % for [Mn(III)-L-SBA-15] and NH_2-SBA-15, respectively, which demonstrate ~14 % loading of chiral metal complex over modified SBA-15.
- Methoxy carbon peak was not observed in the solid state ^{13}C CP MAS NMR spectrum of NH_2-SBA-15, which indicates the proper hydrolysis and anchoring of 3-aminopropyltrimethoxy silane over calcined SBA-15. The presence of aromatic binaphthyl and salicyaldimine groups in the case of

[Mn(III)-L-SBA-15] was demonstrated by the NMR band in the range of 112-170 ppm.

- Moreover additional peak at 28.1 and 34.1 ppm for Mn(III)-L-SBA-15 catalyst was noticed in the ^{13}C CP MAS NMR and it corresponds to the methyl carbon of t-butyl and t-butyl carbon of salicyaldimine group, respectively.
- Calcined SBA-15 showed broad resonance peaks from –93.8 to –102.9 ppm indicative of all Q^2–Q^4 sites in ^{29}Si CP MAS NMR. A decrease in Q^2 and Q^3 site with a corresponding increase in the percentage of Q^4 site was noticed after amino functionalization, indicate that the silylating agents effectively consume the germinal as well as free silanol sites present in the calcined SBA-15. All these NMR results clearly indicating the proper anchoring of amino group as well as metal complex inside the mesoporous SBA-15 material.
- XPS and UV-Vis analysis demonstrate that manganese is in +3 oxidation states in Mn(III)-L-SBA-15 and Mn(III)-L catalyst.
- Sulfoxidation and epoxidation reaction of thioanisole and 1, 2-dihydronaphthalene, respectively demonstrated high catalytic activity, TON and selectivity with heterogeneous Mn(III)-L-SBA-15 catalyst compared to homogeneous counterpart Mn(III)-L.
- During recycling, conversion of thioanisole decreases from ~20 % after use from fresh to fourth recycle over Mn(III)-L-SBA-15. This might be due to partial leaching of metal or active site from the heterogenized metal complex.

Chapter 3: Phosphine free SBA-15-EDTA-Pd highly active recyclable catalyst for Heck, Suzuki and Sonogashira reaction.

- In conclusion, highly stable and recyclable SBA-15-EDTA-Pd catalyst was synthesized by anchoring with different wt. % loading (7 %, 11 %, and 15 %) of Pd-EDTA complex over the inner surface of organo-functionalized SBA-15.
- From the XRD pattern it is clear that after anchoring of different weigh percent of (7 %, 11 %, 15 %) Pd-EDTA complexes; an inconsequential

decrease in peak intensities to the (100), (110) and (200) reflections were observed without changing the peak positions.

- XRD and N_2 sorption analyses of synthesized catalyst confirm that ordered mesoporous channel structure was retained even after the multistep synthetic procedures.
- TGA-DTA results revealed that the heterogenized metal complex catalyst, SAB-15-EDTA-Pd(11) is stable at elevated temperature.
- TEM image of calcined SBA-15 and SBA-15-EDTA-Pd(11) provide structural evidence that the material organized into ordered arrays of two-dimensional hexagonal mesopores. Moreover; TEM image of SBA-15-EDTA-Pd(11) catalyst clearly shows that metal complex was anchored inside the meso channels of the SBA-15.
- XPS, DRS UV-visible techniques revealed that electronic environment and oxidation state of Pd metal as Pd^{+2} in SBA-15-EDTA-Pd(11) catalyst.
- The activity of the heterogeneous catalyst, SBA-15-EDTA-Pd(11) was screened in the Heck, Suzuki and Sonogashira coupling reactions, which shows higher catalytic activity with high TON under phosphine and copper free conditions. In addition, the present catalytic system tolerates a broad range functional group.
- Different varieties of aryl halides (mono substituted, electron rich and electron poor) reacts smoothly with phenyl boronic acid and gave respective Suzuki coupled products. In addition, non aromatic olefins (acrylates) react under high rate with aryl iodide and gave respective Heck C-C coupled products.
- The heterogenization of the EDTA-Pd complex over mesoporous SBA-15 demonstrated the recyclable capability of the catalyst without major loss in activity.

Chapter 4: A recyclable and efficient Pd(II) 4-(2-pyridyl)-1, 2, 3-triazole complex over the solid periodic mesoporous organosilica (PMO) support by "click reactions".

- Benzene containing periodic mesoporous organosilica (B-PMO) materials with uniform hexagonal arrangements was prepared by using C16 alkyl trimethylammonium bromide [CTAB] surfactant under basic conditions.
- Heterogenization of 4-(2-pyridyl)-4-(2-pyridyl)-1, 2, 3 triazole ligand over the inner surface of organo-functionalized B-PMO were achieved by "**Click reaction**" and subsequent complexation with $PdCl_2$ leads to an efficient heterogenized catalyst, B-PMO-TZ-Pd(II).
- The (100), (110) and (200) reflections in small angle XRD patterns of B-PMO and its derivative material showed the existence of long range order with structural stability.
- FT–IR studies confirmed the complete removal of surfactant from the pore channels of the hybrid materials. In addition the presence of benzene fragments in the framework and further modification via triazole ligand (click reaction) over the mesoporous framework was also clearly evident from this study.
- The absence of Q units [Q*n* Si(OSi)*n*$(OH)_4$-*n*] below –100 ppm confirms the negligible hydrolytic Si–C bond cleavage and the bridge-bonded organic group is intact in the silica framework under the synthetic conditions.
- The matrix decomposition [1,2-bis (triethoxysilyl) benzene (BTEB)] fragments bonded in the mesopore frame wall channels is observed in the range of 600-650 °C in all the samples by TG-DTA analysis which attributes that the present mesoporous host materials (B-PMO) are thermally stable up to a temperature of 600 °C.
- The observed increment in the absorption intensity at 220 and 275 nm in UV-Vis analysis surfactant extracted B-PMO demonstrate the increase in π electron interaction in phenylene ring without surfactant molecules. Also the shift in the binding energy value of Pd $3d_{3/2}$ and Pd $3d_{5/2}$ compared $PdCl_2$ explained that the metal species is coordinated with electron rich compound,

i.e. 4-(2-pyridyl)-1, 2, 3 triazole ligand.

- B-PMO shows uniform arrays of mesochannals arrangement and clearly molecular-scale periodicity in the SEM images.
- The present B-PMO-TZ-Pd(II) catalytic system tolerates a broad range functional group of aryl halide in both Stille and Kumada coupling reactions and shows higher catalytic activity, TON and can be recycled efficiently several time without major loss in activity.

Chapter 5: Covalently anchored 2, 4, 6-triallyloxy-1, 3, 5-triazine Pd(II) complex over modified surface of SBA-15.

- In conclusion, stable and recyclable SBA-15-TAT-Pd(II) catalyst was synthesized by anchoring 2, 4, 6-triallyloxy-1, 3, 5-triazine ligand over the surface of organo thiol modified SBA-15 and subsequent complexation with Pd acetate.
- Long range order of the organo thiol and 2, 4, 6-triallyloxy-1, 3, 5-triazine Pd(II) complex modified SBA-15 was demonstrated by the (100), (110) and (200) reflection in X-ray diffraction.
- The proper anchoring of organo thiol and triazine complex was explained by the appearance of C-S, S-H and N-H stretching vibrations at 705, 468 and 3435 cm^{-1}, respectively in FT-IR spectra. This results were further confirmed by the appearance of respective carbon peaks in ^{13}C liquid and solid state NMR.
- Further, Q^2, Q^3 and Q^4 sites were noticed at -93, -102 and -111 ppm, respectively in ^{29}Si NMR of calcined SBA-15 samples. At the same time T^3 (-67 ppm) and T^2 (-60 ppm) sites were observed in the TAT modified SBA-15 supports the FT-IR and ^{13}C NMR results.
- Compared to the calcined SBA-15, 2, 4, 6-triallyloxy-1, 3, 5-triazine Pd(II) complex modified samples show additoinal absorption band in UV-Vis spectra which might be due to metal to ligand charge transfer (MLCT) and π-π^* transition.
- The proper heterogenization of –SH and TAT over SBA-15 were further

revealed by the appearance of weight loss in TGA analysis of the respective samples. The decomposition of thiol groups was observed in the range of 245 to 385 °C. At the same time weight loss in the range of 470 to 500 °C was observed for TAT modified SBA-15 with respective exothermic peaks in DTA.

- The catalytic activity of SBA-15-TAT-Pd(II) was tested in the hydrogenation of a variety of unsaturated olefins and aromatic nitro compounds to their corresponding products.
- It is noteworthy to mention that no ring hydrogenated products were observed with styrene, and α-methyl styrene. Furthermore; non aromatic cyclic olefins cyclo-pentene, cyclohexene, cyclooctene and linear olefins are also hydrogenated within short reaction time period.
- The present SBA-15-TAT-Pd(II) catalytic system tolerates a broad range of olefin compounds in hydrogenation reaction under the mild reaction conditions. The heterogenized solid catalyst SBA-15-TAT-Pd(II) can be and reused several time without major loss in activity.

Publications

Symposium

Conferences

PUBLICATIONS

[1] Mn(III) based binaphthyl Schiff base complex heterogenized over organo-modified SBA-15: Synthesis, Characterization and Catalytic Application.
Priti Sharma, Anish Lazar, A. P. Singh
Applied Catalysis A: General. 440 (2012) 101-110.

[2] Chiral VOIV-Sal-Indanol complex over modified SBA-15: an efficient, reusable enantioselective catalyst for asymmetric sulfoxidation reaction.
Anish Lazar, **Priti Sharma**, A. P. Singh
Microporous and mesoporous materials. 170 (2013) 331-339.

[3] Binapthyl schiff base diamine complex covalently bonded to modified SBA-15: Synthesis, Characterization and Catalytic Application.
Priti Sharma, A. P. Singh
Catalysis Today. 198 (2012) 184-188.

[4] Clay encapsulated Cu(OH)x promoted homocoupling of arylboronic acids: An efficient and eco-friendly protocol.
Bashir Ahmad Dara, A. P. Singh, **Priti Sharma**, Anish Lazar.
Applied Catalysis A: General. 470 (2014) 232-238.

[5] Phosphine free SBA-15-EDTA-Pd highly active recyclable catalyst: Synthesis Characterization and application for Suzuki and Sonogoshira reaction.
Priti Sharma, A. P. Singh,
Catalysis science & Technology. 4 (2014) 2978-2989.

[6] Synthesis of a recyclable and efficient Pd(II) 4-(2-pyridyl)-1, 2, 3-Triazole Complex over the solid Periodic Mesoporous Organosilica support by "Click reactions" for the Stille coupling reaction.
Priti Sharma, A. P. Singh
(RSC Advance Accepted)

[7] Covalently Anchored 2, 4, 6-triallyloxy-1, 3, 5-triazine (TAT) Pd(II) Complex over Modified Surface of SBA-15: Catalytic Applications in Hydrogenation Reaction.
Priti Sharma, A. P. Singh (In press)

[8] Pd-EDTA-SBA-15 highly active recyclable catalyst for Heck reaction.
Priti Sharma, A. P. Singh (In Press).

[9] PMO supported Pd(II) 4-(2-pyridyl)-1, 2, 3-Triazole Complex Heterogeneous catalyst For Kumada Coupling Reaction.
Priti Sharma, A. P. Singh (Manuscript submitted).

[10] Heck, Suzuki, Sonogashira and Hiyama cross coupling reactions catalyzed by Covalently Anchored 2, 4, 6-triallyloxy-1, 3, 5-triazine (TAT) Pd(II) Complex over Modified Surface of SBA-15.
Chandani R. Singh, Pradeep Kumar, **Priti Sharma**, A. P. Singh
(Manuscript under preparation)

POSTER AND ORAL PRESENTATIONS

[1] Heterogenization of $Rh(PPh_3)_3Cl$ over PMO for hydrogenation of olefins.
Anish Lazar, Shoy George C, **Priti Sharma**, Jithesh P. R, A. P. Singh,
15th National Workshop on the Role of New Material in Catalysis.
Indian Institute of Technology (IIT), Chennai, India, December 11-13, 2011.(Poster)

[2] Mn(III) based (S,S)(−)[N-3-tert-butyl-5-chloromethyl salicylidene]-N-[3,5-di tert-butyl salicylidene] 1,1-binapthyl-2,2-diamine complex covalently bonded to modified SBA-15: Synthesis Characterization and Catalytic application.
Priti Sharma, A. P. Singh,
One day National Seminar on Current Trends in Industrial Catalysis.
CSIR-National Chemical Laboratory, Pune, India, June 11 2012.(Poster)

[3] Mn(III) based binapthyl Schiff base complex heterogenized over organo-modified SBA-15: Synthesis, characterization and catalytic application.
Priti Sharma A. P. Singh,
2nd International Indo-German Symposium on Green Chemistry & Catalysis for Sustainable Development. ICT, Matunga, Mumbai, India, October 29-31, 2012.(Poster)

[4] Binapthyl schiff base diamine complex covalently bonded to modified SBA-15: Synthesis, Characterization and Catalytic Application.
Priti Sharma, A. P. Singh
International Conference on Technological Innovations for All Inclusive Growth alongside WAITRO 21st Biennial Congress & General Assembly.
Shree Ram Institute for Industrial *Research (SRI), New Delhi, India, November 8-9, 2012 India. (Poster)*

[5] Mn(III) based binaphthyl Schiff base complex heterogenized over organo-modified SBA-15:Synthesis, Characterization and Catalytic Application.
Priti Sharma, Anish. Lazar, S. Silpa, M. Mirajkar and A. P. Singh
21st National Symposium on catalysis "catalysis for sustainable Development" (CATSYMP-21)
CSIR-IICT, Hyderabad, India, February 11-13, 2013. (Oral)

[6] Mn(III) based binapthyl Schiff base complex heterogenized over organo-modified SBA-15: Synthesis, characterization and catalytic application.
Priti Sharma, A. P. Singh,
Science Day celebration on Green Chemistry & Catalysis. CSIR-NCL Pune, February 27, 2013 (Poster)

[7] Mn(III) based binapthyl Schiff base complex heterogenized over organo-modified SBA-15: Synthesis, characterization and catalytic application.
Priti Sharma, A. P. Singh
7th International Symposium on Feedstock Recycling of Polymeric Material. India Habitate Centre, New Delhi, India. October 23-26, 2013.(Poster)

[8] Schiff base complex heterogenized over organo-modified SBA-15: Synthesis, characterization and catalytic application. (Hindi Symposium)
Priti Sharma, A. P. Singh
Use of Catalyst in Organic Transformation
CSIR-National Chemical Laboratory, Pune, India, May 7th 2013, (Oral presentation in Hindi)

APPENDIX

Suzuki reaction, Stille coupling reaction and Corriu-Tamao-Kumada coupling reaction (NMR results)

(2a) (4a) biphenyl

^{1}H NMR ($CDCl_3$): 7.34-7.62 (m, 10H).

^{13}C NMR ($CDCl_3$): 127.20 (s, 5C), 128.79 (s, 5C).

(2b) (4b) 4-nitro 1,1' biphenyl

^{1}H NMR ($CDCl_3$): 7.40-7.44 (m, 3H), 7.54-7.59 (m, 2H), 7.65-7.69 (m, 2H), 8.21-8.26 (d, 2H).

^{13}C NMR ($CDCl_3$): 123.09 (s, 2C), 126.37 (s, 2C), 126.78 (s, 2C), 127.89 (s, 1C) 128.13 (s, 2C), 137.77 (s, 2C), 146.62 (s, 2C).

(2c) (4c) 4-methyl -1, 1'biphenyl

^{1}H NMR ($CDCl_3$): 2.32 (s, 3H), 7.16-7.53 (m, 9H)

^{13}C NMR ($CDCl_3$): 21.14 (s, 1C), 127.02 (s, 5C), 128.75 (s, 2C), 129.52 (s, 2C), 137.06 (s, 1C) 138.39 (s, 1C), 141.19 (s, 1C).

(2d) (4d) 4-methoxy-1, 1'bibhenyl

^{1}H NMR ($CDCl_3$): 3.83 (s, 3H), 6.96-6.99 (d, 2H), 7.29-7.32 (m, 1H), 7.37-7.41 (m, 2H), 7.50-7.57 (m, 4H).

^{13}C NMR ($CDCl_3$): 55.38 (s, 1C), 114.26 (s, 2C), 126.71 (s, 1C) 126.78 (s, 2C), 128.20 (s, 2C), 128.77 (s, 2C), 133.83 (s, 1C), 140.88 (s, 1C), 159.21 (s, 1C).

Sonogashira reaction (NMR results)

(3a) 1, 2-diphenylethyne

^{1}H NMR ($CDCl_3$): 6.93-7.79 (m, 10H)

^{13}C NMR ($CDCl_3$): 125-136 (m, 12C), 77.25 (d, 2C).

(3b) 1-nitro-4-(phenylethynyl) benzene

^{1}H NMR ($CDCl_3$): 7.07-8.31 (m, 9H)

^{13}C NMR ($CDCl_3$): 68.17 (s, 2C), 122.53 (s, 1C), 123.68 (s, 1C), 127.22 (s, 1C), 128.03 (s, 2C), 120.72 (s, 1C), 129.83 (s, 2C), 130.90 (s, 1C), 131.72 (s, 1C), 132.50 (s, 1C), 142.36 (s, 1C).

(3c) 1-methyl-4-(phenylethynyl) benzene

^{1}H NMR ($CDCl_3$): 4.0 (3H), 7.32-8.7 (9H)

^{13}C NMR ($CDCl_3$): 28.24 (s,1C), 97.95 (s,1C), 80.95(s,1C), 120.76(s, 1C), 121.10 (s,1C), 123.47(s,1C), 124.11 (s,1C), 127.38 (s,1C), 131.14 (s,1C), 132.89 (s,1C), 134.83 (s,1C), 139.89 (s,1C), 140.94 (s,1C), 154.20 (s,1C), 154.95 (s,1C).

Heck Coupling Reaction (NMR Results)

(6a) E Stilbene

^{1}H NMR ($CDCl_3$): 7.11(s, 2H), 7.22-7.40 (m, 6H), 7.50 (m, 4H).

^{13}C NMR ($CDCl_3$): 126.55 (2C), 127.66 (2C), 128.72 (8C), 137.36 (2C).

(6b) Methyl Cinnamate

^{1}H NMR ($CDCl_3$): 3.76 (s, 3H), 6.40-6.48 (d, 1H), 7.38-7.73 (m, 6H).

^{13}C NMR ($CDCl_3$): 51.73 (1C), 117.82 (1C), 128.11 (2C), 128.92 (2C), 130.33 (1C), 134.40 (1C) 144.90(1C), 167.45(1C).

(6c) Ethyl Cinnamate

^{1}H NMR ($CDCl_3$): 1.18-1.25 (t, 3H), 4.09-4.19 (q, 2H), 6.28-6.36 (d, 1H), 7.22-7.61 (m, 6H)s

^{13}C NMR ($CDCl_3$): 14.06 (s, 1C), 60.17 (s, 1C), 118 (s, 1C), 127.78 (s, 1C), 128.60 (s,1C), 129.94 (s,1C),134.18 (s,1c),144.27 (s,1C), 166.62 (s,1C).

(6d) (E)-methyl 2-methyl-3-phenylacrylate

^{1}H NMR ($CDCl_3$): 2.04-2.05 (d, 3H), 3.74 (s, 3H) 7.13-7.14 (m, 4H) 7.62 (d, 1H), 7.86 (s, 1H).

^{13}C NMR ($CDCl_3$): 13.04 (s, 1C), 51.04 (s, 1C), 127.34 (s, 2C), 128.16 (s, 1C), 128.61 (s, 2C), 134.83 (s, 1C), 137.93 (s, 1C), 139.95 (s, 1C), 168.13 (s, 1C).

(6e) (E)-methyl 3-(4-nitropheyl) acrylate

^{1}H NMR ($CDCl_3$): 3.84 (s, 3H), 6.51-6.63 (d, 1H), 7.66-7.77 (m, 3H), 8.23-8.28 (d, 2H).

^{13}C NMR ($CDCl_3$): 51.99 (s, 1C), 121.97 (s, 1C), 124.08 (s, 2C), 128.58 (s, 2C), 140.38 (s, 1C), 141.81 (s, 1C), 148.39 (s, 1C), 166.39 (s, 1C).

(6f) (E)-ethyl 3-(4-nitropheyl) acrylate

^{1}H NMR ($CDCl_3$): 1.24-1.32 (t, 3H), 4.7-4.27 (q, 2H), 6.45-6.53 (d, 1H), 7.58-7.68 (m, 3H), 8.15-8.20 (d, 2H)

^{13}C NMR ($CDCl_3$): 14.28 (s, 1C), 61.03 (s, 1C), 122.59 (s, 2C), 128.64 (s, 2C), 140.60 (s, 1C), 141.63 (s, 2C), 148.47 (s, 1C), 166.06 (s, 1C).

(6g) (E)-1-nitro stilbene

^{1}H NMR ($CDCl_3$): 7.17 (s, 1H) 7.23 (s, 1H), 7.30-7.44 (m, 3H), 7.53-7.65 (m, 4H), 8.19 (s, 1H), 8.23 (s, 1H).

^{13}C NMR ($CDCl_3$): 124.19 (s, 2C), 126.30 (s, 2C), 126.89 (s, 1C), 127.06 (s, 2C), 128.89 (s, 2C), 128.93 (s, 2C), 133.33 (s, 1C), 136.19 (s, 1C), 143.88 (s, 1C)

(6h) 4-nitro cinnamic acid

^{1}H NMR ($CDCl_3$): 6.72-6.80 (d, 1H), 7.68-7.76 (d, 1H), 7.98-8.01 (d, 2H), 8.23-8.27 (d, 2H)

^{13}C NMR ($CDCl_3$): 14.06 (s, 1C), 60.17(s, 1C), 118 (s, 1C), 127.78 (s, 1C), 128.60 (s, 1C), 129.94 (s, 1C), 134.18 (s, 1c), 144.27 (s, 1C), 166.62 (s, 1C).

(6i) Cinnamic acid

^{1}H NMR ($CDCl_3$): 6.42-6.50 (d, 1H), 7.39-7.34 (m, 3H), 7.53-7.58 (m, 2H), 7.76 7.84 (d, 1H).

^{13}C NMR ($CDCl_3$): 117.36 (s, 1C), 128.43 (s, 2C), 129.01 (s, 2C), 130.81 (s, 1C), 134.05 (s, 1C), 147.17 (s, 1C), 172.68 (s, 1C).

(6j) E-methyl 2-methyl-3-(4-nitrophenyl) acrylate

^{1}H NMR ($CDCl_3$): 2.04 (d, 3H), 3.77 (s, 3H), 7.43-7.47 (d, 2H), 7.62 (s, 1H), 8.15-8.19 (d, 2H).

^{13}C NMR ($CDCl_3$): 14.23 (s, 1C), 52.41 (s, 1C), 123.66 (s, 2C), 130.21 (s, 2C), 131.93 (s, 1C), 136.29 (s, 1C), 142.42 (s, 1C), 147.21 (s, 1C), 168.30 (s, 1C).

(6l) Cinnamonitrile

^{1}H NMR ($CDCl_3$): 5.74-5.82 (d, 1H), 7.01-7.07 (d, 1H), 7.34-7.74 (m, 5H).

^{13}C NMR ($CDCl_3$): 96.31 (s, 1C), 118.2 (s, 1C), 127.41 (s, 2C), 129.16 (s, 2C), 131.26 (s, 1C), 133.55 (s, 1C), 150.61 (s, 1C).

(6k) 4-Methyl transtilbene

^{1}H NMR ($CDCl_3$): 7.55 (d, 2H), 7.47 (d, 2H), 7.40 (t, 2H), 7.26-7.33 (m, 1H), 7.22 (d, 2H), 7.13 (d, 2H), 2.41 (s, 3H).

^{13}C NMR ($CDCl_3$): 137.56, 134.53, 129.41, 128.66, 127.74, 127.42, 126.44, 21.27.